WELL LOG ANALYSIS

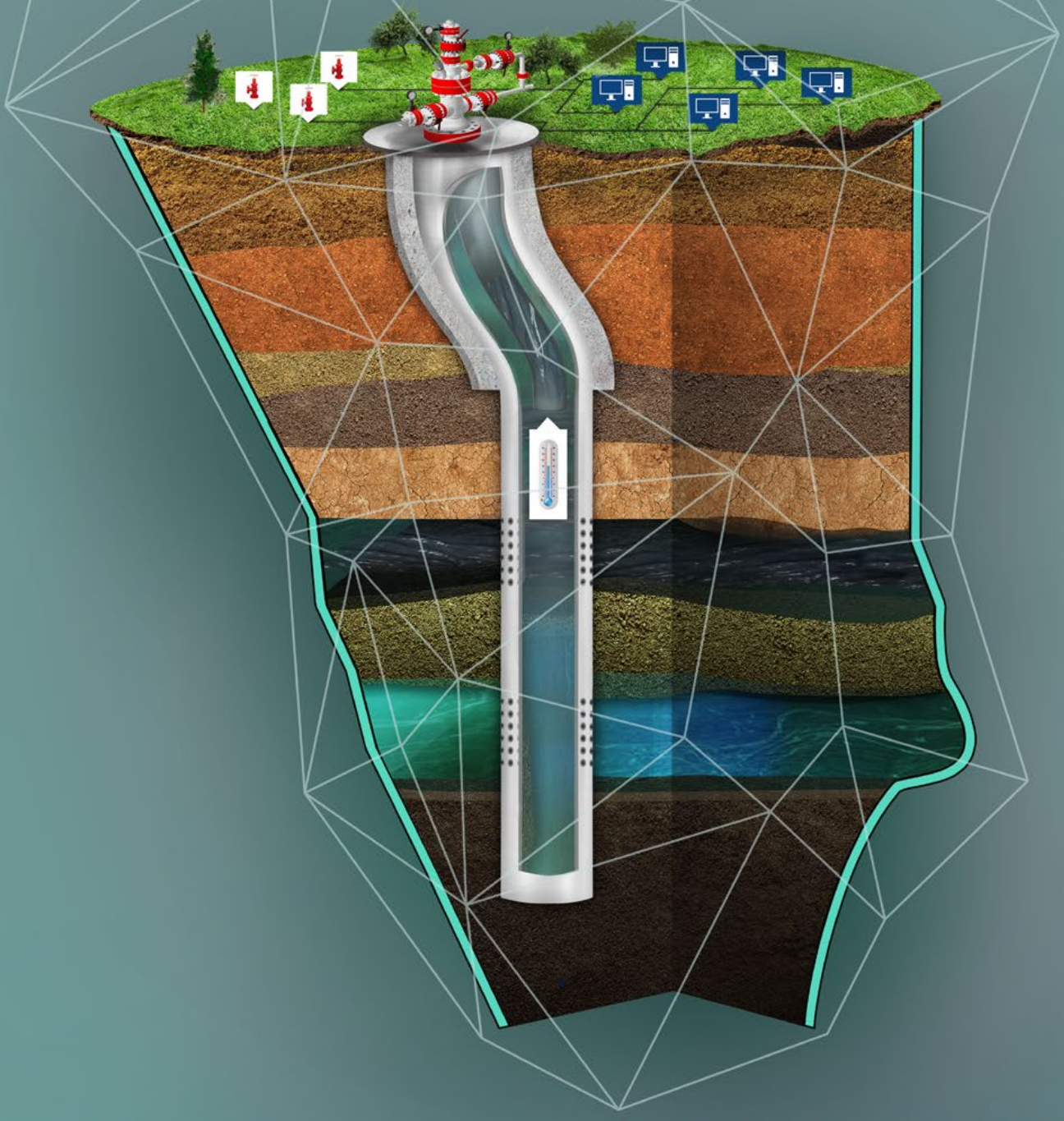

HANDBOOK

www.tgtoil.com

This handbook is the result of many years of work in some areas of cased-hole logging that TGT specialises in.

After a brief introduction to technology basics, most of the handbook's chapters expand on case studies with references to SPE papers in which the reader can get even more details. Sixty cases have been selected out of thousands of cases worldwide as the most representative for particular applications, technologies or certain situations that can puzzle even the most experienced log analyst.

The geography of the cases covers 25 countries, on-shore and off-shore locations from Arctic ice through deep forests to sunburnt deserts, sandstone and limestone formations, from high-permeability to shale deposits, matrix and fractured formations, vertical, deviated and horizontal wells, hydraulically fractured wells, a wide variety of single and dual completions, various types of packers and zonal isolations, production by natural flow, artificial gas-lift, rod pumps and ESPs, oil and gas producers, water, gas and water-alternated gas injection, steam and polymer injectors in green, brown and mature fields, from no-pressure-support to gas-cap-drive, aquifer-drive and water-flood production.

The handbook is split into three major parts – well integrity, borehole flow profiling and reservoir flow profiling, although the last two often overlap and make it difficult to determine to which part of the book a case should belong – and aims to attract interest from cased-hole log interpreters, petrophysicists, reservoir engineers and production technologists.

It particularly focuses on the tools that TGT has been developing over the last 18 years for PLT, spectral noise logging, temperature logging, temperature simulations and pulsed electromagnetic corrosion logging.

Most importantly, this handbook shares TGT's experience in integrated logging employing several tools that provide more information than a simple sum of individual logs. In some case, such integration can be tricky, and searching for a workaround can be a long chain of trials and failures.

Overall, it was a really exciting project and it will surely be continued to present new tools and applications.

We hope that our accumulated experience will be useful to log analysts across the world and that you will enjoy your journey through this Handbook!

You are cordially invited to send your feedback to wla@tgtoil.com.

Dr. Arthur Aslanyan
Chief Technology Advisor

CONTENTS

1. FUNDAMENTALS

1.1 PRODUCTION LOGGING

1.1.1 PRODUCTION LOGGING APPLICATIONS

Production logging (PL) is an essential part of reservoir management as it is used to measure multiphase wellbore flow and detect well integrity problems. The PLT survey is conducted in both cased and open-hole sections of wells in quasi-steady flow/injection or/and shut-in well regimes.

Generally, production logging is used for

- Location of wellbore fluid entry points and fluid types (water, oil or gas)
- Location of fluid injection zones (water or gas)
- Detection of leaks in the completion components and downhole equipment of the first pipe barrier, i.e. tubing, casing, bridge plug, SSD, etc.
- Determination of flow rates for each phase (oil, water and gas) from each producing zone
- Determination of water or gas injection rates for each injection zone

The combination of production logging other technologies, such as Spectral Noise Logging (SNL), Pulsed Neutron-Neutron Logging (PNNL) and Magnetic Imaging Defectoscopy (MID) along with the use of state-of-the-art data processing and mathematical modelling techniques to analyse processes in the wellbore and near-wellbore zone brings well logging to a totally new level.

1.1.2. PRODUCTION LOGGING TOOLSTRING COMPONENTS

A PLT string consists of the following modules measuring the corresponding parameters (with well log mnemonics abbreviated in parentheses):

- INDIGO NAV-2 (GR, CCL and INCL)
- INDIGO PT-2 and Micro-T (PRES and TEMP)
- INDIGO Flowmeters (FBS and ILS)
- INDIGO HEX-2 (HEX)
- INDIGO ReCap-2 (COND and CAP)
- INDIGO XYCaliper-2 (ID)
- INDIGO Three-Arm Roller Centraliser (RC-3)
- INDIGO Four-Arm Roller Centraliser (RC-4)

A typical configuration of an INDIGO-based production logging toolstring is shown in Fig. 1.1.1.

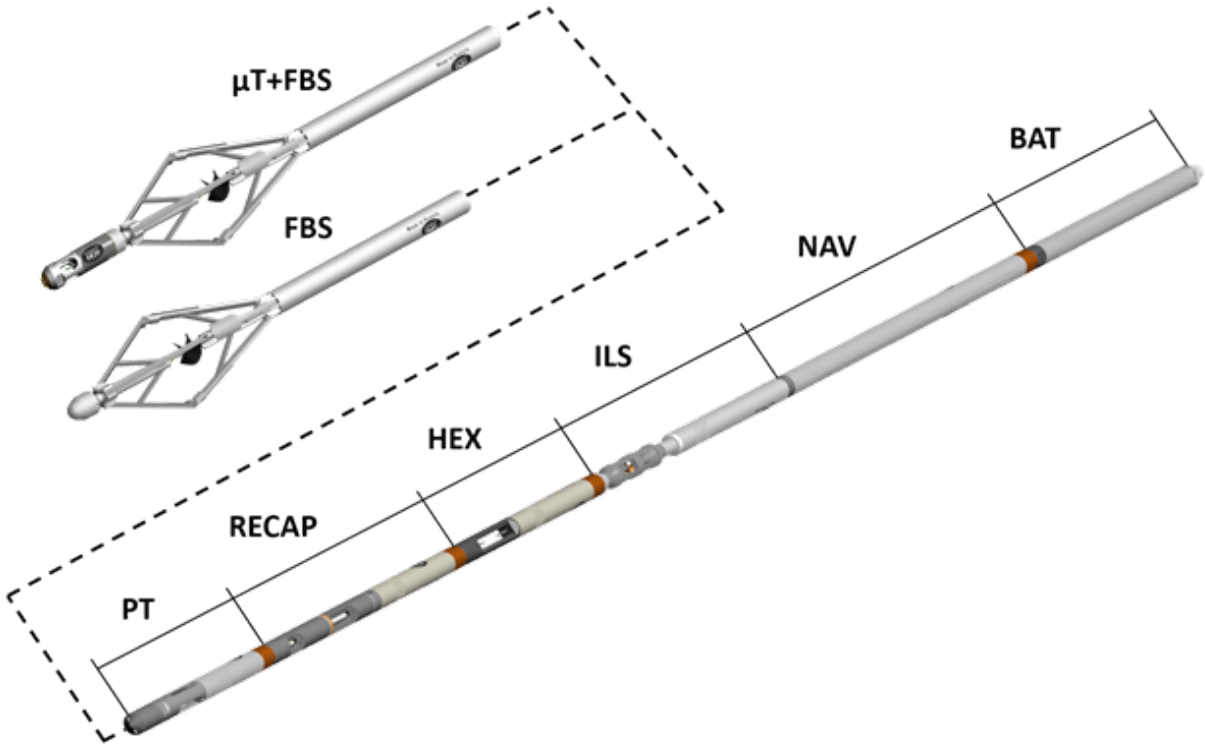

Fig. 1.1.1. INDIGO production logging toolstring

1.1.3. OVERVIEW OF PLT MODULES

The INDIGO tool line is designed for logging and other operations in oil and gas wells, both open and cased.

THE INDIGO CONCEPT

The INDIGO line of tools has the following main features:

- Modularity
  Each module is a full-fledged tool with its own memory, so that individual modules can be assembled into the tool configuration required by the objective
- Power supply independence
  All modules of the INDIGO line can operate independently on batteries (Fig. 1.1.1).
- On-line operation
  Various modules can be configured to operate with a surface recording station through single-core logging cable or coiled tubing
- Single-line power supply
  This provides an opportunity to combine different tool modules in one toolstring in a required order, synchronise time and optimise tool performance
- Clean environment
  The INDIGO multi-module toolstring does not emit electromagnetic or acoustic waves
- INDIGO Suite® software system

The INDIGO Suite® software system is used to set calibration parameters, programme on and off times according to the survey procedure, download recorded survey data from the tools, perform depth correlation and upload data for further processing and interpretation in LAS and DLIS formats

- Compatibility
  Different modules are compatible in one toolstring

Detailed descriptions of all modules and their sensors are given below.

INDIGO NAV-2

The INDIGO NAV-2 module contains three sensors: Gamma-Ray (GR), Casing Collar Locator (CCL) and XYZ Inclination Accelerometer (INCL) measuring the deviation angle (Fig. 1.1.2).

Gamma-Ray Sensor (GR)

Operating principle
Gamma-ray logging measures natural gamma radiation that is specific to individual geological facies.

Measurement unit
The measured value is the count rate. The recorded parameter is the exposure dose rate (EDR) in microroentgen per hour *(μR/hr)*. The American Petroleum Institute gamma ray units (GAPI) were introduced to provide an arbitrary gamma activity scale. The GAPI scale was defined at a calibration facility at the University of Houston, Texas. The gamma-ray API unit is defined as 1/200 of the difference between the count rate recorded by a logging tool in the middle of the radioactive section and that recorded in the middle of the nonradioactive section of the calibration pit.

Application
This sensor is used in radioactivity logging (RL) to correlate recorded logs with lithologies and for other purposes:

- Lithological differentiation and correlation of sedimentary rocks
- Identification of radiogeochemical anomalies caused by oil-water displacement in cased wells
- Identification of reservoirs
- Identification of minerals with higher or lower gamma activity
- Rock shaliness evaluation

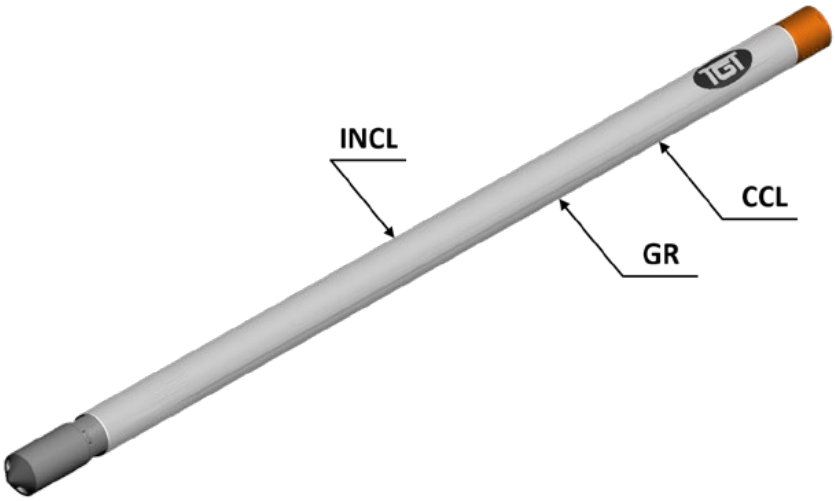

Fig. 1.1.2. INDIGO NAV-2

Casing Collar Locator (CCL)

Operating principle
The Casing Collar Locator detects variations in the magnetic conductivity of metal drill pipes, casing and tubing that are caused by integrity failures. The CCL is an active system containing two coils – generating and receiving. The alternating magnetic field generated by the alternating voltage fed to the generating coil induces an alternating voltage in the receiving coil that depends on the magnetic properties of the environment.

Measurement unit
The informative parameter is the voltage difference between the receiving coils that depends on the integrity of the metal pipe barriers.

Application
This sensor is used to correlate data from other sensors of the toolstring with completion components. In addition to correlation, the Casing Collar Locator provides the following solutions:
- Location of casing collars
- Precise determination of tubing and downhole equipment setting depths
- Hold-up depth determination
- Location of perforated intervals and casing damage

XYZ Inclination Accelerometer (INCL)

Operating principle
The inclinometer is a three-axis accelerometer that measures the projections of gravity acceleration onto the coordinate axis that is parallel to the tool. These projections are transformed into polar coordinates to calculate the angle of deviation of the tool axis from the gravity vector, i.e. from the vertical.

Measurement units
The measurement unit is the degree of the angle of wellbore deviation from the vertical *(°).*

Application
The inclinometer is used to measure the inclination angle of the wellbore, both open and cased.

INDIGO PT-2 FOR PRESSURE AND TEMPERATURE AND MICRO-T FOR TEMPERATURE

The Indigo PT-2 module (Fig. 1.1.3a) is designed to measure wellbore pressure and temperature and contains two sensors: a fast response high-precision temperature (FRT) sensor and a pressure sensor (PRES). This module is installed at the bottom of the tool string to record the temperature of undisturbed wellbore fluid during a downward pass.

To combine mechanical PLT flow-metering with High Precision Temperature (HPT) Logging in one logging trip, the tool string is complemented with the high-precision memory temperature end module Micro-T containing the fast response high-precision temperature (FRT) sensor (Fig. 1.1.3b), which reduces the total number of logging runs.

Fast Response High-Precision Temperature Sensor (FRT)

Operating principle
The temperature sensor is a platinum-wire thermistor. The sensor resistance changes with ambient temperature, and the changing output voltage of the sensor is fed to the input of an analogue-digital converter. Then, temperature is calculated through a calibration.

Measurement units
The measurement unit is degrees Celsius *(°C)* or Fahrenheit *(°F)*.

Application
Qualitative interpretation of recorded logs for:

- Determination of wellbore temperature at any depth
- Location of producing and receiving reservoir intervals
- Location of wellbore and behind-casing cross-flows
- Location of leaks in the downhole components nearest to the sensor, including casings, tubing, packers, mandrels, etc

High-precision temperature (HPT) logging data can be quantitatively interpreted for inflow and injectivity profiling.

Pressure Sensor (PRES)

Operating principle
The pressure sensor is a sapphire pressure transducer, the electrical resistance of which is proportional to substrate deformation, which is in turn proportional to pressure. The pressure transducer is integrated into a measuring bridge, and pressure variation causes an imbalance in its diagonal generating a voltage difference that is measured using an analogue-digital converter and is then recalculated to pressure through a calibration.

Measurement units
The measurement unit is the pascal *(Pa)*, pound-force per square inch *(psi)* or atmosphere *(atm).*

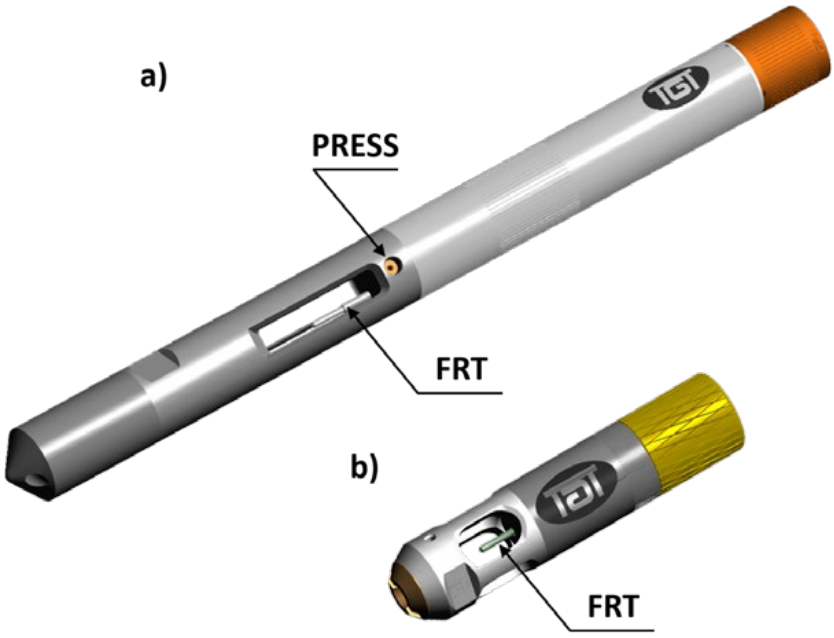

Fig. 1.1.3. (a) Indigo PT-2; (b) Micro-T

Application

The pressure sensor is used to measure

- Bottom-hole pressure
- Wellbore pressure at any depth
- Wellbore fluid levels
- Wellbore fluid density

INDIGO FLOWMETERS

Mechanical flow meters measure the average velocity of mixture flow. The full-bore spinner FBS (Figs. 1.1.4a and 1.1.4b) and in-line spinner ILS (Fig. 1.1.4c) are mechanical flowmeters for both open-hole and cased-hole wells. FBS is equipped with expanding fingers and has a larger diameter than ILS to measure flow velocity inside casing. The ILS's internal diameter does not exceed that of the main toolstring and can be used in small-diameter casing and tubing.

Operating principle

The sensor of a mechanical flowmeter is a multi-blade turbine generating electrical signals that are then recorded. The frequency of electrical pulses is converted into rotational speed, which is directly proportional to linear flow velocity. FBS is sensitive to both axial and radial flow (Fig. 1.1.5), and its material and geometry provide high momentum transfer between fluid flow and spinner blades, thus ensuring a low spinner threshold.

The limitations of this technique are low

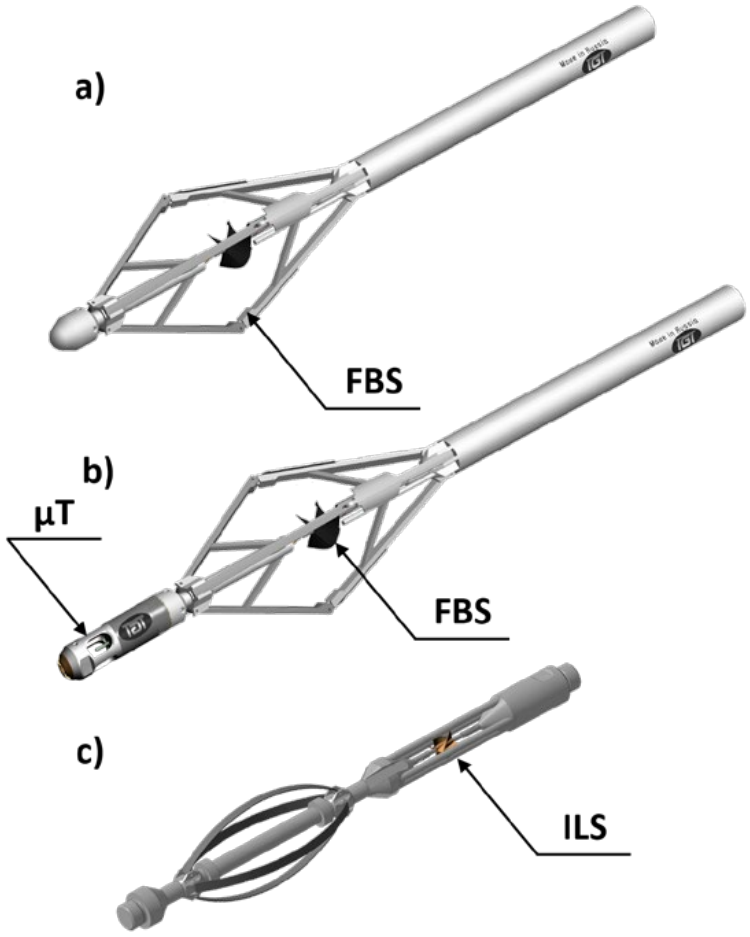

Fig. 1.1.4. (a) Full-bore spinner; (b) Full-bore spinner + Micro-T; (c) In-line spinner

sensitivity to low-velocity flows and the dependence of the sensitivity threshold on survey conditions, presence of solid particles and flow composition.

Measurement units

The spinner module reads out turbine rotational speed in RPS that is converted into flow velocity in meters per minute *(m/min)*, meters per second *(m/s)*, feet per minute *(ft/min)* or feet per second *(ft/s)* through a calibration.

Application

Mechanical flow metering determines the flow velocity of fluid, gas or their mixture in the wellbore and is used for the following applications:

- Location of inflow intervals in production wells and injection intervals in injection wells
- Determination of interval and total flow rates
- Detection of wellbore cross-flows after well shut-in

INDIGO HEX-2

The Indigo HEX-2 module (Fig. 1.1.6) has two sensors: the fast response high-precision temperature (FRT) sensor and a wellbore fluid heat exchange sensor (HEX). The temperature sensor is integrated into this module to determine the ambient fluid temperature.

Operating principle

The HEX sensor is a heat flowmeter that measures the variation of the sensor's temperature (Fig. 1.1.7) occurring with variations in the velocity of the fluid that flows around the sensor [1]. It consists of a heating element that heats the HEX sensor and a temperature sensor that measures its temperature. The temperature sensor and heating element are accommodated in one housing filled with thermal grease. The sensor is sensitive to the temperature and velocity of the wellbore fluid that flows around it. HEX data are recorded during upward and downward tool passes and/or at stations.

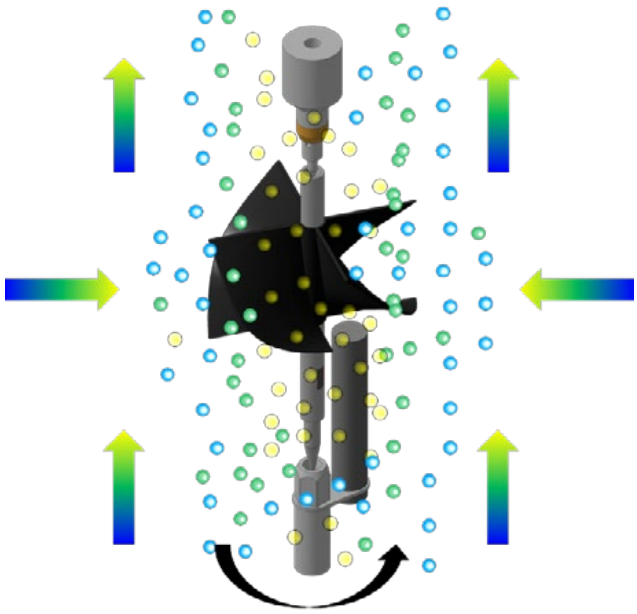

Fig. 1.1.5. An FBS turbine and the directions of the flows pushing against its blades

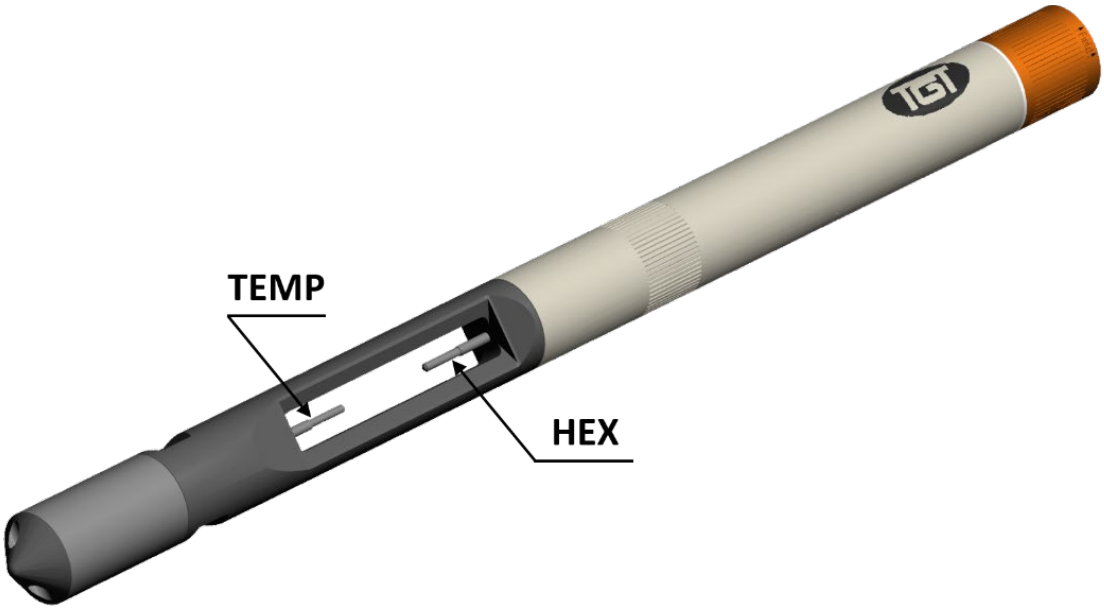

Fig. 1.1.6. Indigo HEX-2

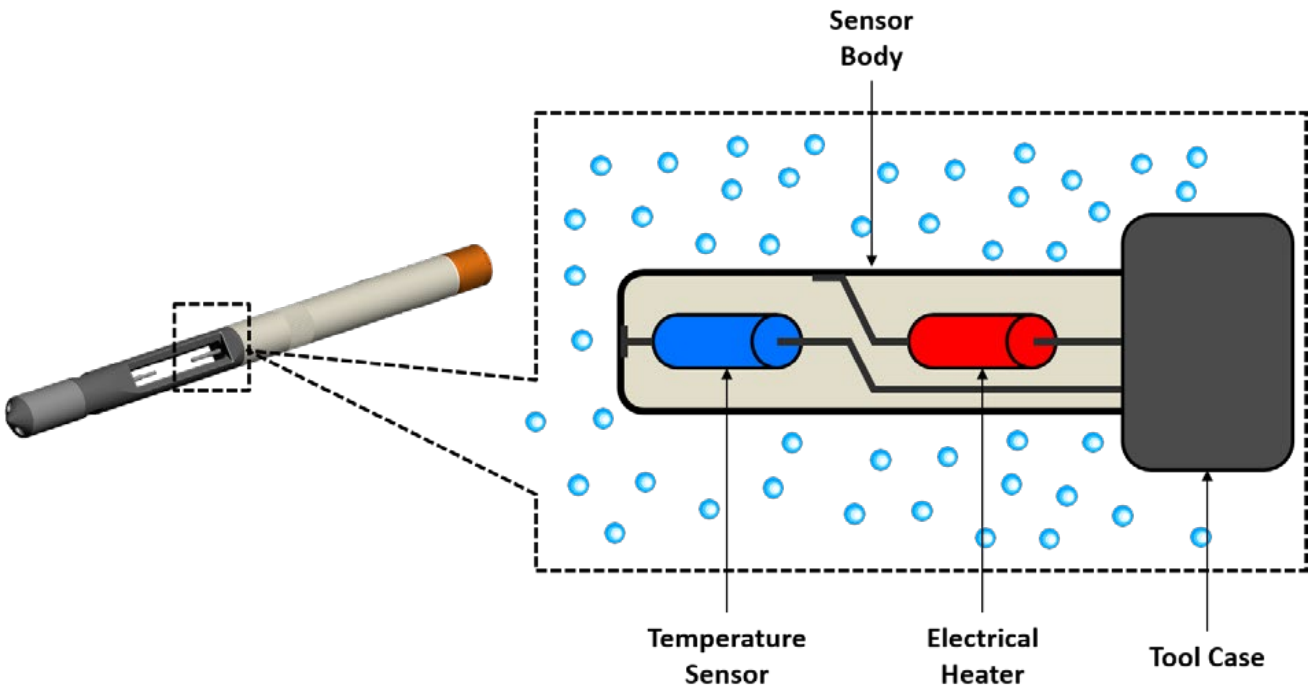

Fig. 1.1.7. HEX sensor schematic

Measurement units
The module reads out the temperature difference between the HEX sensor and the ambient temperature measured by the fast response high-precision temperature (FRT) sensor. The measurement unit is degrees Celsius *(°C)* or Fahrenheit *(°F).*

Application
The HEX module is used for the following applications:

- Inflow and injection location, especially in low-velocity flows
- Location of leak points in the pipe nearest to the sensor

INDIGO RECAP-2 TOOL MODULE

The Indigo ReCap-2 module (Fig. 1.1.8) contains two sensors: a capacitance meter (CAP) to determine water hold-up and a conductivity meter (COND) to determine induction resistivity.

Wellbore fluid electrical conductivity sensor (COND)

Operating principle
The induction resistivity sensor (COND) measures the electrical conductivity of wellbore fluids of varying salinity in production and injection wells (Fig. 1.1.9). The sensor consists of two toroidal coils (generating and receiving) that are spaced apart along the axis.
The coils are housed in a cylinder of nonconductive material flowed around by wellbore fluid through windows in the tool case. The sensor employs an inductive technique to measure fluid electrical conductivity. High-frequency current is supplied to the generator coil, and an electromagnetic force (EMF) is induced in the receiver coil. The signal recorded by the receiver coil is proportional to the conductivity of the fluid flowing around it. Fig. 1.1.10 shows a graph of resistivity variation depending on the water holdup in a two-phase (oil-water) mixture in the effective volume of the tool.

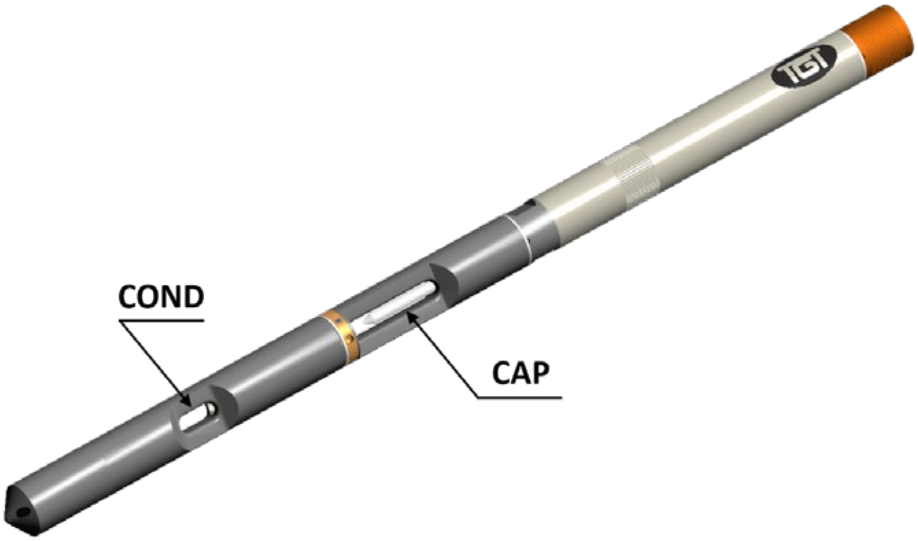

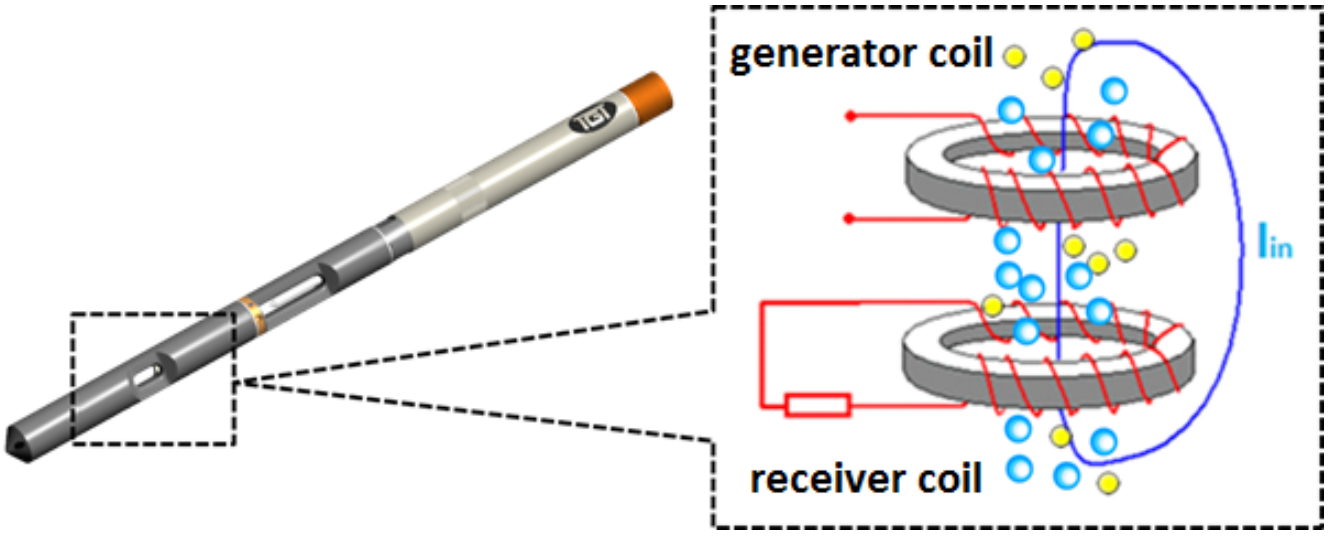

Fig. 1.1.9. Conductivity sensor schematic

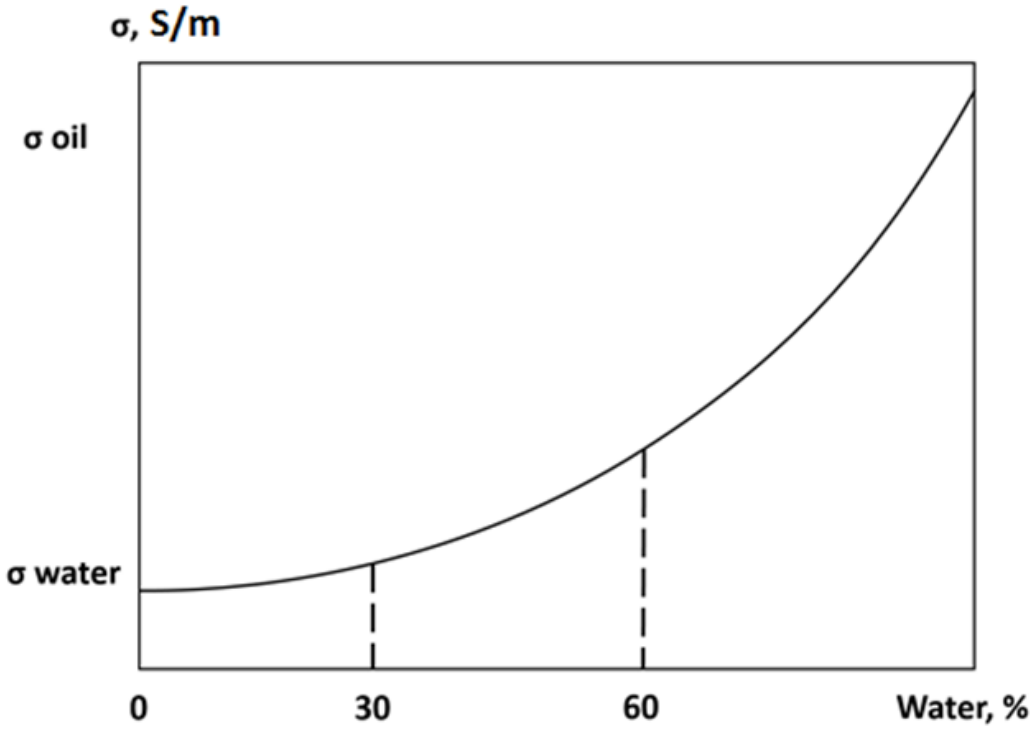

Fig. 1.1.10. Resistivity vs. water holdup for a two-phase (oil-water) mixture in the effective volume of the toolFig. 1.1.8. Indigo ReCap-2

The sensor is most sensitive in the water holdup range of 60–100%. At lower water contents, the tool's response to water content variations is weak. For this reason, the conductivity sensor is used in water-dominant flows with a water holdup of more than 60%. It should be noted that its readings can be substantially affected by the multiphase flow structure, oil viscosity and presence or absence of centralisers in the tool string.

Measurement units

Conductivity is measured in siemens per meter *(S/m).*

Application

The wellbore fluid electrical conductivity sensor is used for the following applications:

- Wellbore water holdup measurement
- Location of water inflow intervals
- Determination of wellbore water salinity in NaCl equivalent units
- Location of leaks in casing and downhole equipment

Wellbore electrical capacitance sensor (CAP)

Operating principle

The operation of the electrical capacitance sensor (CAP) is based on different dielectric responses of gas, oil and water in the wellbore. Fig. 1.1.11 shows the schematic of the capacitance sensor.

The sensor is a resistor-capacitor generator (RC-generator) with a measuring flow-through capacitor integrated into its oscillating circuit. Wellbore fluid that flows around the sensor serves as the capacitor's dielectric, and mixtures of varying-phase compositions flowing between the capacitor's plates change its capacity, which in turn changes the circuit oscillation frequency. Fig. 1.1.12 shows a graph of circuit oscillation frequency variation depending on the water holdup in a two-phase (oil-water) mixture in the effective volume of the tool.

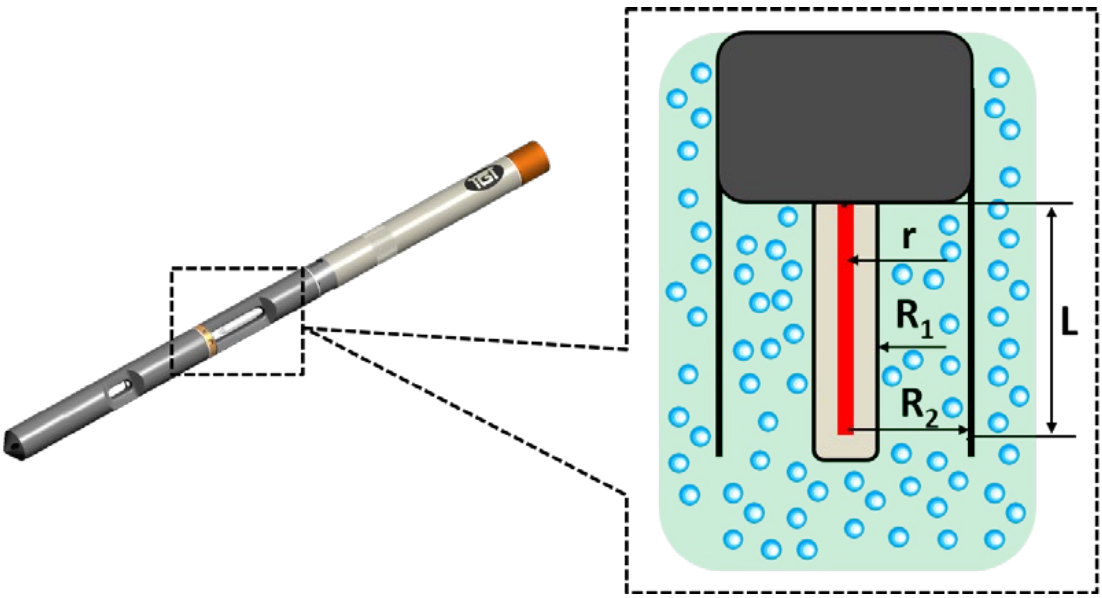

Fig. 1.1.11. Capacitance sensor schematic

The dielectric permittivity, which is linearly proportional to capacitance, varies between 50 and 80 relative units for water, 2 and 4 for oil, and is 1 for gas. As a result, the capacitance sensor responds non-linearly to different phases in the wellbore and is more sensitive to water. Accordingly, its sensitivity changes with water content. Fig. 1.1.12 shows that the sensor has the highest sensitivity at a water holdup of up to 40%. At higher water contents, the tool's response to water content variations is weak. Therefore, the capacitance sensor is used in oil-dominant flows at a water holdup of less than 40%. It should be noted that capacitance readings can be substantially affected by the multiphase flow structure, oil viscosity and presence or absence of centralisers in the tool string.

Measurement units

The output reading of the capacitance sensor is frequency measured in hertz *(Hz).*

Application

The wellbore electrical capacitance sensor is used for the following applications:

- Wellbore water holdup measurement
- Location of water inflow intervals
- Phase analysis of wellbore fluids (when used in combination with the conductivity sensor)
- Location of leaks in casing and downhole equipment

INDIGO XYCALIPER-2

The Indigo XYCaliper-2 module is a pipe caliper tool (Fig. 1.1.13). Adding INDIGO XYCaliper-2 to the PLT tool string substantially improves the quality of inflow and injection profiling and determining total and interval flow rates, as the actual inner wellbore diameters may significantly differ from the initial or specified ones.

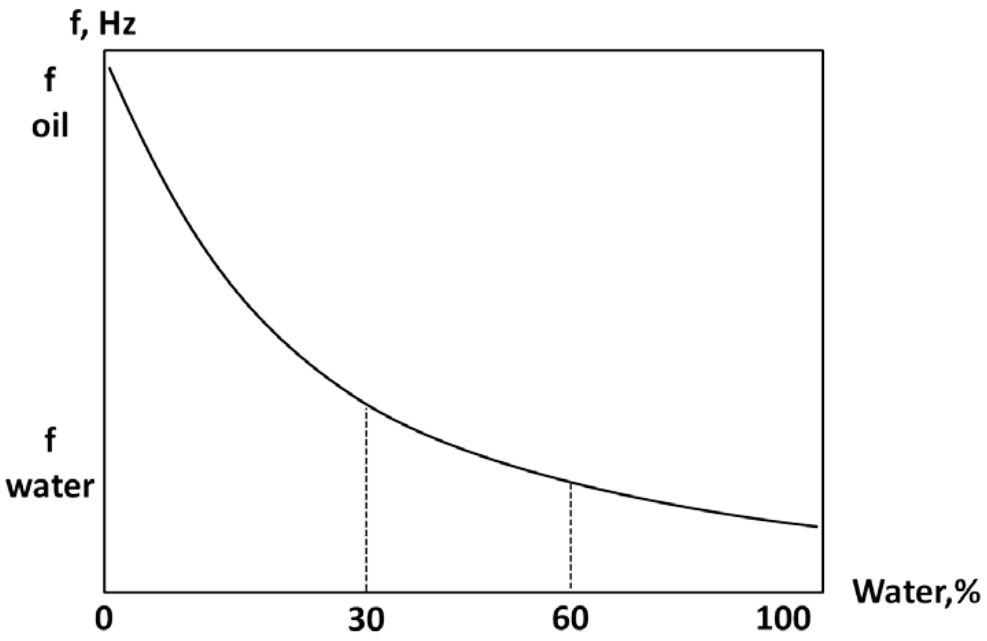

Fig. 1.1.12. Frequency variation vs. water holdup for a two-phase (oil-water) mixture in the effective volume of the tool

Operating principle
The module is an electromechanical system for independent measurements of two diameters and is used to continuously and simultaneously measure and record two inner casing and/or open-hole diameters.

Measurement units
The measurement units of XYCaliper-2 are metres *(m),* centimetres *(cm),* feet *(ft)* and inches *(in).*

Application
The Indigo XYCaliper-2 module is used for the following applications:
- Inner diameter measurement
- Detection of casing ovality and collapse
- Detection of casing breaks and collar disconnections
- Precise wellbore diameter measurement in uncased intervals with caverns or deposits

The application of the technique is limited by deposits on the pipe's inner surface, decentralisation of the downhole tool in deviated and horizontal wells, and inner wellbore diameters that are too large to be measured by the tool.

INDIGO THREE-ARM ROLLER CENTRALISER

The compact Three-Arm Production Roller Centraliser RC-3 (Fig. 1.1.14) accurately centralises production logging tools in vertical and deviated wells. Due to an electrical feed-through, it can be used at any point of the string. The rollers ensure minimum friction on the way down the well.

INDIGO FOUR-ARM ROLLER CENTRALISER

The compact Four-Arm Production Roller Centraliser RC-4 (Fig. 1.1.15) accurately centralises production logging tools in horizontal wells. Due to an electrical feed-through, it can be used at any point of the string. The rollers ensure minimum friction on the way down the well.

Fig. 1.1.13. Indigo XYCaliper-2

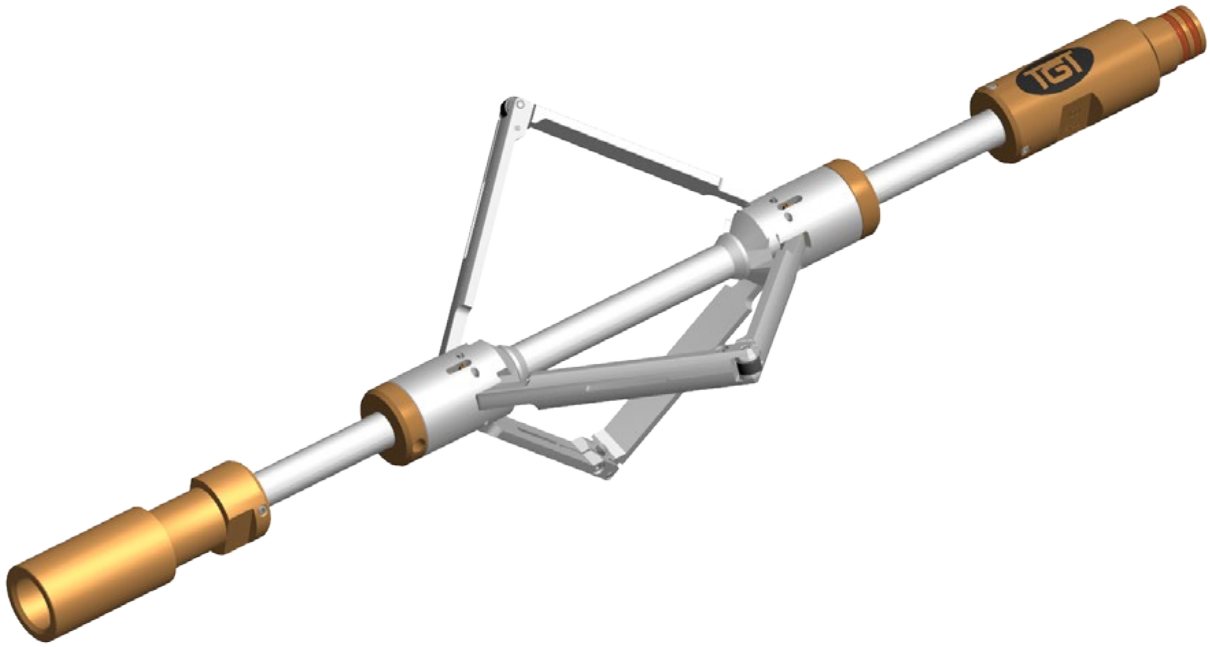

Fig. 1.1.14. Three-Arm Roller Centraliser RC-3

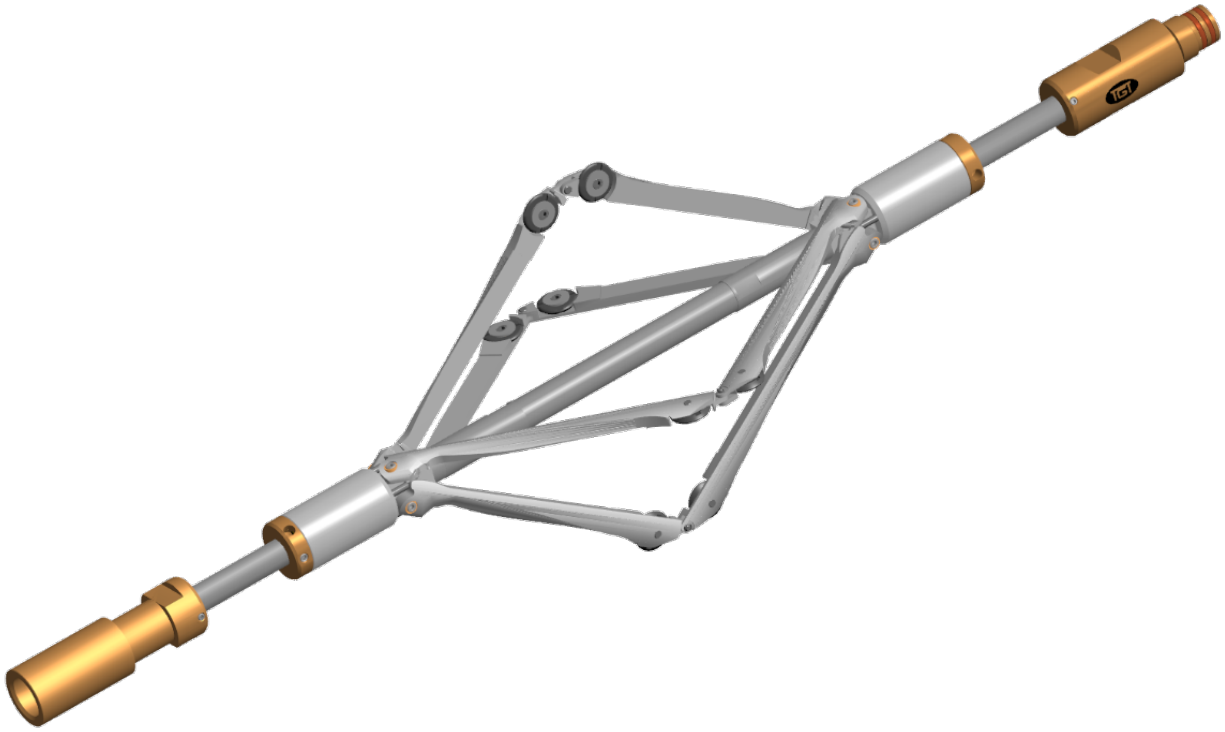

Fig. 1.1.15. Four-Arm Roller Centraliser RC-4

1.1.4. FLOW PHYSICS

Depending on the composition, fluid flow can be classified as single- or multi-phase flow. The first type is in most cases found in gas or water injection wells, new oil or gas production wells or watered production wells, while the second in the majority of mature production wells. In the most general case, multiphase analysis can be performed for four-phase fluid flow containing the following components:

- Formation water
- Injected water
- Oil or gas condensate
- Gas

FLOW PHYSICS BASICS

Determination of flow rates for fluid, gas or a multiphase composition requires knowing their mean linear velocities. The flow rate Q is related to the mean linear flow velocity $\bar{v}$ as follows:

$$Q=\bar{v}A, \qquad (1.1.1)$$

where Q is the well flow rate in m^3/D, and A is the cross-sectional area in m^2.

The spinner and heat exchange sensor data provide the apparent linear flow velocity v_{APP}. The mean flow velocity is linearly proportional to the apparent flow velocity:

$$\bar{v}=k_{VPCF}\cdot v_{APP}, \qquad (1.1.2)$$

where k_{VPCF} is the velocity profile correction factor that depends on the wellbore flow regime and the spinner's geometry and defined as a function of the Reynolds number Re and the ratio of the spinner's blade area radius r to the inner wellbore radius R [2]:

$$k_{VPCF}=f(Re,\frac{r}{R}), \qquad (1.1.3)$$

In fluid mechanics, the Reynolds number Re is a dimensionless number that provides a measure of the ratio of inertial forces to viscous forces for given flow conditions [2]:

$$Re=\frac{inertial\ forces}{viscous\ forces}=\frac{\rho v d}{\mu}, \qquad (1.1.4)$$

where
ρ – mixture density
v – flow velocity
d – inner pipe diameter
μ – dynamic viscosity

The Reynolds number depends on the flow velocity and is an important parameter that describes whether flow is laminar or turbulent [2]:

- Laminar flow occurs at low Reynolds numbers, where viscous forces are dominant, and is characterised by smooth, constant fluid motion. Typically, Re is lower than 2300
- Turbulent flow occurs at high Reynolds numbers and is dominated by inertial forces, which tend to produce chaotic eddies, vortices and other flow instabilities. Typically, Re is higher than 2300

MULTIPHASE FLOW

The flow-rate and multiphase sensors included in the Indigo PLT toolstring measure some average characteristics in the tool's cross-section that depend on the multiphase mixture flow regime.

In multiphase flow, typical flow regimes can be distinguished in terms of the relationship between phase superficial velocities.

Examples of gas-liquid flow regimes in vertical and horizontal tubes are shown in Figs. 1.1.16 and 1.1.17, respectively.

Vertical flows are conventionally classified as follows: bubble flow, slug flow, churn flow, annular flow with droplets and annular flow (Fig. 1.1.16). When the gas-phase superficial velocity is low, the bubble flow regime dominates. As the gas-phase superficial velocity increases, bubbles tend to coalesce and form Taylor bubbles, so that slug flow becomes predominant. With further increases in the gas-phase superficial velocity, slug flow changes into churn flow and then into annular flow, when gas moves in the flow core and fluid along the pipe wall. If the gas velocity is relatively low, some fluid may move in the gas flow core in form of droplets [3].

Horizontal flows are conventionally classified as annular flow, dispersed bubble flow, slug flow, elongated bubble flow, stratified wavy flow and stratified flow (Fig. 1.1.17). Horizontal and inclined pipes are characterised by an asymmetric distribution of phases in the cross-section of a flow channel due to gravity [3].

In multiphase flow, each phase has a different relative velocity. The difference between phase velocities depends on the physical properties of the phases, well inclination and flow regime. The difference between the velocities of dispersed and continuous phases is called slip velocity, v_{21}:

$$v_{21}=\overline{v}_2-\overline{v}_1, \qquad (1.1.5)$$

where v_1 is the continuous phase velocity and v_2 is the dispersed phase velocity. Due to the slippage effect, measured cross-sectional phase holdups do not correspond to their input volume fractions. A cross-sectional phase holdup is defined as the fraction of the wellbore's cross-section occupied by a particular phase [4,5]:

$$\alpha_i=\frac{A_i}{A}. \qquad (1.1.6)$$

There are a number of correlations – empirical, based on experimental data, and mechanistic, based on the fluid mechanics principles – to determine flow regimes and the slippage velocity

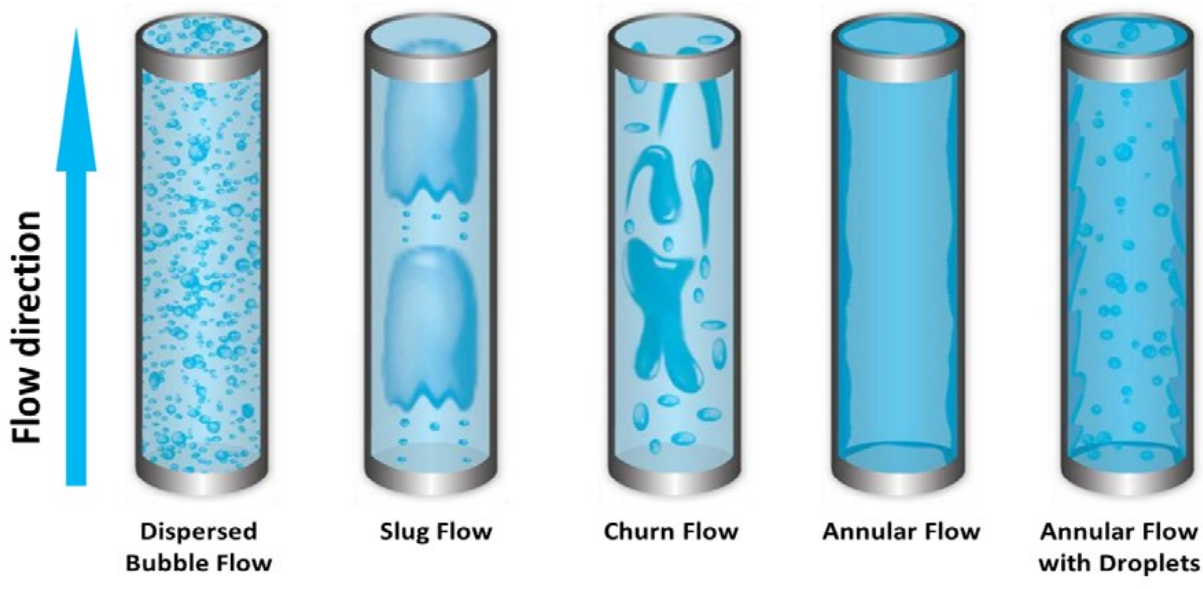

Fig. 1.1.16. Gas-liquid flow patterns in a vertical tube [4,5]

v_{21}. A brief description of the most widely used correlations and the scope of their applications are given in Table 1.1.1-Table 1.1.3.

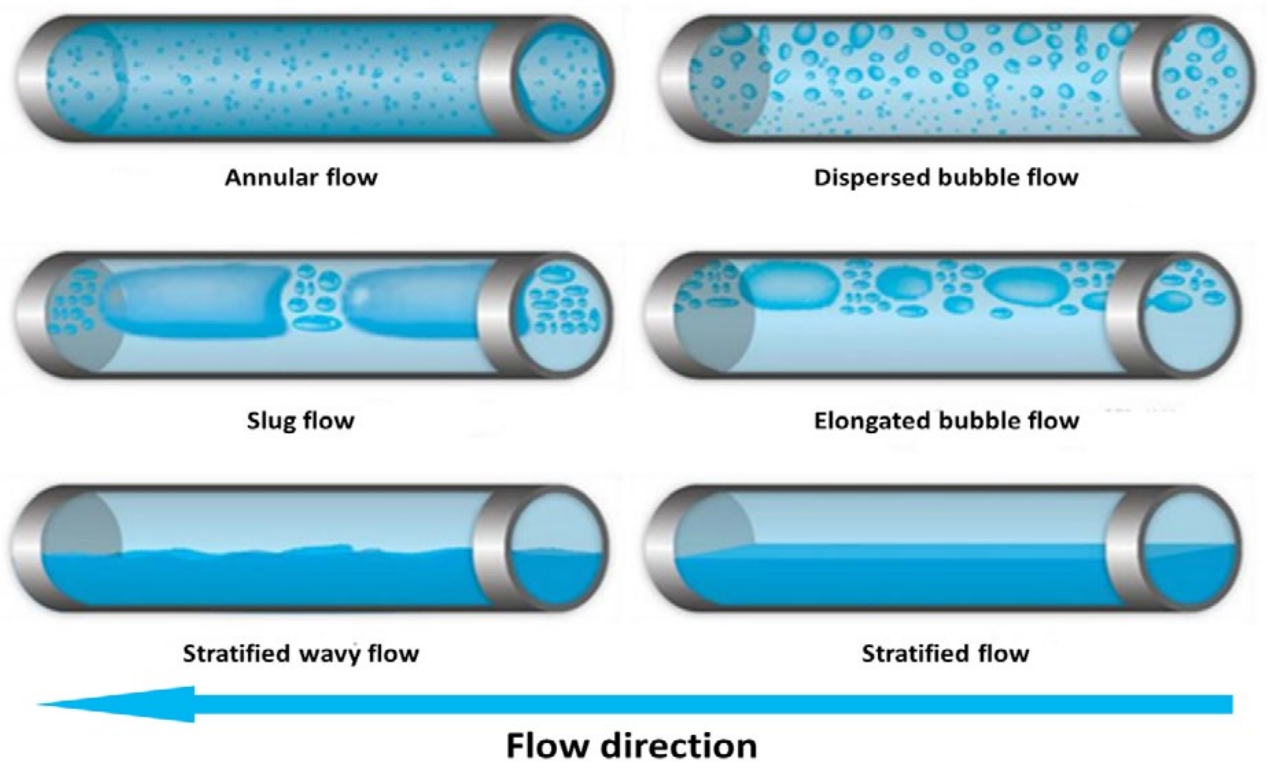

Fig. 1.1.17. Gas-liquid flow patterns in a horizontal tube [4,5]

Table 1.1.1 Gas-liquid (gas-oil or gas-water)

Model	Deviation	Regimes	Comments
Ansari [6]	Vertical and nearly vertical wells	Bubble, slug and dispersed	Mechanistic model
Beggs & Brill [7]	Horizontal and highly deviated wells	Stratified, intermittent (slug) and dispersed (bubble)	Empirical model
Stanford Drift Flux Three- Phase Flow Model (Gas-Liquid) [8,9]	0–88°	Bubble to annular	A semi-mechanistic model based on drift flux theory and using empirically determined parameters with continuity between different flow regimes. Applicable for gas holdups greater than 0.06

Table 1.1.2 Liquid-liquid (oil-water)

Model	Deviation	Regimes	Comments
Choquette	Vertical and nearly vertical wells	Bubble	An empirical model in which slip velocity is determined using a family of curves representing the dependence of slip velocity on the phase density difference and specific heavy phase content α_w (water hold-up). The model does not distinguish between hydrophilic (oil droplets in water) and hydrophobic (water droplets in oil) mixtures
Nicolas & Witterholt [10]	Vertical and deviated wells deviations of up to 70°	Bubble and pseudo-slug	A semi-empirical model based on experimental survey data and drift flow model assumptions. The model does not distinguish between hydrophilic (oil droplets in water) and hydrophobic (water droplets in oil) mixtures
Stanford Drift Flux Three-Phase Flow Model (Liquid-Liquid) [8,9]	0–88°	Bubble and pseudo-slug	A semi-mechanistic model based on drift flux theory and using empirically determined parameters

Table 1.1.3 Three-phase (gas-oil-water)

Model	Deviation	Regimes	Comments
Stanford Drift Flux Three-Phase Flow Model (Three phase) [8,9]	0–88°	Bubble to annular	A semi-mechanistic model based on drift flux theory and using empirically determined parameters with continuity between different flow regimes. Applicable for gas holdups greater than 0.06

1.2 SPECTRAL NOISE LOGGING

1.2.1 FLOW NOISE PHYSICS

This section describes the physical principles of Spectral Noise Logging (SNL) and provides an overview of papers on the generation of acoustic noise by fluid or gas flows in a reservoir formation.

Although the theory of the generation of acoustic noise by turbulent fluid or gas flow through a pipe has been elaborated in detail [11], its generation by fluid flow through a reservoir formation is still poorly understood. Numerous physical models have been proposed in the last several decades to analyse this process. Many of them are based on the generation of acoustic noise by micro-vortices appearing near pore walls due to their roughness and at pore throats due to an abrupt change in diameter when a fluid flows through a heterogeneous porous medium. They also take into account elastic rock properties that have an additional resonance effect on acoustic noise propagating through a reservoir. An experimental verification of this noise generation model is described in a paper [12]. Another paper [13] describes the physical mechanism of acoustic noise generation by gas percolation through a porous medium partially saturated with fluid wetting pore walls. An aerodynamic model of acoustic noise generation in a reservoir based on turbulence occurring when a fluid passes through a pore throat is given in the paper [14].

Another model, focused on fluid percolation through a reservoir as a source of acoustic noise, resulted from many years of well tests and laboratory studies (see the "Laboratory tests" section).

According to these tests, oil or water flows through a porous reservoir intermittently: a fluid initially accumulates in a pore and then, after a certain pressure is reached, slips into an adjacent pore through a pore throat. The paper [15] presents an observation of oil flow through a heterogeneous porous medium. Fig. 1.2.1 shows how oil drops go into nearby pores through pore throats (indicated by red arrows).

The paper [16] shows how frequency maxima in the acoustic noise spectrum of a reservoir correlated with maxima in porosity histograms. This study was carried out using core data from the wells that were then surveyed by Spectral Noise Logging and shows that the spectral pattern of acoustic reservoir noise is governed primarily by the reservoir formation structure.

In the general case, the frequency distribution of the spectral density of acoustic noise generated by fluid flow through a porous reservoir depends on the Rock Quality Index (RQI)

$$RQI=0.0314\sqrt{\frac{k}{\Phi}} \qquad (1.2.1)$$

i.e. on reservoir porosity ϕ and permeability k.

Thus, the frequency of spectral maxima would remain the same for different reservoir flow velocities but noise amplitudes would vary, as defined by the geometry of porous media. In other words, the amplitude, or power, of acoustic noise depends primarily on the fluid flow velocity and, therefore, on the differential pressure related to the flow velocity by the motion equation. In general, noise power increases with the product of flow velocity and differential pressure because this product is equivalent to the work performed by acoustic noise.

Notably, motion equations that relate flow velocity to differential pressure are different for fluids and gases. Therefore, noise power also depends on the fluid type. Laboratory studies show that the noise power is much higher for gas than for water or oil, when determined for equal flow rates and differential pressures in the same reservoir.

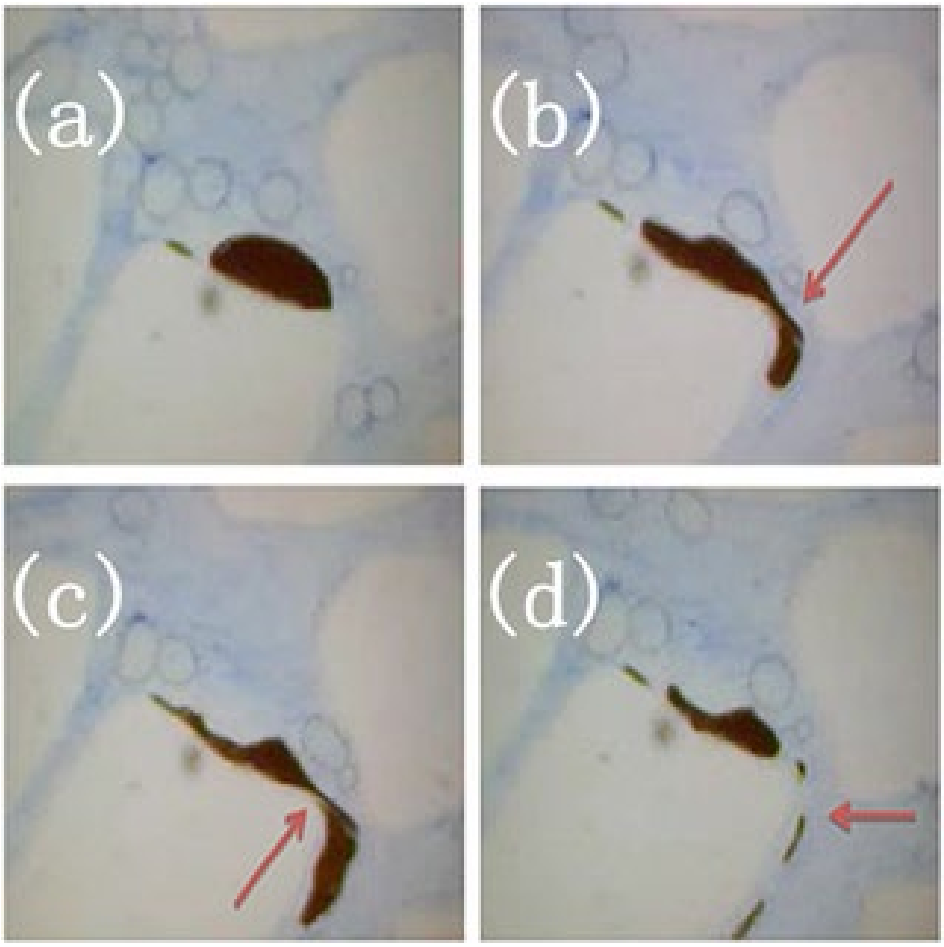

Fig. 1.2.1 Oil drop's movement through a heterogeneous porous medium

1.2.2 SNL APPLICATIONS

Acoustic noise can be generated in a well by fluid or gas flow through a reservoir or leaks in completion components and, for this reason, Spectral Noise Logging (SNL) can be used in a wide range of applications including Reservoir Flow Analysis and Leak Detection in downhole completion components. The reservoir noise amplitude also depends on the differential pressure, and SNL can therefore be used to analyse Formation Pressure in each flowing reservoir unit.

SNL TOOL OVERVIEW

The Spectral Noise Logging tool is designed to record sound in a wide frequency range. The key component of the SNL tool is a highly sensitive hydrophone, which is a piezocrystal sensor placed in an oil-filled chamber (Fig. 1.2.2). Oil reduces the density difference between the wellbore fluid and the sensor's environment, thus minimising the reflection of acoustic waves from the interface and maximising the sensor's sensitivity.

The recorded time-domain data are written to the tool's internal memory using high-frequency analogue-to-digital converters. Further analysis of SNL data is conducted after reading the data from the tool. In the spectral domain, the recorded noise logging data fall in a wide frequency range from 8 *Hz* to 58.5 *kHz*.

A battery pack contained in the tool can power all its electronic components for a continuous period of 48 hours.

The tool operates in memory mode on slickline and can be used in both vertical and horizontal wells. In the latter case, coiled tubing or slickline with a tractor has to be used.

All components of the tool are made of high-strength materials, and its electronic circuits are assembled from high-temperature components. As a result, the SNL Tool can be used to survey wells at temperatures of up to 150°*C* and pressures of up to 60 *MPa*. The tool housing is made of titanium and can be used to log wells containing up to 30% hydrogen sulphide (H2S).

SNL-9 is the ninth generation of Spectral Noise Logging tools and has a wider dynamic range of 90 *dB* to record even very low noise, but still can record data even in the presence of intense low-frequency noise generated by turbulent fluid flow in the wellbore. This has become possible due to the use of state-of-the-art high-quality electronic components and specialised filters. The detailed technical specifications of the SNL-9 tool are given in Table 1.2.1.

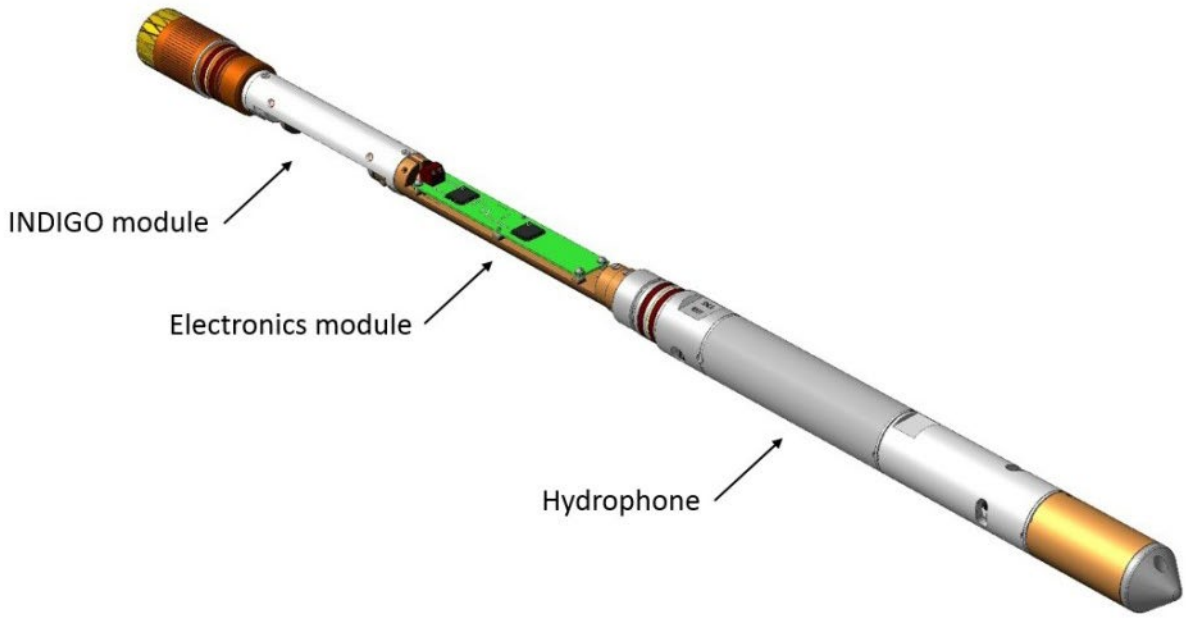

Fig. 1.2.2 SNL tool schematic

Table 1.2.1 SNL-9 tool specifications

Pressure rating	< 60 *MPa* (8,700 *psi*)
Temperature rating	< 150°*C* (302°*F*)
Operating frequency range	LFP 8 *Hz* – 5 *kHz*
	HFP 3 *kHz* – 58.5 *kHz*
Frequency channels	1024 (or more)
Dynamic range	90 *dB*
Battery lifetime	70 *hour*s
Casing material	Titanium/Bronze
H2S resistance	up to 30%
Diameter	42 *mm* (1.65 *in*)
Length	816 *mm* (2.68 *ft*)
Weight	7 *kg* (15.4 *lb*)

SNL-9 has the specialised Indigo interface that can synchronise measurements from several tools, as described in more detail in Section 1.1.3 . This substantially enhances Spectral Noise Logging, and it will, for example, be able to differentiate noise sources from the near and far zones around the well. The use of three synchronised noise logging tools will reduce the total survey time three-fold without loss of spatial resolution.

All SNL equipment is certified for compliance with the GOST Certification System of the Federal Agency for Technical Regulation and Metrology.

RESERVOIR FLOW ANALYSIS

SNL is a powerful technique for reservoir flow analysis due to its ability to locate active reservoir flow units, although it cannot reliably calibrate noise volume in terms of flow rates because noise is a complex function of several flow parameters, most of which, including differential pressure, fluid type and reservoir rock properties, are unknown.

SNL data are visualised in the SNL data panel to locate active flow units that can also be used as an input for TermoSim pTSM to start a matching procedure.

The integration of temperature simulation (Section 1.4) and Spectral Noise Logging provides a unique technique for volumetric assessment of behind-casing flow profiles.

SNL data can also be used to analyse the origin and character of flow: for example, it can distinguish between noises generated by the wellbore, completion components, channelling, reservoir rock matrix, casing leaks, gas bubbling and others.

Another application of SNL is the determination of formation pressure in each reservoir unit of a multi-layer field by conducting a survey in three well regimes without shut-ins.

FORMATION PRESSURE ANALYSIS

Formation pressure is an important indicator of the amount of fluid left in the reservoir, which in turn indicates the amount of energy available to drive fluid out.

There are two conventional techniques to determine the formation pressure in wells that produce from single reservoirs:

1. Long-term pressure transient testing for a bounded reservoir in which wellbore pressure build-up/fall-off is analysed. The wellbore pressure tends to, and at late times becomes, the average formation pressure
2. A static wellbore pressure survey several days after well shut-in when the wellbore pressure is expected to recover to the average formation pressure

If a well penetrates several reservoirs, the measured wellbore pressure is equal to the weighted average formation pressure for all formations that communicate with the wellbore. In this case, the above techniques cannot be used to determine the formation pressure in each reservoir.

Triple Production Logging (TPLT)

This section describes a technique for determining reservoir pressure by measurements at three well flow rates in each flowing zone with spinner logging and Spectral Noise Logging.

PLT profiling is conventionally employed in cased wells to determine the formation pressure in multi-reservoir systems by measuring inflows from each perforated zone at different stable flow rates. However, its results in this application are far from adequate.

In a model case with a well of zero radius, or a line source well, drilled through an infinite homogeneous reservoir, the pressure at any distance from the well and at any time is determined using the exact solution of the diffusion equation:

$$P\,(r,t) = P_e + \frac{QB}{4\pi\sigma}\left[E_i\left(-\frac{r^2}{4\chi t}\right) - 2S\right] \quad \text{....(1.2.2)}$$

$\chi = \frac{k}{\mu\varphi C_t}$, $\sigma = \frac{kh}{\mu}$ – hydraulic conductivity and transmissibility, respectively.

Thus, the determination of the pressure P_e at the external boundary requires setting the rate Q at the sand face, duration Δt and the pressure P_{wf} for each flow rate. The formation pressure is determined by fitting the measured and modelled operating pressures for the above parameters (Fig. 1.2.3). In addition to the formation pressure, two other parameters are determined: the skin factor S, and mobile ratio .

This approach implies the assumption that the formation pressure does not change throughout the test, which can be the case when production or injection is negligible relative to the amount of oil in place and the test period should be as short as days but not months.

As flow rate changes, the flow stabilisation duration Δt at each flow rate must be set so that Infinite Acting Radial Flow (IARF) is achieved before flow-rate measurements are made because equation (1.2.2) cannot be applied to transient flows. Another factor is that the boundary conditions are often not known precisely, and flow-rate measurements should therefore be made within the IARF time window.

A Pressure Transient Analysis is normally performed to determine a time window for IARF. A typical log-log diagnostic plot is shown in Fig. 1.2.4, with IARF displayed as a plateau.

The TPLT method did not become a regular practice to determine formation pressure because numerous cross-flows behind casing prevent fluid from entering the wellbore laterally. As a result, well inflows are difficult to correlate with their reservoir sources, which can lead to substantial errors in the selection of input parameters.

Triple Spectral Noise Logging (TSNL)

An alternative method for determining formation pressure, Triple Spectral Noise Logging (TSNL), is based on the analysis of noise measured at several flow rates.

The core of the method is the correlation between flow rate and noise amplitude, and noise amplitude is to be used in equation (1.2.2) instead of inflows through perforations Q_i. Reservoir noise, generated by fluid flow through the rock matrix, can be distinguished from other noises because of its specific frequency pattern (see Section SNL type library).

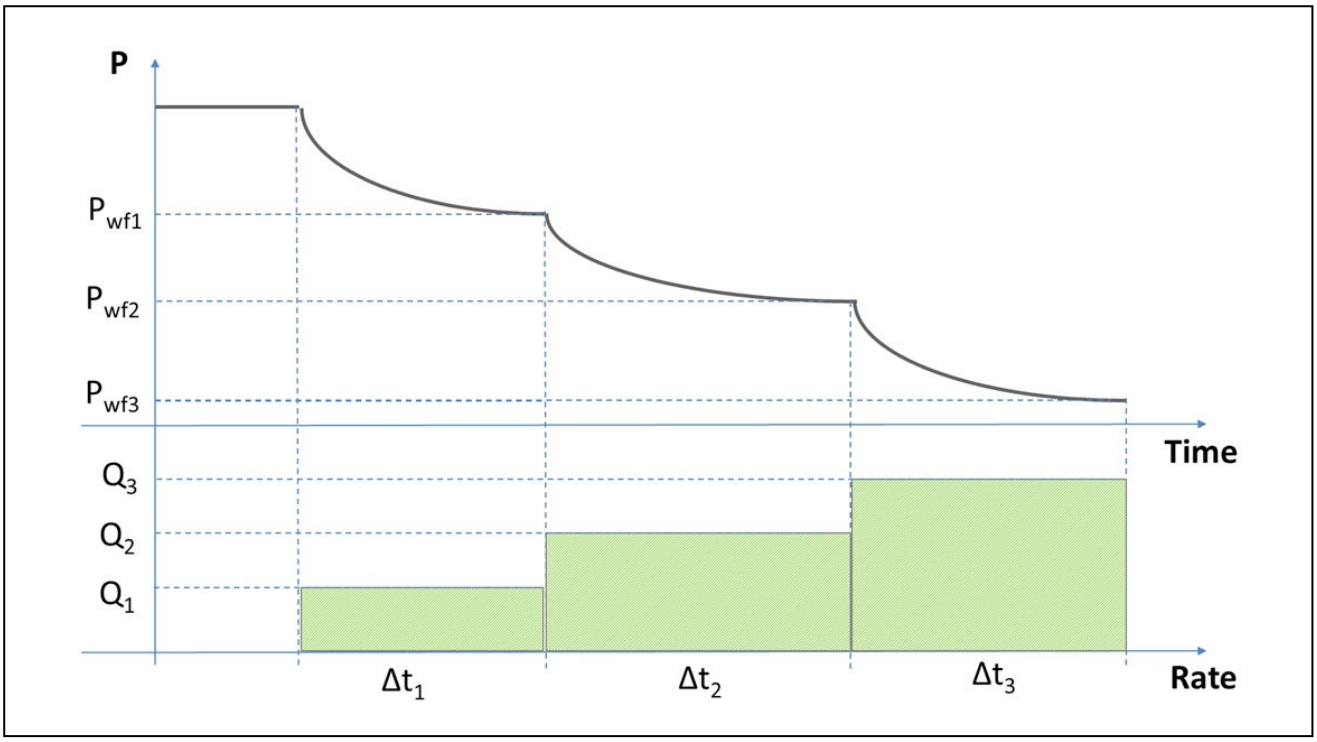

Fig. 1.2.3 A PLT survey procedure for the determination of formation pressure, permeability and skin factor

Numerous field and laboratory tests have shown that the amplitude A of the noise generated by fluid flow from a reservoir is directly proportional to the flow rate *Q*. The noise power *N*, actually used in calculations instead of the amplitude *A*, is proportional to its square.

In broader terms, it has been found experimentally that the reservoir flow noise power is proportional to the product of flow rate and differential pressure generated to create this flow:

$$N \propto Q^{*}\Delta P \qquad (1.2.3)$$

This correlation was obtained and published in 1994 by Prof. McKinley (USA) and verified by TGT under laboratory conditions on the CAS-2 laboratory unit (Fig. 1.2.5).

Fig. 1.2.6 shows the results of the noise power vs. flow rate and differential pressure tests on the CAS-2 unit.

Reservoir noise extraction

For accurate calculation of formation pressure, it is required to determine the reservoir noise power. Taking into account equations (1.2.2) and (1.2.3), the reservoir noise power N is related to the flow rate *Q* as follows:

$$N \propto \frac{Q^2 B}{4\pi\sigma}\left[E_i\left(-\frac{r^2}{4\chi\sigma}\right) - 2S\right]\ldots\ldots\ldots \qquad (1.2.4)$$

In reality, any noise recorded at any depth contains not only reservoir noise but also a wide range of frequencies from other sound sources: wellbore fluid flow, cross-flows behind casing, fluid seepage through perforations and others. The noise, generated by fluid flow through the rock matrix and fractures, depends on the formation pressure in each hydrodynamically isolated zone.

In a spectrogram, reservoir noise is seen as cloud-shaped zones localised in depth and frequency.

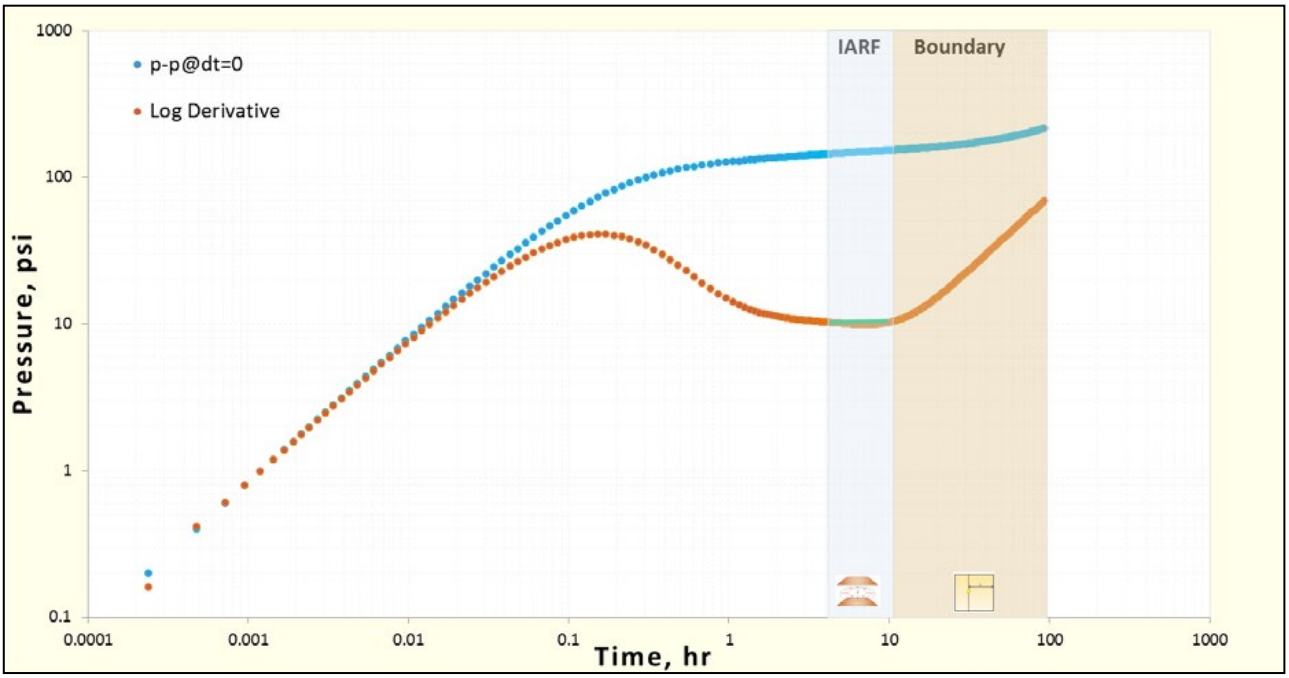

Fig. 1.2.4. A log-log diagnostic plot for a typical PTA survey with the IARF regime over the 3 hours

Fig. 1.2.5. The CAS-2 laboratory unit with the SNL sensor for the analysis of core samples measuring 25x50x70 *mm* at a maximum differential pressure *dP* of 10 bars.

Normally, rock-matrix flow produces noise between 10 *kHz* and 15 *kHz*, but it can also occupy a wider frequency range. Tight formations produce ultrasound above 20 *kHz*. In exceptionally tight formations with less than *1-mD* permeability, only gas can percolate, producing noise in a wide range including frequencies above *30 kHz*. Wellbore flow and cross-flow behind casing are characterised by low-frequency noise below 3 *kHz* that does not correlate with permeability and is spatially limited by cement channel boundaries.

The frequency patterns of noise generated by flows through the rock matrix, fracture and wellbore displayed in an SNL data spectrum and a calculated reservoir noise power profile are shown in Fig. 1.2.7.

Mathematical modelling. PolyGon™ software application

Real cases are normally more complicated than line-source ones and can be analysed by the dedicated PolyGon™ multi-well 3D pressure simulator.

PolyGon™ can simulate flowing wellbore pressure P_{wf} for the known reservoir noise power N determined from SNL data for each flowing unit and for any time. Once a pressure diffusion model – consisting of a wellbore storage model, a well model, a reservoir model and a boundary model – is specified, PolyGon™runs an optimisation loop over the current external boundary pressure P_e, skin factor S and permeability k to fit the measured bottom-hole pressures P_{wf1},P_{wf2} and P_{wf3} and noise powers NP_1, NP_2 and NP_3, recorded at three times t_1,t_2 and t_3 and three surface flow rates Q_1,Q_2 and Q_3 with three durations Δt_1,Δt_2 and Δt_3 (see Fig. 1.2.8).

The net reservoir thickness ^{h} of each flowing unit is determined from SNL panel data.

Out of the three fitting parameters (*Pe*, *S* and *k*), the current formation pressure *Pe* usually reaches its highest accuracy at the end of the fitting process.

As mentioned above, a TSNL procedure, based on flow-rate durations and pressure timings, must be carefully planned to ensure that pressure readings are taken when the wellbore storage has disappeared for the SNL

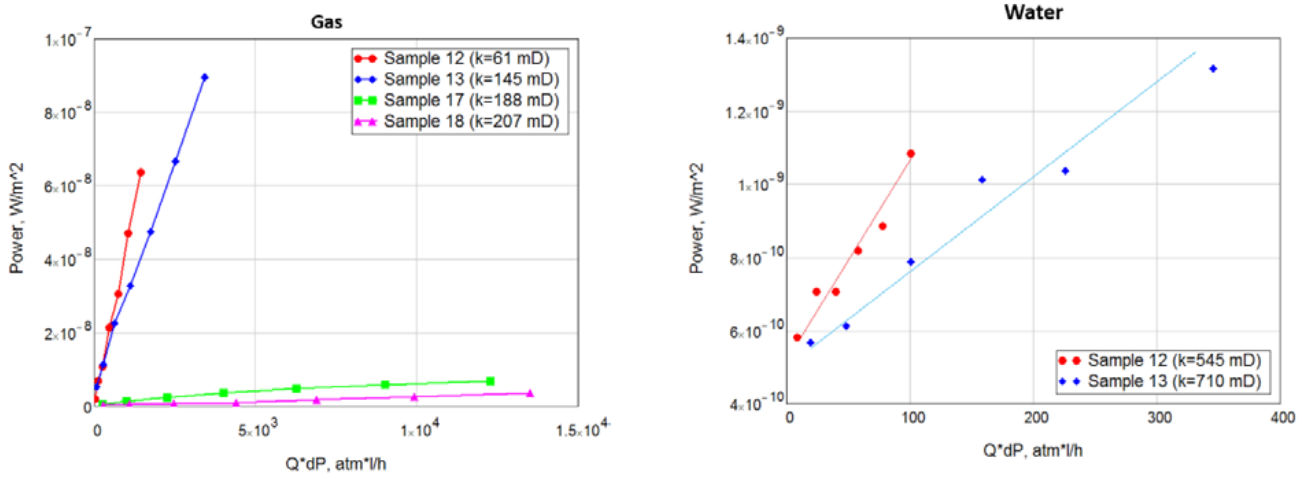

Fig. 1.2.6. Noise power vs. flow rate and differential pressure data obtained on the CAS-2 laboratory unit

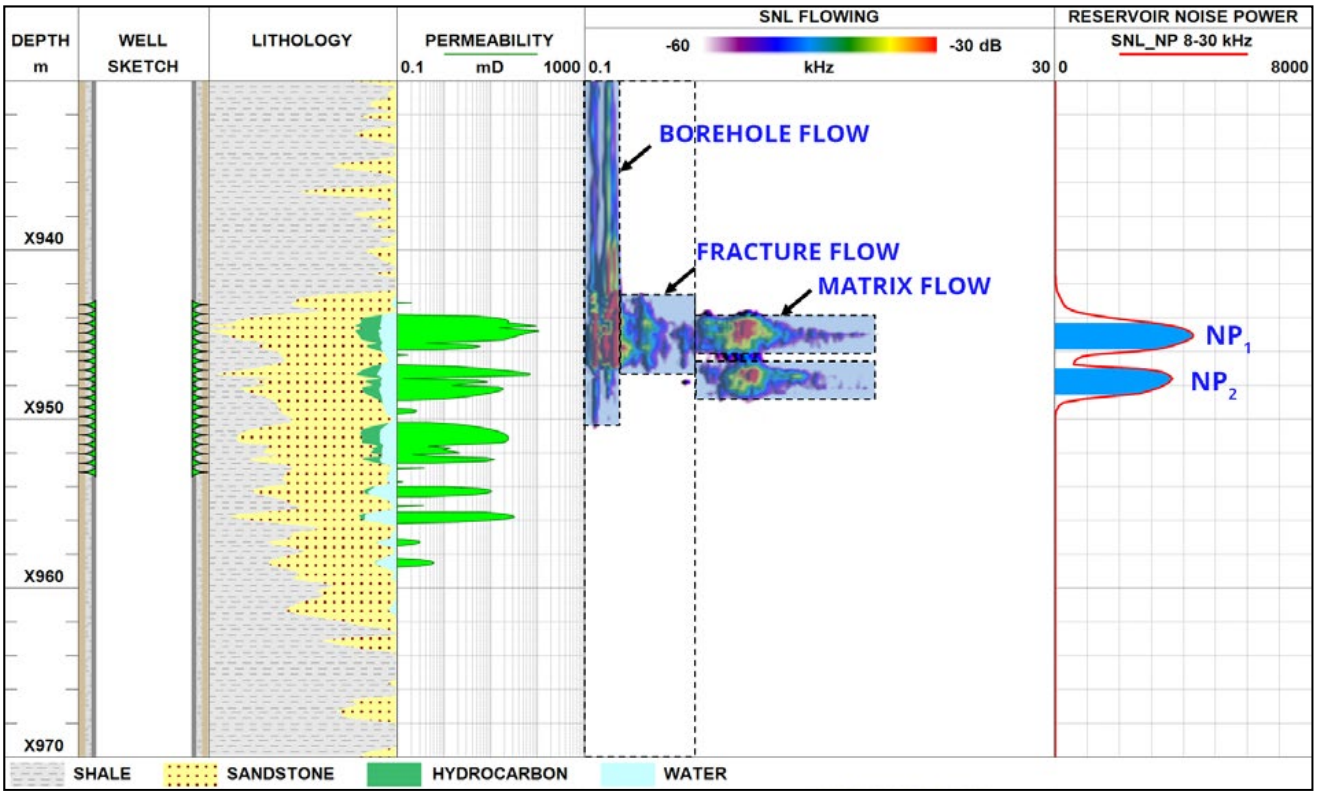

Fig. 1.2.7. Reservoir noise in an SNL data spectrum** SPE 177620-MS [16]

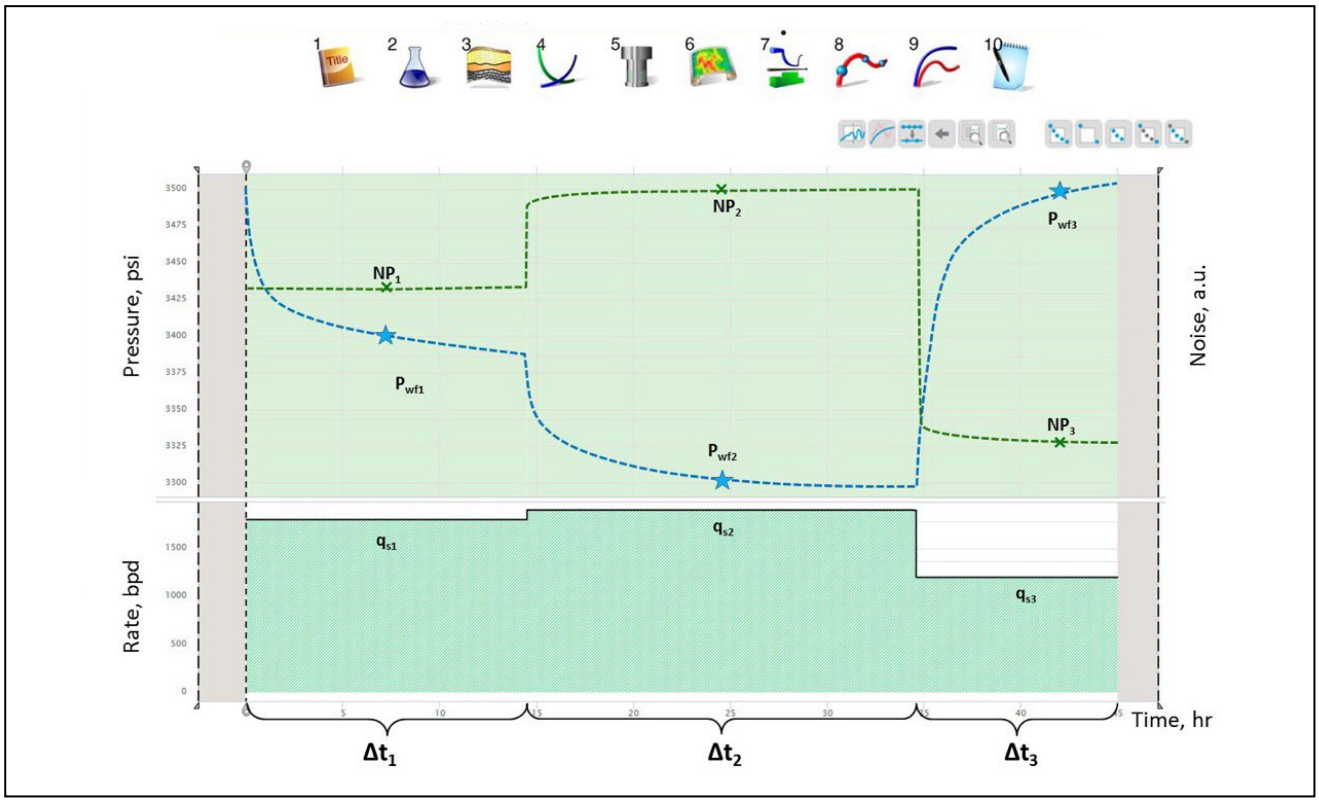

Fig. 1.2.8. Determination of formation pressure and skin factor by PolyGon™

tool to record sand-face flow noise that should bestable by the time of recording. In practice, there is more than one pressure reading at each rate that PolyGon™ should fit, which usually increases the accuracy of formation pressure, skin factor and permeability estimations.

TSNL's advantages and limitations

The TSNL method has some limitations. One of the most significant limitations is that it cannot be applied to no-flow zones with zero noise power, and the formation pressure can be determined only for active flow zones.

However, if an active zone is not perforated or covered by completion components – for instance, when a reservoir of a dual-string well is producing through the shorter string – the pressure in it can still be determined. However, measurements in such a well should be made in both strings to determine all required parameters: in the long string to survey the entire upper formation and in the short one to determine the bottom-hole pressure gradient and extrapolate it to the top of the formation.

Notably, cross-flows behind casing do not affect pressure determination for each hydrodynamically independent unit, which is an advantage over Pressure Transient Analysis (PTA), Static Pressure Survey (SPS) and even Triple Production Logging (TPLT) that is used to determine individual formation pressures in multi-zone wells.

The major advantage of this technology in terms of cost effectiveness is that it does not require a well to be shut in, which minimises deferred oil production and maintains injection at a desired level.

LEAK DETECTION

Turbulent fluid flow through a hole-type defect in a well completion component generates acoustic noise and creates anomalies in the temperature profile. This noise is therefore clearly confined to a certain depth and in most cases stands out as a peak in a total noise log. These two phenomena can be jointly analysed for leak location.

The leaking fluid usually comes from or drains into the nearest reservoir. If the reservoir is located above or below the leak, communication occurs through cement channels indicated in a noise log as a characteristic increase in noise power. Cross-flows behind casing can also be tracked by the difference between shut-in and bleed-off temperatures and by the characteristic shape of the temperature curves.

To make lead detection more reliable, noise and temperature logging data are complemented with well design, lithology and other data, for instance, salinity and capacitance.

LOGGING PROCEDURE

This section describes the specific features of Spectral Noise Logging.

Unlike many conventional logging techniques, noise logging is conducted at stations to eliminate noise generated by tool motion – for instance, through the friction of centralisers against the tool housing or the casing wall.

The accumulation of data recorded at stations increases their statistical reliability. The standard station time ranges from 40 seconds for leak detection to 60 seconds for reservoir flow analysis to ensure that enough data are accumulated with one standard 8-ms long noise record made every second. The SNL-9 tool makes records that are twice as long, i.e. 16 ms per second, which halves the station time. The maximum tool running time

is also reduced two-fold from 72 to 36 hours.

In the zone of interest, stations are located at 1-m intervals. In some cases – for instance, in leak detection when the entire wellbore has to be logged – the distance between stations can be increased to up to 3 m. To minimise the logging time in long horizontal wells, measurements can be made at 3-m intervals.

Noise logging can be carried out during both upward and downward passes. However, apart from the SNL tool, the tool string often includes a temperature sensor that can measure the temperature accurately and continuously during downward passes, and stationary SNL measurements are made afterwards during upward passes. An example of such a survey visualised in the LogDesigner application is shown in Fig. 1.2.3.

SNL DATA PROCESSING

According to the SNL tool's specifications, the digitisation frequency for high-frequency noise data is 120 *kHz* and the total operation time is 72 hours. The SNL tool records large volumes of data – 200 *Mb* to 2 *Gb*, depending on the duration of the survey – which complicates their real-time transmission to the surface by cable. For this reason, all recorded data are written to the tool's internal memory in both memory and cable versions.

The tool has to be withdrawn to the surface after each survey to download the recorded time-domain acoustic data to a computer. The dedicated SNL 2.0 plug-in synchronises the obtained data with the depth sensor's

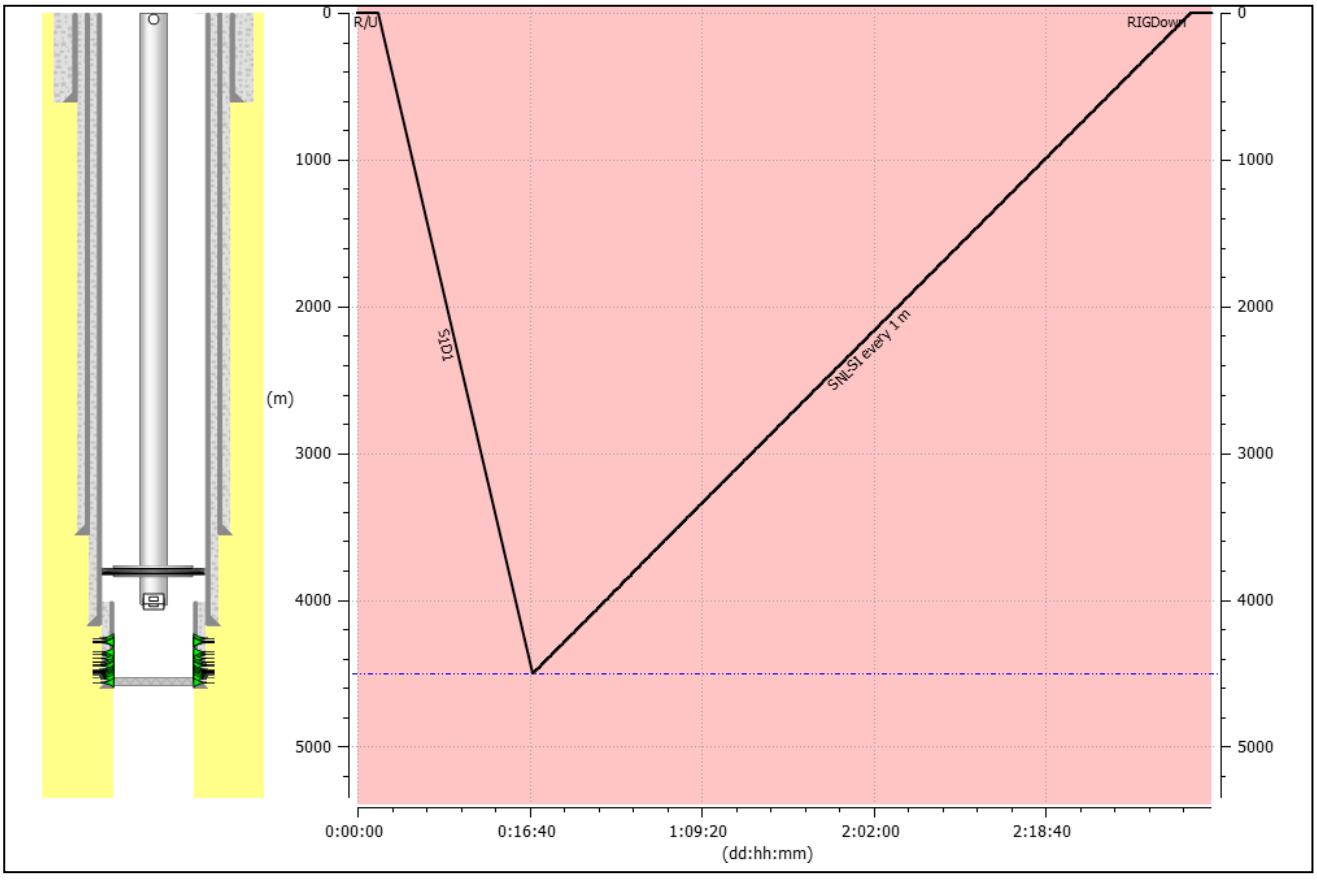

Fig. 1.2.3. SNL survey procedure

readings for further analysis and removal of uninformative signals generated by tool motion. This data analysis is performed on a set of time-domain acoustic noise records made solely at stations.

During data processing, a noise frequency spectrum is calculated for each time-domain acoustic noise record by Fast Fourier Transformation (FFT). The resulting spectra are averaged for each station and saved in LAS 2.0 format. The overall spectrum for the entire depth interval is visualised as a colour spectral data panel (Fig. 1.2.5, SNL FLOWING data panel).

SNL data panel

The calculated and averaged noise spectra for various depths can be visualised as a colour spectral data panel (Fig. 1.2.5). Noise levels are indicated in colours: red for high-volume noise; yellow, green, blue and violet for noise of lower volumes in decreasing order; and white for noise below the tool's threshold. It should be noted here that noises of both high and low amplitudes simultaneously occurring in the SNL data panel impede noise visualisation and interpretation.

DREQ data panel

Contrast equalisation and feature highlighting in the spectral data panel can be implemented by the Dynamic Range Equalisation (DREQ), a post-processing technique to improve the contrast in the SNL data panel. Contrasting spectral data panels are particularly useful for visualising all significant noises in one dynamic range and making weak signals stronger and strong ones weaker when both high- and low-intensity signals are present simultaneously.

An example of the SNL DREQ data panel is shown in Fig. 1.2.5. As seen in the figure, the spectral features have become equalised in intensity, and noise detected at Line A, previously invisible in the SNL FLOWING data panel, has become distinct. Also, temperature modelling indicates a flowing streak at this depth. The production profile determined by temperature modelling is shown in the QZI column.

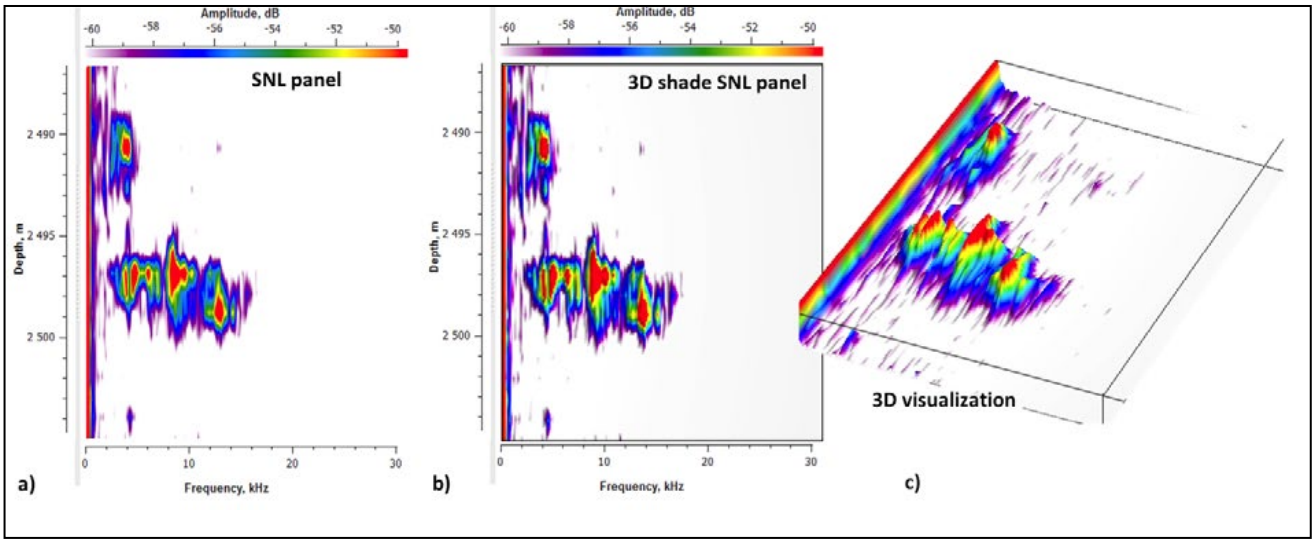

Fig. 1.2.4. (a) A standard SNL data panel; (b) A 3D shade data panel in a top view; (c) A 3D visualisation of an SNL data panel in a side view

SNL relief shading

In many cases, small spectral features may be poorly visible against large ones. This can be improved by relief shading visualisation in the spectral data panels, as shown in Fig. 1.2.4. Fig. 1.2.4 shows a standard SNL data panel (a), a 3D data panel in a top view (b) and the same panel in a side view (c). These representations make some signal features more distinct.

SND data panel

Noises generated by flows through the reservoir or holes are confined to certain depths (Fig. 1.2.5). Low-frequency high-intensity noise, usually generated by wellbore fluid flow or pump equipment, is not informative but often complicates the identification of localised noise sources. The Spectral Noise Drift (SND) technique has been developed to pin-point such depth-confined noise, both in the reservoir and at leaks. SND is a noise data processing technique that takes into account both the time and frequency parameters of recorded noise signals to determine their significance.

A detailed description of the SND algorithm can be found in the paper [17].

The resulting SND data panel contains only noise generated by flow through the reservoir or holes in casing, with no background or depthwise-extended noise (Fig. 1.2.5, SND FLOWING data panel).

Generally, the inner well diameter in the survey interval may vary greatly, for instance, at the tubing end. The character of acoustic noise

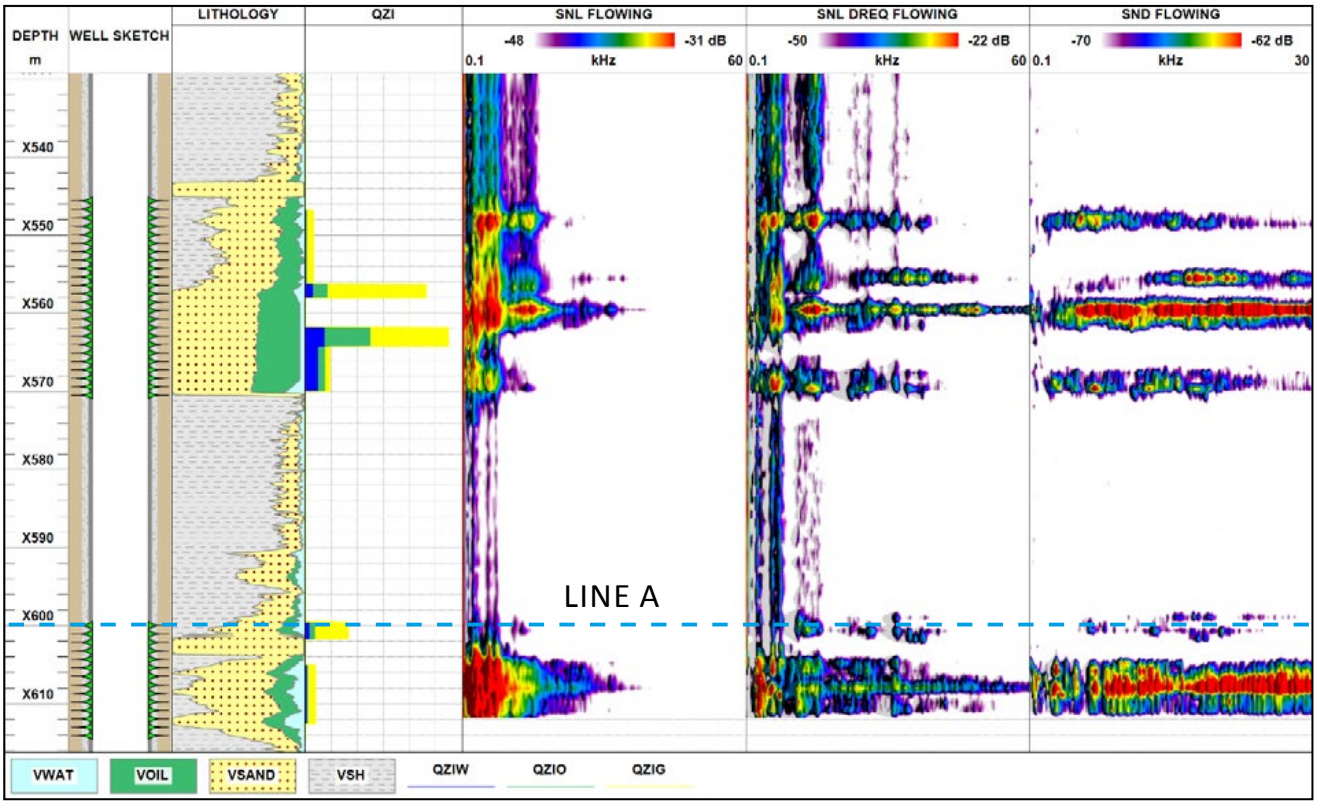

Fig. 1.2.5. SNL, DREQ and SND panels for flowing conditions in a production well

generated by fluid flow through completion components can also vary substantially, both in amplitude and in spectral composition. In such a case, the SNDZ (Spectral Noise Drift by Zone) technique needs to be used to remove the wellbore noise component. This technique divides the survey interval into subintervals and selects optimal processing parameters for each of them.

1.3 PULSED NEUTRON LOGGING

1.3.1 APPLICATION

The Pulsed Neutron Logging (PNL) tool is used to locate watered, bypassed and uninvaded hydrocarbon zones in both open-hole and cased-hole wells.
PNL can be applied in the following cases:

WATER INVASION

Determination of water saturation is based on the different abilities of water and oil to capture thermal neutrons. Chlorine present in salt water enlarges its thermal neutron capture cross-section. For this reason, PNL can distinguish high-salinity formation or injected water from hydrocarbons and can therefore estimate water saturation.

GAS INVASION

Another application of PNL is gas invasion monitoring. The location of gas zones using neutron logging techniques is based on the phenomenon that gas contains less hydrogen than water or oil, and the neutron count in a gas reservoir is therefore lower.

HYDROGEN POROSITY

In addition to saturation quantification, PNL is effectively used to determine hydrogen porosity, even in cased wells. Hydrogen atoms are present in both water- and oil-filled reservoirs, and neutron counts can therefore be used to estimate hydrogen porosity.

1.3.2 PHYSICS

Pulsed neutron logging (PNL) is a well logging technique based on the diffusion of thermal neutrons resulting from collisions of fast neutrons. Thermal neutron diffusion is characterised by such parameters as Thermal Neutron Mean Lifetime T; Neutron Mean Free Path Λ between the point at which a neutron becomes thermal and the point at which it is absorbed by an atom's nucleus; and Thermal Neutron Macroscopic Capture Cross-Section Σ (Sigma). The PNL-determined Sigma parameter is conventionally used to characterise reservoir saturation and reflects the probability for a thermal neutron to be captured while moving a 1-cm distance. Sigma is measured in capture units *(c.u.*).

Table 1.3.1 shows capture cross-sections for some fluids under normal conditions *(t = 20°C, P = 0.1 MPa)*.

Nonstationary thermalisation and capture of neutrons in pulsed neutron logging occurs as follows.

Table 1.3.1

Fluid	$\sum$, *c.u.*
Fresh water	20–22
Saline water, 20 *g/l NaCl*	29
Saline water, 30 *g/l NaCl*	32.5
Saline water, 250 *g/l NaCl*	109.5
Light oil	16–18
Heavy oil	20–22

Initial fast 14 *MeV* neutrons collide with nuclei in the wellbore, completion components and formation rocks. The first collisions are mostly inelastic. Inelastic scattering occurs when a neutron loses part of its kinetic energy to the scattering nucleus. When a nucleus returns from an excited state, inelastic scattering produces gamma rays (ISGR) with characteristic energy lines for all elements.

Inelastic scattering reduces the neutron energy to 1 *MeV* and then neutrons gradually slow down to a thermal energy of 0.025 *eV* (Fig. 1.3.1). Thermalisation of fast neutrons takes approximately 10 μs. A neutron loses most of its energy when it collides with a nucleus of the same mass. On the other hand, when colliding with nuclei of different masses, the neutrons are not slowed down. Neutron energy loss upon collision is 100% for a hydrogen nucleus, 11% for an oxygen nucleus and 6% for a silicon nucleus. Therefore, neutron slowing-down depends primarily on the number of hydrogen atoms in the reservoir.

When slowed down to thermal energy, neutrons are captured by nuclei, and this process is accompanied by the emission of prompt capture gamma rays (CGR). Each rock-forming element has its own CGR energy

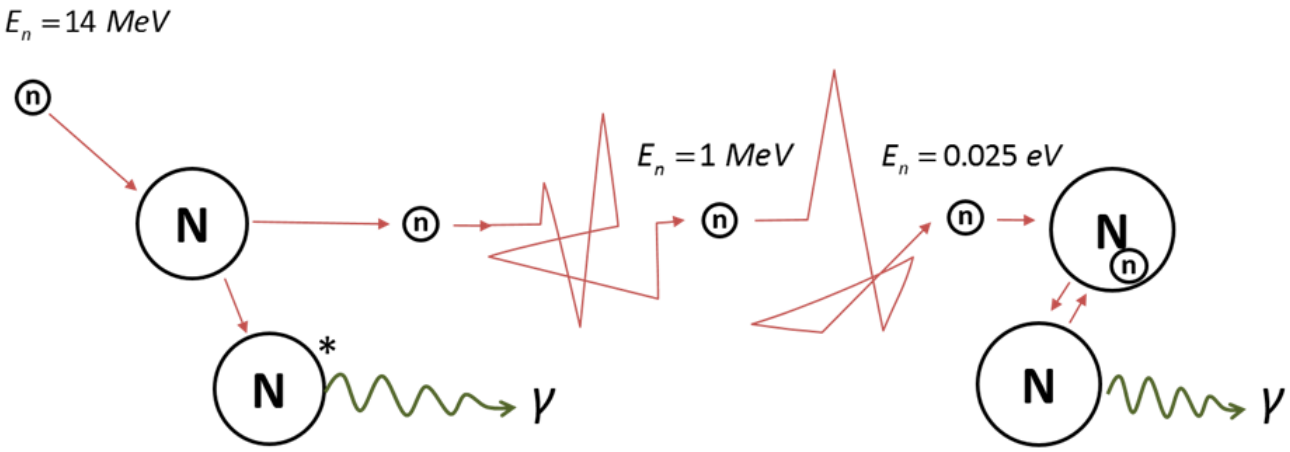

Fig. 1.3.1 A neutron moderation cycle. A 14-MeV neutron "n" collides with a nucleus "N". The nucleus becomes excited ("N") and emits a gamma quantum, and the neutron energy is reduced. This process is called inelastic scattering. Several inelastic scattering events reduce the neutron energy to 1 *MeV*. At that point, the contribution of elastic scattering to overall slowing down of neutrons increases. Neutron gradually slow down to thermal energy (0.025 *eV*).

spectrum, and CGR data can therefore be used for lithological analysis.

Thermal neutrons reaching the near and far detectors are of primary interest in pulsed neutron-neutron (PNN) logging. Capture gamma rays generated by the absorption of slow, or thermal, neutrons after a neutron pulse are analysed in pulsed neutron-gamma (PNG) logging.

1.3.3 PNL TOOL OVERVIEW

Reservoir saturation in cased wells, including those with tubing, is conventionally determined by small-size PNL tools that measure Sigma (Σ).

MINK-1 PNN LOGGING TOOL DESCRIPTION

The MINK-1 PNN logging tool (Fig. 1.3.2) is a new, unconventional memory tool that records all neutron count decays.
The sensors of a conventional PNN logging tool record 200-ms long neutron decays. Within a 10-cm distance, 80 to 100 different neutron decays are recorded and then averaged into one neutron decay as a tool output. Although each neutron decay recorded at each depth is characterised by a minimum scattering of points, the averaged one is a noisy cloud of points. This averaged decay is approximated using the least square method. In the process, some information may be lost at late times where most information about the reservoir resides. Then, this averaged decay is used in processing and interpreting PNN logging data.

Sigma is determined more accurately by processing unaveraged data using the maximum likelihood method because of low scattering of points in each neutron count recorded at each depth, as said above. As a result, processing each decay makes Sigma determination approximately twice more accurate [18].

GENERATOR

The powerful pulsed neutron generator used in MINK-1 produces an output of 108 14-*MeV* neutrons per second. The generator contains a neutron tube that in turn contains a tritium-filled target (3H), a source of deuterium gas (1H) and a deuterium ioniser gun for tritium bombardment. A nuclear fusion reaction between deuterium and tritium occurring in the target results in the generation of high-energy neutrons according to the following formula:

$$ {}^{2}_{1}H+{}^{3}_{1}H\rightarrow{}^{4}_{2}He+{}^{1}_{0}n \qquad (1.3.1) $$

DETECTORS

MINK-1 contains two neutron detectors, near and far, located at different distances from the generator (Fig. 1.3.2 and Table 1.3.2.) and filled with 3*He*. The detectors of this type are very sensitive, and the thermal neutrons entering them are absorbed.

TOOL SPECIFICATION

The basic technical specifications of the tool are shown in Table 1.3.2

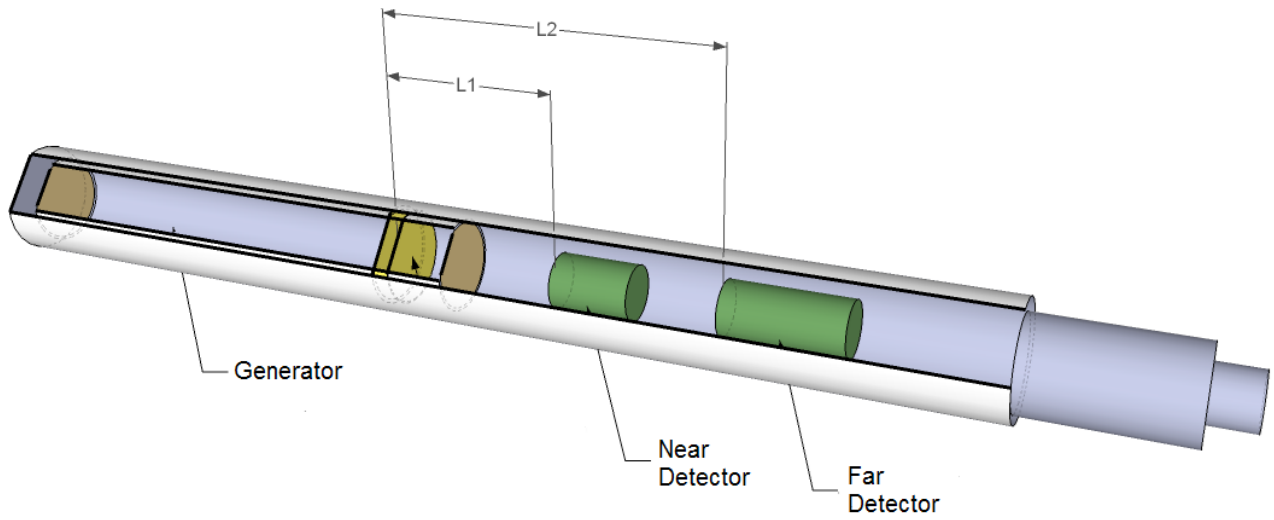

Fig. 1.3.2 A simplified sketch of the downhole pulsed neutron logging tool. The tool includes a generator and two, near and far, thermal neutron detectors

Table 1.3.2

Parameter	Unit	Specification
Tool OD	*mm (in)*	43 (17)
Tool length	*m (ft)*	2.3 (7.5)
Tool weight	*kg (lb)*	18 (40)
Neutron burst rate	*n/s*	$\geq 10^8$
Burst duration	μs	≤ 2.0
Recording time	μs	2000
Distance from generator to near detector	*cm (in)*	32 (12.5)
Distance from generator to far detector	*cm (in)*	59 (23)
Depth of investigation	*см (in)*	60 (24)
Temperature	*°C (°F)*	125 (260)
Pressure	*MPa (psi)*	100 (14,500)

PNN LOGGING TOOL TESTING AND CALIBRATION

Calibration interval

MINK-1 is tested and calibrated in the following cases:

1. Before putting the tool into operation
2. After repair, including replacement of the detectors or pulsed generator of fast neutrons
3. Every three months of operation

Initially, PNN logging tools are calibrated by the manufacturer. The calibration results are always provided in the technical documentation. Calibrations are performed periodically to check the operational stability of the tool and its sensitivity to the measured parameter, i.e. Sigma, as well as the difference with the first calibration results.

Calibration is also performed in a fresh water tank before each logging job.

Requirements for a calibration tank with fresh water

A calibration tank for the MINK-1 tool must comply with the following requirements:

1. The content of salt and other substances in water must not exceed 0.5 *g/l.*
2. The size of the tank must prevent the environment from affecting the tank's contents, and must be at least 1.5 *m* in diameter and 2 *m* in height.

Calibration measurements are made in sampling mode with a time step of 3 to 10 sec. Such a long time sequence is required for accurate statistical analysis and justifiable PNN log data errors.

The tool is considered calibrated if the Sigma error does not exceed 10%.

1.3.4 PNN LOGGING DATA INTERPRETATION

Pulsed neutron-neutron logging data are interpreted to determine neutron porosity (TPHI) and formation water saturation *(S_w).*

NEUTRON COUNT DECAY ANALYSIS

Fig. 1.3.3 shows typical neutron count rate decays in linear and logarithmic scales recorded after a pulse was emitted by a generator. The recording was about 2-ms long, and neutron count rates were averaged in 60 time windows, each 32-μs long.

All neutrons recorded by the detector are initially emitted by the generator, pass the through wellbore fluid and are reflected by its atoms. Then, unabsorbed neutrons are scattered and absorbed by the fluid contained in rock pores and by a minor amount of neutrons in the rock matrix, after which the remaining unabsorbed neutrons reach the detector.

Thus, neutron count rate decay at early times mainly reflects neutrons' interaction with wellbore fluid, and at late times their interaction with formation fluid and rocks. In the general case, neutron count rate decay is described by a double-exponential function in which one

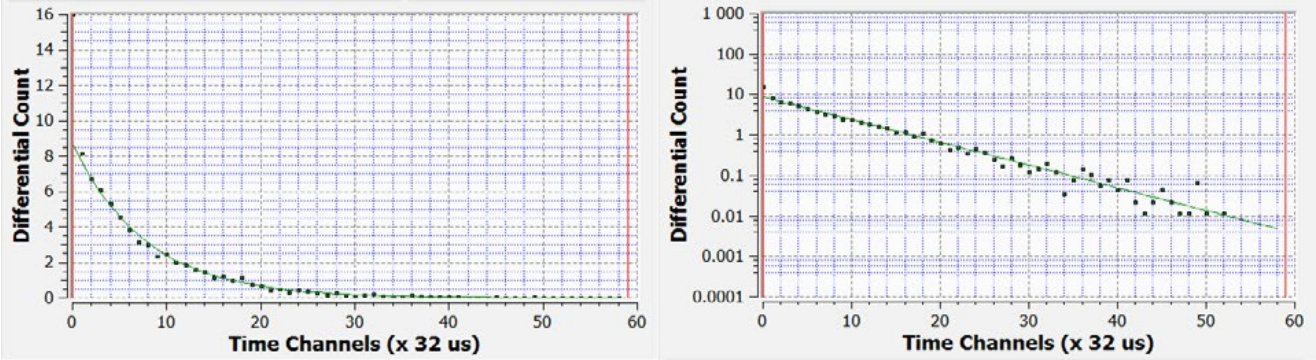

Fig. 1.3.3. Neutron count rate decays in linear (left) and logarithmic (right) scales

component characterises wellbore fluid and the other formation fluid and rocks, each of them depending on both scattering and absorption properties:

$$N(t)=A_{borh}exp\{-\Sigma_{borh}t_i\}+A_{form}exp\{-\Sigma_{form}t_i\} \quad (1.3.2)$$

NEUTRON POROSITY

The exponential coefficients Aborh and Aform depend on scattering properties. Hydrogen atoms have the lowest mass and, therefore, the highest scattering capacity. For this reason, the neutron porosity determined by pulsed neutron logging is a measure of hydrogen concentration and is in some cases called the hydrogen index.

Because most hydrogen resides in the fluid, i.e. in rock pores, the scattering properties depend on rock porosity.

Noteworthily, the difference between the hydrogen contents of water and oil is small, and logging data therefore reflect the total neutron porosity of the formation. However, the displacement of oil or water by gas significantly reduces the apparent neutron porosity, which should be taken into account.

As neutrons move and undergo multiple elastic collisions with neutrons in the environment, they slow down, and this process is called neutron diffusion.

The A_{borh} and A_{form} coefficients are proportional to the integral neutron count at each detector (TOTAL COUNT NEAR/FAR), i.e. the total number of thermal neutrons detected at a certain depth during the entire survey period, normally 2 *ms.* Logging data processing includes the calculation of the total selected counts of neutrons recorded by the near and far detectors (TSC N/F) in a selected time window.

The neutron porosity is determined by the ratio between the numbers of neutrons at the near and far detectors in a selected window (12–24) in which information is not affected by wellbore fluid and characterises the reservoir formation – TRAT (Total Count Ratio).
The neutron porosity is normalised by the known value of hydrogen concentration in fresh

water under normal conditions, TRATwater, equalling 8.4 *c.u.* (capture units).

CROSS-PLOTS FOR POROSITY CORRECTION FOR DIFFUSION

The hydrogen index changes with formation lithology and well parameters, including well diameter and fluid salinity, and therefore requires minor correction, normally 1 to 2 percent. Corrections for wellbore conditions, i.e. cross-plots for diffusion corrections, are determined in the laboratory [19].

THE SIGMA PARAMETER

The exponential factors *Σ*borh and *Σ*form in Formula (1.3.2) characterise absorption properties. The atom of chlorine, a constituent of many salts dissolved in water, is an element with an extremely large thermal neutron capture cross-section. For instance, that of halite *(NaCl)* is 770 *c.u.* [20].

Fluid salinity in c.u. can be expressed as the NaCl salt content of fluid using the following equation:

$$\Sigma_{wat}[c.u.]=22[c.u.]+0.35*(NaCl)[ppk] \quad (1.3.3),$$

where 22 *c.u.* is the Sigma of fresh water. Therefore, salinity defines the Sigma parameter. The faster the neutron count rate decay, the higher the fluid salinity and, accordingly, the water content.

In laboratory tests, the response of wellbore fluid in neutron rate decay records is displayed in Time Channels 1 to 3, while the response of the formation may vary depending on the reservoir formation's mineralogy and on the well fluid and diameter, and normally starts from Time Channel 8 or later.

The curves used for salinity calculation are

1. SBND (Sigma Borehole Near Detector) – Sigma of the borehole fluid at the near detector
2. SBFD (Sigma Borehole Far Detector) – Sigma of the borehole fluid at the far detector
3. SFND (Sigma Formation Near Detector) – Sigma of the reservoir formation at the near detector
4. SFFD (Sigma Formation Far Detector) – Sigma of the reservoir formation at the far detector

DETERMINATION OF CURRENT WATER SATURATION. VOLUMETRIC MODEL

The salinity and water saturation are determined using a petrophysical reservoir-well model in which the rock consists of the rock matrix and the pores filled with fluid, gas or their mixture, and the wellbore is filled with saline fluid.

In this case, the general formula to determine water saturation using the rock, formation fluid and wellbore fluid Sigma values and the formation porosity is as follows:

$$S_{w(PNL)} = \frac{(\Sigma_{log} - \Sigma_m) - \phi * (\Sigma_o - \Sigma_m) - V_{sh} * (\Sigma_{sh} - \Sigma_m)}{\varphi * (\Sigma_{wf} - \Sigma_o)} \quad (1.3.4),$$

where ϕ – total fluid-filled pore volume
Σ_m, Σ_{sh}, – Sigma values of the rock matrix and shale
Σ_o, Σ_{wf} – Sigma values of pore-filling fluids
V_o, V_{wf}, V_i, – Volumes of pores filled with oil, formation water and injection water

Changes in the formation's saturation relative to its initial water saturation are assessed by determining the Invasion parameter as the invading fluid content in pores, which

requires setting an invading fluid salinity. However, this information may not always be available, particularly if the invading fluid is different from the formation one, and this makes current saturation determination less certain. The salinity of an invading fluid can be determined by complementing pulsed neutron-neutron logging with, for instance, temperature measurements under shut-in conditions. A temperature increase in the formation interval could mean formation water encroachment from below, and a temperature decrease could be caused by lateral breakthrough of injected water.

QUALITY CONTROL

After processing all log data files, the following primary data are checked for quality:

1. Repeatability in the recording overlap interval.
1. Standard deviations STDN (relative data approximation error for the near detector) and STDF (relative data approximation error for the far detector). If the error exceeds 10%, the measurement is considered unreliable.

1.4 TEMPERATURE MODELLING

1.4.1 INTRODUCTION

Temperature logging conducted throughout the wellbore is one of the most informative well-surveying techniques widely used for qualitative analysis of processes in wells and reservoirs. For a long time, it was impossible to analyse temperature logs quantitatively because of the thermohydrodynamic complexity of the well-reservoir system. As computer technology developed, temperature measurements came into use to quantify inflow and injection and unwanted injection and production as well as to analyse well integrity issues including channelling.

The TERMOSIM™ software application is designed for temperature and hydrodynamic simulations. It quantitatively analyses temperature logs and can be used in the following applications:

For injectors

- Injection profiling across flowing reservoir units
- Quantification of injection loss outside survey intervals
- Identification and quantification of behind-casing channelling and wellbore cross-flows including those into unperforated zones
- Quantitative characterisation of historical injection zones

For producers

- Production profiling across flowing reservoir units
- Identification and quantification of behind-casing channelling and wellbore cross-flows including those from unperforated zones
- Location of zones of water breakthrough from nearby injectors

The TERMOSIM™ software numerically solves the problems of flow hydrodynamics and heat exchange between the wellbore fluid, completion components, surrounding

anisotropic rocks and reservoirs. TERMOSIM™ can flexibly tune a multi-parameter thermohydrodynamic model (described below) to match simulated and measured temperatures. It operates in two modes: injection mode for injection temperature modelling and production mode for production temperature modelling.

The simulation is based on the assumption that fluid and gas flow in the reservoir radially from and to the well. It also takes into consideration thermodynamic effects caused by fluid and gas flows through a reservoir, behind casing and along the wellbore as well as wellbore and behind-casing cross-flows.

1.4.2 TEMPERATURE AND HYDRODYNAMIC WELL MODEL

A well penetrates horizontal strata of different mineral compositions, porosities, saturations, permeabilities and, therefore, different thermophysical properties. A formation and rocks above and below it initially have a certain temperature distribution that depends on the geometry and thermal conductivity of the formation and rocks λ and on the Earth's heat flux q. Heat exchange between the reservoir rocks and the produced or injected fluids causes temperature variations in the formation and rocks.

The hydrodynamic flow pattern significantly affects the temperature distribution in the wellbore, reservoir and non-reservoir rocks. A TERMOSIM™ hydrodynamic model was developed to take cross-flows into account.

Fluid production from and injection into a reservoir cause temperature perturbations in the near-wellbore zone. In injectors, it occurs because the injected fluid temperature differs from the formation temperature. In producers, the near-wellbore temperature deviates from the geothermal profile because of thermodynamic processes triggered by differential pressure. These temperature variations decrease with distance from the wellbore, and the temperature ultimately tends towards the geothermal profile. As fluid flows through a reservoir, it exchanges heat with the reservoir itself and overlying and underlying rocks. In the wellbore, fluid exchanges heat with surrounding rocks, and this process depends on isolation conditions.

To take into consideration all these factors and determine injection and production profiles using temperature measurements, it is necessary to create a thermohydrodynamic model that takes into account processes in the well and reservoir based on the following parameters, conditions and submodels associated with heat-exchange processes in the well and reservoir:

- Rock properties and geothermal profile
- Well isolation conditions
- Heat exchange between air and rocks at the Earth's surface
- Well and reservoir temperature submodels for injectors and producers
- Hydrodynamic submodel of the well-reservoir system

ROCK PROPERTIES AND GEOTHERMAL PROFILE

The Earth's heat flux is measured in energy per square metre *[W/m²]*. This flux has already stabilised and, therefore, the amount of energy is the same at any depth. The Earth's heat flux ranges from 0.04 *W/m²* to 0.15 *W/m²* averaging at 0.06 *W/m²*. Different regions may have different heat fluxes. For example, the Earth's heat flux through a tectonic plate is low because of low seismic activity but is typically high in seismically active regions.

Importantly, the thermal conductivity of rocks increases with temperature and depends on the type of rock fluid.

The initial temperature profile of a small oil or gas field depends only on depth and does not vary laterally, although the geothermal temperature of large fields does vary laterally.

The rock temperature initially formed by the Earth's heat flux can be disturbed by both recent and secular lateral flows. For this reason, the geothermal profile T_g (Fig. 1.4.1) is calculated by the following formula:

$$T_g(z) = T_{ref} - q_g \int_{z_{ref}}^{z} \left(1 + \int_0^z S_g(\zeta) d\zeta\right) \frac{dz}{\lambda^{(z)}(z)} \quad (1.4.1)$$

where

Z – upward vertical coordinate, or the distance from the reservoir bottom

q_g – Earth's local heat flux

Z_{ref} – geothermal temperature reference depth

T_{ref} – geothermal temperature at reference depth (z_{ref})

$\lambda^{(z)}(z)$ – thermal conductivity of surrounding rocks

S_g – heat source of secular lateral flow

Secular lateral flows (Fig. 1.4.2, left) are fluid flows through reservoirs occurring for as long

Average thermal conductivities for different rock types at 20°C are given in the table below.

Rock	**Average thermal conductivity,** *W/(M*K)*	**Thermal conductivity range,** *W/(M*K)*
Claystone	1.3	0.25–3.1
Shale	1.6	0.12–3.1
Dolomite	3.2	1.6–6.5
Limestone	2.3	0.64–4.4
Salt	3.6	1.7–5.5
Chalk	1.6	0.82–2.2
Sandstone	1.8	0.24–4.4
Quartz	1.38	-

as hundreds or thousands of years. Secular lateral flows in rocks substantially change the geothermal profile above and below a flowing reservoir.

Recent lateral flows (Fig. 1.4.2, right) are fluid flows caused by industrial activities taking place for up to several decades. Recent lateral flows in rocks create additional temperature perturbations (Θ_r) in the initial temperature gradient T_g and the regional geothermal profile is described as follows:

$$T_r = \Theta_r + T_g \qquad (1.4.2)$$

The vertical extent and amplitudes of the temperature anomalies Θ_r developing over a certain period of time *(t)* are defined by the thickness of lateral flow, heat source power and thermophysical properties of rocks.

Heat insulation properties of completion components

Heat exchange between wellbore fluid, well components and surrounding rocks must be taken into account for temperature calculations. This heat exchange depends on flow rate, well completion, wellbore fluid temperature T_f, rock temperature T_w and flow type (laminar or turbulent).

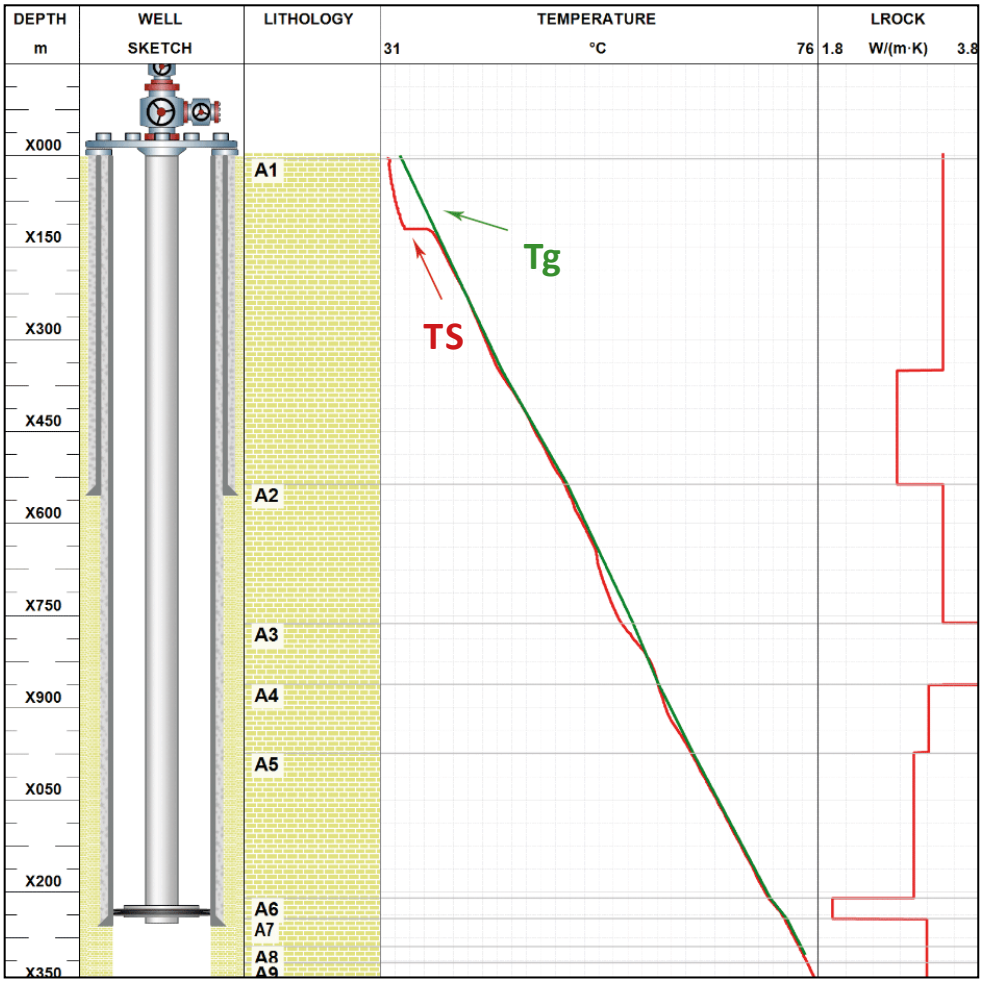

Fig. 1.4.1. Geothermal profile. T_S – temperature measured in a remote observation well; T_g – simulated geothermal profile

The components of a complex well completion model include tubing, casing, annulus and cement sheath (Fig. 1.4.3). Heat flow passes through all well completion components from tubing fluid through the casing annulus and cement sheath to rocks. A specific temperature is set for each layer: T_f – wellbore fluid temperature; T_a – annulus fluid temperature; T_c – cement temperature; T_w – rock temperature. Also, the following radii are precisely set: r_f – inner tubing radius; r_c – inner casing radius; r_w – cement sheath radius. The following fluid properties must be taken into account for accurate calculations: λ_a – thermal conductivity of annulus fluid; λ_c – thermal conductivity of the cement sheath.

A procedure has been developed to calculate heat-exchange coefficients for all well completion components by taking into account the properties of their materials and well fluids. The calculated heat-exchange coefficients are used to calculate the temperature for each well completion layer.

Temperature modelling can identify anomaly sources. For instance, a packer usually produces a temperature anomaly under shut-in conditions, and modelling can tell if it was caused by reservoir fluid flow or by the difference in material properties between the packer and behind-casing fluids, which often leads to temperature anomalies.

HEAT EXCHANGE BETWEEN THE AIR AND THE EARTH'S SURFACE

The near-surface rock layers are exposed to seasonal and daily temperature variations caused by solar activity and air temperature changes.

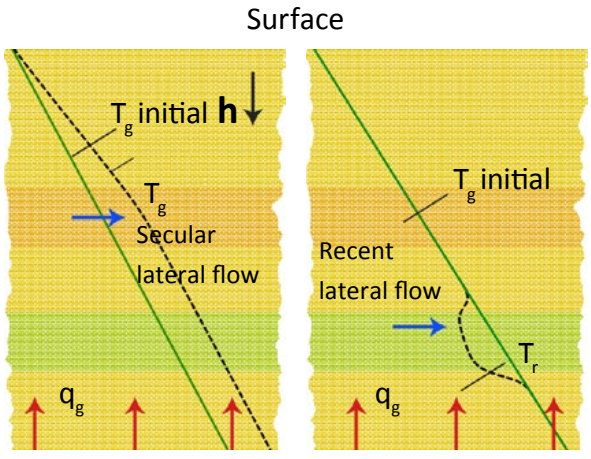

Fig. 1.4.2. Geothermal profile affected by lateral (right) and secular (left) flows. T_g initial – geothermal profile; T_g – geothermal profile affected by secular lateral flows; T_r – geothermal profile affected by recent lateral flow; q_g – Earth's heatv flux

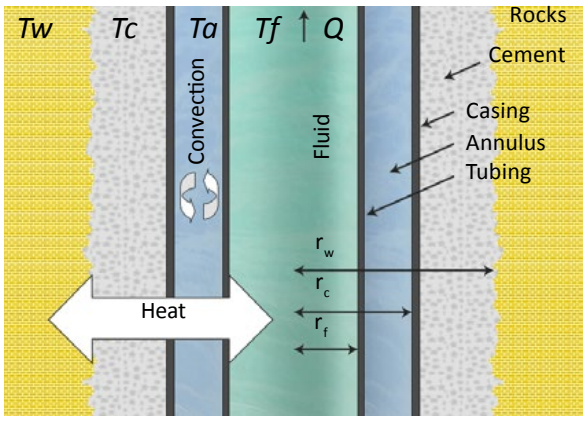

Fig. 1.4.3. A well schematic showing completion components and temperatures in each cylindrical layer: T_f – wellbore fluid temperature; T_a – annulus fluid temperature; T_c – cement temperature; T_w – rock temperature; Q – fluid flow rate; r_f – inner tubing radius; r_c – inner casing radius; r_w – cement sheath radius

Therefore, surface temperature variations are periodic and can be assumed to have the following form:

$$T(t)=A\cos\omega t, \quad (1.4.3)$$

In this ideal case, the amplitude of temperature variations depends on depth z as follows:

$$A(z) = Ae^{-\sqrt{\frac{\omega}{2a^2}}z} \quad (1.4.4)$$

The greater the period of temperature variations, the deeper their penetration. Another factor that affects the amplitude of temperature variations at depth is their amplitude at the surface. Daily air temperature variations occur in the soil layer to a depth of 1–1.5 *m*. Temperature variations do not propagate instantaneously and occur at depth some time after they do at the surface. Seasonal temperature variations penetrate to a depth of 20–40 *m* where heat is transferred mainly due to thermal conductivity. For this reason, the neutral layer, i.e. the constant temperature zone, occurs in a depth interval of 20–40 *m*. The neutral-layer temperature is always 3.7°*C* higher than the average annual air temperature.

The following boundary condition is set to model the temperature at the Earth's surface: the temperature at the interface between the air and the Earth's surface is $T_{surf}(t)$, which changes in time and results from seasonal and daily temperature variations. The intensity of heat exchange between the air and the Earth's surface is defined by the heat-exchange coefficient α_{surf}.

THERMOHYDRODYNAMIC MODEL

To model the thermodynamic processes occurring in the well and reservoir during injection and production, the TERMOSIM™ simulator numerically solves two systems of coupled equations – hydrodynamic and thermodynamic, the TERMOSIM™ simulator numerically solves two systems of coupled

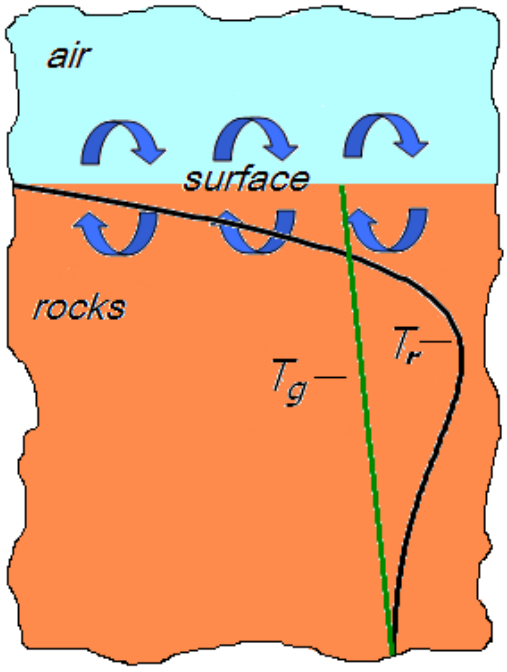

Fig. 1.4.4. Heat exchange at the Earth's surface
T_g – Geothermal profile
T_r – Rock temperature profile

equations – hydrodynamic and thermodynamic. The production/injection history of the well is divided into steps. A flow pattern is set for the well and reservoir, which is followed by the calculation of temperature perturbations for each time step.

The simulator can model various flow patterns including those for wellbore and behind-casing cross-flows under both flowing and shut-in conditions.

Hydrodynamic model of single-phase well-reservoir flow

The hydrodynamic models of well and reservoir with single-phase flows are identical for injection and production wells. For this reason, this case describes a generalised hydrodynamic model valid for both types of wells.

The fluid is assumed to flow radially in the reservoir. Fluid flows in the well and reservoir depend on the bottom-hole pressure P_{wf}, formation pressure P_e at the external radial boundary r_e (at a 100-*m* radius from the well or half the distance between neighbouring wells), permeability k and skin factor *S* for each production or injection zone. For producers $P_e > P_{wf}$, and for injectors $P_{wf} > P_e$.

A hydrodynamic model can include two or more perforated or unperforated reservoir units, if the latter communicate with the wellbore through the casing annulus. Fig. 1.4.5 shows a hydrodynamic model for a two formations.

The model accounts for a wide variety of fluid flow patterns under both flowing and shut-in conditions. It should be taken into account that wellbore and behind-casing cross-flows, often appearing in multi-reservoir wells under shut-in conditions, mask the true reservoir temperature. As a result, the resulting measured temperature profile is smoothed, which substantially complicates modelling.

The hydrodynamic well model takes into account unsteady pressure build-up in a multi-reservoir system. To calculate pressure for both the well and the reservoir, TERMOSIM™ numerically solves the pressure diffusion equation for communicating reservoir layers and radial fluid flow. Each reservoir unit is characterised by pressure diffusivity *(χ)*. All reservoir units are assumed to communicate with the wellbore. Generally, formation pressures are different in different layers, and this causes cross-flows between them during shut-in periods. In a shut-in well, pressures in reservoir units build up differently because of different pressure diffusivities. During the first hours, it can lead to cross-flow from a layer of high pressure diffusivity to one of low pressure diffusivity. Then, after the reservoir pressure is stabilised, cross-flow can change direction in accordance with the pressure at the external boundary. Depending on reservoir characteristics, the flow direction may change during the first hours or days after well shut-in.

Flow velocity *(u)* and flow rate *(V)* in each formation are defined by Darcy's law:

$$u = -\frac{k}{\mu}\nabla p \quad (1.4.5) \qquad V = -2\pi r \frac{kh}{\mu}\nabla p \quad (1.4.6)$$

The flow rate depends on reservoir permeability (k), reservoir thickness (h) and fluid viscosity (μ). To describe flow in a disturbed zone, its radius (r_s) and skin factor (S) need to be set as well.

Mass balance for each layer is determined by the following equation:

$$Q + W_{bot} = V + W_{top} \qquad (1.4.7)$$

where V – rate of inflow from the reservoir, W_{bot} – rate of behind-casing cross-flow from the bottom unit, Q – wellbore inflow rate, W_{top} – rate of behind-casing cross-flow to the top unit (Fig. 1.4.5).

This equation implies that the total volume of fluid coming from the reservoir and behind the casing from lower formations has to be equal to that of fluid entering the wellbore and then flowing behind the casing into overlying intervals.

In many wells, inflow or injection profiles are not uniform within the reservoir interval, which has been taken into account in modelling. A reservoir inflow profile may be different from a wellbore inflow profile – for instance, in the presence of cross-flows behind casing – and these profiles can be set differently.

Thermodynamic well and reservoir model

In addition to the hydrodynamic equations described in the previous section, the TERMOSIM™ simulator numerically solves a system of thermodynamic equations to calculate well and rock temperatures. The models of injection and production wells are different because temperature anomalies in them are of different origins. For this reason, each model has to be described separately.

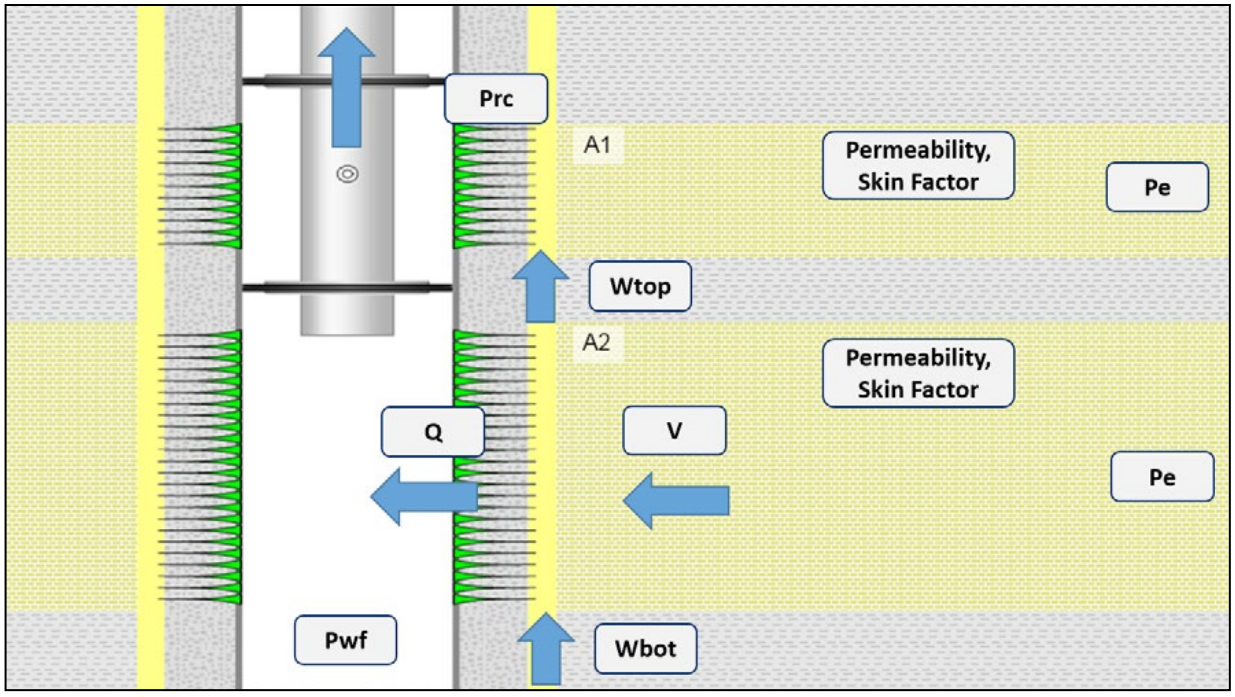

Fig. 1.4.5. A generic hydrodynamic model for a two-layer formation. P_e – formation pressure at the external boundary, P_{wf} – bottom-hole pressure, Pr_c – pressure at casing radius, V – reservoir fluid flow rate, Q – wellbore inflow rate, W_{bot} – rate of cross-flow from the underlying zone, W_{top} – rate of cross-flow into the overlying zone

Injection wells

In the generic thermodynamic model of an injection well, fluid injection changes the temperature of surrounding rocks through conductive heat exchange. Generally, the temperature of injection fluid is lower than the geothermal temperature, and surrounding rocks therefore cool down. Then, as the fluid flows through the reservoir due to convective and conductive heat exchange, a cooling anomaly appears in the initial temperature distribution. The more fluid enters the reservoir, the larger and farther from the well the temperature anomaly develops. The scale of temperature perturbations in the reservoir depends on a large number of factors: injection rate history, seasonal and daily injection temperature variations, the thermohydrodynamic characteristics of the reservoir and the heat insulation properties of completion components. At the same time, fluid flow through the reservoir is accompanied by conductive heat exchange between fluid and overlying and underlying rocks. Fig. 1.4.6 illustrates heat exchange in an injection well.

Injection fluid temperature plays a key role in forming reservoir temperature anomalies. It may vary in time in a complex manner, depending on the water-supply system: fluid flowing through onshore pipes to an onshore well is affected by daily temperature variations, while an offshore well would receive injection fluid of nearly constant temperature. Another factor that affects the formation of temperature anomalies is specific flow rate: the higher the specific flow rate, the deeper the penetration of temperature anomalies into the reservoir.

Quantitative injection profiling is based on the combined analysis of flowing and shut-in temperature measurements to minimise the number of uncertain input parameters. The formation injection profile can be determined with minimal error by generating a temperature pulse in the reservoir and analysing its response.

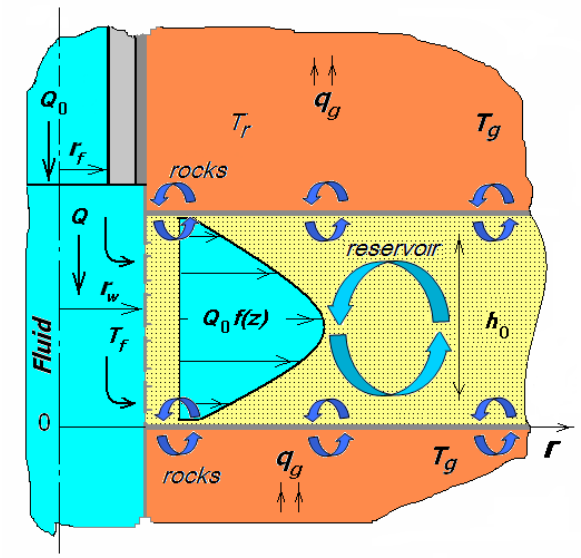

Fig. 1.4.6. A generic flow pattern for an injection well

T_f – Wellbore fluid temperature,
T_r – Rock temperature,
T_g – Geothermal profile,
q_g – Earth's heat flux,
Q – Wellbore flow rate at a certain depth,
$QO_{(t)}$ – Total surface flow rate,
$f_{(z)}$ – Normalised injection profile,
r_f – Inner tubing radius,
r_w – Cement sheath radius,
Blue arrows denote conductive heat exchange between reservoir rocks and fluid and overlying and underlying rocks;
Cyan arrows denote conductive and convective heat exchange between fluid and reservoir rocks.

There are two main techniques for injectivity profiling: DTR (Daily Temperature Response) and STR (Step Temperature Response). In the DTR technique, the fluid injected into the reservoir is affected by daily temperature variations. Therefore, this technique is used in onshore wells. The STR technique employing artificial temperature pulsing is used in offshore wells in which daily temperature variations do not reach reservoirs. To generate temperature pulses in a reservoir, a well is shut-in for some time, during which the wellbore fluid above the reservoir is warmed by surrounding rocks, and then the warmed fluid column is injected into the reservoir.

Production wells

In the thermodynamic model of a production well, wellbore temperature is defined by two factors: the Joule-Thompson effect and thermal mixing.

Joule-Thompson effect

As fluid moves radially through the reservoir towards the wellbore, it warms up or cools down due to the Joule-Thompson effect leading to both conductive and convective heat exchange with the reservoir as well as conductive heat exchange with overlying and underlying rocks (Fig. 1.4.7). The Joule-Thompson effect in turn has two components: friction heating and adiabatic cooling. For liquids, when they are forced through pores, the friction heating effect prevails over the adiabatic effect and a heating anomaly appears in the water/oil inflow interval. Because the adiabatic effect for gas is greater than the friction heating effect, a cooling anomaly appears in a gas inflow interval. The maximum Joule-Thomson coefficient is 0.4*°C/MPa* for oil, 0.22*°C/MPa* for water and -4*°C/MPa* for gas.

Water, oil and gas entering a producing well affect wellbore temperature differently (Fig. 1.4.8). Water and oil production results in heating and gas production in cooling. Pure oil produces the greatest heating effect. Some water in oil reduces the temperature because of a lower Joule-Thompson coefficient. For a mixture containing 50% oil and 50% gas, heating will be lower than for an oil-water mixture because pure oil flow produces a heating effect, while pure gas flow produces a cooling effect.

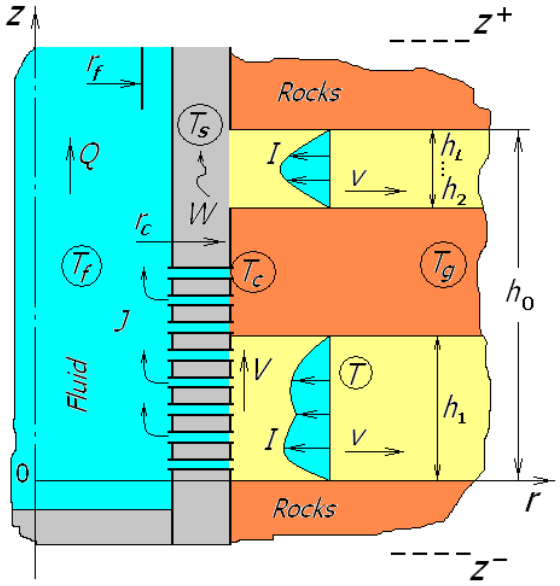

Fig. 1.4.7. A generic flow pattern for a dual producer
T_f – Wellbore fluid temperature,
T_r – Rock temperature,
T_s – Cement sheath temperature,
Q – Wellbore flow rate,
r_f – Inner tubing radius,
r_c – Wellbore radius,
r_w – Cement sheath radius,
I – Reservoir flow density,
J – Wellbore inflow density,
V – Reservoir fluid volume,
W – Cross-flow behind casing.

For a large amount of gas, the cooling effect is greater than the heating effect and the resulting temperature is lower than the geothermal temperature (Fig. 1.4.8).

Thermal mixing

Inflow of fluids of different temperatures from different reservoir units into the borehole results in their thermal mixing.

Thermal mixing plays an important role in case of more than one flowing reservoir unit. The thermal mixing effect is displayed in temperature logs as a temperature gradient change. This effect is normally caused by the difference between the temperatures of upward flow and wellbore inflow due to the geothermal gradient. The resulting temperature is defined by the heat capacities, flow rates and temperatures of mixing fluids.

In the case when a heating effect occurs due to water inflow from the lower production interval (Fig. 1.4.9), the heated water goes up and its temperature slowly decreases as a result of heat exchange with surrounding rocks. The degree of temperature decrease depends on the flow rate, well design and the thermal conductivity

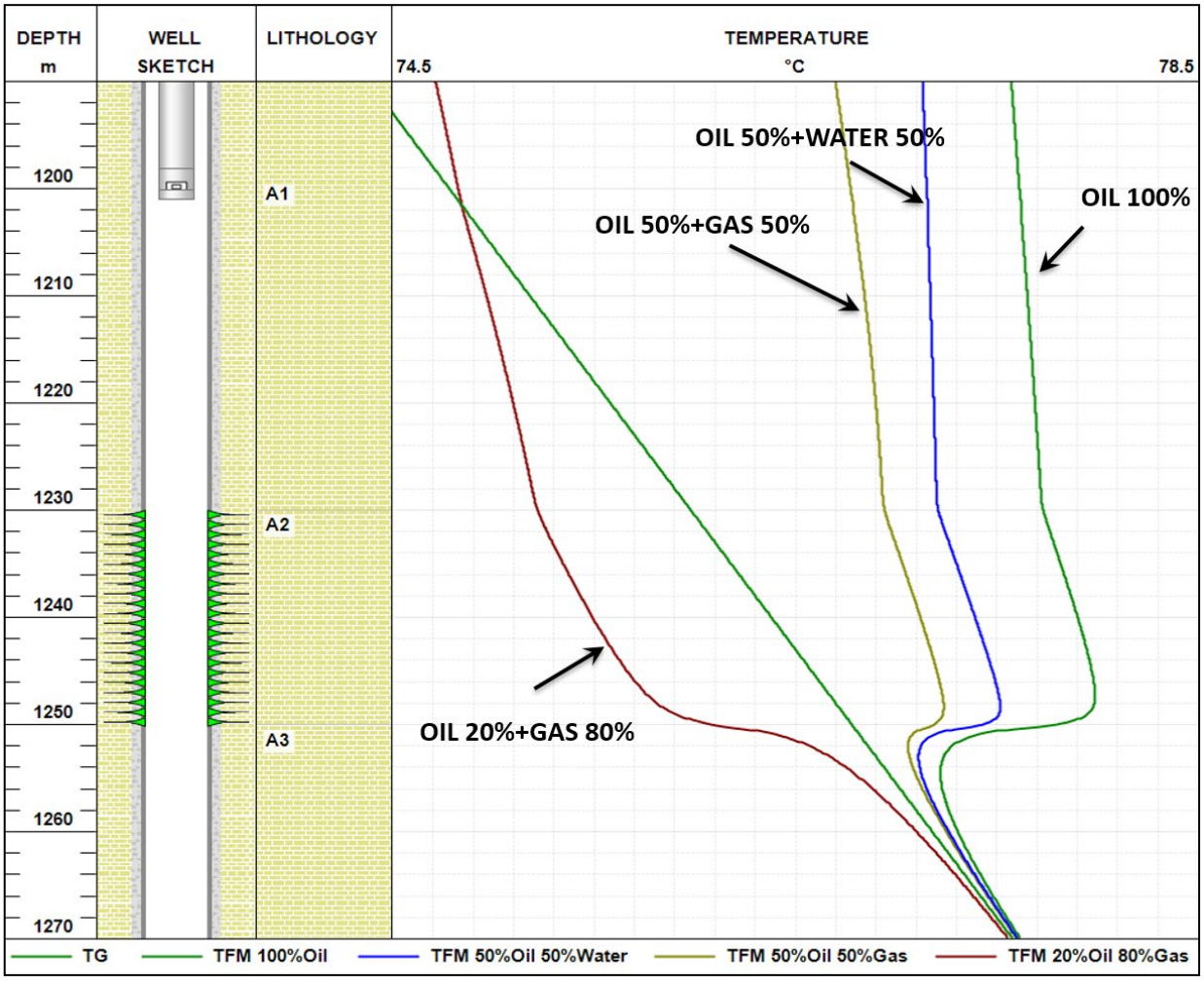

Fig. 1.4.8. Effect of phase composition on temperature

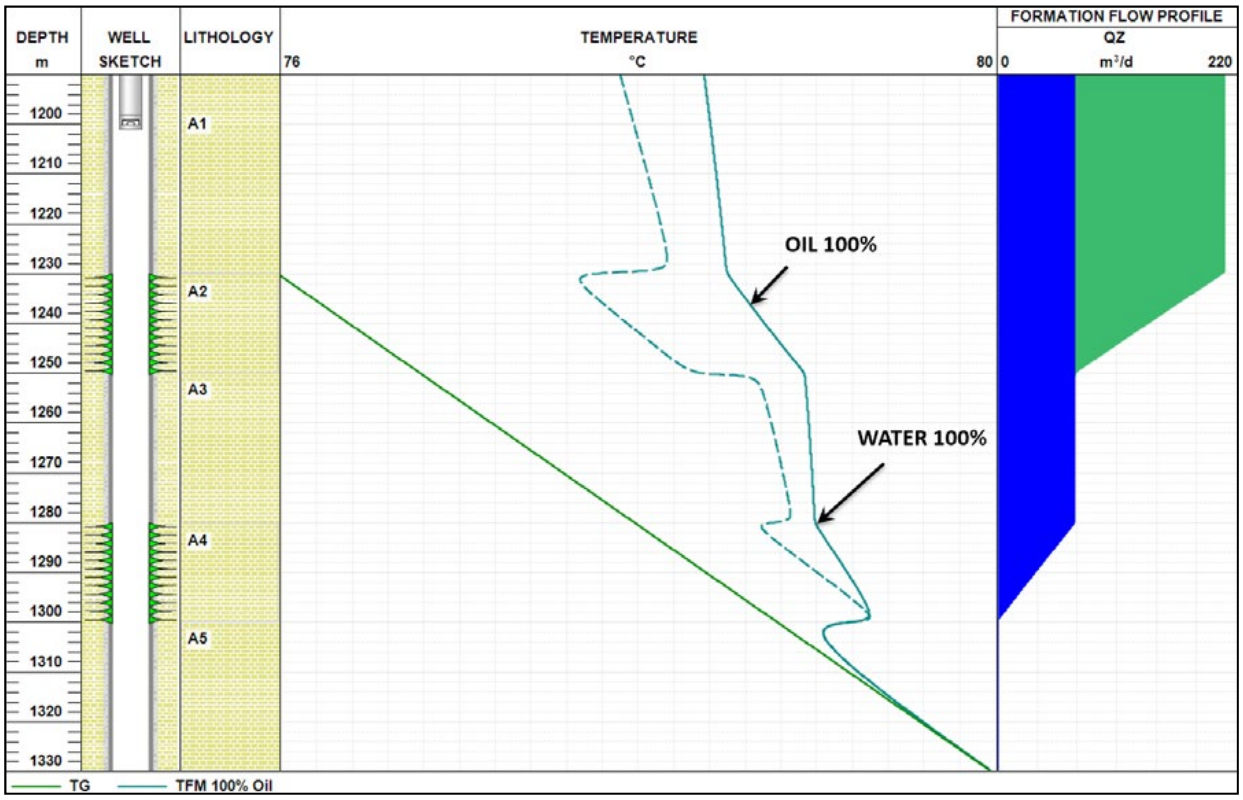

Fig. 1.4.9. A thermal mixing effect for a two-layer reservoir. The solid blue line indicates wellbore temperature, the dashed blue line indicates inflow fluid temperature, and the green line indicates the geothermal profile. The rightmost data panel displays an inflow profile showing uniform water flow from the lower formation and uniform oil flow from the upper one.

of surrounding rocks. The temperature of the oil entering the wellbore from the upper production interval is also higher than the geothermal temperature but lower than the temperature of the water moving up from the lower production interval because of the geothermal gradient. The final temperature of mixed fluids is higher than the temperature of the oil from the upper formation but lower than that of the water flowing up the wellbore.

Reservoir temperature

The simulator can also take into consideration fluid breakthrough in the reservoir, and in this case uses the changed temperature profile as the initial temperature distribution. This temperature profile features a local temperature anomaly against the geothermal temperature.

A more detailed description of temperature survey technologies and the specific temperature modelling features of the TERMOSIM™ simulator for injection and production wells is given in the following sections.

1.5 MAGNETIC IMAGING DEFECTOSCOPE

1.5.1 CORROSION LOGGING OVERVIEW

The average operating life of production and injection wells varies between 20 to 30 years in a non-aggressive environment and two to five years in the presence of hydrogen sulphide or carbon dioxide. Statistically, every fifth production well and every third injection well have integrity-related issues, including corrosion in tubing, casing, collars and other completion components. Continuous corrosion monitoring can substantially improve production performance by preventive workovers and prevent environmental issues by factoring survey findings into abandonment procedures.

Corrosion can be monitored using different downhole electronic tools, such as defectoscopes and other wall thickness measuring instruments. Defectoscopes can be acoustic, mechanical or electromagnetic, depending on the types of generated and detected signals. Each type has its advantages and disadvantages, as described in detail below in this handbook.

1.5.2 INDIGO MAGNETIC IMAGING DEFECTOSCOPE (MID)

TECHNOLOGY INTRODUCTION

The operation of the Magnetic Imaging Defectoscope is based on the phenomenon of the decay of eddy currents induced in metal pipes by electromagnetic pulses. A magnetic coil, as part of the logging tool, is placed coaxially within concentric pipes to generate eddy currents in them (Fig. 1.5.1). The generated pulses are rectangular, and eddy currents are generated twice, on its leading and trailing edges.

The response is generally measured after the pulse's trailing edge decays because this process is well studied and is easier to take into account for further interpretation. The electromagnetic pulse amplitude is selected so that all transient processes on the leading edge cease before the detection of the response. For the same pulse amplitude, the thicker the pipe wall, the longer the eddy currents take to die out. The induced currents decay faster due to defects and corrosion because these currents flow around the defects or are disrupted by them, and corrosion leads to pipe wall thinning, which in turn increases electrical resistance. The eddy current decay rate is analysed to identify defects in pipe barriers. The long-range electromagnetic coverage enables the analysis of several coaxial pipes of different diameters surveyed in one run.

A coil sensor effectively scans pipes with diameters of up to three fourths of its length. To scan various barriers, the tool usually contains several coils of different lengths, each for a pipe of corresponding diameter.

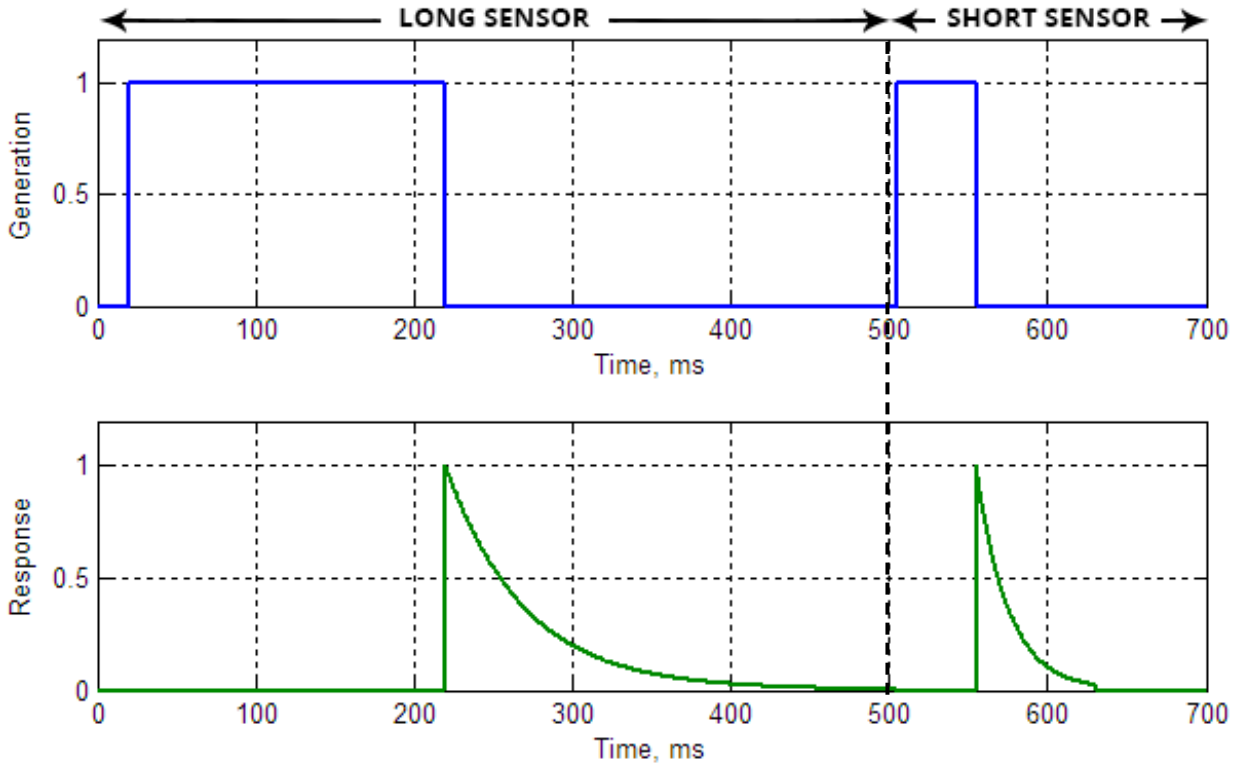

Fig. 1.5.1. A typical measurement cycle for a two-coil logging tool, with generator-coil current shown as the blue curve and receiving-coil current as the green one

The coaxial receiving and generating coils and placed together to ignore ghost signals that can be interpreted as defects. The decaying eddy currents induce an electromotive force (EMF) in the receiving coil, and its amplitude can be assessed by their decay rate.

The electromotive force recorded by the sensor is proportional to the electromagnetic field at sensor locations:

$$U_{reciever} = C_{coil} E_{\varphi}(r,z,t) \qquad (1.5.1)$$

where C_{coil} are the coefficients characterising the geometry and electromagnetic parameters of the generating and receiving coils that should be defined by factory calibration.

Magnetic field variation can generally be described by Maxwell's equations:

$$rot(E)=-\frac{\partial B}{\partial t}; div(D)=\rho; rot(H)=j+\frac{\partial D}{\partial t}; \; div(B)=0, \qquad (1.5.2)$$

where $\vec{E}$ – electric-field strength, $\vec{B}$ – magnetic induction, $\vec{D}$ – electric induction, ρ – electric charge density, $\vec{H}$ – magnetic field strength, j – current density.

In reality, downhole pipes make up an axisymmetric layered system. Because a logging tool is positioned along the wellbore, Maxwell's equations can be reduced for them to one equation:

$$\frac{\sigma(r,z)\cdot\mu_0}{r}\cdot\frac{\partial rE_{\varphi}(r,z)}{\partial t} = \mathrm{div}\left\{\frac{1}{\mu(r,z)\cdot r}\cdot \mathrm{grad}(r\, E_{\varphi}(r,z))\right\} + \mu_0\frac{\partial j(r,z)}{\partial t} \qquad (1.5.3)$$

where z – distance along hole, r – radial distance from hole, $\sigma\ (r, z)$ – electrical conductivity, $\mu\ (r, z)$ –magnetic permeability, $E_{\varphi}\ (r, z)$ – axial component of electromagnetic field, $j\ (r, z)$ – generating coil current density, and μ_0 – vacuum magnetic permeability.

Equation 1.5.2 describes the variation of the tangential component of the electric field for the two-dimensional distribution of parameters – in the radial *(r)* and axial *(z)* directions.

It can be seen that the response recorded by the tool is governed by the magnetic permeability, conductivity, the strength of the magnetic field generated by the coils, diameter and thickness of pipes as well as by the design of the tool itself including its dimensions, current strength, etc.

EmPulse tool specification

The EmPulse tool can contain up to three electromagnetic sensors (short, medium and long). Each sensor consists of two coils: generating and receiving. Both coils are mounted concentrically around a composite core (see Fig 1.5.2). The EmPulse tool can detect and analyse transverse and longitudinal defects in each of the first three coaxial metal barriers. The tool is effective in surveying pipes of various steel grades and weights, including those with high chrome contents, and its titanium housing enables operation in corrosive environments with a hydrogen sulphide content of up to 30% (Fig. 1.5.2).

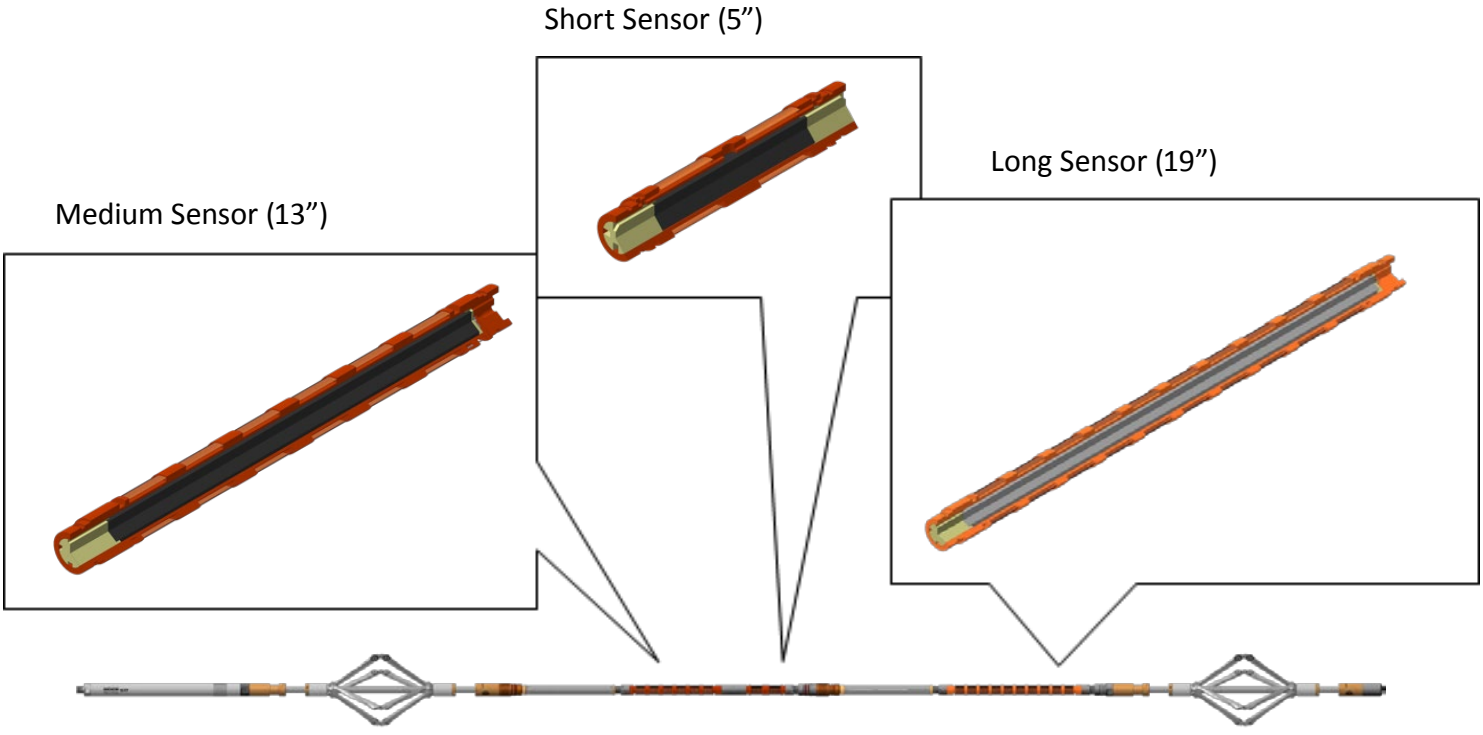

Figure 1.5.2. EmPulse-2 and EmPulse -3 tool designs

General tool specifications are given in the table below.

Table 1.5.1. EmPulse tool specifications

Parameter	Value
Operating temperature range	-20…150 *°C* (-4…302 *°F)*
Maximum pressure	100 *MPa* (14,500 *psi*)
Maximum H_2S concentration	30%
Maximum pipe wall thickness	38 *mm* (1.5")
Pipe diameter	51–381 *mm* (2"–15")
Recommended tool speed	2–4 *m*/*min* (6–12 *ft*/*min*)
Stand-alone operating time	48 *h*

The Indigo Concept

The main common feature of the EmPulse tools with the Indigo interface is the Indigo single-line bus 2.0 that supplies power to the tool and performs data exchange. This provides an opportunity to combine different tool modules (MID, Navigator, Hex, PT, ReCap, SNL and others) in one toolstring in a required order.

The single-line bus enables the user to acquire information about the connected tools, their current configuration and logging interval duration, switch the recording sensors on and off, upload a required survey scenario to the tools (in memory mode), and read out data directly from the toolstring using a hardware adaptor and the unified Indigo Suite software.

The EmPulse tools can perform automatic self-tests. Operation algorithms can be set for the tools to provide specific pulse durations and periods. Several tool modules in one toolstring can be synchronised to avoid their mutual interference.

The EmPulse tool comes in two versions for different well completions: Indigo EmPulse -2 and EmPulse -3. EmPulse -2 scans the first and second metal pipe barriers up to 9-5/8" in diameter, and EmPulse-3 detects defects in pipes with larger diameters of up to 14". These modules can be integrated or used separately. If combined, the modules can evaluate the thicknesses of the first, second and third concentric pipes in one run.

The complete generation-and-recording cycle takes 0.8 seconds for EmPulse-2, 1.2 seconds for EmPulse -3 and 2 seconds for their combination. If possible, the modules should be used separately to log at a higher speed of 4 *m/min,* while the recommended speed limit for their combination is 1–2 *m/min*.

EmPulse-2 defect sensitivity data are given in the table below.

Table 1.5.2. Sensitivity of EmPulse -2 to defects

Completion pipes (in)	Thickness		Minimum hole size in Barrier 1		Minimum hole size in Barrier 2	
	Barrier 1	Barrier 2				
2 ⅞	+		15 *mm*	0.6 *in*		
3 ½	+		20 *mm*	0.8 *in*		
3 ½ (stainless steel)	+		7 *mm*	0.3 *in*		
4 ½	+		25 *mm*	0.9 *in*		
5 ½	+		40 *mm*	1.5 *in*		
7	+		50 *mm*	2 *in*		
9 ⅝	+		65 *mm*	2.5 *in*		
13 ⅜	+		90 *mm*	3.5 *in*		
2 ⅞ + 5 ½	+	+	20 *mm*	0.7 *in*	65 *mm*	2.5 *in*
3 ½ + 5 ½	+	+	20 *mm*	0.8 *in*	65 *mm*	2.5 *in*
3 ½ + 7	+	+	20 *mm*	0.8 *in*	68 *mm*	2.7 *in*
4 ½ + 7	+	+	25 *mm*	0.9 *in*	70 *mm*	2.8 *in*
5 ½ + 7	+	+	41 *mm*	1.6 *in*	100 *mm*	4 *in*
3 ½ + 9 ⅝	+	+	20 *mm*	0.8 *in*	100 *mm*	4 *in*
4 ½ + 9 ⅝	+	+	25 *mm*	0.9 *in*	100 *mm*	4 *in*
5 ½ + 9 ⅝	+	+	41 *mm*	1.6 *in*	115 *mm*	4.5 *in*
7 + 9 ⅝	+	+	53 *mm*	2.1 *in*	115 *mm*	4.5 *in*
4 ½ + 7 + 9 ⅝	+	+	25 *mm*	0.9 *in*	86 *mm*	3.4 *in*
3 ½ + 9 ⅝ + 13 ⅜	+	+	20 *mm*	0.8 *in*	140 *mm*	5.5 *in*
4 ½ + 9 ⅝ + 13 ⅜	+	+	25 *mm*	0.9 *in*	140 *mm*	5.5 *in*
7 + 9 ⅝ + 13 ⅜	+	+	53 *mm*	2.1 *in*	140 *mm*	5.5 *in*
3 ½ dual string + 9 ⅝	+	+	25 *mm*	1 *in*	152 *mm*	6 *in*

Barrier thickness accuracy	Specification
Barrier 1	±3.5% (±0.01 *in*. or ± 0.25 *mm* for 3 ½'' tubing with 7 *mm* wall thickness)
Barrier 2	±6% (±0.03 *in*. or ± 0.75 *mm* for 9 ⅝'' casing with 12 *mm* wall thickness)

EmPulse -3 defect sensitivity data are given in the table below.

Table 1.5.3. Sensitivity of EmPulse -3 to defects

Completion, inch	Minimum hole size in Barrier 1		Minimum hole size in Barrier 2		Minimum hole size in Barrier 3	
7	2 *in*	51 *mm*				
9 ⅝	2.5 *in*	65 *mm*				
13 ⅜	3.5 *in*	89 *mm*				
2 ⅞ + 7	0.7 *in*	18 *mm*	2.7 *in*	69 *mm*		
3 ½ + 7	0.8 *in*	20 *mm*	2.7 *in*	69 *mm*		
4 ½ + 7	0.9 *in*	23 *mm*	2.8 *in*	71 *mm*		
5 ½ + 7	1.6 *in*	41 *mm*	4 *in*	102 *mm*		
2 ⅞ + 9 ⅝	0.7 *in*	18 *mm*	3 *in*	76 *mm*		
3 ½ + 9 ⅝	0.8 *in*	20 *mm*	4 *in*	102 *mm*		
4 ½ + 9 ⅝	0.9 *in*	23 *mm*	4 *in*	102 *mm*		
5 ½ + 9 ⅝	1.6 *in*	41 *mm*	4.5 *in*	114 *mm*		
7 + 9 ⅝	2.1 *in*	53 *mm*	4.5 *in*	114 *mm*		
2 ⅞ + 13 3/8	0.7 *in*	18 *mm*	6 *in*	152 *mm*		
3 1/2 + 13 3/8	0.8 *in*	20 *mm*	6 *in*	152 *mm*		
4 1/2 + 13 3/8	0.9 *in*	23 *mm*	6 *in*	152 *mm*		
5 1/2 + 13 3/8	1.6 *in*	41 *mm*	6 *in*	152 *mm*		

Completion, inch	Minimum hole size in Barrier 1		Minimum hole size in Barrier 2		Minimum hole size in Barrier 3	
7 + 13 3/8	2.1 *in*	53 *mm*	6 *in*	152 *mm*		
9 ⅝ + 13 ⅜	2.6 *in*	66 *mm*	6 *in*	152 *mm*		
2 ⅞ + 5 ½ + 7	0.7 *in*	18 *mm*	3 *in*	76 *mm*	6 *in*	152 *mm*
3 1/2 + 5 ½ + 7	0.8 *in*	20 *mm*	3 *in*	76 mm	6 *in*	152 *mm*
4 1/2 + 5 ½ + 7	0.9 *in*	23 *mm*	3 *in*	76 *mm*	6 *in*	152 *mm*
2 ⅞ + 5 ½ + 9 ⅝	0.7 *in*	18 *mm*	3 *in*	76 *mm*	7 *in*	178 *mm*
3 1/2 + 5 ½ + 9 ⅝	0.8 *in*	20 *mm*	3 *in*	76 *mm*	7 *in*	178 *mm*
4 1/2 + 5 ½ + 9 ⅝	0.9 *in*	23 *mm*	3 *in*	76 *mm*	7 *in*	178 *mm*
2 ⅞ + 7 + 9 ⅝	0.7 *in*	18 *mm*	3.3 *in*	84 *mm*	7 *in*	178 *mm*
3 ½ + 7 + 9 ⅝	0.8 *in*	20 *mm*	3.3 *in*	84 *mm*	7 *in*	178 *mm*
4 ½ + 7 + 9 ⅝	0.9 *in*	23 *mm*	3.4 *in*	86 *mm*	7 *in*	178 *mm*
5 ½ + 7 + 9 ⅝	1.6 *in*	41 *mm*	4.9 *in*	124 *mm*	7 *in*	178 *mm*
2 ⅞ + 5 ½ + 13 ⅜	0.7 *in*	18 *mm*	3 *in*	76 *mm*	7.5 *in*	191 *mm*
3 1/2 + 5 ½ + 13 ⅜	0.8 *in*	20 *mm*	3 *in*	76 *mm*	7.5 *in*	191 *mm*
4 1/2 + 5 ½ + 13 ⅜	0.9 *in*	23 *mm*	3 *in*	76 *mm*	7.5 *in*	191 *mm*
2 ⅞ + 7 + 13 ⅜	0.7 *in*	18 *mm*	3.2 *in*	81 *mm*	7.5 *in*	191 *mm*
3 1/2 + 7 + 13 ⅜	0.8 *in*	20 *mm*	3.2 *in*	81 *mm*	7.5 *in*	191 *mm*
4 1/2 + 7 + 13 ⅜	0.9 *in*	23 *mm*	3.4 *in*	86 *mm*	7.5 *in*	191 *mm*
5 1/2 + 7 + 13 ⅜	1.6 *in*	41 *mm*	4.8 *in*	122 *mm*	7.5 *in*	191 *mm*
2 7/8 + 9 ⅝ + 13 ⅜	0.7 *in*	18 *mm*	4.5 *in*	114 *mm*	7.5 *in*	191 *mm*
3 ½ + 9 ⅝ + 13 ⅜	0.8 *in*	20 *mm*	5.5 *in*	140 *mm*	7.5 *in*	191 *mm*
4 ½ + 9 ⅝ + 13 ⅜	0.9 *in*	23 *mm*	5.5 *in*	140 *mm*	7.5 *in*	191 *mm*
5 ½ + 9 ⅝ + 13 ⅜	1.6 *in*	41 *mm*	5.5 *in*	140 *mm*	8 *in*	203 *mm*
7 + 9 ⅝ + 13 ⅜	2.1 *in*	53 *mm*	5.5 *in*	140 *mm*	8 *in*	203 *mm*

DATA ACQUISITION

The short EmPulse -2 sensor generates short, low-amplitude electromagnetic pulses that magnetise mainly the first barrier and then records magnetisation time decays. It is most commonly used for tubing inspection but can also work in moderate-size casing of up to 5" in diameter. The length of the sensor defines the minimum detectable size of defects, which is 0.9" for the short one. If a defect is larger than the smallest detectable one, magnetisation decay in this zone is faster than for nominal. Accordingly, if any extra metal, such as a collar, gets into the tool's radius of investigation, the magnetisation decays longer than nominal. Therefore, the magnetic-field amplitude recorded in the collar zone would remains larger than nominal throughout the decay (Fig. 1.5.3). Magnetisation decay starts to deviate from nominal not at the beginning but 0.003 seconds after the start of decay recording.

The medium EmPulse -2 sensor is optimised to scan metal barriers from 5" to 13" in diameter for the first one and up to 9-5/8" for the second one. This sensor generates electromagnetic pulses with an amplitude larger than that for the short sensor. Before 0.05 seconds (Fig. 1.5.4), magnetisation decays uniformly throughout the second barrier in all its components including collars. The magnetisation decay starts to deviate from nominal 0.05 seconds after recording begins, i.e. much later than could be expected due to a defect in the first barrier (Fig. 1.5.3). This observation can be used to distinguish corrosion occurrences in the first, second and third barriers (Fig. 1.5.4).

The long EmPulse-3 sensor generates long, high-amplitude electromagnetic pulses and records longer magnetisation decays. The

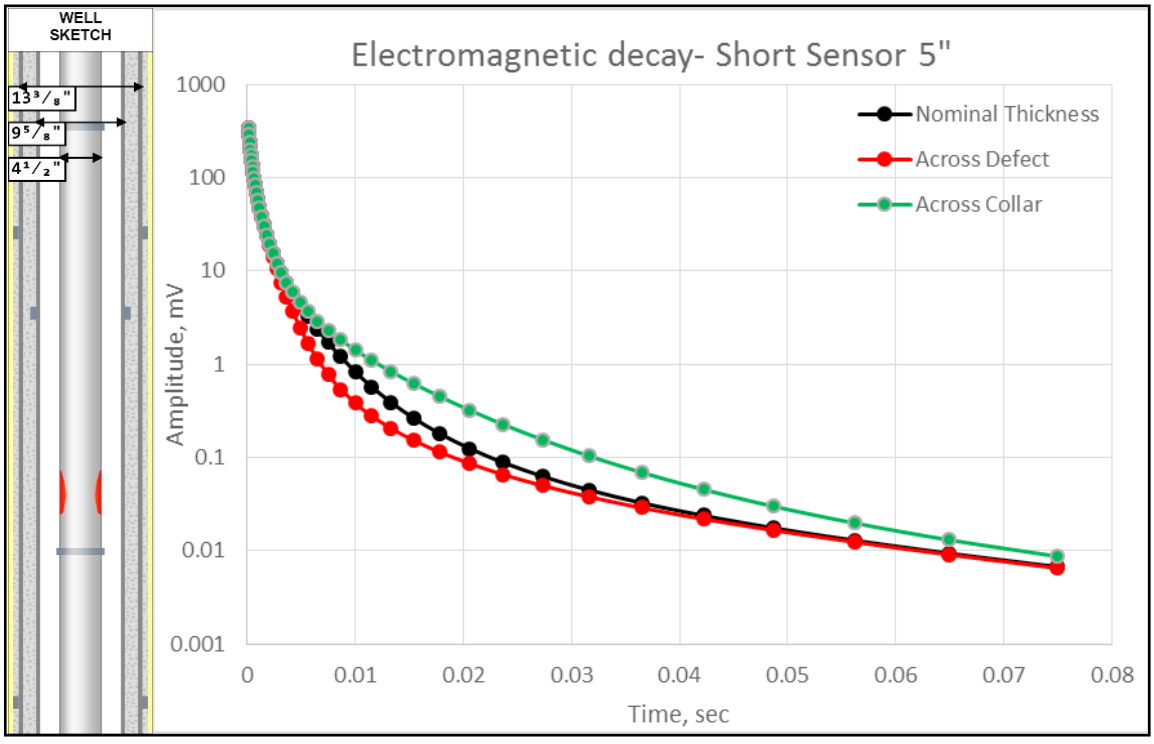

Fig. 1.5.3. Electromagnetic decays recorded by the short 5" sensor in the 4-½" metal barrier for a nominal thickness zone (black curve), a 10% corrosion zone (red curve) and a collar (green curve).

recorded responses reflect the conditions of the first, second and third barriers of up to 14" in diameter. The deviation of magnetisation decay from nominal at collars and defects in the third barrier occurs later than at those in the first and second barriers (Fig. 1.5.5). The presence of corrosion or a defect speeds up magnetisation decay while collars slow it down. Notably, corrosion and collars are displayed in magnetisation decays at different times because the deviation of the recorded electromagnetic decay from nominal in corrosion zones occurs earlier than at collars. Corrosion in each barrier appears in magnetisation decay data within the same time interval in which the response of the corresponding collar is detected.

Electromagnetic decay data recorded by the short 5" sensor are digitised into 42 channels. The medium 13" sensor records decay into 51 channels, while the long 19" sensor is characterised by the longest observation time and digitises decay data into 91 channels. Thus, the tool records a total of 181 channels in one run.

Data Acquisition Procedure

A MID survey can be conducted during both downward and upward tool runs. However, recording is recommended to be performed during upward runs because of the more stable tool speed. Although there are no special requirements for well operation, the tool may move intermittently and thus affect the data recording quality if the first metal barrier has a small diameter or if the well is producing at a high rate. Any downhole electrical equipment, such as an ESP, cathodic protection or pressure and temperature gauges, may also affect tool operation and recorded data. For this reason, all downhole equipment must be turned off before a well survey.

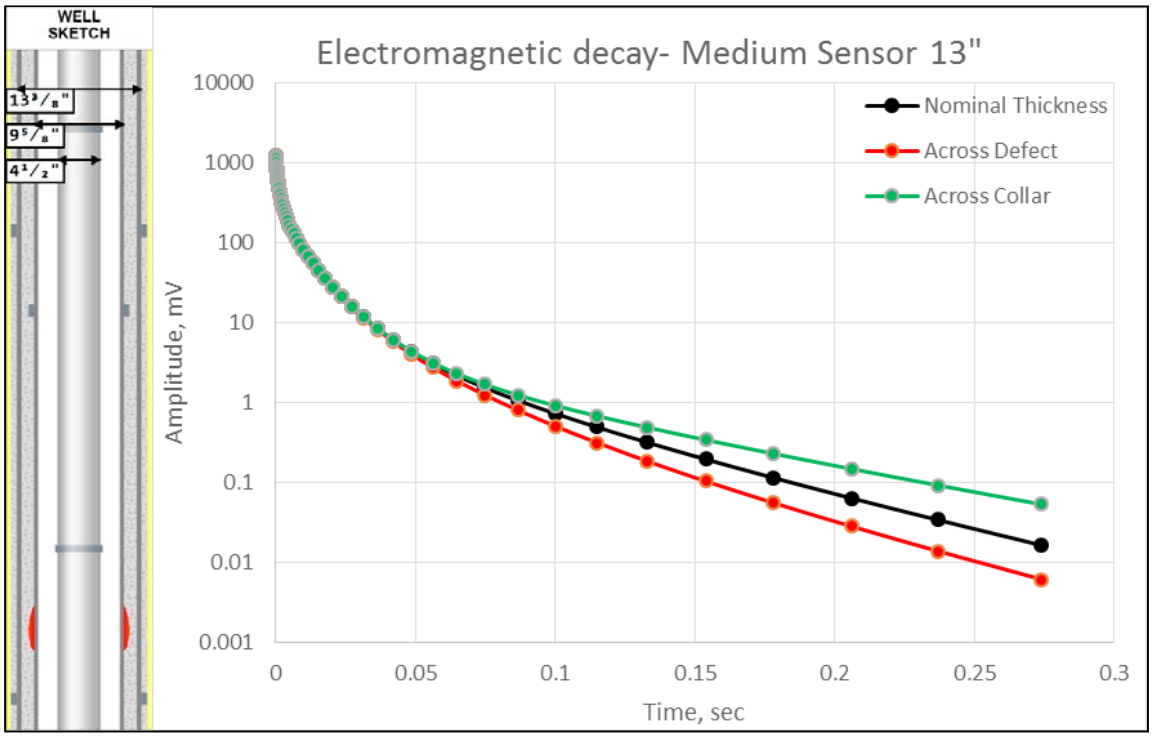

Fig. 1.5.4. Electromagnetic decays recorded by the medium 13" sensor through the 4-½" tubing for a nominal thickness zone (black curve), 10% corrosion (red curve) and a collar in the 9-5/8" casing (green curve).

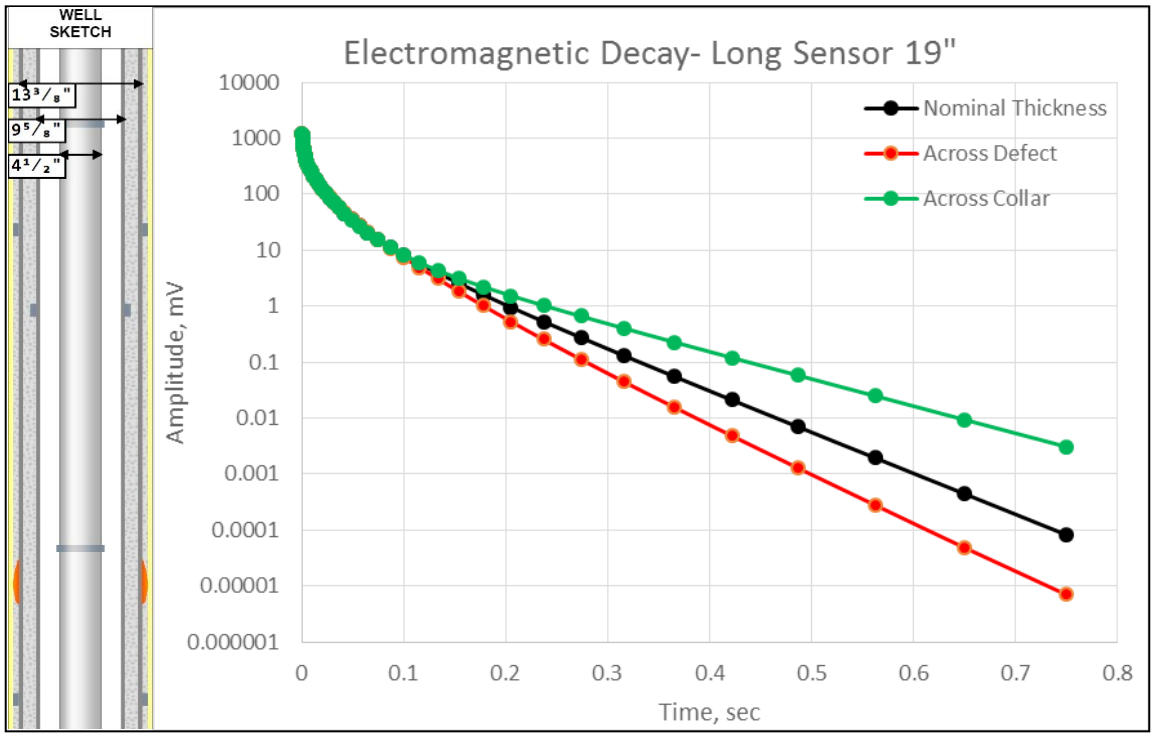

Fig. 1.5.5. Electromagnetic decays recorded by the long EmPulse -3 sensor through the 4-½" tubing and 9-5/8" casing for a nominal thickness zone (black curve), 10% corrosion (red curve) and a collar in the 13-3/8" casing (green curve).

A typical survey procedure for a multi-barrier well is given below.

Fig. 1.5.7 shows a complete digitised data set for the integrated MID toolstring: the short 5" sensor's data are displayed in the SS (Short Sensor) Response data panel and the medium sensor's data in the MS (Medium Sensor) Response data panel for the EmPulse -2 module. The long sensor's data are shown in the LS (Long Sensor) Response data panel for the EmPulse -3 module.

Fig. 1.5.7 also displays zoomed-in logs recorded by the long 19" sensor and shows collars for each of the three barriers, which indicates that each log contains information about all scanned barriers. For this reason, downhole corrosion quantification requires not just data from a particular sensor or a time channel but combined analysis of all data from all sensors.

DATA PROCESSING

Modelling in Magnetic Imaging Defectoscopy

In Magnetic Imaging Defectoscopy, the thickness of metal pipe walls is determined by mathematical modelling and comparing responses recorded in a well by the EmPulse tool with model responses for a well with a particular design. The recorded magnetisation decays can be used to determine not only the wall thicknesses of all metal pipes but also their electromagnetic properties: magnetic permeability and electromagnetic conductivity.

As an advantage, this method is more flexible in adapting the model to any particular well with its own design, metal type, etc.

The EmPulse tool records integrated signals from

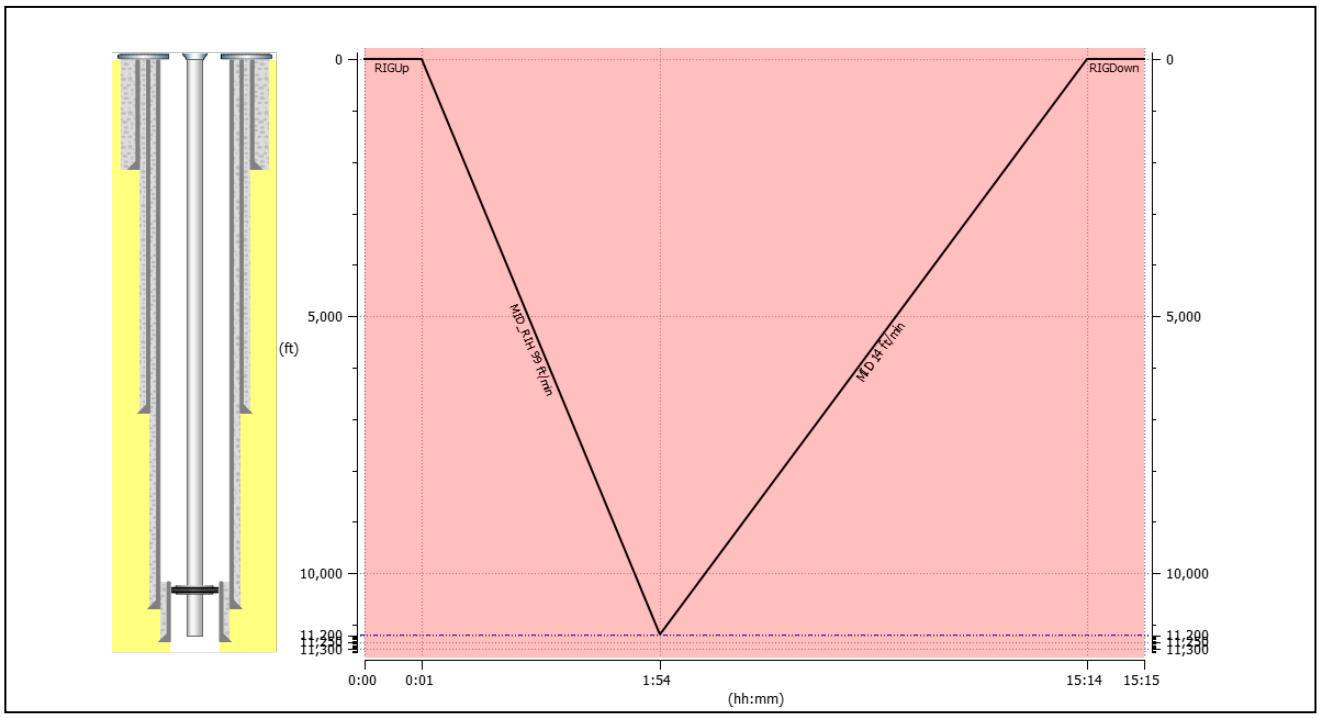

Fig. 1.5.6. A typical MID logging procedure, with the logging tool run to the bottom of the survey interval and recording made during an upward pass at a stable speed of not more than 6 *m/min* to the top of the interval.

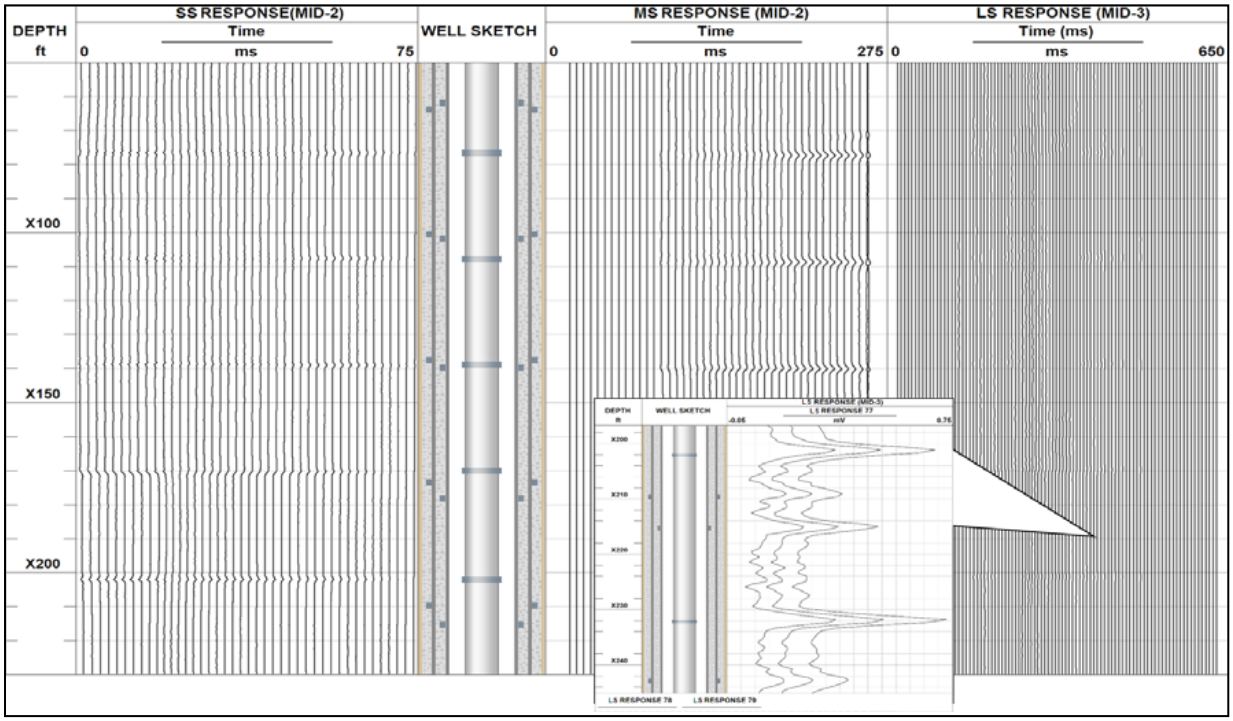

Fig. 1.5.7. Raw data from the integrated MID tool. The SS Response (EmPulse -2) data panel displays the magnetisation decays digitised in 42 time channels of the 5" sensor, the MS Response (EmPulse -2) data panel displays 51 channels of the 13" sensor, and the LS Response (EmPulse -3) data panel displays 91 channels of the 19" sensor. A zoomed-in fragment shows response variations at the collars of the first, second and third barriers

A

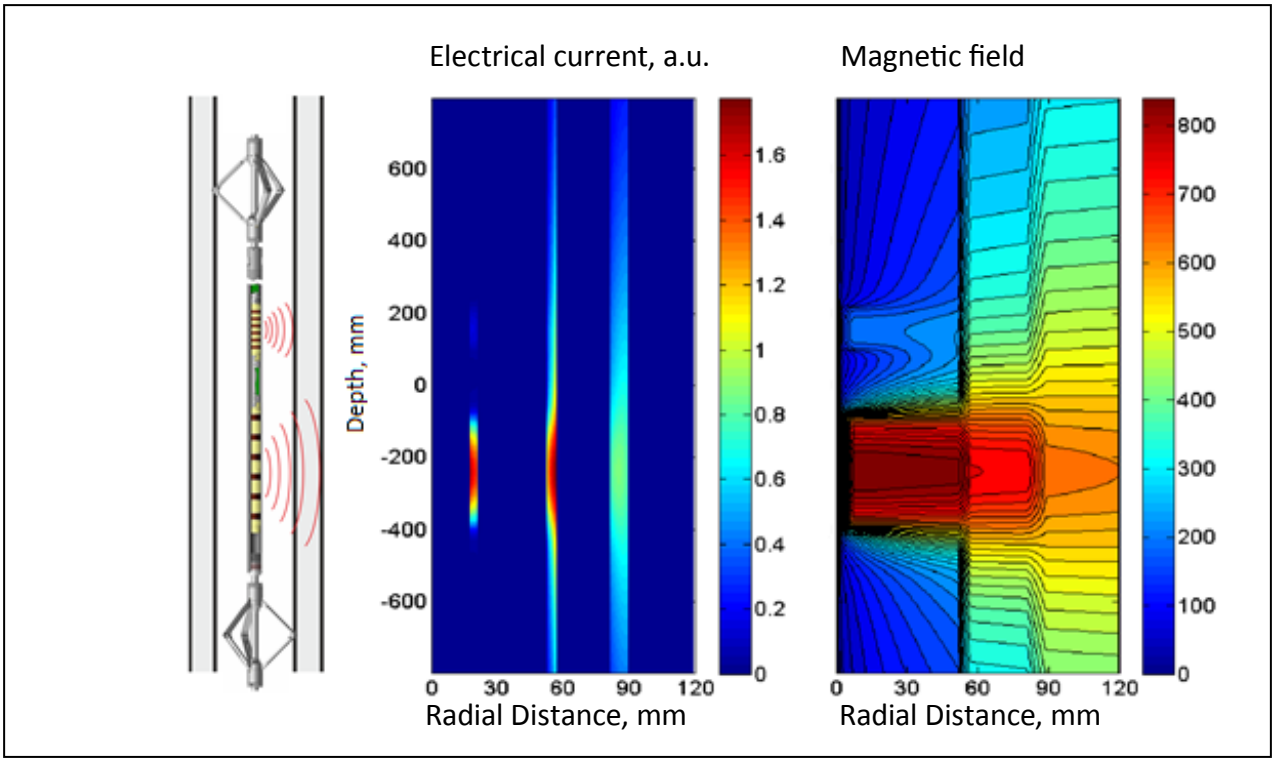

B

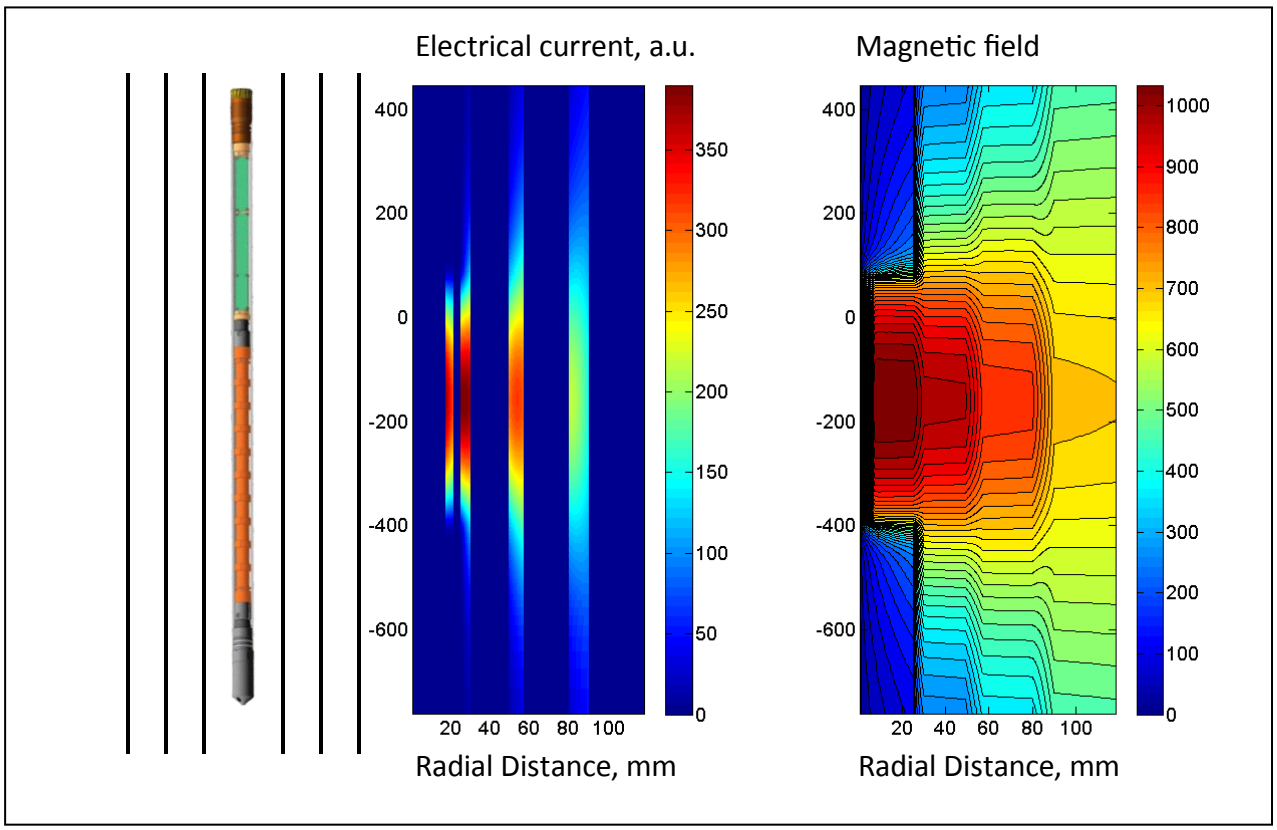

Fig. 1.5.8. 2D MID model. Modelling the distribution of electric currents (left) and the magnetic field (right) induced and measured by EmPulse -2 and EmPulse -3 in tubing and two casings.

all metal barriers in a well, and each recorded time channel therefore contains information about all metal barriers under study including the mutual influence of adjacent barriers. For this reason, a simulation should take into account the individual responses of all barriers to determine pipe properties and accurately calculate pipe wall thicknesses.

This is implemented with the 2D MID simulation software, based on the numerical solution of Maxwell's 2D axial symmetric equations (2), that uses an algorithm simulating sensor responses. The simulator takes into account the tool's geometry including centralisers and simulates the responses of several sensors simultaneously in two dimensions – along the well and radially (Fig. 1.5.8).

Fig. 1.5.9 shows how accurately EmPulse tool readings can be matched with the 2D numerical model.

Thickness determination

The thickness of a pipe wall barrier under study is determined by matching modelled magnetisation decay with measured one by varying the electrical conductivity, magnetic permeability and thicknesses of all barriers for each depth. The modelled and recorded decays are matched for each sensor (Fig. 1.5.10).

MID modelling is a highly complex multi-parameter mathematical process. Numerous laboratory tests suggest that electrical conductivity and magnetic permeability remain reasonably constant along a factory pipe joint (usually 33-ft long each) and depend on the steel type and aging, while completion components and corrosion zones are unlikely to occur throughout the joint.

This observation allows the modelling procedure to be done in several stages. In the first stage,

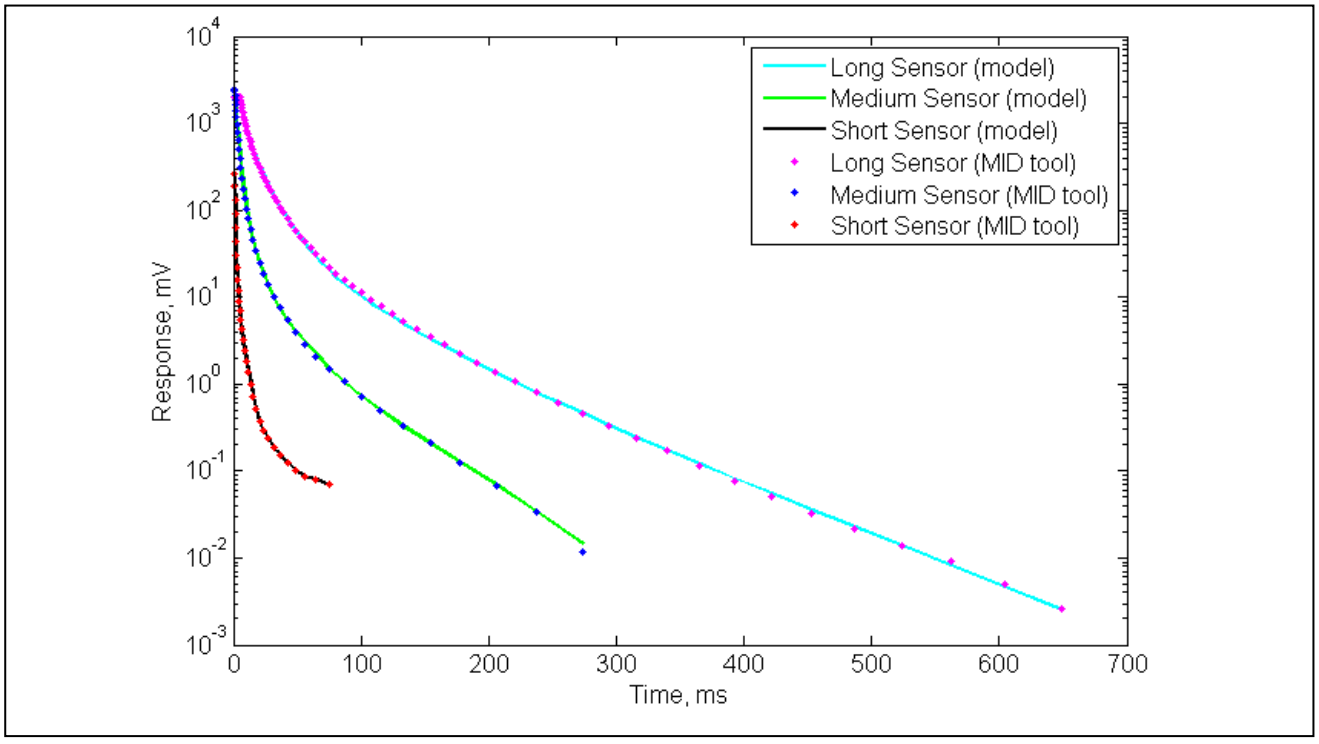

Fig. 1.5.9. Fitting the measured magnetisation decays (dots) and modelled ones (solid lines) for all three sensors of the EmPulse tool.

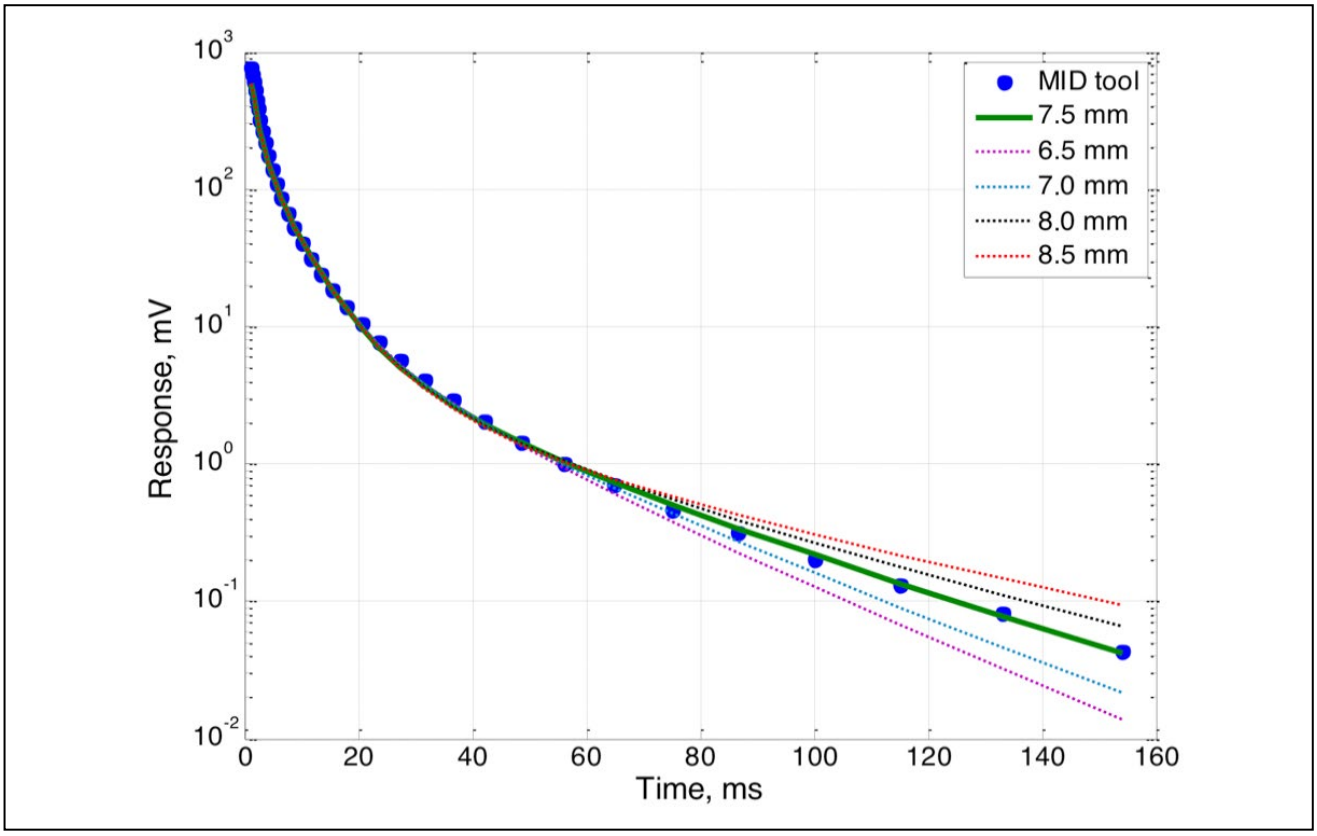

Fig. 1.5.10. MID modelling results for the first barrier (7" casing) with the best fit obtained at 7.5-*mm* pipe wall thickness (green curve)

the algorithm analyses tool responses at all depths using depth-correlated trends and recognises pipe collars and joints in all barriers. Then it decomposes each barrier into numerous joints between the collars and creates a list of wellbore intervals containing all barriers but no collars. As the next step, it analyses all decays for each joint, selects statistically representative decays and, assuming that electrical conductivity and magnetic permeability are constant along the pipe joint (although they can be different for different pipe barriers), changes these two parameters and thickness across the pipe joint to provide the best fit to the tool response (Fig. 1.5.11). Ultimately, it generates a thickness profile, an electrical conductivity profile and a magnetic permeability profile for each of the three barriers (Fig. 1.5.11).

This algorithm is called Real-Time Fitting (RTF) because it models responses and performs fitting for modelled and measured ones immediately in the process of thickness calculations.

The RTF algorithm is auto-calibrated and accounts for any combination of concentric pipes without requiring inputs on the steel grade, aging factor or specific completion designs because the steel types can be determined by the product $\mu \cdot \sigma$ of magnetic permeability and electrical conductivity and are output in the modelling process put into a separate data panel. This often allows the recognition of non-standard pipes, such as those of alloy steels that may contain different concentrations of chromium or magnesium.

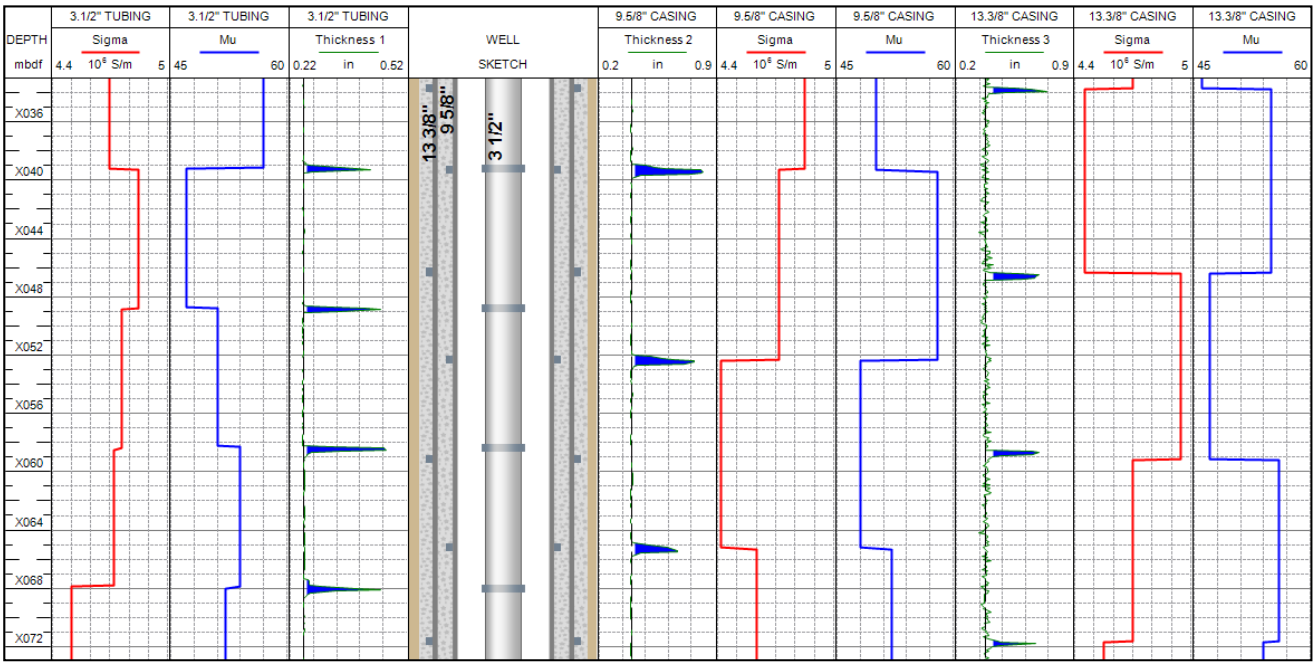

Fig. 1.5.11. The results of numerical modelling for thickness determination. Black dashed lines in the TUBING and CASING columns denote nominal tubing and casing thicknesses, and green solid lines in the Thickness 1, Thickness 2 and Thickness 3 columns denote simulated tubing and casing thicknesses from the MID response. The blue filling indicates the zones in which the simulated thickness is higher than the nominal, and the brown filling indicates the zones in which the thickness is lower than the nominal. Electrical conductivity (σ) and magnetic permeability (μ) in their respective columns are for steel types in each tubing or casing joint.

Pipes may have remanent magnetisation due to the following factors:

- Downhole electrical equipment
- Mechanical stress caused by torsion, bending, etc
- Friction between a drill pipe and a casing during drilling
- Transportation and storage

Remanent magnetisation significantly distorts the recorded signal, especially when the tool speed increases. This distortion can be filtered out because it produces the same effect in each time channel of the tool. At late times, when the eddy current dies out, the signal recorded by the EmPulse tool contains only a background remnant magnetisation signal. The MID simulator automatically filters out this parasitic magnetic signal from the response recorded by the tool.

TECHNOLOGY VERIFICATION BY LABORATORY TESTS

Intensive laboratory tests were conducted to determine how the EmPulse tool responds to various defects in the first, second and third downhole pipe barriers. Such tests can evaluate the quality, sensitivity and reliability of tool sensors and electronics and the technology in general by modelling different well completion designs with various combinations of pipes.

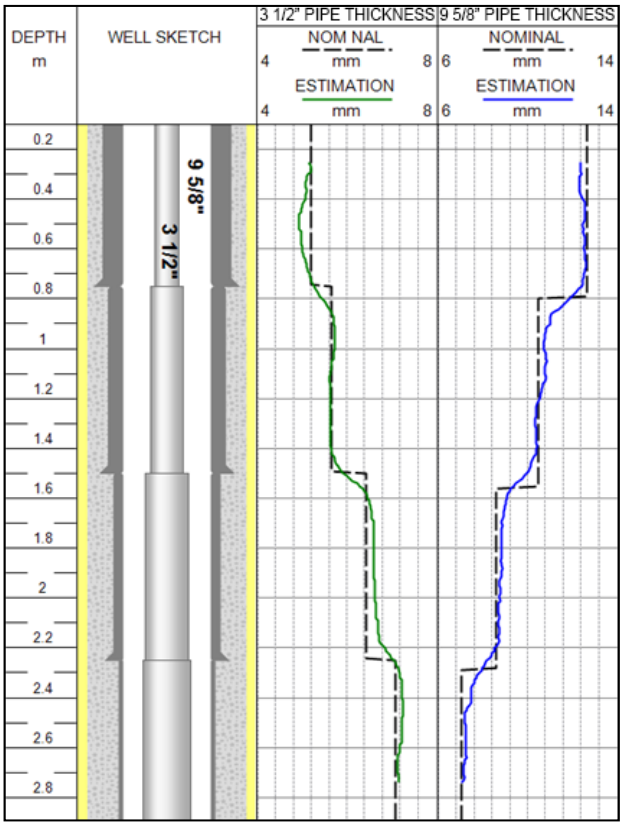

Fig. 1.5.12b. Laboratory test results: inversely-correlated variation of the measured and nominal wall thicknesses of 3-½" and 9-5/8" pipes. The green and blue curves indicate the modelled wall thicknesses of both pipes and take into account their variations in the first barrier that affected the wall thickness calculation for the second one.

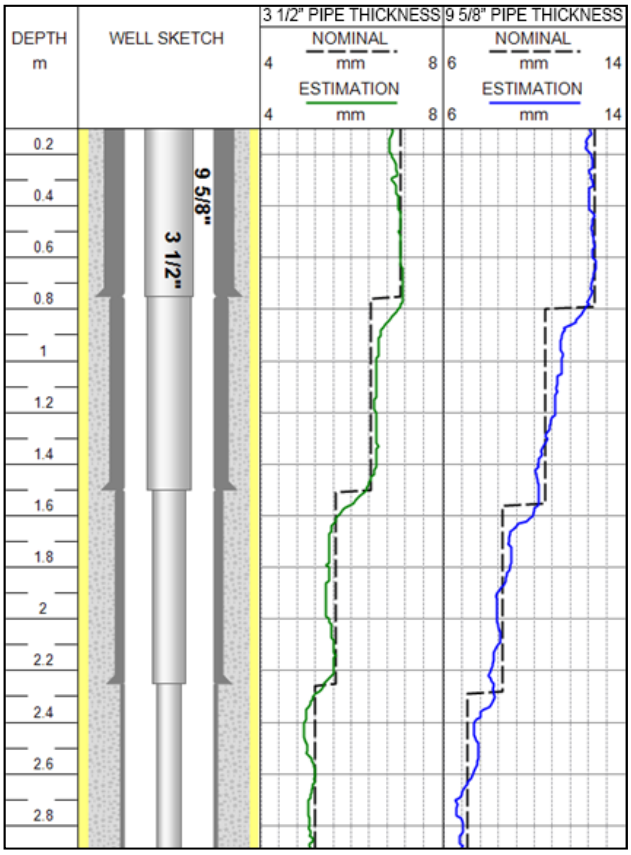

Fig. 1.5.12a. Laboratory test results: measured and nominal wall thicknesses of the first and second pipe barriers, 3-½" and 9-5/8", change in a correlated manner. The green and blue curves indicate the modelled wall thicknesses of both pipes and take into account their variations in the first barrier that affected the wall thickness calculation for the second one.

Test 1. Determination of minimum wall thickness loss for each barrier in a dual-barrier pipe assembly

A laboratory test conducted to determine the tool's sensitivity to minor metal loss in a dual-barrier completion is described below. A dual-barrier system used in the test consisted of 3-½" and 9-5/8" pipes, both 3 metres long and evenly ground circumferentially at 0.75-metre intervals to gradually reduce pipe wall thickness.

Fig. 1.5.12a illustrates a laboratory test using a setup including both pipes (3-½" and 9-5/8"), with thicknesses decreasing with depth in a correlated manner.

Fig. 1.5.12b shows the results of laboratory tests on a system in which the wall thickness of a 3-½" pipe increased as that of a 9-5/8" pipe decreases.The discrepancy between the modelled and actual thicknesses was less than 0.4 *mm* (6%) for the first barrier and less than 0.8 *mm* (8%) for the second one.

Test 2. Quantifying the smallest defect in the third barrier (13-3/8" pipe)

These laboratory tests were conducted to examine the tool's ability to identify defects in the third pipe barrier, which is normally 13-3/8" surface casing, as well as to demonstrate the tool's sensitivity to defects in large-diameter pipes in general and its ability to determine the thicknesses of the first three barriers.

One of the test setup arrangements is described below. The setup included a 3-1/2" pipe, a

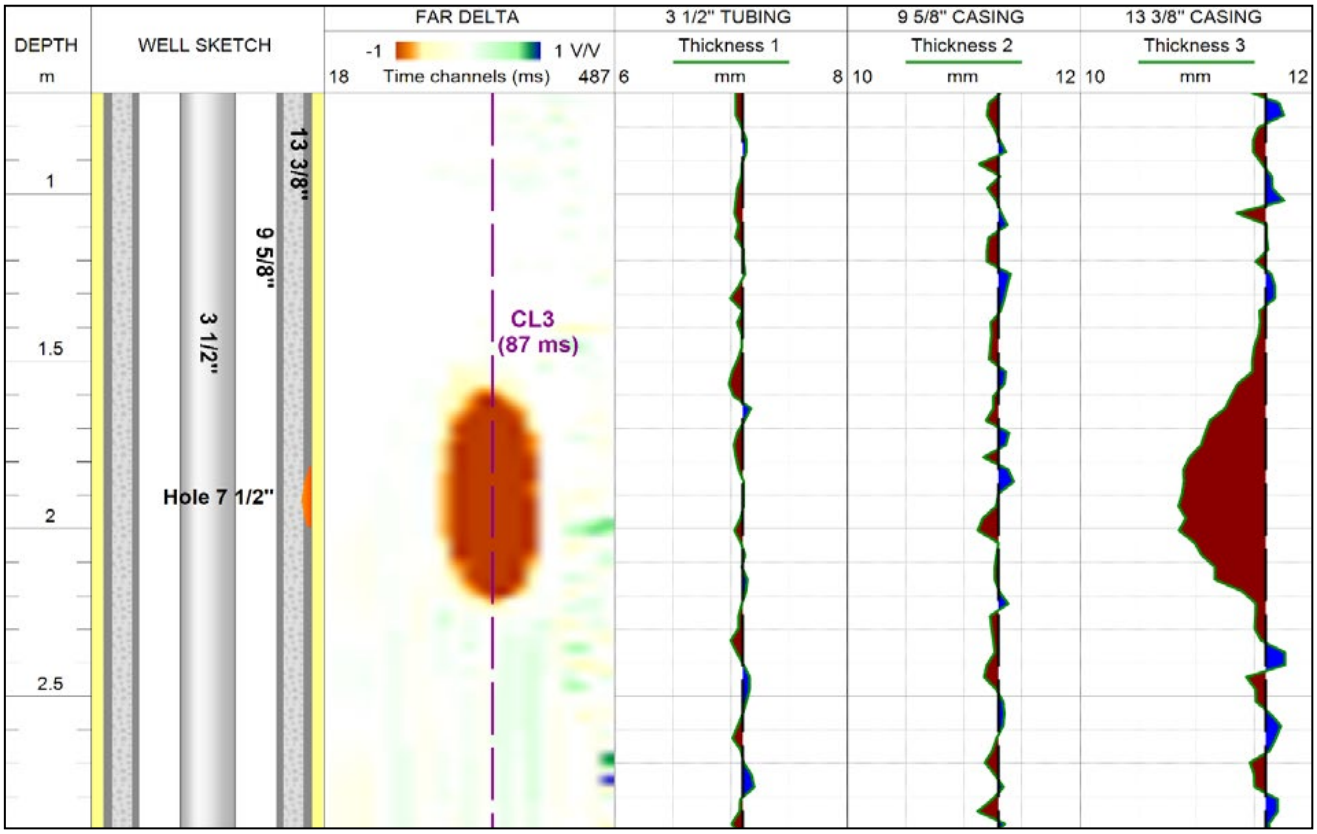

Fig. 1.5.13. EmPulse -3 laboratory test results: a defect detected in the third barrier (13-3/8" pipe) and a defect in the third barrier producing no effect on thickness calculations for the first and second barriers

9-5/8" pipe as an intermediate casing, and a 13-3/8" pipe. A 7-½" hole was drilled in the last casing joint, which is equivalent to a uniform metal loss of 8.8%.

Fig 1.5.13 shows the results of this laboratory test. The modelled wall thickness curve for the 13-3/8" pipe clearly indicates a defect. The metal loss at this defect was calculated at 6.7%. No significant deviations from the first and second barriers' responses were observed in the defect's time interval.

Test 3. Quantifying the smallest defect in a 13-3/8" pipe string in the presence of a 18" pipe string

Another laboratory test was conducted to examine the ability of the EmPulse tool to identify a defect in the second pipe barrier of a three-barrier completion and to calculate the thicknesses of the first three barriers.

The test model consisted of 9-5/8", 13-3/8" and 18" casing joints inserted into one another. A 7-½" hole was made in the 13-3/8" pipe, which is equivalent to a uniform metal loss of 8.8%. The objective was to identify defects in the first three barriers.

Fig. 1.5.14 illustrates the results of this laboratory test. A defect in the second barrier (13-3/8" pipe), clearly identified as considerable metal loss, was calculated at 6.7%.

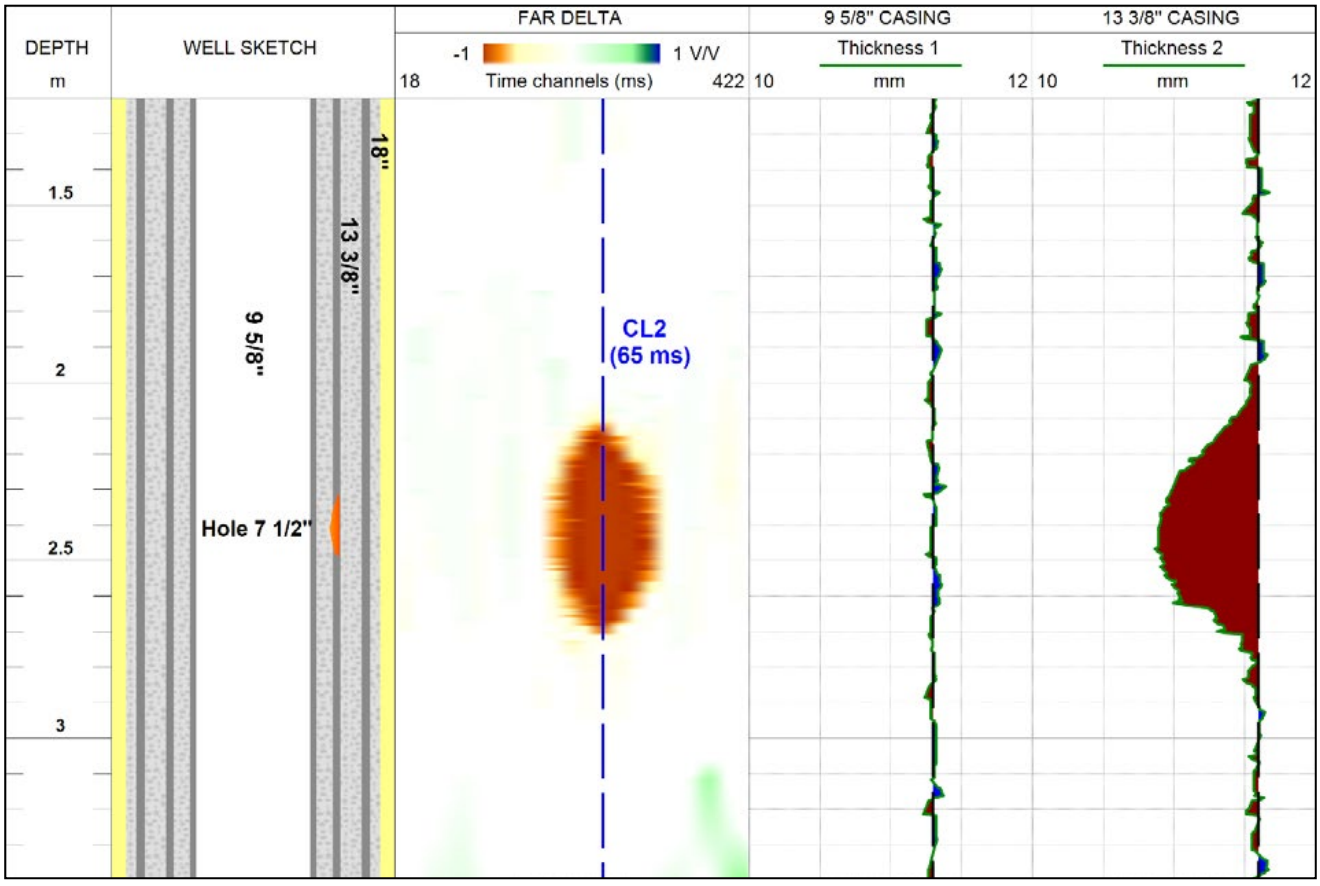

Fig. 1.5.14. EmPulse -3 laboratory test results: (a) A defect made and detected in the second barrier of a triple-barrier setup of 9-5/8", 13-3/8" and 18" pipes

ADVANTAGES AND LIMITATIONS OF THE INDIGO MID TECHNOLOGY

The Indigo MID technology is based on time domain data recording and magnetisation decay modelling providing a cutting-edge advantage in the analysis of multi-barrier structures for accurate evaluation of the effect of pipe wall thickness variations in one barrier on determining the thicknesses of the others.

The Indigo MID technology has the following advantages and limitations.

Advantages:

- **Determination of the individual thicknesses of the first three metal pipe barriers in one run**
  The major advantage of the Indigo MID technology is that deviations from the nominal wall thickness and defects in metal pipes can be detected and quantified for the first, second and third barriers at the same time. As a result, a triple-barrier survey can be completed in a single run, which makes this technology cost and time effective.

- **Deposits present on pipe walls do not affect the accuracy of thickness determination**
  Non - magnetic deposits inside the pipe such as salt or paraffin, fluids or downhole conditions do not produce any effect on the EmPulse tool readings, which saves time on preparing the well for the survey and thus minimises the impact on operations and production.

- **No calibration needed for steel type or completion**
  The survey can be conducted in pipes of unknown steel grades. This advantage makes it possible to conduct the survey in old wells for which completion records are lost or in wells with erroneous completion records.

- **Evaluation of corrosion in stainless steel pipes**
  The survey can also be conducted in corrosion-resistant stainless-steel pipes.

- **Operation in memory or surface read-out mode**
  The EmPulse tool can be run on slickline or in surface read-out (SRO) mode. Depending on client preferences and cable availability, the tool could be adapted to run in both modes, which eliminates logistical problems.

Limitations:

- **Low logging speed**
  The survey has to be conducted at low logging speed to ensure that there is sample time for magnetisation and recording the responses of pipe barriers. However, the slow logging speed reduces the risk of tool sticking in the well and logging cable tangling, and data become more detailed and less prone to errors associated with cable speed. Because of the low logging speed and long survey interval, which is normally the entire wellbore, logging may take up to a day or even more.

- **Cannot distinguish internal from external metal loss**
  The tool records the average response of the tubing without distinguishing internal from external corrosion, and thickness deviations may occur on either inner or outer side of the pipe wall. However, this can be achieved by integrating MID with caliper logging.

- **The defects identified cannot be located azimuthally**
  The current version of EmPulse tool does not locate defects azimuthally but averages the recorded response circumferentially.

- **Time and processing power consuming interpretation**
  The algorithm for thickness modelling is based on time-domain analysis of responses recorded by the tool, and this algorithm is quite complex. For this reason, this technology requires computers with high CPU power ensuring accurate and efficient thickness and metal loss calculations.

2. CASE STUDIES

2.1 ADVANCED BOREHOLE FLOW ANALYSIS

Objectives
Multiphase wellbore flow quantification

Technology
1. Hardware and software tools
- PLT – Production Logging Tool string
- Micro T – High precision temperature sensor
- RFI/RFP Temperature Simulators – temperature modelling software for Radial Flow Injection (RFI) and Radial Flow Production (RFP)

2. Methodology
- Location of injection and inflow zones across perforated intervals
- Evaluation of multiphase and injection flow rates across perforations
- Identification of wellbore cross-flows under shut-in conditions

Criteria for Candidate Selection
1. Wellbore accessibility
2. Premature water/gas breakthrough
3. Anomalously high or low production/ injection performance
4. Poor communication between producers and injectors before/after workover
5. Evaluation of new reservoir treatment techniques

Inputs for Candidate Selection
1. Production History and latest tests for all offset wells
2. Formation tops and perforations for all offset wells

Inputs for Job Proposals
1. Latest production tests
2. Well sketch
3. Formation tops

Inputs for Interpretation and Analysis
Raw logs recorded by TGT

1. Inflow profiling by a mechanical spinner and a salinity and capacitance tool

Example 1 (Model case)

The example below shows how PLT captures the inflow zones across two perforated intervals. Spinner readings show a very good resolution and stability which allows for the identification of a fine-structure inflow profile: one can clearly discern two inflow streaks against the upper perforations.

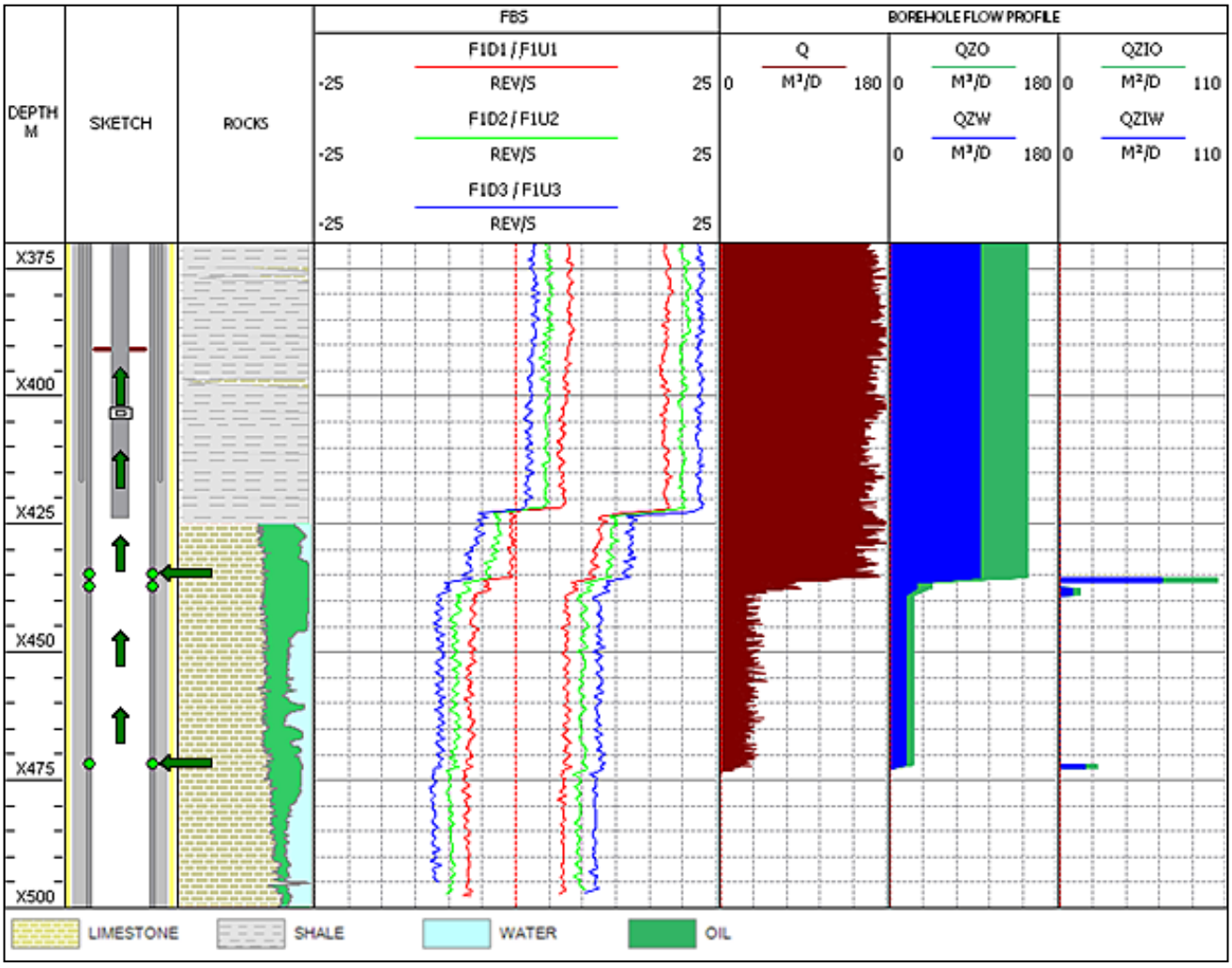

The table below shows a good match between the fullbore spinner and surface test data:

	Oil, *m³/d*	**Water, *m³/d***	**Total, *m³/d***
Surface Test Data	60	96	156
Fullbore Spinner	52	98	150

2. Injectivity profiling by a mechanical spinner

Example 2 (Model case)

This example shows how the fullbore spinner provides a high resolution injection profile. Spinner data shows 5 injection intervals localized within perforated zones.

The table below shows a good match between the fullbore spinner and surface test data:

	Water, *m³/d*
Surface Test Data	183
Fullbore Spinner	190

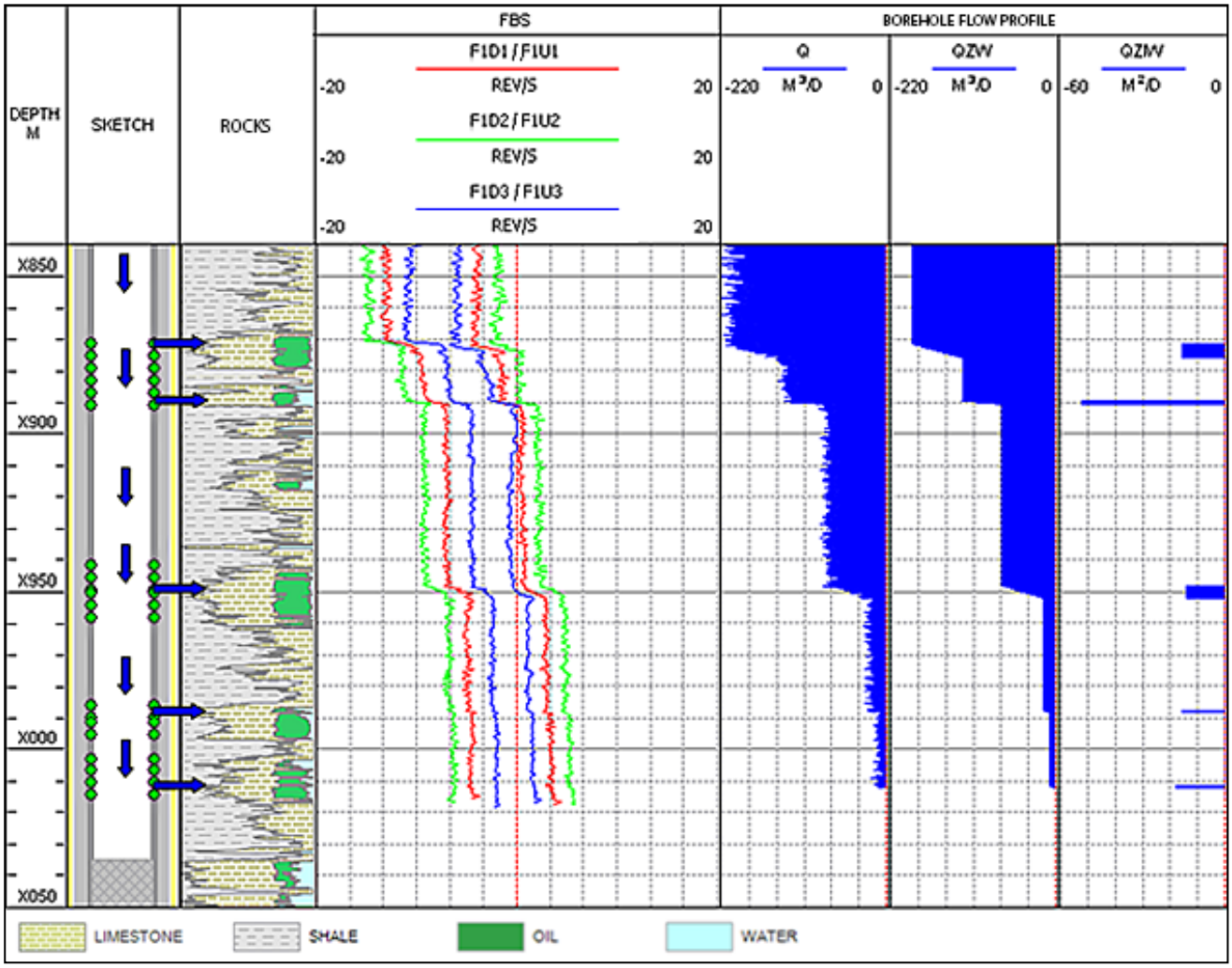

3. Comparison of the injectivity profiles obtained by a mechanical spinner and the HEX tool

Example 1 (Model case)

The example below shows a good match between HEX and spinner profiles. One can see that injection profile QZI_HEX from HEX survey is less noisy than spinner profile and provides better resolution. It clearly shows fine structure of injection units which is missed on spinner.

Injection rates are evaluated through the HEX calibration – similar to the one used in spinner interpretation. The table below shows a good match between HEX and surface test data:

	Water, m^3/d
Surface Test Data	242
HEX	245
Fullbore Spinner	240

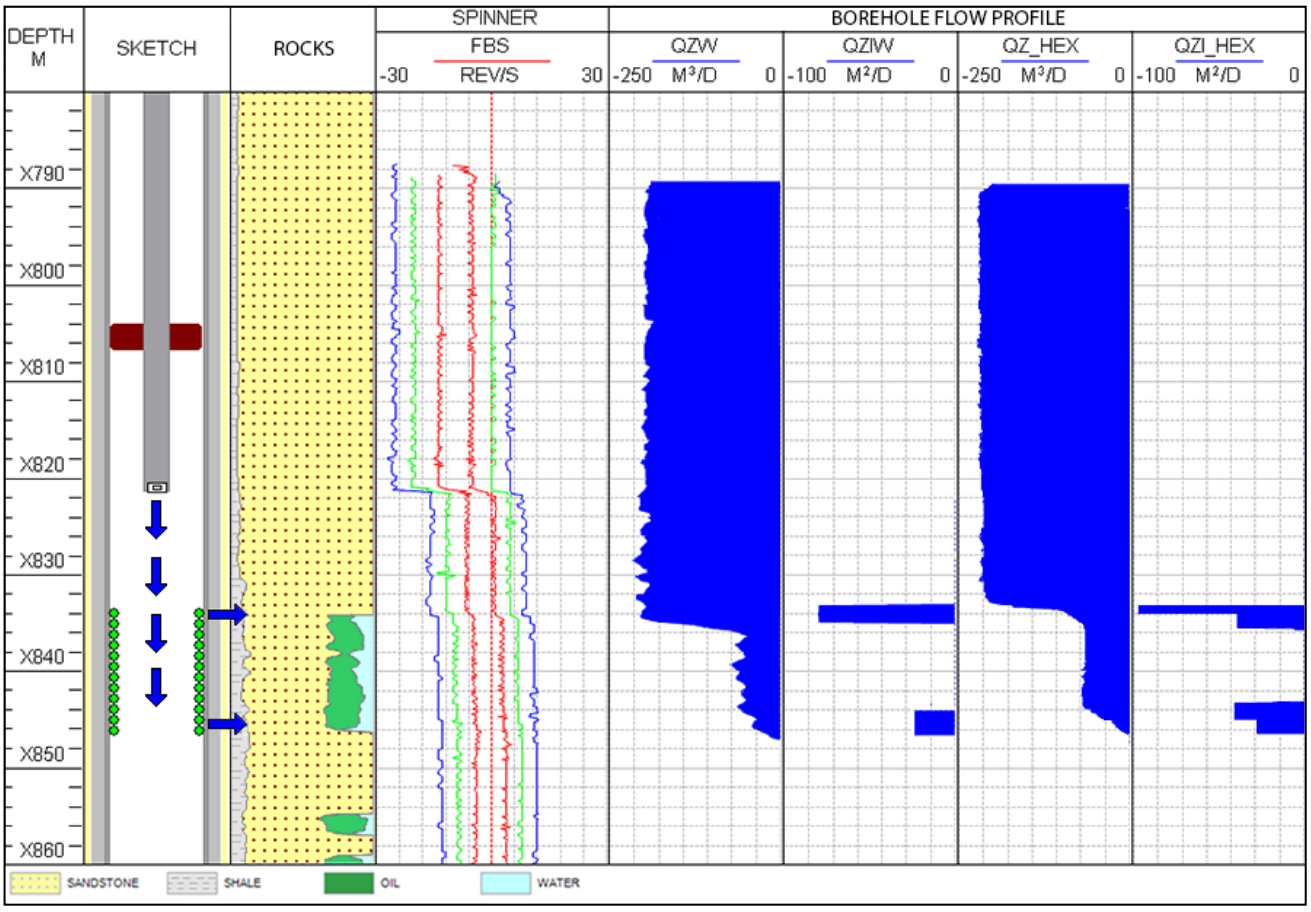

Example 2 (Model case)

The example below shows HEX survey in horizontal well where spinner readings are poor and missing large zones of injection. Spinner has captured only one injection zone which is attributed to the open fracture while the injection into the matrix reservoir was completely missed. HEX survey provides more accurate description of injection scenario and clearly shows the zones of fracture and matrix injection.

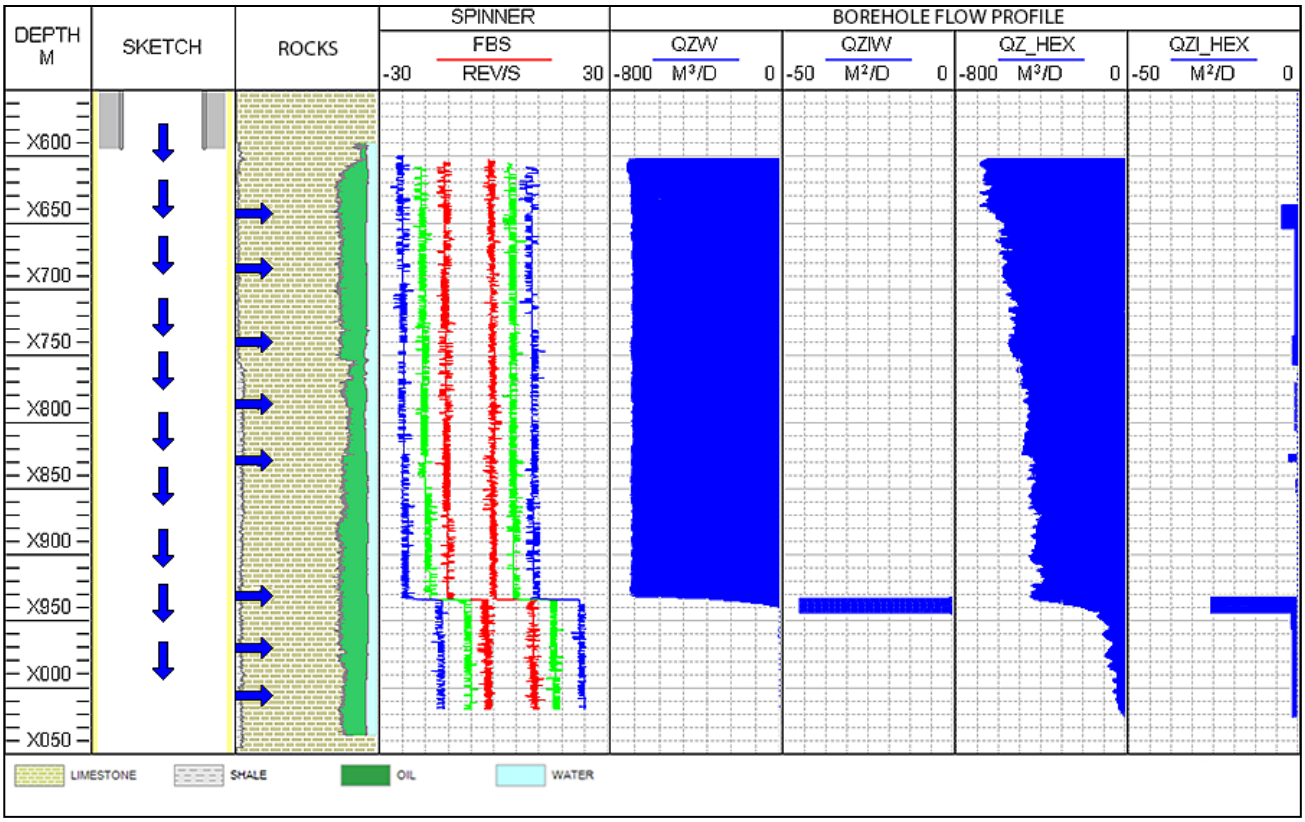

Injection rates are evaluated through HEX calibration. The table below shows a good match between HEX and surface test data:

	Water, *m³/d*
Surface Test Data	680
HEX	672
Fullbore Spinner	700

2.2 SPECTRAL RESERVOIR PLATFORM

Objectives
Quantification of behind-casing/near-wellbore reservoir flow profile with characterisation of matrix/fracture flow contribution

Technology
1. Hardware and software tools
- SNL – Spectral Noise Logging tool
- Micro T – High precision temperature sensor
- RFI/RFP Temperature Simulators – temperature modelling software for Radial Flow Injection (RFI) and Radial Flow Production (RFP)

2. Methodology
- Location of flows behind casing and in the reservoir
- Evaluation of behind-casing/reservoir flow rates
- Characterisation of matrix/fracture flow contribution
- Identification of cross-flows behind casing under shut-in conditions

Criteria for Candidate Selection
1. Wellbore accessibility
2. Availability of conveyance equipment for stationary measurements
3. Premature water/gas breakthrough
4. Anomalously high or low production/ injection performance
5. Poor communication between producers and injectors before/after workover
6. Evaluation of new reservoir treatment techniques

Inputs for Candidate Selection
1. Production history and latest tests for all offset wells
2. Formation tops and perforations for all offset wells

Inputs for Job Proposals
1. Production history and latest tests for selected well
2. Well sketch
3. Formation tops

Inputs for Interpretation and Analysis
1. Raw logs recorded by TGT
2. Open-hole logs in LAS format for lithology, porosity, saturation and permeability

2.2.1 RESERVOIR FLOW ANALYSIS

2.2.1.1 CHANNELLING IDENTIFICATION

Example 1 (Job ID-10046)
This example shows how spinner and SNL profiles are correlated to locate flowing reservoir units, open and closed perforations and cross-flows behind casing in a production well with three permeable perforated intervals (Fig. 1). Spinner data indicated that fluid entered the wellbore from three zones and that the most permeable zone E produced no fluid. SNL indicated two high-amplitude flow units as Zone 1 and Zone 3 of the three production zones identified by spinner data [24].

In the upper production zone (AB), high-amplitude low-frequency noise indicated fluid flow through fractures. SNL-detected features appear slightly above the spinner response in this zone, probably because of fluid cross-flow. Low-frequency noise was detected by SNL also in Zone 2.

Statistically significant SNL-detected inflow zones were identified by wavelet thresholding. Wavelet filtration located one more flowing interval in Zone D of Zone 2 that was not located by spinner data.

Two scenarios could unfold there: (1) The spinner could have failed to detect any flow from the middle perforations due to its limitations; (2) This perforated section could be plugged/damaged and small upflow could occur from this part of the reservoir behind the casing to enter the wellbore through the upper perforations. The quality of the second perforated interval should be checked by magnetic imaging defectoscopy (MID).

The most interesting observation was on production evaluation for the lower perforated section including Zones 3 and 4. According to SNL, a thin streak in Zone 3 was the main source of well production. Open-hole data confirmed the high permeability of this interval. It should be mentioned that this was the only streak that produced fluid mainly through the matrix. The fact that spinner indicated a much thicker

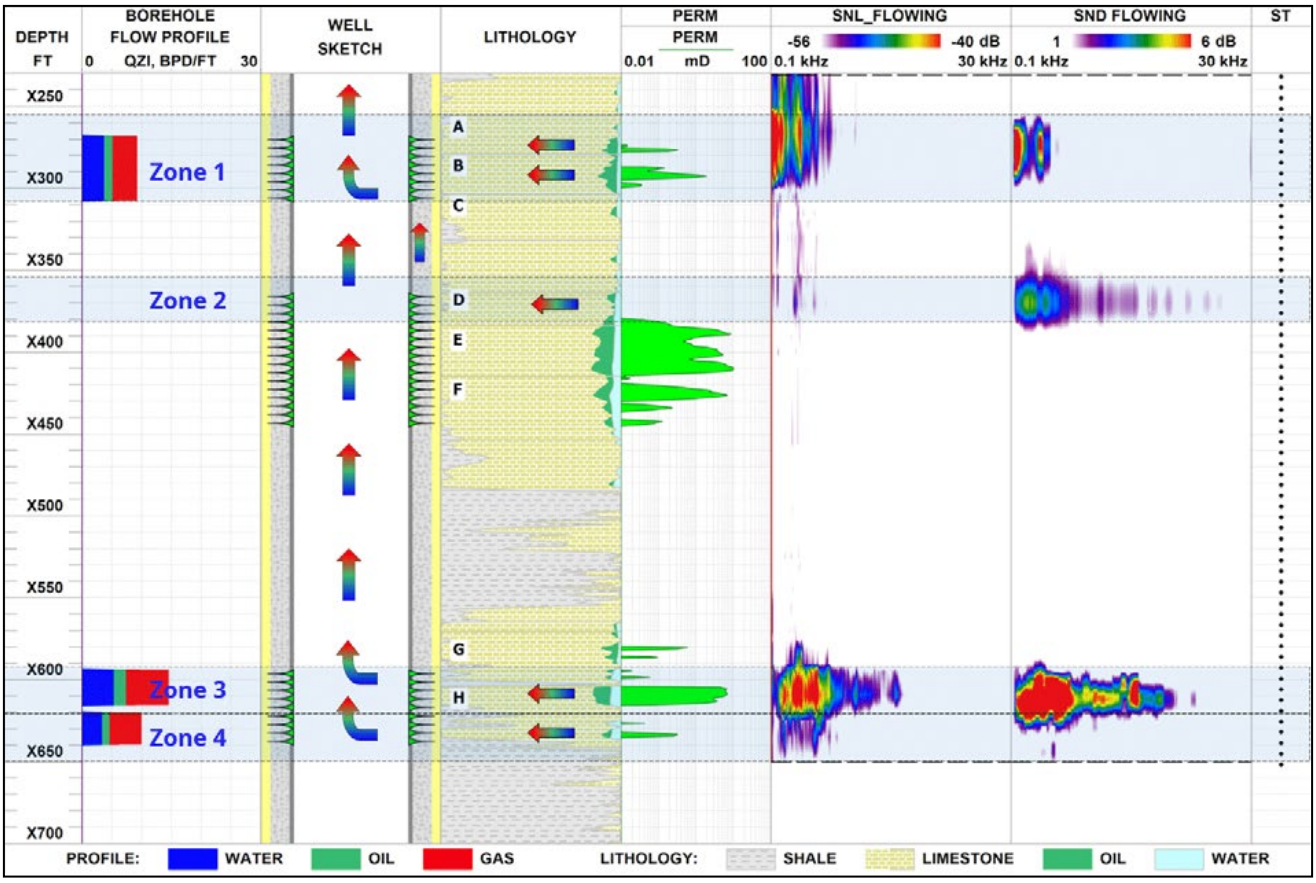

Fig. 1. Inflow profiling and cross-flow detection by spinner and SNL data. Wavelet filtration of SNL data enabled accurate sizing of flow intervals

production interval in Zones 3 and 4 means that the quality of the bottom perforations was goodbut the reservoir was inactive, most probabely due to depletion or scale deposition. Some fluid from Zone 4 entered the wellbore through the lower perforations, most probably due to cross-flow in this well section. This should be taken into account when designing workovers.

On the whole, SNL in a straightforward fashion located flow streaks. These streaks correlate perfectly with the open-hole permeability profile, unlike spinner data which was noisy and less accurate. The comparison of SNL and spinner data gives an idea about cross-flows in Zones 1 and 2 that should also be taken into account in workover planning, as for Zone 4. In this particular case, re-perforation and stimulation of all perforated intervals can be recommended, although the obtained results suggest that selective re-perforation of the middle perforations would bring little reward due to poor cement quality behind the casing and that good cement should thus be restored first.

Example 2 (Job ID-11014)

This well was drilled as a water injector for the B and C reservoirs separated by the C1 seal. Analysis of PLT-HPT-SNL data clearly showed flows in the receiving intervals X253.9–X264.5 mbdf in reservoir B and X276.3–X279.4 mbdf in reservoir C.

SNL enables differentiation between matrix and fracture injections. Low-frequency noise detected by SNL indicated that injection was mainly into fractures, while injection within the narrow interval X279.9–X282.0 mbdf of the C4 reservoir unit occurred into the matrix. This correlates with the open-hole permeability profile.

High-amplitude noise was detected in a wide frequency range, 9–19 *kHz*, within the interval X280.0–X285.0 mbdf. Noises detected during shut-in and injection had equal amplitudes and frequencies. Moreover, the static and flowing temperature curves TS and TF merged into a curve with a temperature lower than geothermal below a depth of X285.0 mbdf. These facts all indicate lateral flow in the well area and suggest that this cooling was caused by water breakthrough from a nearby injector (Fig. 1).

A temperature drop and low-frequency noise were detected above the perforations, which indicated upward cross-flow behind casing from the perforated interval X254–X269 mbdf into the B2 reservoir unit. This low-frequency noise is characteristic of flow through a fracture.

The static temperature curve TSM was simulated to determine the injection profile using the matrix injection model. The deviation of the TSM curve from the static temperature curve indicated fracturing and injection into fractures, as detected by SNL.

A median filter was applied in drift mode to extract low-amplitude noise. As a result, it became apparent that small amounts of fluid were injected into the B2 reservoir unit through the rock matrix and into the B3 unit.

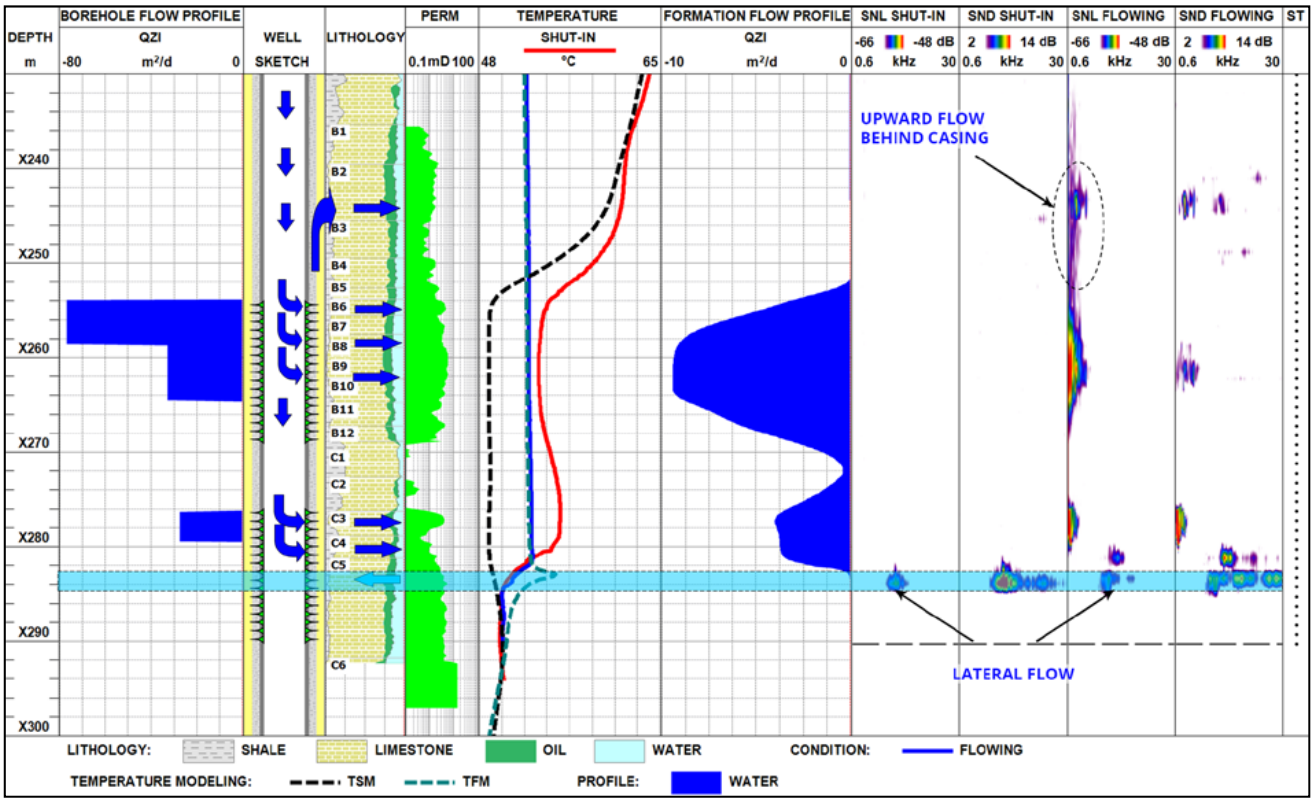

Fig. 1. Identification of water breakthrough from a nearby injection well and upward cross-flow behind casing by integrated PLT, SNL and temperature simulation

Example 3 (Job ID-10025)

This case illustrates the application of integrated high-precision temperature (HPT) logging, Spectral Noise Logging (SNL) and spinner logging (PLT) for constructing historical and current injection profiles and detecting cross-flows behind casing in an onshore injection well.

Flowing PLT data identified two narrow perforated flow intervals (Fig. 2). Temperature and noise surveys were conducted to determine the geometry of injection fluid flow in the reservoir. The static temperature curve showed major cooling relative to the geothermal profile within and above the perforations. The temperature curve has two characteristic cooling peaks. However, a static temperature simulation located the point of maximum water injection not at the point of the maximum cooling, as could be expected, but in the heated intervals of Zone 2 within a cooling background anomaly. This was due to seasonal variations of the injection fluid temperature. This injection well was surveyed in April, while the minimum annual temperature of the injected water was recorded in early January. According to the well history, the highest injection rate was recorded in winter at 230–240 m^3/d (Fig. 1). At that time, intense injection created a reservoir cooling anomaly. Then warm water entered the well, in smaller amounts than in winter, and created local heated zones within

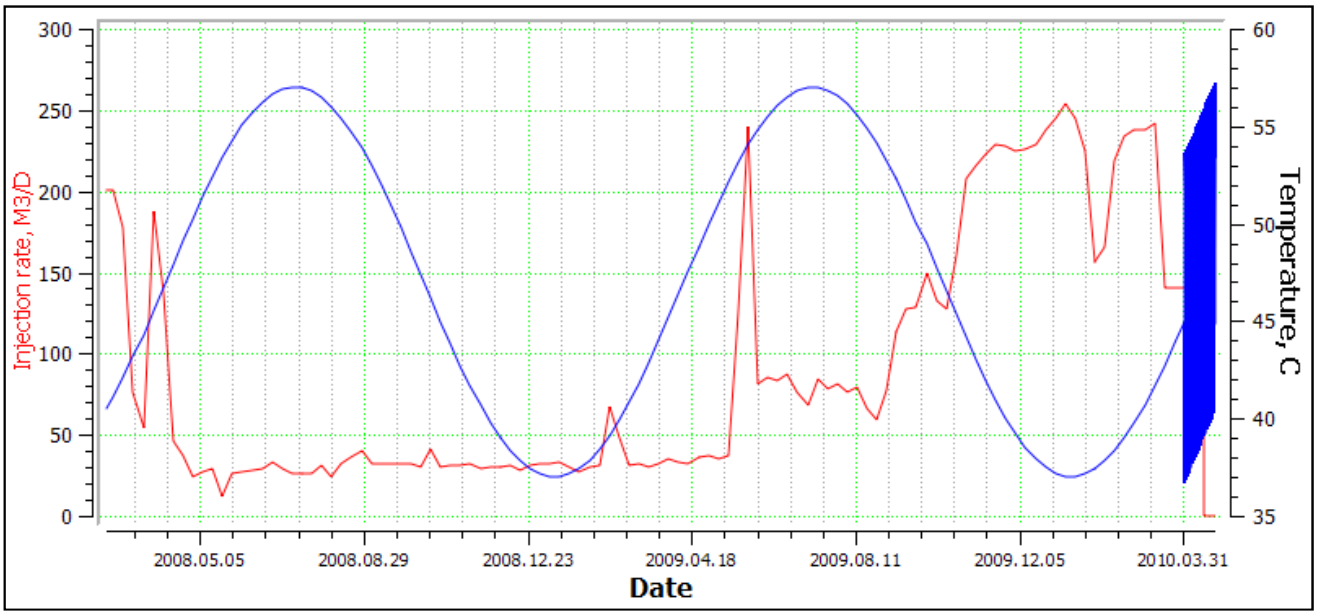

Fig. 1. Injection and temperature history

the general cooling anomaly.

The results of the static temperature simulation were confirmed by flowing SNL. The high-amplitude in Zone 1 was generated by intense water filtration through the reservoir rock matrix. However, the simulated profile indicated a relatively small volume of injected fluid in this interval, which in turn suggested that injection here started recently and is now at its most intense.

Noise with a frequency of less than 5 *kHz* detected in Zone 2 is characteristic of water flow through fractures. The low-frequency 2.5-*kHz* component of the noise signal in this zone was produced by fluid flow behind casing from the perforated interval to Zone 1. In Zone 3, SNL detected low-frequency noise lower than 2 *kHz* generated by the filtration of the injected water through the perforated interval. Low-amplitude 5.6–7.9-*kHz* noise was produced by low water filtration through the rock matrix.

Importantly, the static temperature simulation showed that the injected fluid flowed up the casing annulus into the overlying, unperforated reservoir units of Zones 1 and 2, thus bypassing the target reservoir. Interestingly, open-hole gamma-ray readings increased across the target reservoir. It can be assumed that the increased open-hole gamma-ray readings in the perforated reservoir interval of Zone 3 were due to the deposition of radioactive salts in the near-wellbore zone that probably clogged this interval.

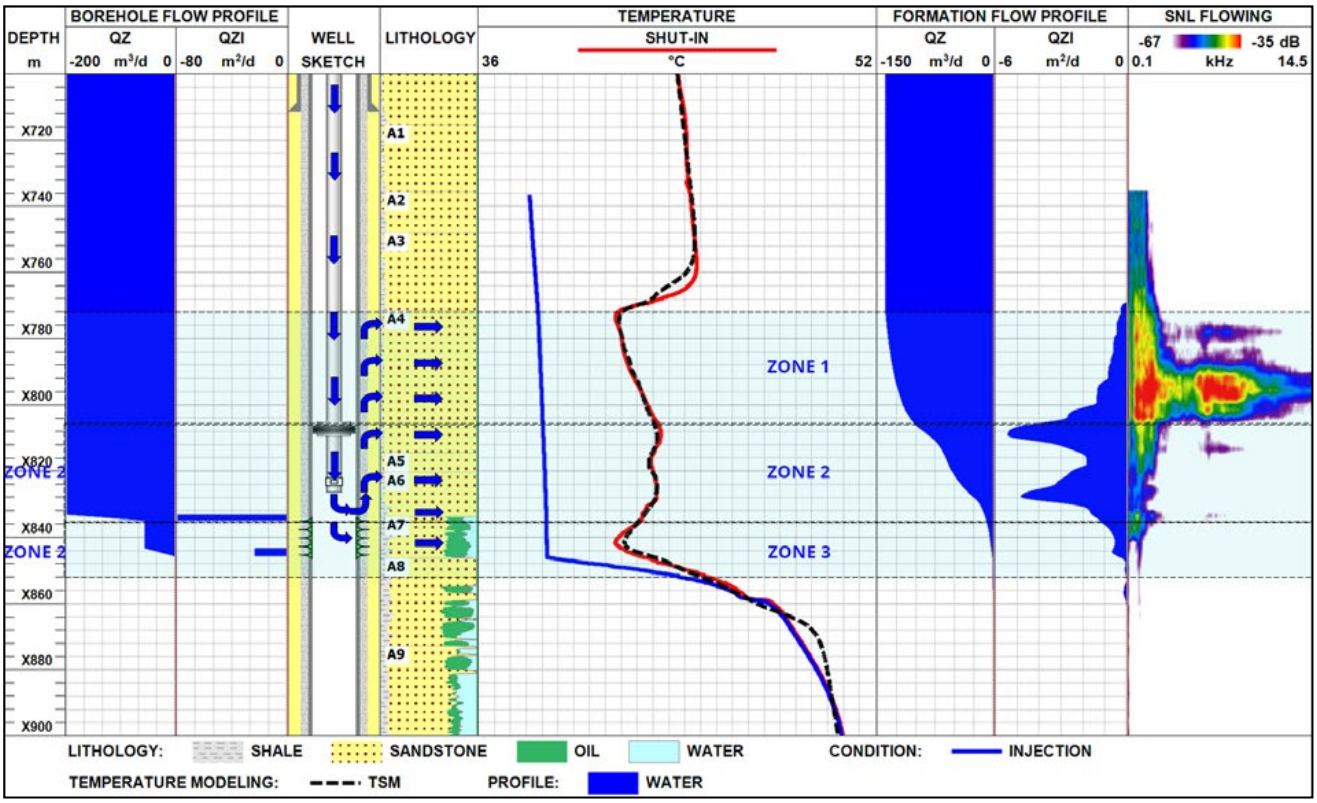

Fig. 2. Detection of cross-flow behind casing by SNL and temperature simulation

Example 4 (Job ID-10048)

The production well WP-1 was drilled in December 1977 for gas-lift production from the carbonaceous reservoir B. In 2008, it was shut-in because of a high water cut of about 80%. In March 2009, the well resumed production.

The well was surveyed to locate the source of water encroachment, construct an inflow profile and determine reservoir saturation. This was undertaken by integrated high-precision temperature logging, spinner logging (flow-rate metering), pulsed neutron-neutron (Sigma) logging and spectral noise logging.

A static high-precision temperature log (red line in Fig. 1) indicated communication between Reservoirs B4 and C1. This was confirmed by a vertical static temperature gradient within the B4–C1 interval. Static noise logging detected intense noise in fluid flow intervals.

Shut-in spinner logging identified downward wellbore cross-flow from a perforated interval of Reservoir B4 to Reservoirs B6, B7 and B9 through perforations and to Reservoir C1, possibly through a casing leak. This cross-flow was caused by unscheduled gas bleed-off less than a day before the survey. As a result, the temperature distribution in the zone of interest could not be accurately assessed.

Flowing high-precision temperature logging detected fluid inflow from both perforated and unperforated intervals. Flowing temperature simulations showed that 45% of the fluid was

produced from the unperforated Reservoir C1. Some fluid entered the wellbore through a casing leak within Reservoir C1, and the rest of it was channelled up into a perforated interval of Reservoir B9. A large difference between the flowing and static temperatures at the very bottom of the survey interval indicated inflow from below it.

The spinner survey failed to measure flow rates within the perforated reservoirs because of their instability.

Sigma logging data were used to identify breakthroughs of saline formation water and characterise residual oil saturation. Increased salinity and water-oil displacement were found in Reservoirs B9 and C1. The slightly increased salinity in Reservoirs B3–B8 was most likely caused by fluid flow behind casing within this interval rather than by water encroachment.

Spectral noise logging ensured the clearest identification of flow intervals, as seen in the SNL_SHUT-IN and SNL_FLOWING panels of Fig. 1. As mentioned above, noise detected under shut-in conditions was most likely generated by gas bleed-off, as indicated by similar noise patterns under shut-in and flowing conditions. The high noise amplitude revealed a large fraction of gas in the well production due to a pressure drop below the bubble point pressure. It was found that the main flow units were represented by the upper one and those below the perforations.

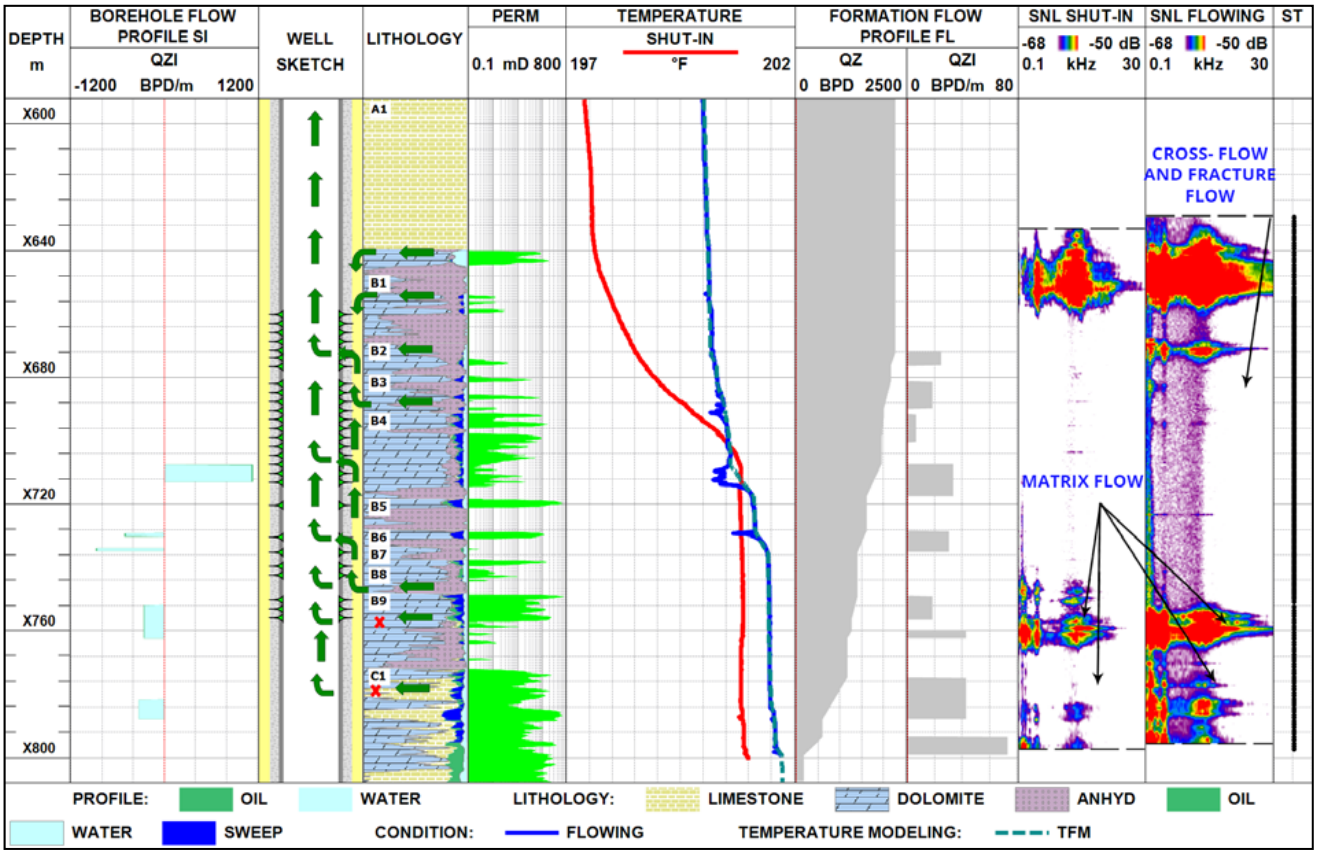

Fig. 1. Flow detection in unperforated reservoir intervals by HPT, PLT, Sigma and SNL

Inflows through the perforations within Reservoirs B3–B8 were mainly caused by cross-flows behind the casing and through fractures from the overlying and underlying formations. Thus, none of the perforated reservoirs under development contributed to the well production. The principal recommendation would therefore be to stimulate and re-perforate Reservoirs B1–B8.

Example 5 (Job ID-11051)

This well, producing from the A reservoir, was surveyed by high-precision temperature (HPT) logging and spinner logging (PLT) to construct behind-casing and wellbore inflow profiles. The survey objective was to identify the source of water encroachment [25].

PLT data indicated that inflow occurred mainly from the middle of the perforated A2 interval. Salinity and water holdup sharply decreased in this interval because of inflow gas. The presence of gas was also indicated by high-amplitude noise, as the production pressure was lower than the bubble-point pressure. It should be noted that the salinity and water holdup data identified some fluid inflow through the middle perforations that was too low to be detected by the flow meter (Fig. 1).

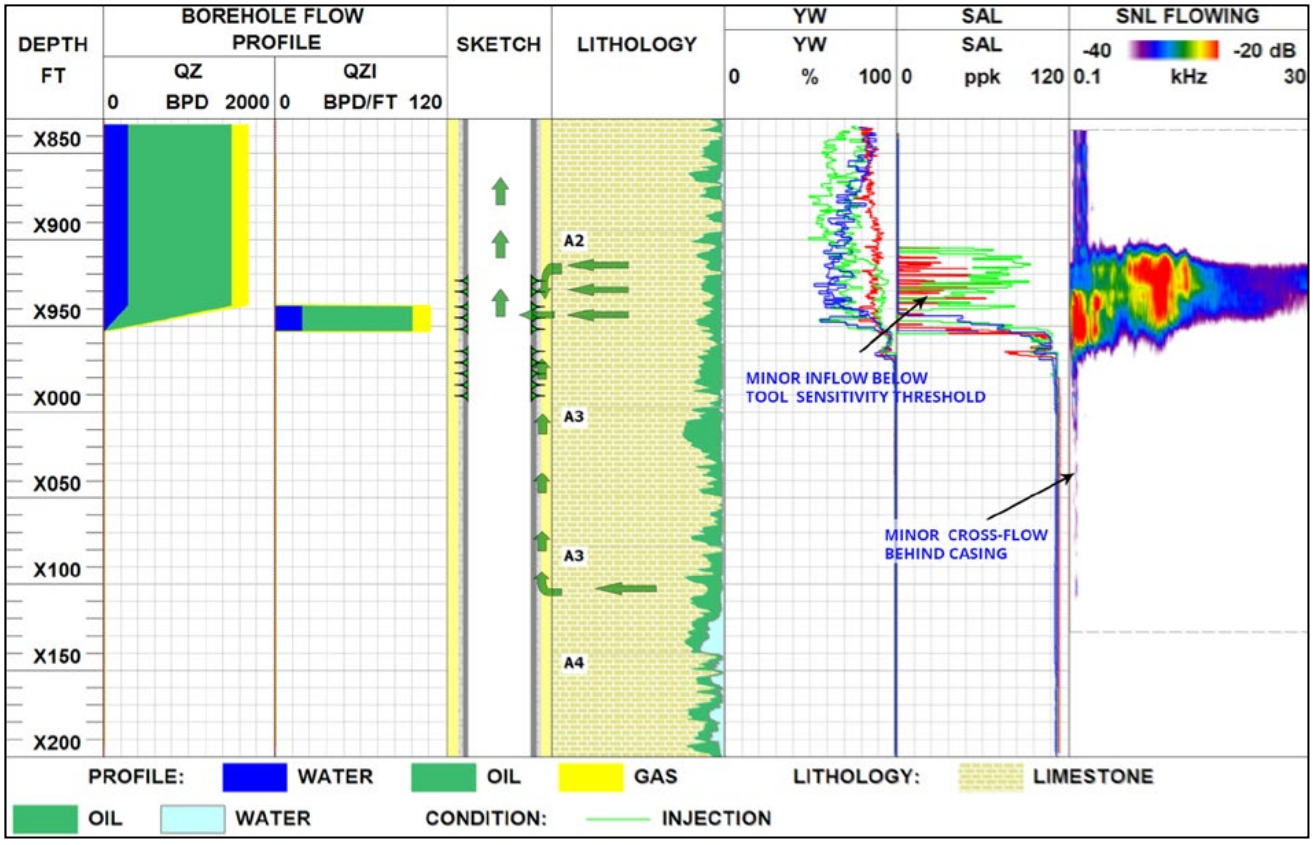

Fig. 1. Identification of upward cross-flow as a source of increased water cut by SNL and multiphase analysis

Noise logging showed that the fluid flowed behind casing both in the middle and in the upper portion of the A2 reservoir. Some fluid entered the perforations behind the casing from above. Ideally for this scenario, magnetic imaging defectoscopy (MID) should be performed to determine the quality of the lower perforations. The poor performance of the upper and lower perforations could also be due to clogging with heavy hydrocarbons. High-frequency noise within the A2 interval indicated that the fluid flowed mainly through the rock matrix, although some fracture noise was also detected within the flowing perforations. In addition, the noise logging tool detected low-frequency noise reaching the perforations from the water-saturated portion of the A4 reservoir below, probably because of upward cross-flow behind casing.

Thus, an integrated analysis of available data delivered the conclusion that water encroachment was caused by cross-flow behind casing from the A4 reservoir.

Example 6 (Job ID-10049)

This case provides a good example of how integrated high-precision temperature (HPT) logging, spectral noise logging (SNL), PLT spinner logging and Sigma logging can be effectively used to detect fluid flow behind casing, flowing through leaking cement, and entering the wellbore through a perforated interval. Initially, the well produced from the bottom of Reservoir C. After 10 years of well operation, the upper portion of Reservoir C (C1 unit) was also put into production and the lower interval was isolated with a cement plug. The well was surveyed to assess its integity and the current condition of producing formations (Fig. 1).

Static spectral noise logging detected no noise generated by producing reservoirs or fluid cross-flows between them. This indicated that the positive static temperature anomaly observed within the perforated interval could be caused by bottom water rise but not by transient wellbore conditions. This assumption was later confirmed by PNN logging data interpretation, as seen in the volumetric model (LITHOLOGY) column of Fig. 1.

The difference between the static and flowing temperatures below the perforated interval was indicative of inflow from below a cement packer, and therefore of its leakage. Spinner logging showed that 65.6% of the well production under flowing conditions came from below the leaking packer.

Spectral noise logging identified a flow zone, Zone 2, within a perforated reservoir section. Fig. 1 shows that noise was also present below the survey interval. Interestingly, numerous fluid flow zones were found in the producing reservoirs A and B above the perforated interval.

Spinner logging indicated two inflow zones across perforations. The upper inflow Zone 1, occurring in the top portion of the perforated interval, yielded most oil. Most probably, oil from the upper producing reservoirs A and B entered the wellbore behind the casing through the upper perforations. This is also evidenced by Sigma logging data indicating that Reservoir C1 of the spinner-detected Zone 1 was flooded during the survey, as shown in blue in the LITHOLOGY column of Fig. 1.

Fluid flow behind casing from the upper unperforated reservoirs A and B entered the wellbore through the upper perforation was clearly illustrated in the transient temperature logs: the temperature within the perforated section was lower than both flowing and static temperatures because of fluid inflow from the upper, colder strata.

It should be noted that SNL data correlated remarkably well with porosity, which as a result can be used to identify narrow flow units of dolomite omitted in the open-hole data interpretation.

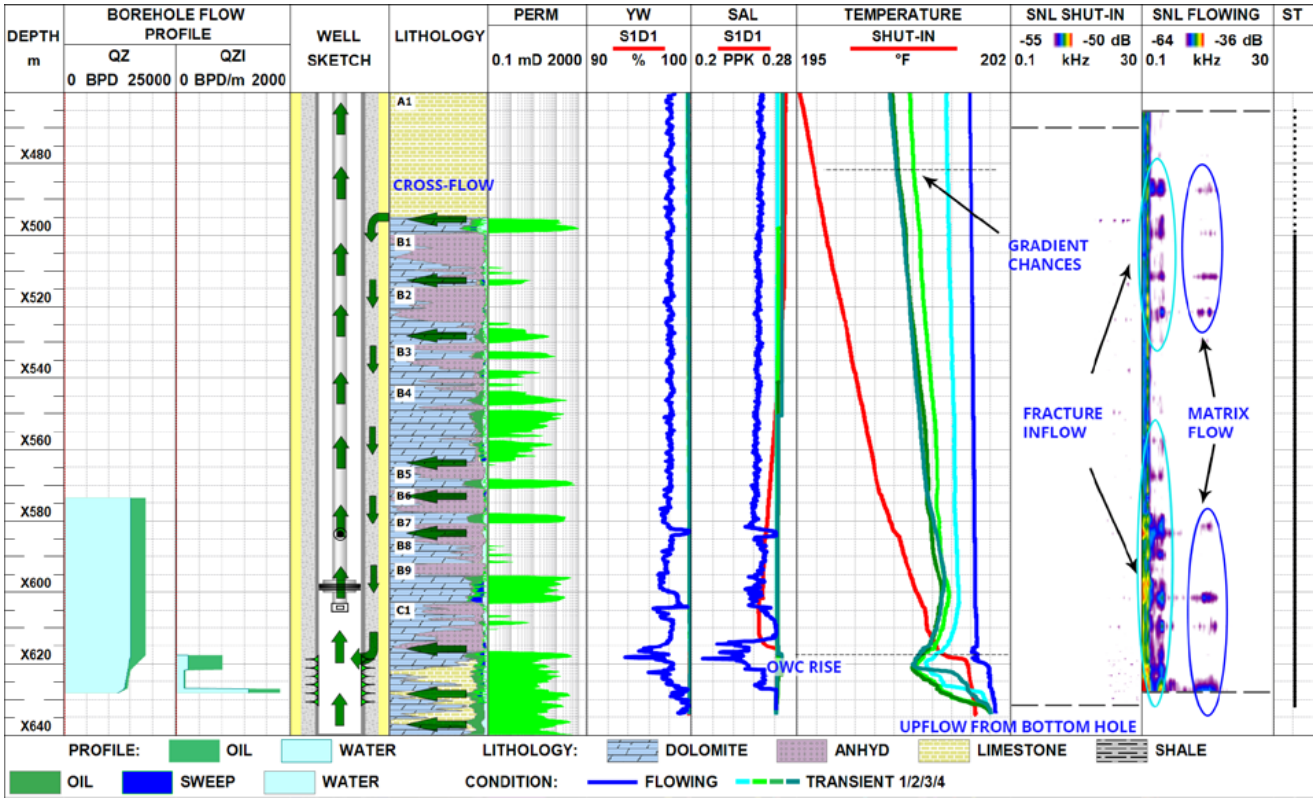

Fig. 1. Detection of fluid channelling behind casing by HPT, PLT, Sigma and SNL

Example 7 (Job ID-14402)

The main objectives of the survey on the given producer well, were to check communication behind casing and quantify the flow distribution across the logged interval.

HPT (High Precision Temperature) – SNL (Spectral Noise Logging) technologies were utilised during the survey. HPT and SNL surveys were conducted under flowing and static conditions. The first HPT-SNL survey was done under shut-in condition. Well was shut-in 3 days before the survey. After that the well was flowing 12 hours and second HPT-SNL survey was performed.

Heating anomaly on temperature curve

recording under flowing condition and high amplitude noise in a wide frequency spectrum indicate inflow of fluid from the formation of A1 and entering into the wellbore through the perforated interval. Moreover, the fluid inflow through the perforated interval is not uniform, the bulk of the fluid supplied to the lower part of the interval.

According to the methods of composition there are no changes in values below perforated interval on shut-in and flowing conditions, indicating the absence of the inflow into the wellbore below perforation. However, the temperature curves recorded on shut-in and flowing conditions did not merge in the sump, and signals with frequency 13.0 *kHz* were detected on SNL FLOWING panel opposite reservoir A3, indicating the inflow from given formation.

In this way, the fluid flows from the reservoir A3 and moves upward behind casing channeling and mixing with the fluid received from the reservoir A1 and exit into the wellbore through the perforated interval.

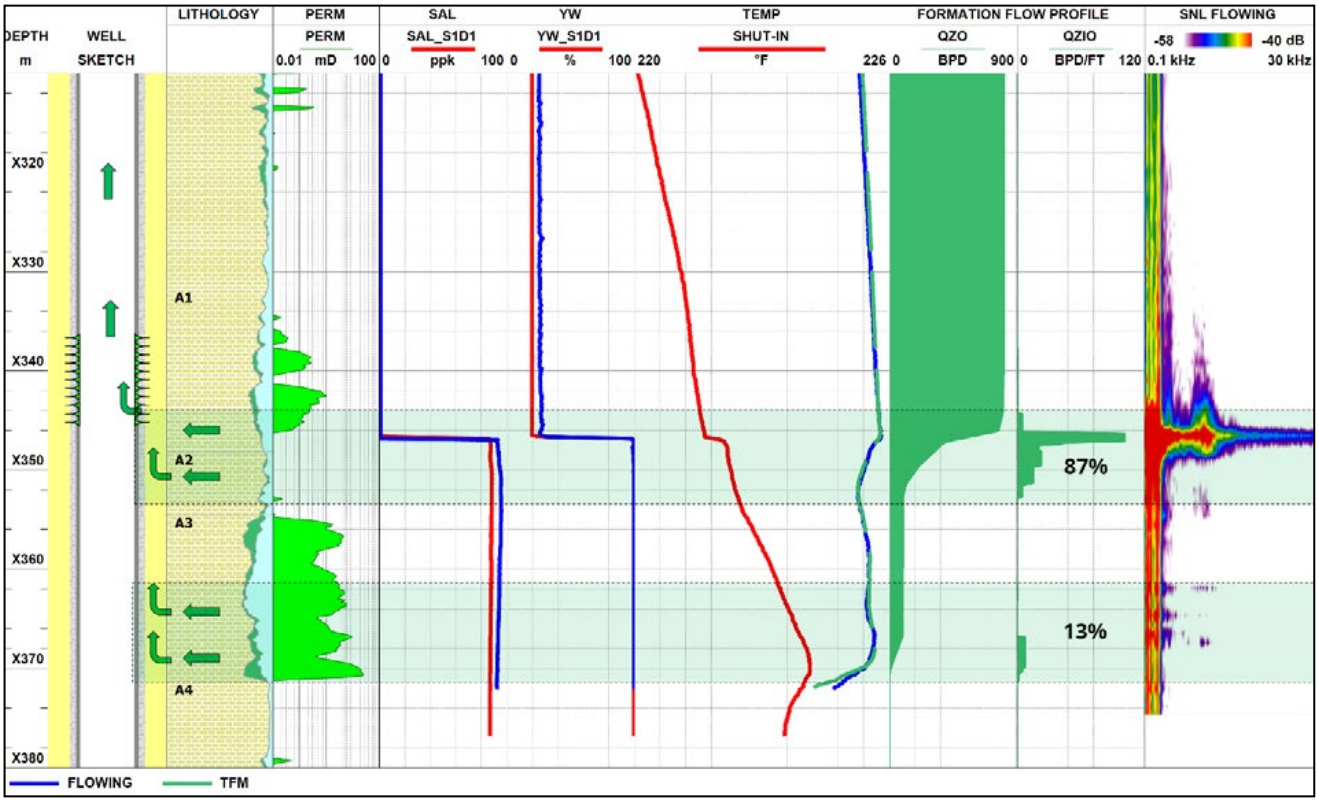

Fig. 1. Channeling Identification

2.2.1.2 LATERAL FLOW IDENTIFICATION

Example 1 (Job ID-11072)

In this well, injection into the D2 and E1 reservoirs, was surveyed by high-precision temperature (HPT) logging, spinner logging (PLT) and Spectral Noise Logging to construct the injection profile and detect cross-flows behind casing and bottom-hole leaks. The static temperature log showed cooling caused by cold fluid injection within the perforated D2 and E1 reservoirs.

The most intense flow of the injected water through perforations was detected by PLT data and a flowing temperature break within D2.

The reservoir-oriented static temperature logging and Spectral Noise Logging techniques also indicated that the injected fluid mainly entered D2: high-amplitude noise was detected during injection in a wide frequency range of 2–16.5 *kHz* and the static temperature curve showed a cooling peak in this reservoir (Fig. 1). Static SNL detected the same 0.8–16.5 *kHz* noise in the D2 reservoir as during injection. It is assumed that this reservoir flowed after injection, as confirmed by the pressure behaviour: the static pressure at the top of the D2 reservoir three days after shut-in was 8.29 MPa, exceeding the initial reservoir pressure by 2.93 MPa. A differential pressure of 10.06 MP, at which the well operated, was apparently off the optimum range. In such a case, the well should be shut-in for a long period of up to a month so that the reservoir pressure in the well area could fall off, and then put in injection mode at lower differential pressure.

Injection flow into the E1 reservoir was detected

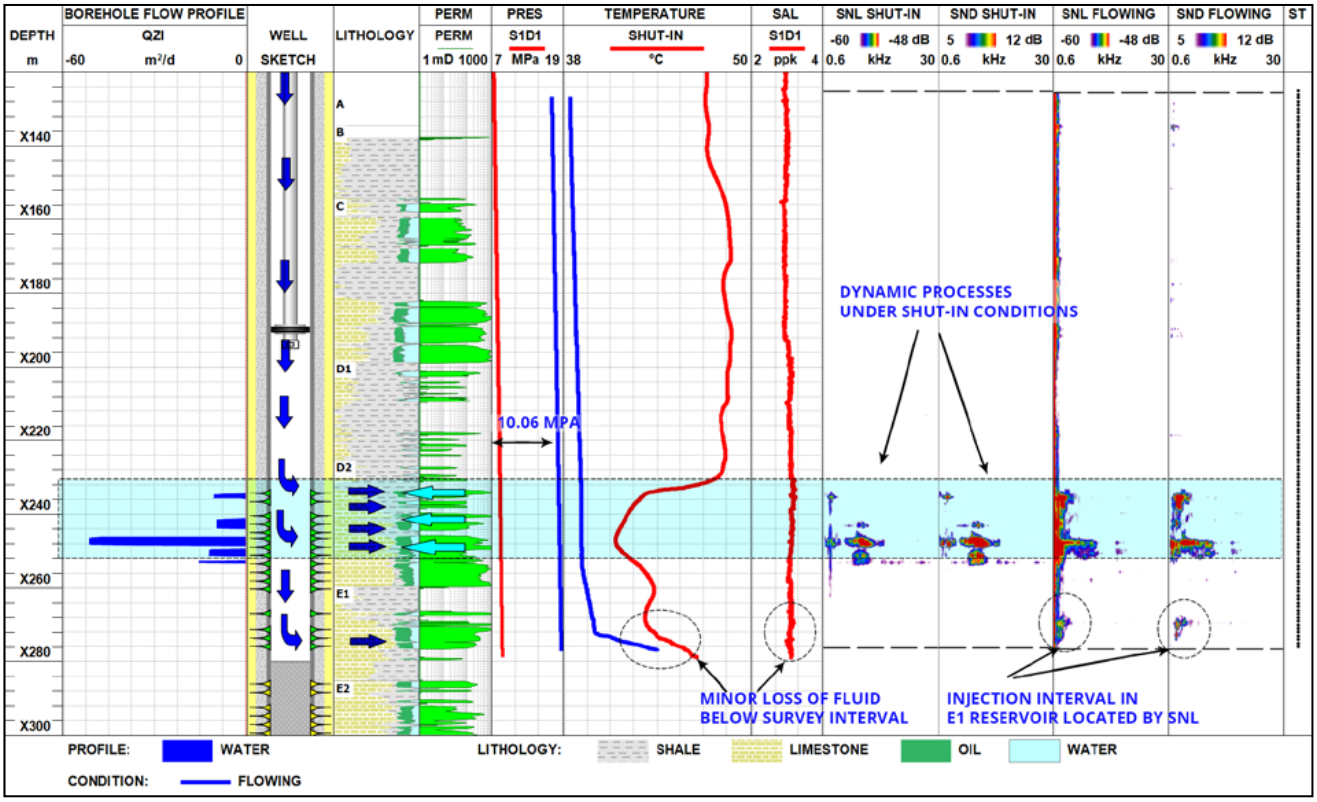

Fig. 1. Location of injection intervals and lateral fluid flows under static conditions by SNL

by 2–5.6 *kHz* noise and a characteristic injection temperature break. The use of a median filter for SNL in drift mode clearly identified injection intervals, in particular the one in the E1 reservoir that was indistinct in raw SNL data.

The facts that the static and flowing temperatures did not merge in the survey interval and that no deposit was found at the bottom hole, as indicated by the static salinity curve, suggest that some injected fluid was lost below the survey interval. However, the calculated PLT profile (middle column) showed no fluid flow below a depth of X254 m. Therefore, the fluid flowed into the E1 reservoir and below the survey interval at a rate that was too low to be detected by the flow meter.

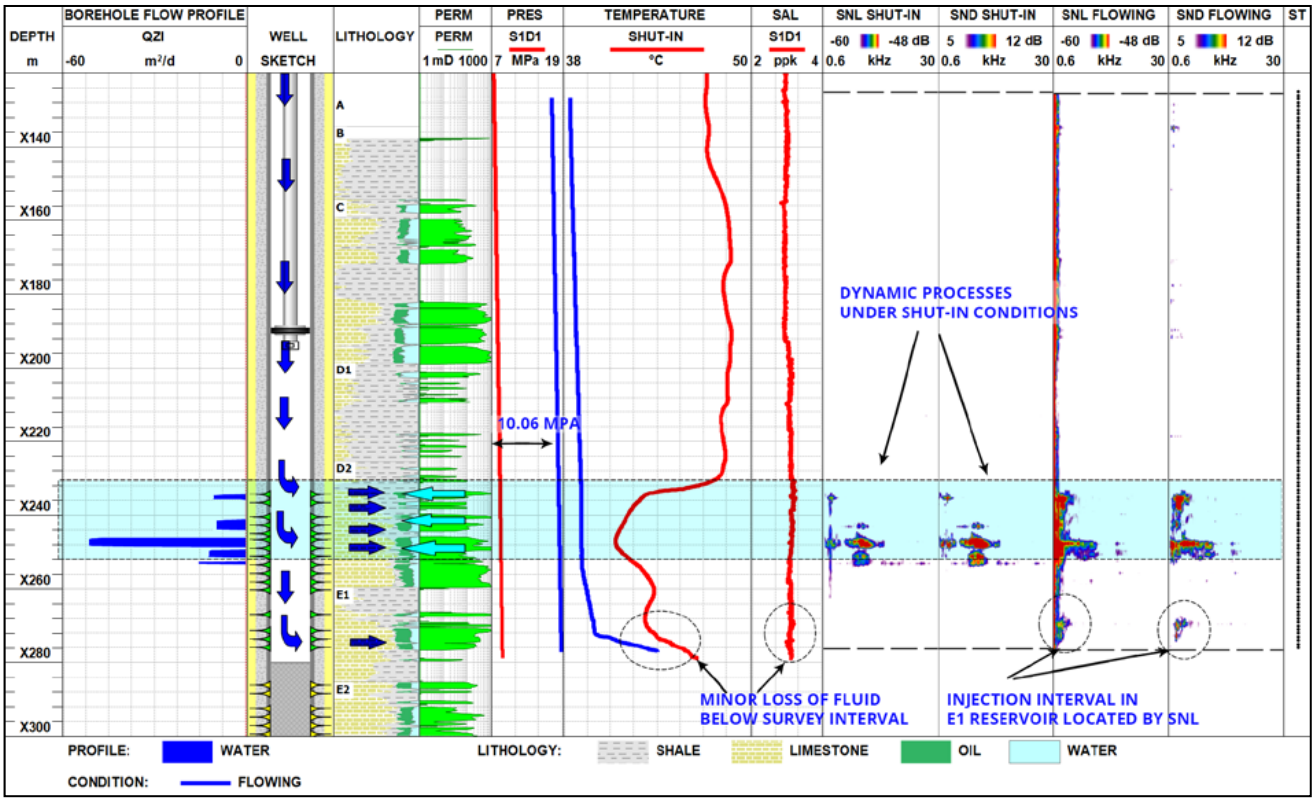

Fig. 1. Location of injection intervals and lateral fluid flows under static conditions by SNL

Example 2 (Job ID-10026)

The deviated well WP-6 was drilled to bottom at the C reservoir sequence in November 1976. In 2006, it was shut-in because of high water cut. The well was surveyed to determine the flow geometry and current oil saturation, and to provide recommendations on additional perforation. This objective was successfully achieved with integrated static high precision temperature (SHPT), Sigma and spectral noise logging (SNL).

In Fig. 1, the geothermal profile is shown in green and measured temperature in red. A positive

measured temperature anomaly detected in the B5 reservoir interval was caused by lateral flow. High-frequency noise detected by SNL was also generated by intense fluid flow through the rock matrix in this zone.

According to Sigma data, the B5 reservoir contained a high-salinity fluid. The sweep profile is shown in blue in a volumetric model (VOL COLUMN in Fig. 1). Moreover, B5 also features high GR values suggesting saline reservoir water flow. Other reservoir units, occurring above the production zone, were apparently unaffected by production processes.

All the above data were taken into account to produce recommendations to sidetrack the upper portion of the B10 reservoir and perforate the B6 and B7 reservoir units. The B5 reservoir was considered unpromising for production in this zone.

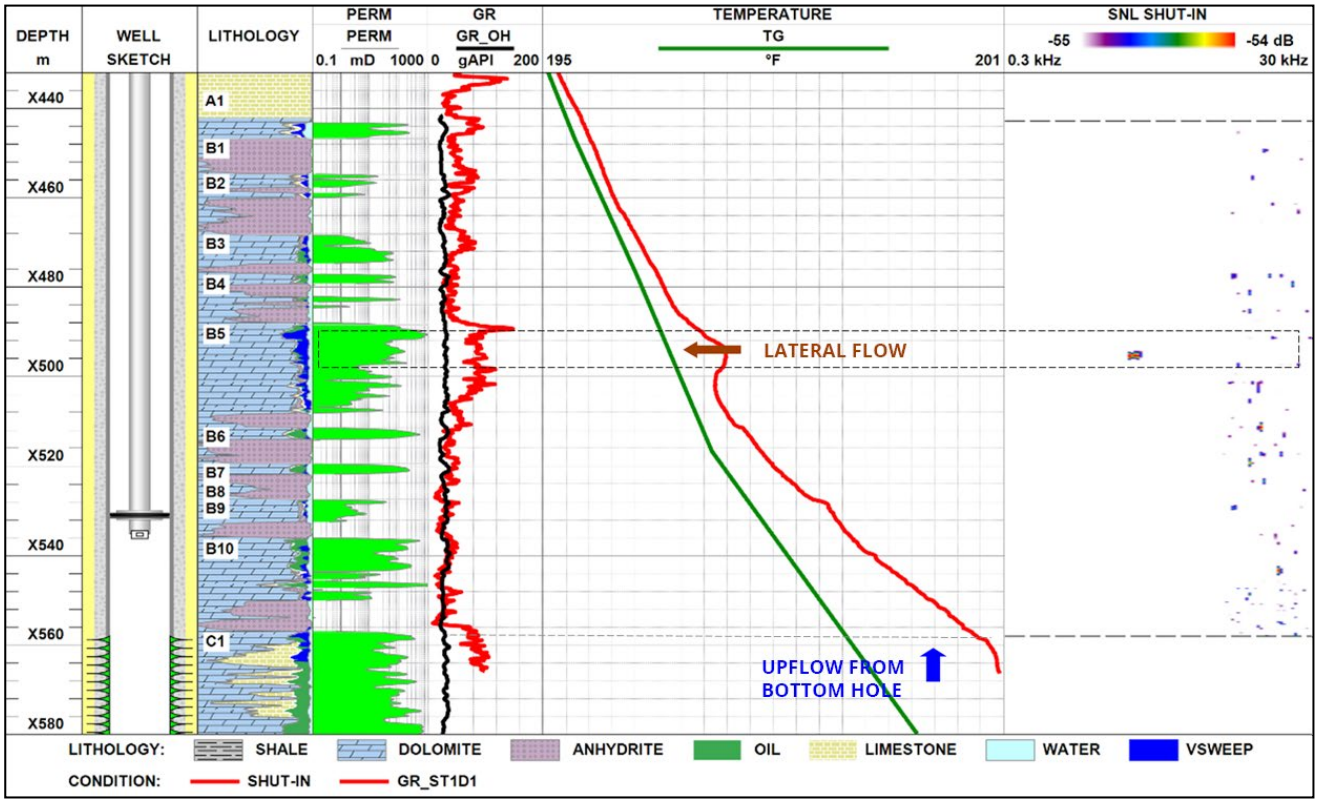

Fig. 1. Geothermal profile of the field, flow geometry and current oil saturation according to integrated HPT-PNN-SNL data

Example 3 (Job ID-12067)

This observation well was surveyed to detect lateral reservoir flows. This objective was achieved by integrating the high-precision temperature (HPT) and spectral noise (SNL) logging techniques.

In the interval between the surface and the zone of interest, the measured static temperature

curve and the geothermal profile coincided. A cooling anomaly was detected in the zone of interest within Zone 1 and Zone 2. The facts that field pressure was maintained by injecting both cold water and gas and that Zone 1 received water while Zone 2 received gas all helped to find the cause of cooling in this observer. It was found that Zone 1 was cooled by water flow from a nearby injector, which was confirmed by a temperature simulation performed to assess its impact. A dense, impermeable unit at the top of Zone 2 and an underlying reservoir were cooled by conductive heat exchange with overlying units of Zone 1. Gas flowing from a gas injector through reservoir units of Zone 2 could also play some role, but heat exchange between the gas and the reservoir is less intense than between the water and the reservoir, and gas breakthroughs could therefore be masked by conductive cooling from Zone 1.

SNL detected low-frequency noise within pay intervals of Zone 1 and Zone 2 and no noise across the dense unit. Therefore, this noise could not be generated by cross-flows behind casing, but was caused by reservoir fluid flows. The presence of low-frequency noise indicated a fracture-flow component in lateral fluid flow, while the absence of high-frequency noise in SNL data indicated that no flow occurred through the rock matrix.

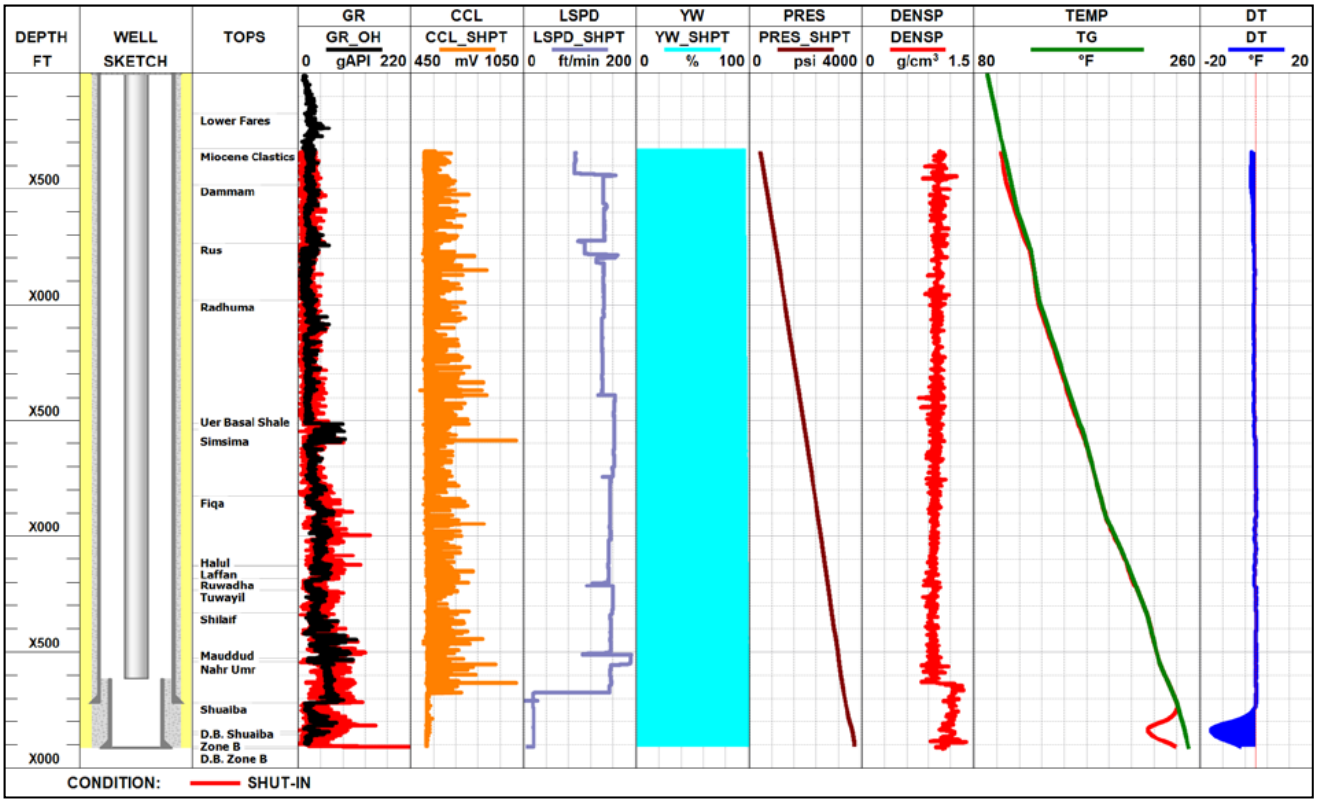

Fig. 1. A static survey of the entire well

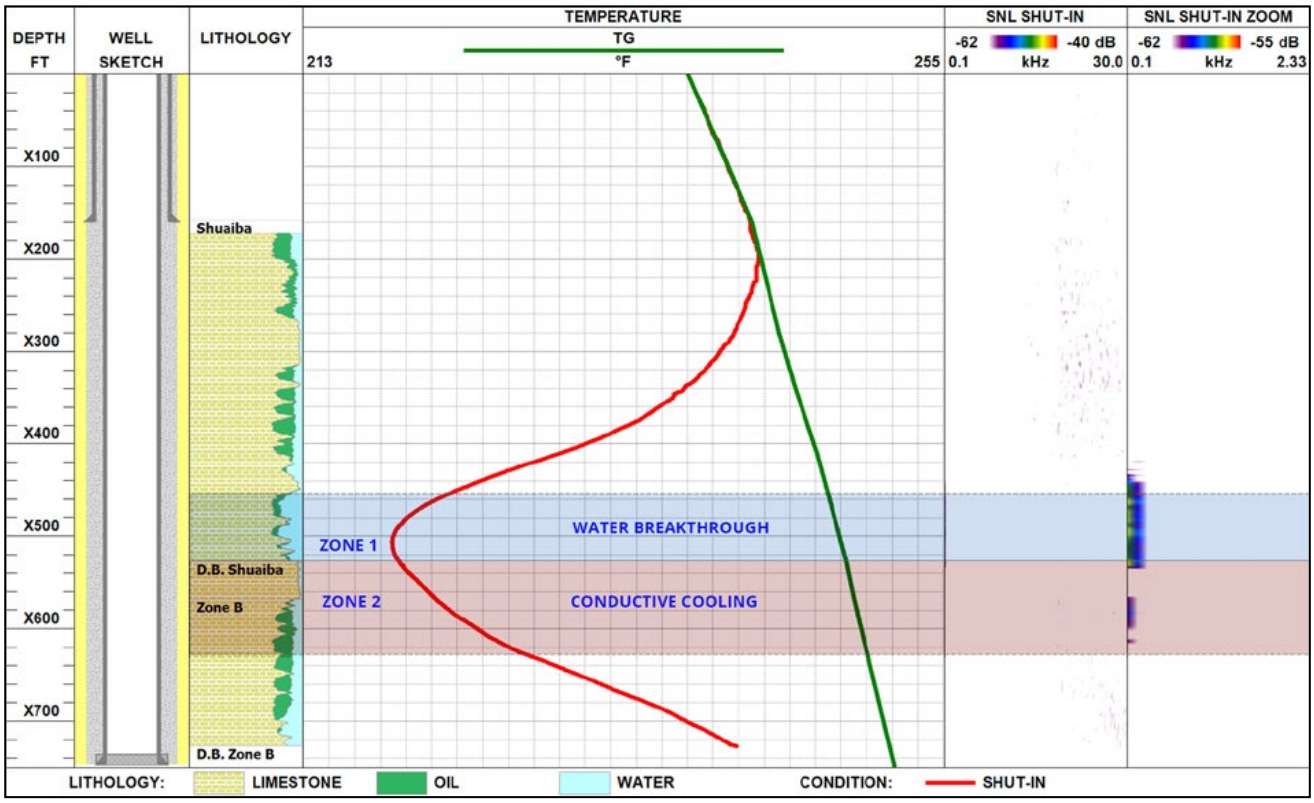

Fig. 2. A static survey of the reservoir interval

2.2.1.3 COMMINGLED PRODUCTION

Example 1 (Job ID-10033)
This case illustrates the application of high-precision temperature (HPT) logging and spectral noise logging (SNL) for locating oil inflows in the perforated deviated and open-hole horizontal sections of the wellbore.

According to client data, the bottom hole was at a depth of X785 ft and the total length of the open-hole horizontal section was X108 ft, the unsurveyed distance being 30 ft.

The static temperature was higher than the geothermal because of the rise of hot fluid from the lower portion of the reservoir towards the wellbore. The flowing temperature did not tend towards the static temperature at the end of the survey interval, which indicated inflow below this depth. A flowing temperature simulation showed that about 7% of the total inflow came from below the tool hold-up depth (Fig. 1), while almost a third of the total oil inflow entered the wellbore within the open-hole survey interval. SNL detected narrow intervals of low and medium frequency noise below 5 *kHz*, characteristic of fluid filtration through faults and fractures.

According to seismic data, the top of the E1 reservoir unit is crossed by a fault (Fig. 2).

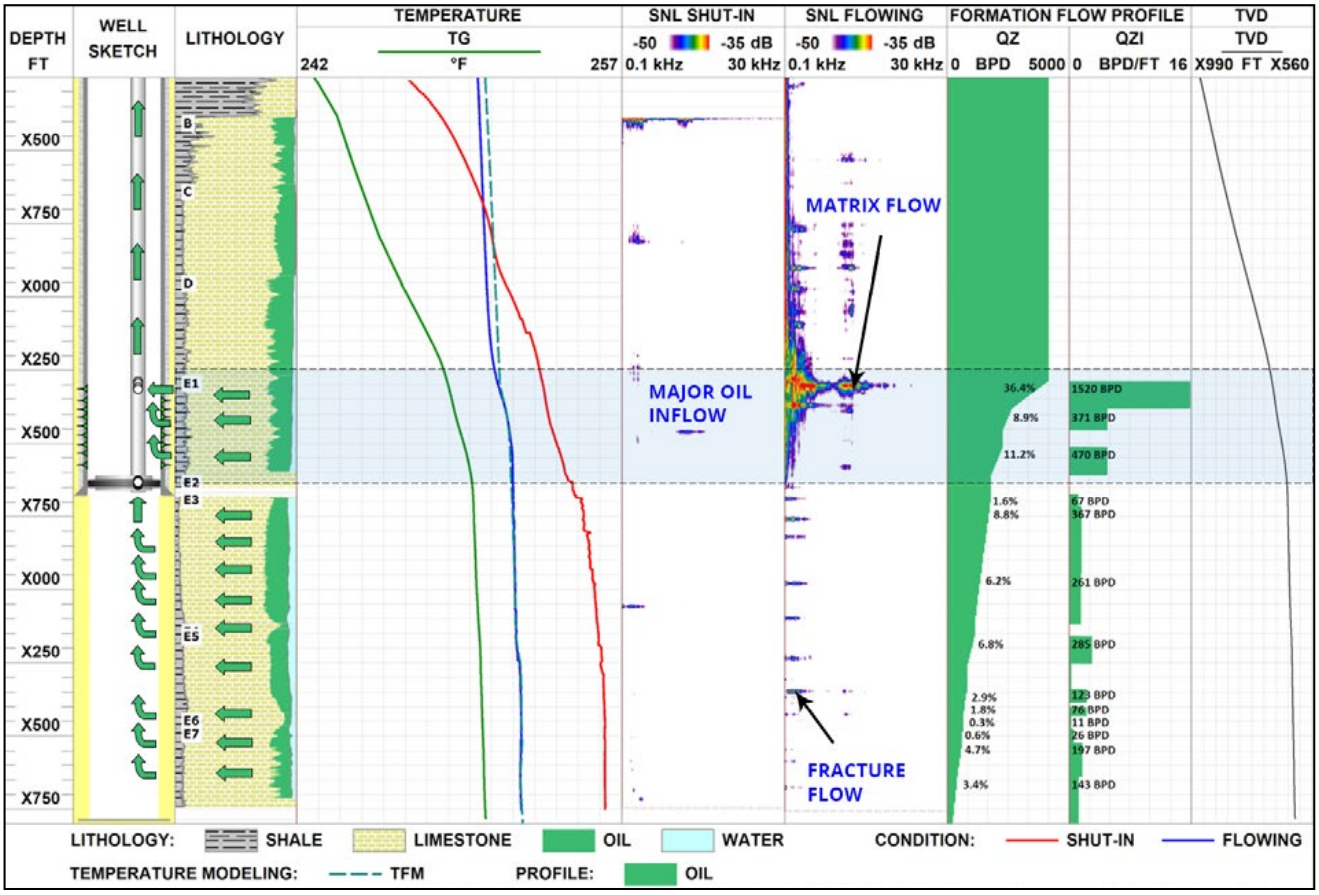

However, flowing SNL detected a thin 20-*kHz* noise streak within the top of E1 that widened as the noise frequency decreased. This noise pattern was generated by oil filtration through a fault, although the high-frequency portion of the noise suggested fluid flow through a porous reservoir. Most probably, the fluid initially flowed through the fault and then entered the rock matrix. The temperature simulation showed that the E1 reservoir unit produced about two-thirds of the total oil inflow. It can thus be concluded that oil entered the wellbore mainly through the fault and fault-related fractures.

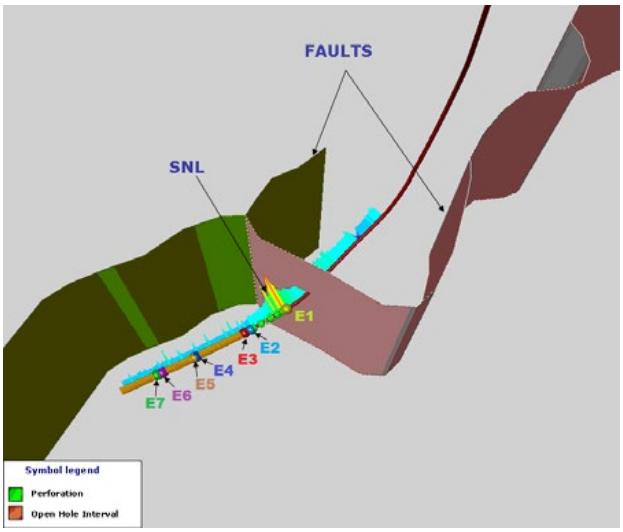

Fig. 2. A fault crossing the wellbore in a 3D model

2.2.1.4 DUAL-STRING COMPLETIONS

Example 1 (Job ID-11058)

This case presents a deviated dual-string well selectively producing from the reservoir units A2 and B through long and short tubing, respectively. All measurements were made in the long tubing string and the A1–A3 interval was therefore logged through a barrier, being the tubing. In this particular case, all conventional techniques—the spinner, multiphase sensors, pressure gauge, etc.—failed to determine an inflow profile. This objective was achieved by integrated high-precision temperature and spectral noise logging (HPT-SNL) [25].

Analysis of SNL data identified reservoir intervals with fluid flows: Zone 1 and Zone 2. According to the noise frequency distribution, most of the fluid was produced through fractures generating 1–1.3 *kHz* noise. Some fluid flowed through the matrix, as indicated by slight 1.7–2.0 *kHz* noise.

The A2 reservoir unit produced through two perforated intervals. However, low-frequency noise recorded within the unperforated A1 reservoir unit and some portion of A2 indicated downflow behind casing from these units that significantly contributed to overall production. Noise generated by another behind-casing flow was detected in the top portion of the unperforated A3 reservoir unit (Fig. 1).

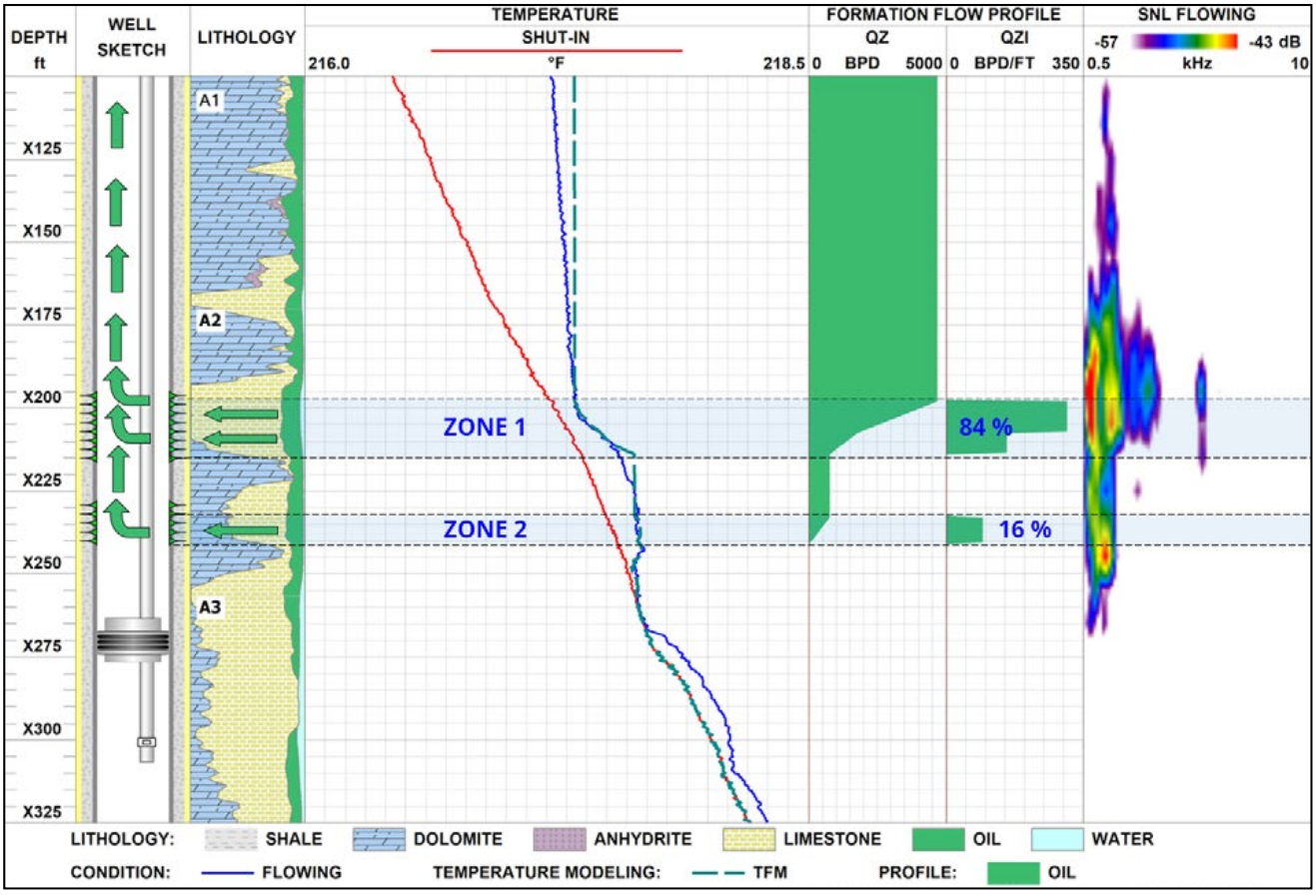

Fig. 1. Identification of inflow intervals behind tubing by temperature simulation and SNL

A production profile was constructed using the temperature simulator. The simulation results showed that the main inflow through the short string (84%) occurred within the upper perforated interval. The lower perforated interval had only minor flow. Thus, the simulated production profile based on temperature measurements correlated with the SNL noise distribution.

Analysis of reservoir fluid at the surface indicated that the gas-oil ratio did not change throughout the production process, which indirectly meant that the pressure in the upper reservoir units was still above the bubble point pressure. This was confirmed by low-amplitude noise recorded by SNL.

The deviation between the static and flowing temperatures below the packer was due to production from the underlying reservoirs through the long string.

Example 2 (Job ID-12035)

This case is an illustration of inflow profiling of a horizontal dual-string production well achieved by integrated High-Precision Temperature and Spectral Noise Logging (HPT-SNL).

The well selectively produced from the A2, A3 and A4 reservoirs through a Short String (SS) and from A6 through Long String (LS). The Long String produced from the horizontal wellbore section. All measurements, including those in the A2–A5 interval, were made in the Long String.

Shut-in survey

A combined analysis of High Precision Temperature and Spectral Noise Logging data identified no intervals with increased noise associated with fluid flow.

Production through the short string

A combined analysis of High Precision Temperature and Spectral Noise Logging data revealed the following:

1. The flowing intervals of A3 and A4 reservoirs were identified. A high-intensity, wide-ranging 0.1 – 30 *kHz* SNL signal and a cooling anomaly were detected by high-precision temperature logging (HPT) under shut-in well conditions during SS inflow indicated free gas.
2. Intervals of inflow through A5 reservoir with upward fluid flow behind casing and subsequent entry into the wellbore at the bottom of the A4 reservoir. High-amplitude 0.1 – 5.1 *kHz* acoustical noise within the A5 reservoir interval indicated fluid flow behind casing.

Spectral Noise Logging detected a 0.4–7.5 *kHz* signal in A5 reservoir. The signal amplitude in Zone 3 was much lower than in Zone 1 or Zone 2. In addition, the F1D1 high-precision temperature curve showed a heating anomaly in the A5 reservoir. The above phenomena suggested the absence of free gas from the A5 reservoir.

Above Zone 1, SNL detected a high-amplitude, low-frequency signal generated by upward wellbore fluid flow. According to temperature modelling, as much as 91 percent of fluid inflow occurred between A3 and A4 reservoirs. Inflow from lower A5 reservoir was small and fluids from A3 and A4 reservoirs had high free gas content. The modelled profile matched the interpreted SNL data (Fig. 1).

Production through the long string

A combined analysis of High Precision Temperature and Spectral Noise Logging data identified inflow intervals for the A6 reservoir

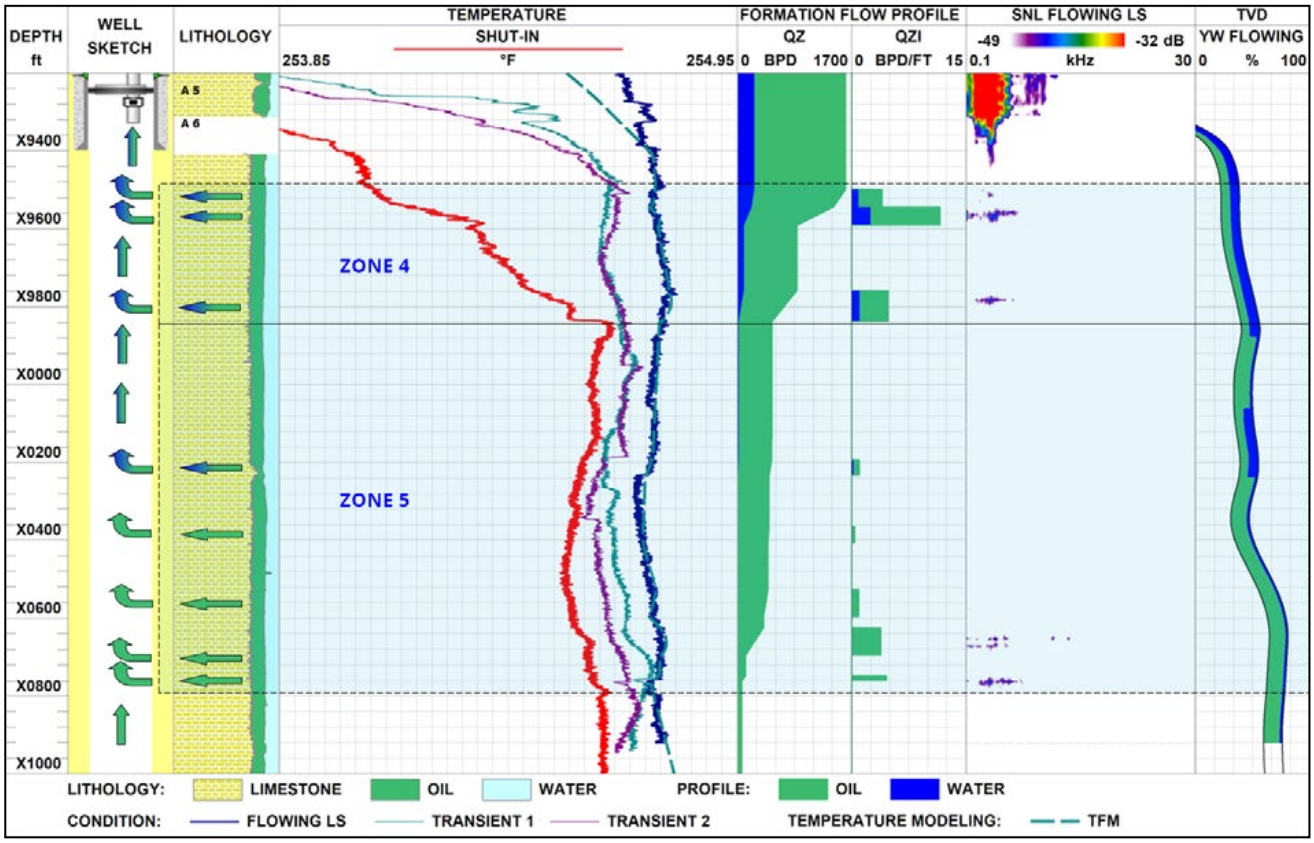

Fig. 2. HPT-SNL during inflow through the Long String

in the open hole section (Zone 4 and Zone 5). At the top of A6 reservoir and above, SNL detected a high-amplitude 0.1–6.3 *kHz* signal generated by upward fluid flow through the long tubing string.

According to temperature modelling, as much as 68 percent of fluid inflow from the A6 reservoir occurred in Zone 3. The salinity, capacitance and temperature modelling data indicated water in this inflow. In Zone 5, fluid inflow was 28 percent of the total inflow under bottom hole conditions. Additionally, about 4 percent of the total inflow was allocated to below the survey interval. No free gas was detected in inflow under bottom hole conditions. Water cut was 21 percent. The modelled profile matched with the interpreted SNL data (Fig. 2).

Temperature modelling and Spectral Noise Logging were used to determine the inflow profile of the A2 – A6 reservoirs and identified intense gas inflow zones in A2 and A3 reservoirs. Another finding was upward cross-flow behind casing from A5 reservoir and subsequent entry into the wellbore at the bottom of A4 reservoir. The survey revealed no leaks in the production casing, tubing or packers and no communication between tubing strings.

Example 3 (Job ID-11036)

This case presents a horizontal dual-string oil well selectively producing from different portions of Reservoir D through long and short tubing. The main objective of the survey conducted in this well was to profile inflow from the perforations within Reservoir Units D1–D3 and to detect communication between the short and long strings.

The well was surveyed by integrated high-precision temperature and spectral noise logging (HPT-SNL). In accordance with safety requirements, all measurements were made through the long string. However, because of this, the tool did not contact oil inflowing from Units D1–D3.

Noise logging indicated flows not only in Units D1–D3 but also above and below them. The main oil flow was detected within the unperforated Reservoir B and the perforated Units D1 and D2. As indicated by the noise frequency distribution, most of the oil was produced through fractures and only a small fraction through the rock matrix (Fig. 1).

Downward cross-flow behind casing from Reservoir B was detected by noise logging and verified by a temperature simulation and analysis of the shape of temperature curves between Reservoir B and Unit D1, where

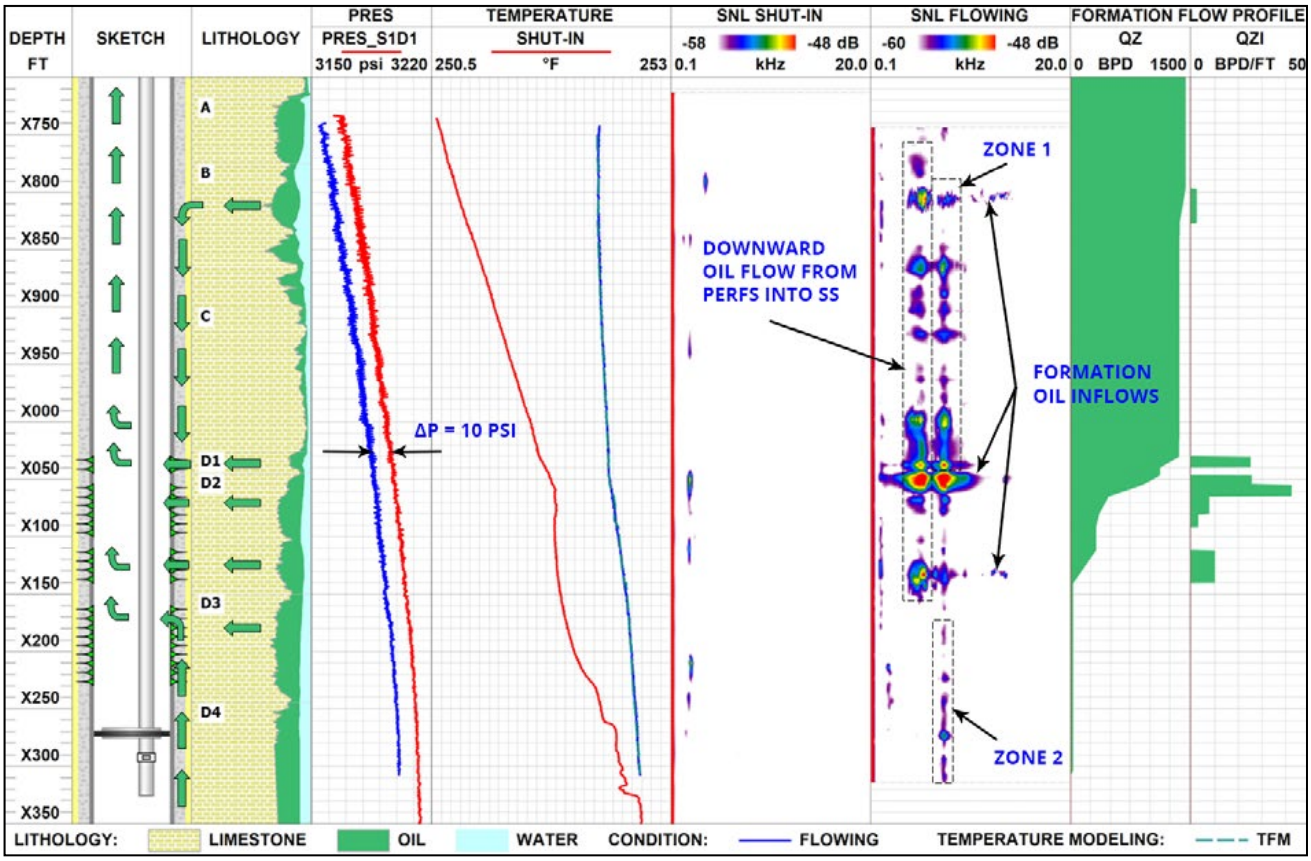

Fig. 1. Inflow profile and cross-flow behind casing during flow in the short tubing string identified using HPT-SNL data from the long tubing string and temperature simulation

production of colder-than-expected fluid from perforations was observed. However, static noise logging identified some low reservoir flow even three days after shut-in, which could have distorted the static temperature profile.

Noise was also detected below the perforations. Low-frequency noise within Zone 2 could be caused by flow behind casing or in the reservoir from the producing Unit D4 into the lower perforations of Unit D2.

A difference of 10 psig between the static and flowing pressures in the short string indicates inter-string communication. This cross-flow most likely occurred behind casing. Alternatively, it could have occurred through a leaking packer, as suggested by minor heating in the static temperature profile and low noise detected by flowing SNL at the packer. Flowing temperature modelling determined a production profile for the perforated intervals through tubing, the tubing being a barrier between the tool and inflowing oil. This barrier was taken into account in the simulation. The simulated profile correlates with porosity.

Example 4 (Job ID-11037)
This case presents a deviated dual-string well selectively producing from Reservoirs B–D through a short tubing string and from Reservoirs F–H through a long one.

The well was surveyed to determine the flow geometry in the survey interval, identify a source of watercut for the short tubing string and to detect communication between the short and long strings. This objective was achieved by integrated high-precision temperature and spectral noise logging (HPT-SNL). In accordance with safety requirements, all measurements were made through the long tubing string. The long and short strings operated alternately.

Below is an analysis of HPT-SNL data recorded both with no flow and with flow through the long tubing string. A static temperature curve within Zone A (Fig. 2) indicated upflow from Reservoir H, apparently through the long string, to Reservoir C. Static SNL detected low-frequency noise in the interval, from below a perforated interval in Reservoir H. to Reservoir B. This noise was probably generated by fluid circulation between the reservoirs, which indicates possible communication between two packer-isolated zones.

Production through the long string
The static and flowing temperatures diverged below the perforated interval whilst flowing in the long tubing string. This indicated fluid upflow behind casing to a perforated interval in Reservoir H. The flowing temperature within Reservoirs F to H was lower than the static, possibly because of gas release from the oil. Gas inflow was also indicated by high-intensity noise in the lower perforated interval.

The fact that the upper perforations had strong flow whilst flowing in the long string also suggests communication between the reservoirs. This communication was found to occur through a leak in the long string. The leak was located by a capacitance sensor (watercut meter). The temperature and water cut decreased rapidly in Zone B (Fig. 1) although the water remained at the same level after putting the well into operation. This can be explained by gas entry from the producing zones of Reservoirs C and D through the leak in the long string, as confirmed by temperature

simulation. It can therefore be deduced that it was this leak that caused communication between the strings. Flow through the upper perforations covered by the tubing during production in the long string can be analysed in more detail. Wavelet filtration of SNL data revealed two producing zones in Reservoirs F and H. They are indicated by noise generated by fluid production through fractures and the rock matrix. Noise of the same frequency range identified fluid flow through Reservoirs C and D.

Production through the short string

Below is an analysis of HPT-SNL data recorded under static conditions and with flow in the short tubing string. The above-mentioned communication between the short and long strings was confirmed by a difference of 570 psig—between pressures measured under static conditions and during production from the short string—detected in the long string. This communication occurred through a leak in the long tubing string [2].

The flowing temperature in Zone C (Fig. 2) was reduced by fluid flow into the tubular annulus through perforations behind the long tubing string. This inflow probably contained gas that cooled the fluid moving up the long string. Part of this gas entered the long string through the leak. In Zone D (Fig. 2), the flowing temperature and capacitance also varied sharply during the operation of the short tubing string due to gas flow into the long one.

Four producing zones were reliably identified within Reservoirs B to D by the noise characteristic of fluid production through fractures and the rock

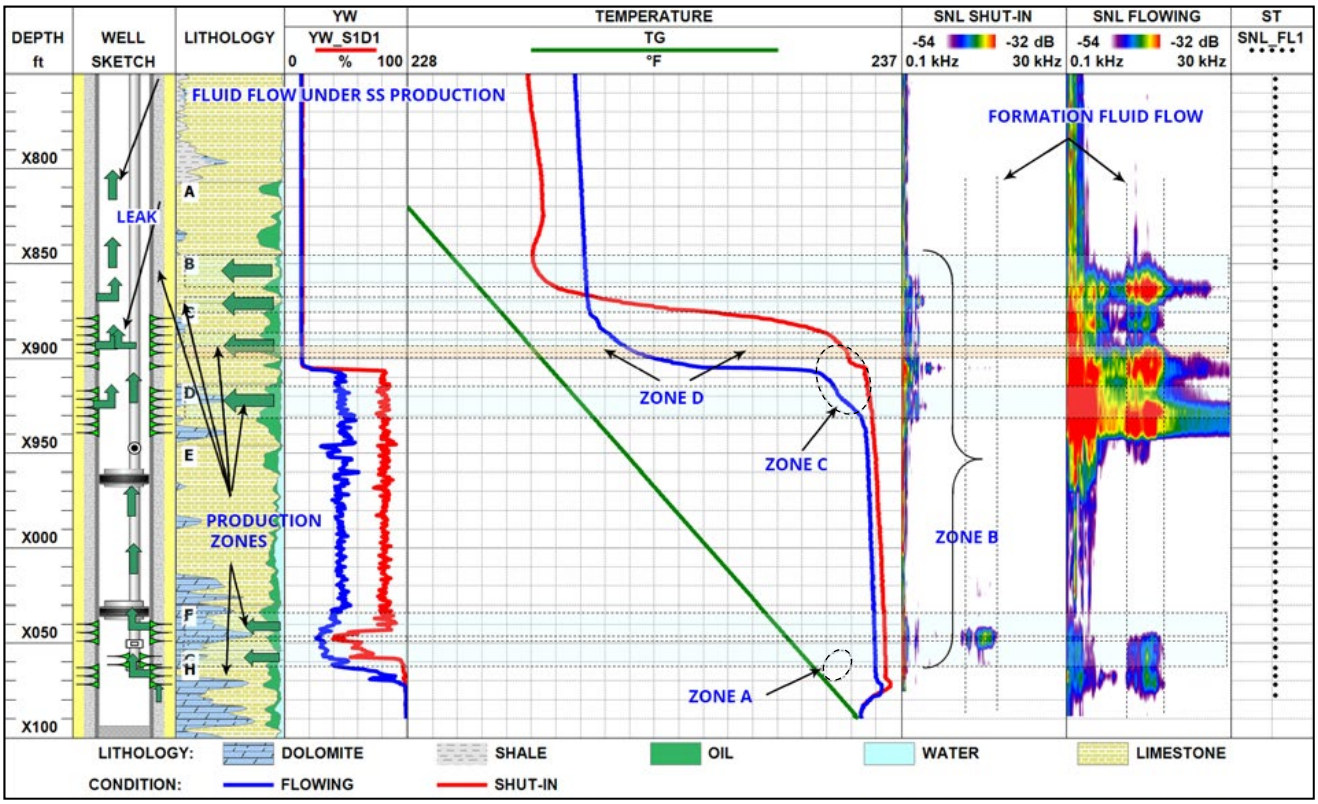

Fig. 2. HPT and SNL data recorded under static conditions and during production through the short string. Detection of leakage in the long string during the operation of the short string.

matrix. SNL data and reservoir porosity correlated remarkably well.

Because of the communication between the strings, lower perforations flowed during the operation of the short string, and the upper perforations flowed (although not to the same extent) during the operation of the long one. This significantly reduced the quality of the well's production.

Metal loss from the long string could be determined by magnetic imaging defectoscopy (MID).

Example 5 (Job ID-13071)

This case describes a survey conducted in the vertical dual string well to determine water injection effectiveness and check well integrity issues. The short string is an injector and the long string is a producer. It was known that whenever injection started in the short string the production from the long string stoped. This indicated communication of short string with long string. This objective was achieved by the integration of high-precision temperature, spinner, multiphase capacitance and salinity, and spectral noise logging techniques.

Recorded temperature, noise and PLT showed leak in the long string at 3343.0m.

Medium-amplitude noise, with frequency up to 30.0 *kHz* in the interval 3401.5–3408.0 m caused

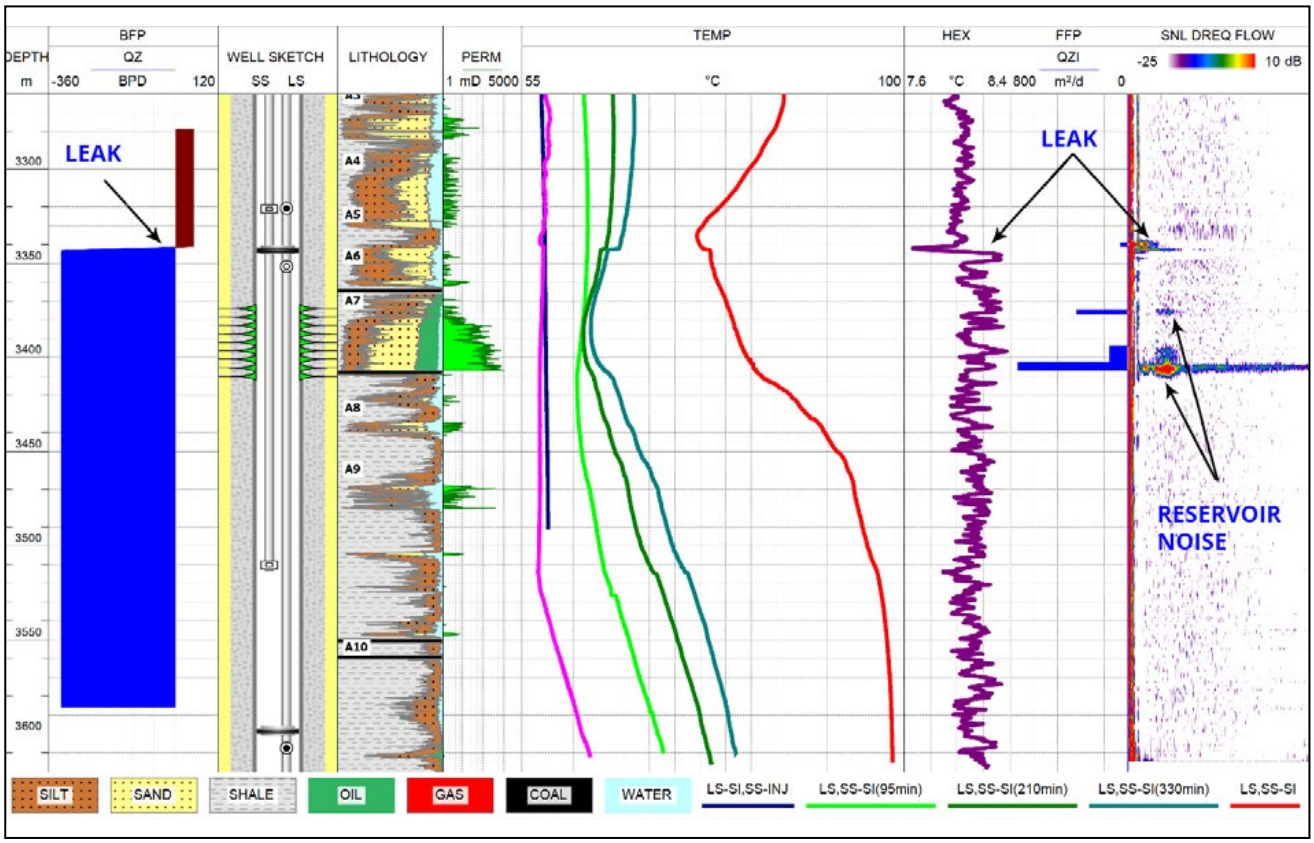

Fig. 1. Logging data integration to determine injection efficiency and integrity issues.

by fluid entry in the reservoir through perforation. Shut in SNL detected no reservoir noise.
According to temperature simulation most of the water (77.8%) absorbed in the interval 3394.1 – 3406.6 m. 13.8% of total injected water absorbed in the interval 3374.9 – 3377.0 m.

Production logging recorded under long string flowing and short string injection. PLT showed both upward and downward flow at the leak depth. Total upward flow rate was 50.9 BPD. Total downward flow rate was 325.2 BPD.

2.2.1.5 ESP-COMPLETED WELLS

Example 1 (Job ID-12028)

The survey described in this example was performed in a vertical well producing from the C carbonate reservoir. The well was equipped with an ESP. The main objective of the survey was to determine whether water encroachment in this well was caused by bottom water coning or injected water breaking through the producing reservoir. At the time of the survey, the water cut was 92% and the total flow rate was 3,433 BPD. The well was surveyed by integrated high-precision temperature, spinner and spectral

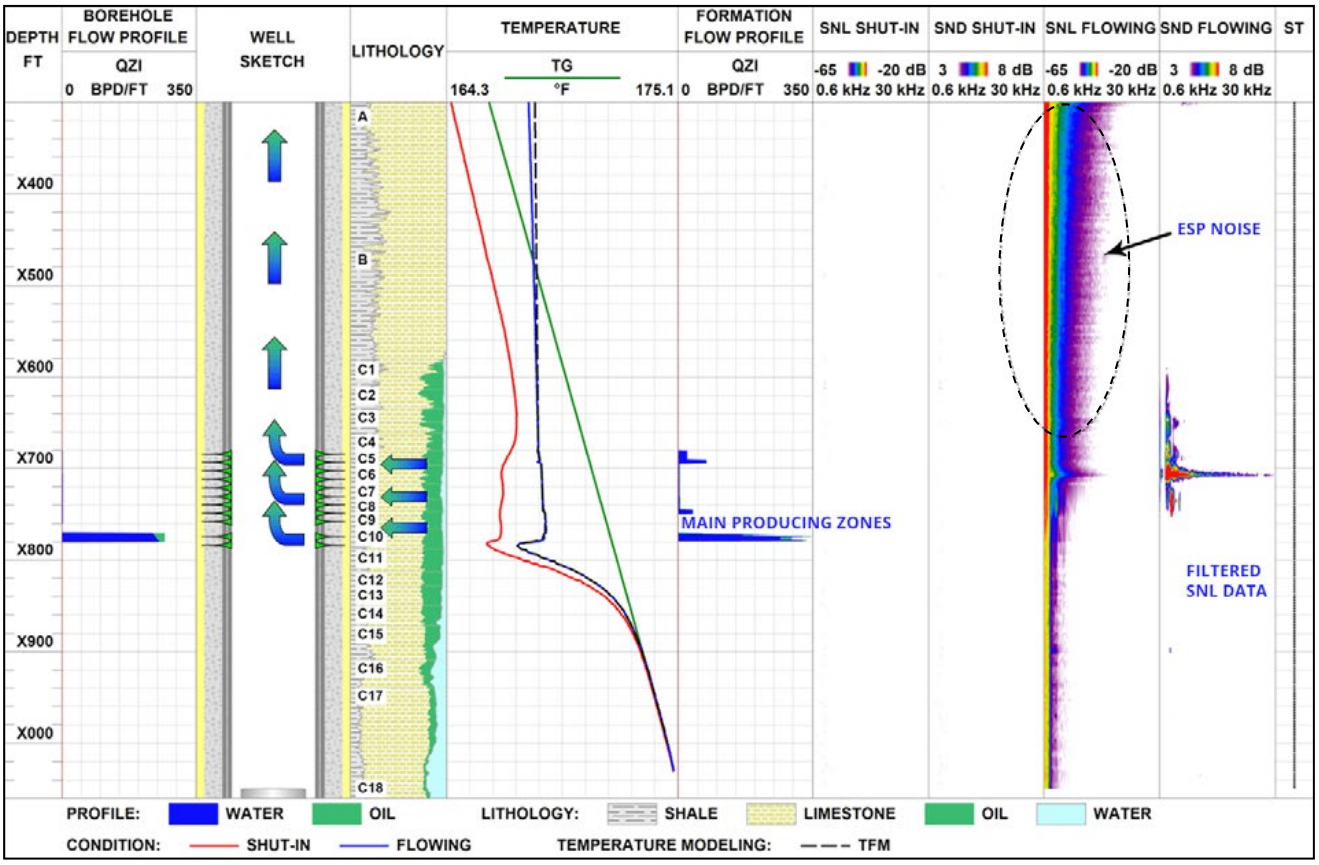

Fig. 1. Inflow profile constructed by PLT-based temperature simulation and SNL. (Uninformative ESP noise was removed from SNL data using a median filter)

noise logging (HPT-PLT-SNL).

HPT data analysis showed that fluid flowed in non-uniformly through the perforated section—mainly from the lower interval C8—and flowing temperature simulations for this well indicated that C8 accounted for 72% of the total flow rate. Importantly, the static temperature decreased in comparison with the geothermal profile throughout the perforated interval of the C formation, indicating breakthrough of cold injected water into the well (Fig. 1).

According to the PLT survey, 94% of the fluid entered the wellbore through the C8 lower perforated interval and the remaining 6% through the C4-C7upper perforated interval.
SNL data acquired under inflow conditions were affected by an operating ESP. The intensity of noise recorded by the SNL tool increased as it approached the ESP. A median filter was applied in drift mode to extract the reservoir signal from the noise and minimise the effect of ESP operation on SNL readings. As a result, the C4-C7reservoir units were identified as the main producing zones, with the most intense noise detected in the C5 unit.

The correlation of production profiles based on HPT-PLT-SNL data allowed analysis of the inflow geometry. It was found that fluid from the C5 unit flowed behind the casing or through the near-wellbore zone, entering the wellbore through the lower perforated interval.

The lack of increase in noise intensity within the C8 reservoir was probably due to its high degree of fracturing. Consequently, low-frequency low-amplitude noise in this interval could have been masked by ESP noise.

Example 2 (Job ID-11021)
The survey described in this example was performed in a vertical high water cut producer developing the B carbonate reservoir. The well was equipped with an ESP.
The main objective of the survey was to determine whether water encroachment in this well was caused by bottom water coning or injected water breaking through the producing reservoir. At the time of the survey, the water cut was 61% and the total flow rate was 4,630 BPD. The well was surveyed by integrated high-precision temperature, spinner and spectral noise logging (HPT-PLT-SNL).

An HPT data analysis showed that fluid flowed in non-uniformly through the perforated section—mainly from the lower interval B10—and flowing temperature simulations for this well indicated that B10 accounted for 67% of the total flow rate. The temperature within the perforated reservoirs exceeded the temperature that would have resulted from the average temperature gradient in a sump, and this suggests that water in the produced fluid was mainly hot formation water (Fig. 1).

The PLT survey failed to measure flow rates within perforated reservoirs, because the spinner was clogged with paraffin hydrocarbons.

For this reason, the production profile was constructed using only SNL and temperature logging data.

SNL conducted under inflow conditions was

affected by an operating ESP. The ESP generated additional low-frequency noise within the entire SNL interval. However, low-frequency noises generated by fluid flows in the reservoir differed from the background noise generated by the ESP. A detailed analysis of the low-frequency noise component by data filtration located flow intervals, and a logarithmic representation of SNL data illustrated them more clearly. The Flowing SNL panel shows the results of wavelet averaging of input data and clearly separates 0.5–1 *kHz* noise generated by the ESP from local 0.1–0.4 *kHz* noises generated by reservoir fluids flowing through perforations.

Below the perforations, 1–5.5 *kHz* noise was detected within the B11–B14 reservoir units under both static and flowing conditions. The static and flowing temperature curves merged within the B11–B14 interval and their shape suggested the presence of constant lateral flow. Interestingly, open-hole data from this recently drilled well indicated high water content within B11–B14. It would therefore be logical to suppose that formation water breakthrough occurred in these reservoir units. The increased noise amplitude detected after opening the well indicated behind-casing communication. Thus, it can also be assumed that it is water from the B11–B14 interval that entered the perforations. It should be noted that the salinity curve indicated water within the lower perforated interval B10–B11. This is in line with the hypothesis that water approached

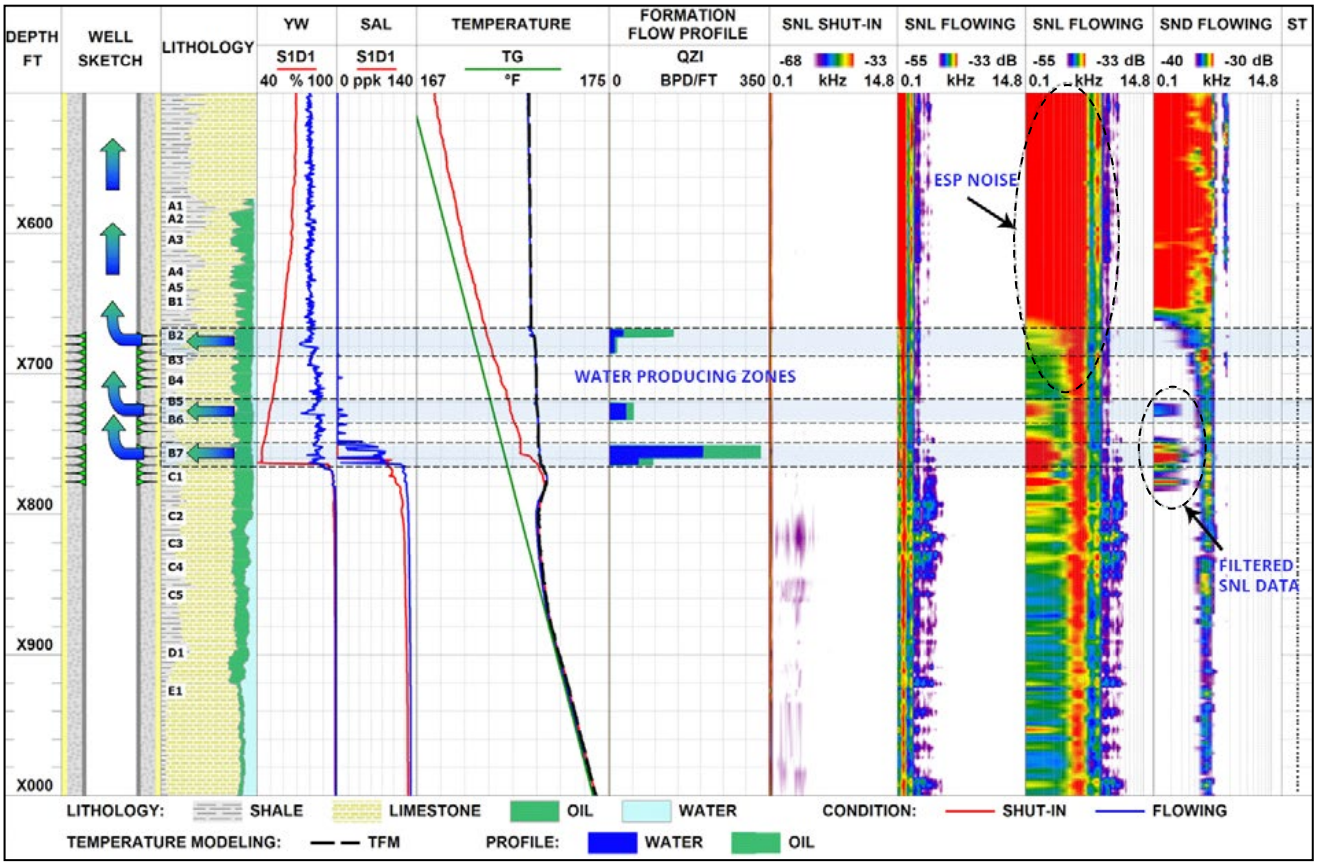

Fig. 1. Identification of a water entry interval by integrated HPT-SNL, multiphase analysis and temperature simulation. (Uninformative ESP noise was removed from SNL data using a wavelet filter)

the perforations from below and then entered the wellbore through the lower perforated interval. The salinity above the top of the B10 reservoir unit was zero, which indicated that the hydrocarbon concentration in the wellbore was higher and that the water was mainly produced from below.
The recommendation generated for this well was to repair the cement sheath and shut-off water production from the B11–B14 reservoir interval.

2.2.1.6 SMART COMPLETION WELLS

Example 1 (Job ID-13041)
This case study exemplifies the High Precision Temperature (HPT), Spectral Noise Logging (SNL) and Production Logging (PLT) capabilities in surveying a horizontal Dual String Oil Producer. This well is completed as a dual string multi-lateral oil producer. The short string is producing from the upper lateral and the long string from the lower lateral. Special emphasis in this case study is laid upon performance of one of the horizontal sections of the wellbore, which is producing through the long string and is equipped with Inflow Control Devices (ICD's). The horizontal section of the wellbore is divided into several segments by packers and each of those segments is equipped with Inflow Control Devices with Sliding Sleeve Door (SSD). There are ten ICD's installed in this well.

The first HPT-SNL survey was run for qualitative and quantitative analysis of the inflow zones and identification of any possible communication between the intervals separated by packers.

During the repeat run, the HPT-SNL suite was supplemented with a Production Logging Tool, because in addition to identification of flow zones and quantifying the fluid volumes it was also decided to check the current status of each ICD. Prior to the survey, some of the ICDs were closed. According to the information provided by the client, during the survey ICD #1, #2, #3, #4, and #5 were closed and #6, #7, #8, #9 and #10 were open.

During the first run, HPT identified some local heating anomalies associated with fluid inflow into the liner through ICDs and found some zones of formation fluid inflow from the open hole into the interval between ICDs where no packers were installed. An inflow profile was constructed on the basis of temperature simulation data. It was observed that formation fluid enters the liner from several flow units. From Unit-A1, the fluid moves downwards through the casing annulus to the perforation and then enters the liner through ICD#1. Some inflow from the formation into the intervals between the packers where ICDs are installed and two inflow zones between the packers where the liner is not equipped with ICD were detected within Unit A2. The fluid from those intervals travels behind the liner and then enter the liner through ICD#3. Two flow zones from which fluid enters through ICD#4 and ICD#5 were identified within Unit A4. Static and flowing temperature curves do not merge in the lower part of the well, which means that inflow occurs from Unit A5 through ICD#10. The reservoir flow zones identified by HPT data are in good correlation with SNL data. Signals of different amplitude in a wide frequency range were captured within the inflow zones. The low-frequency component of the captured noise signals is associated with the ingress of fluid into ICDs, while the high-frequency

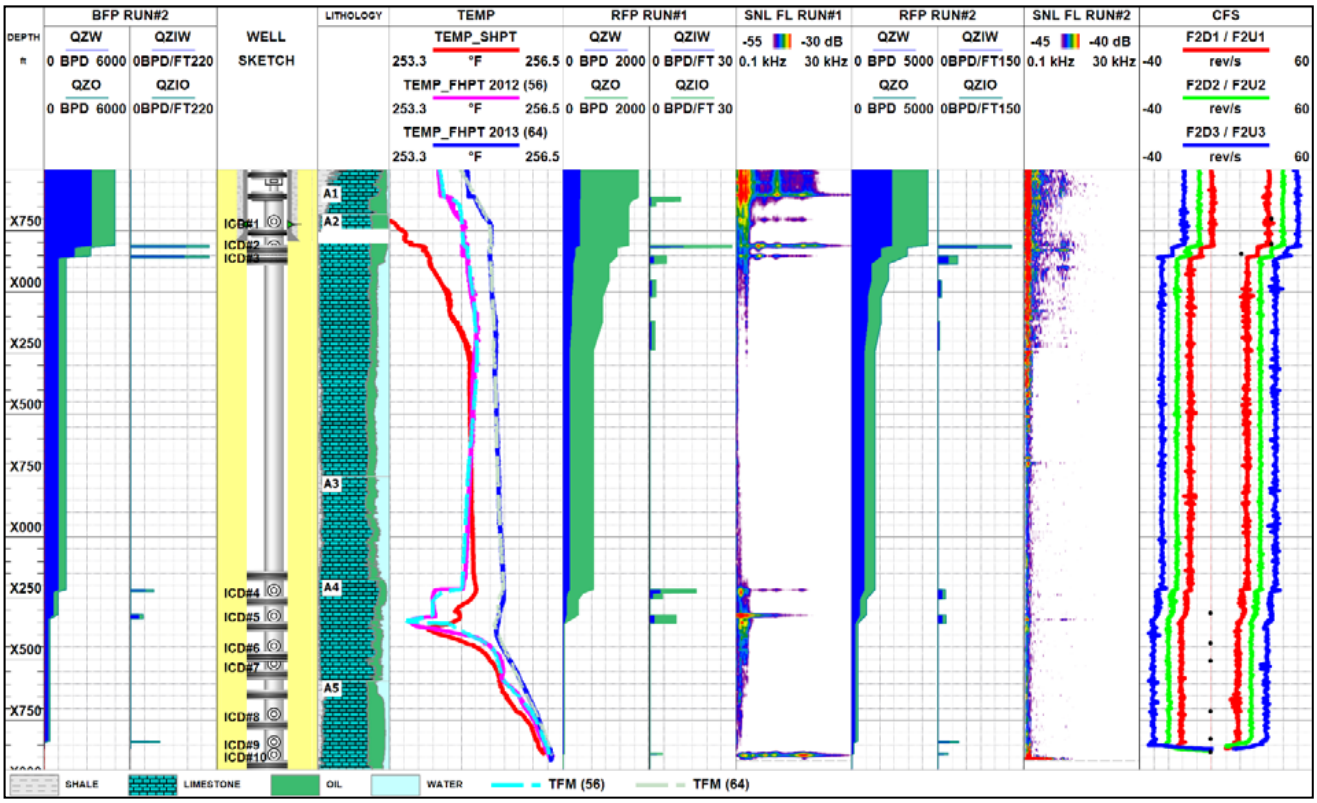

Fig. 1. HPT, SNL, and PLT logs recorded in the reservoir zone

component is associated with the formation fluid flow through the rock matrix.

ICDs from #1 to #5 were closed prior to the repeat run that included PLT measurements in addition to the HPT-SNL suite. Based on the processed HPT-SNL data, some temperature variations and noise signals associated with formation fluid inflow were identified. The inflow profile was constructed using temperature simulation technique. In comparison with the previous survey (run #1), this one indicated no flow from Unit A1 and showed another flow zone in A5. Application of PLT technique enabled precise identification of the ICDs through which the produced fluid entering the liner. According to the logging suite data, it could be concluded that ICD#2, ICD#3, ICD#4, ICD#5, and ICD#9 are flowing even though ICD #1 to #5 were closed prior to the logging run.

Using this well as an example, we could conclude that application of HPT-SNL technique will assist in identification of flow patterns behind the liner, and addition of PLT to the logging suite will provide additional information to locate the zones where inflows occur directly into the wellbore, i.e. to determine current status of the (Inflow Control Devices) ICD's.

2.2.1.7 HORIZONTAL WELLS

Example 1 (Job ID-10032)

This case describes a survey conducted in the horizontal well to determine flow patterns in a screen and reservoir as well as oil sweep efficiency. A screen with an outside diameter of 5-1/2” installed in an open-hole section complicated the identification of flow zones in the reservoir. This challenging objective was achieved by the integration of PNN, high-precision temperature, spinner, multiphase capacitance and salinity, and spectral noise logging techniques. The survey was performed in three modes: flowing, static and transient.

These techniques have different radii of investigation, and the combined interpretation of their data enable the reconstruction of flow patterns around a well. The correlation of temperature, spinner and noise measurements showed that the producing reservoir interval was far away from the entry zone of the screen due to significant intertubular cross-flows.

Neutron logging is the key technique to control oil displacement by water in cased wells including those with sand screens. Despite the small radius of investigation, it can yield sweep information. In this case, the correlation of open-hole porosity and TPHI

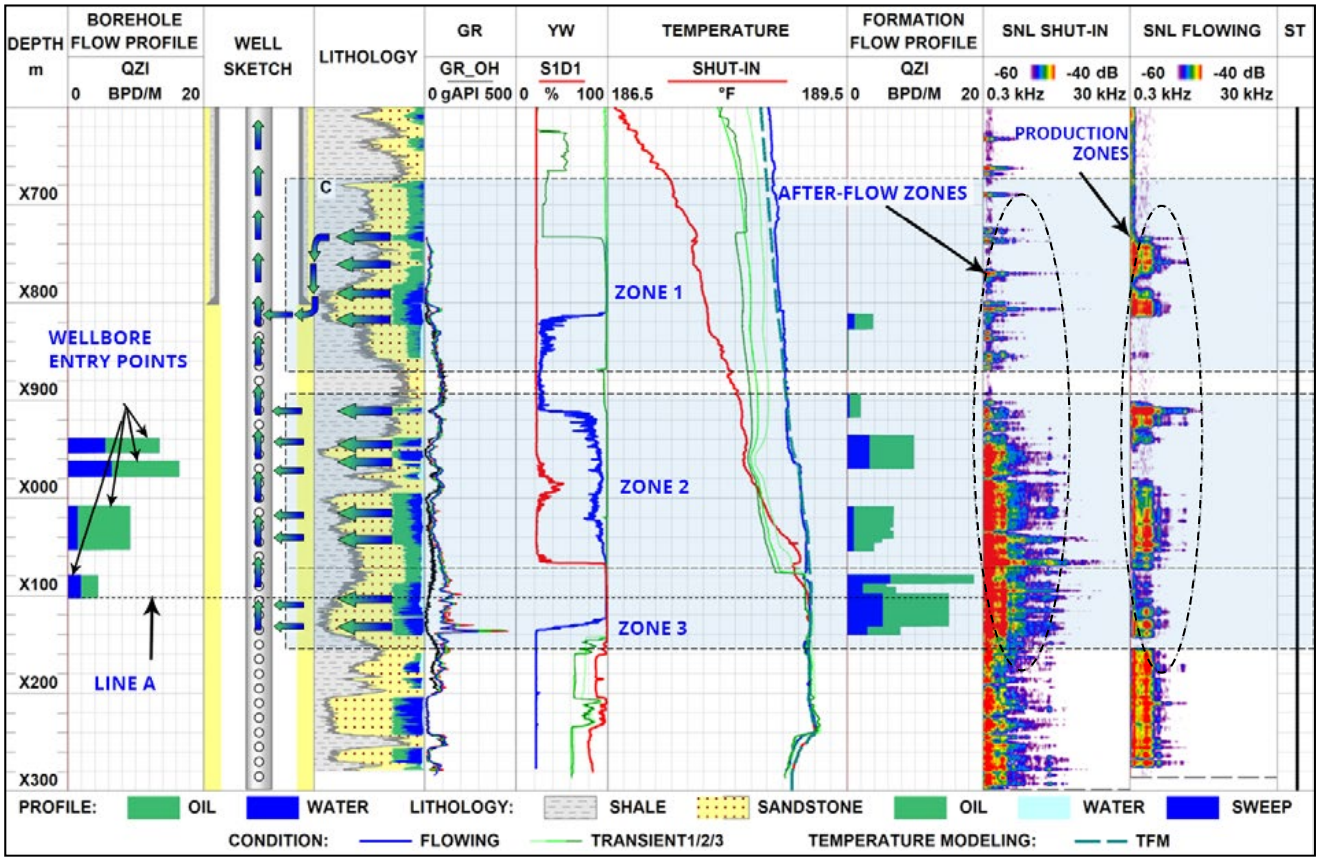

Fig. 1. Logging data integration to determine oil sweep efficiency and flow patterns in a screen and reservoir.

neutron porosity logging data indicated the largest sweep in the lowest, horizontal portion of the well (Zone 3) and, supposedly, a bottom water rise in this zone, in agreement with GR values disturbed relative to the background (Fig. 1).

Shut-in spectral noise logging data revealed high-frequency noise behind casing in the top portion of the C reservoir (Zone 1). The signal from this zone features noise streaks, probably indicating reservoir fluid flow that was still there after well shut-in.

High-frequency noise streaks detected in Zone 2 under flowing conditions have been interpreted as reservoir flows. The spinner and flowing temperature data showed that the sand screen received the maximum amount of fluid in this zone.

Zone 1 was not found by SNL to contain any fluid flows and is therefore considered a no-flow zone. This is in agreement with PNN logging data showing that the zone contains virtually untapped amounts of oil.

The lower portion of the screen had no flow either, according to temperature and spinner data, and all the fluid from the reservoir entered the screen above Line A. A deviation of gamma-ray values from the initial background in the lower portion of Zone 2 and in Zone 3 indicated scale deposition preventing fluid from entering the screen. In contrast, noise data showed major flow in the reservoir within this interval.

It was also found that well production was contributed not only by the target zone but also by the top, cased section of the reservoir, where transient temperature curves indicated downward cross-flow. PNN logging showed that this was a low-sweep zone, and it could be supposed that mainly oil was produced from its upper portion.

Example 2 (Job ID-11036)

This case presents a horizontal dual-string oil well selectively producing from different portions of Reservoir D through long and short tubing. Flow-rate metering (PLT), high precision temperature (HPT) logging and spectral noise logging (SNL) performed in this well determined the inflow profile for the horizontal open-hole section of the wellbore below the long tubing string shoe.

The tool was in direct contact with the inflowing oil. Noise and spinner logging yielded identical results indicating that the production was from several thin streaks, mainly from the shallow Zone 1 of the D4 reservoir unit located in the open-hole section. Four more thin flowing streaks were located below Zone 1, with the wellbore section below Line A only slightly contributing to production, which is consistent with the PLT profile (Fig. 1).

The flowing temperature was simulated to accurately locate inflow intervals. The results were in agreement with the PLT profile and additionally identified an inflow interval in Zone 2 that could not be identified by the spinner due to its threshold limitations. Notably, the flowing Zone 2 was clearly displayed in SNL panel.

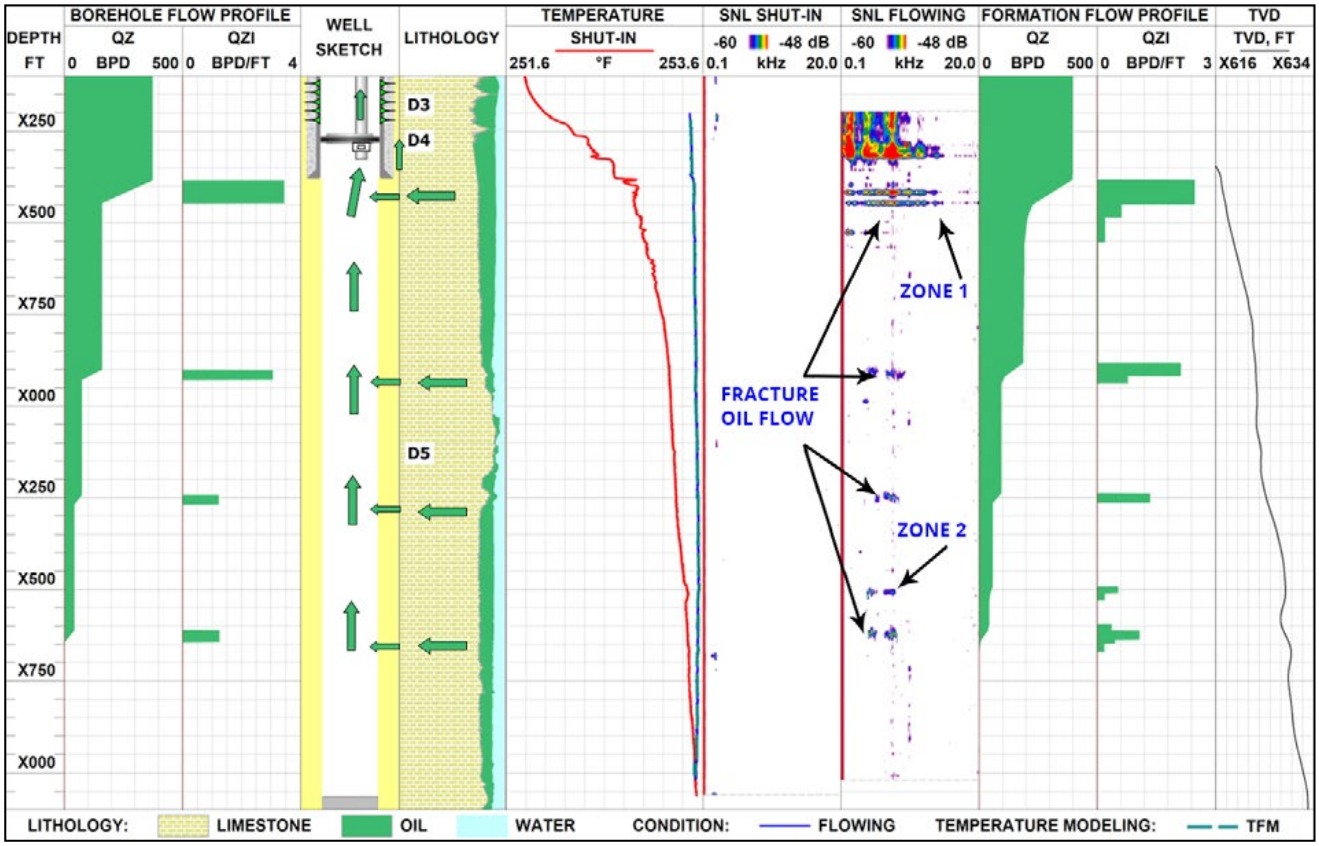

Fig. 1. Correlation of PLT and SNL data and temperature simulation for the identification of inflow intervals in a horizontal open-hole section

The fact that noise logging data correlated perfectly with the simulated temperature indicated lateral inflow, normally occurring in uncased horizontal wells. The frequency of the noise within the identified inflow intervals was characteristic of fluid flow through wide faults.

Example 3 (Job ID-14173)

This case describes a survey conducted in the horizontal well to determine gas entry points and identify any communication behind the casing/liner with A5.

To achieve the objectives, High Precision Temperature (HPT) and Spectral Noise Logging (SNL) surveys were carried out in this well under static and flowing conditions on one choke (32/64") at a differential pressure of 566.5 psi. The pressure values are lower than the initial reservoir pressure of 4,300 psia.

Under static conditions, water was injected to push coil tubing along the wellbore. Injection zones can be identified by multiphase sensor data and by pressure gradient change. Also, the coil tubing

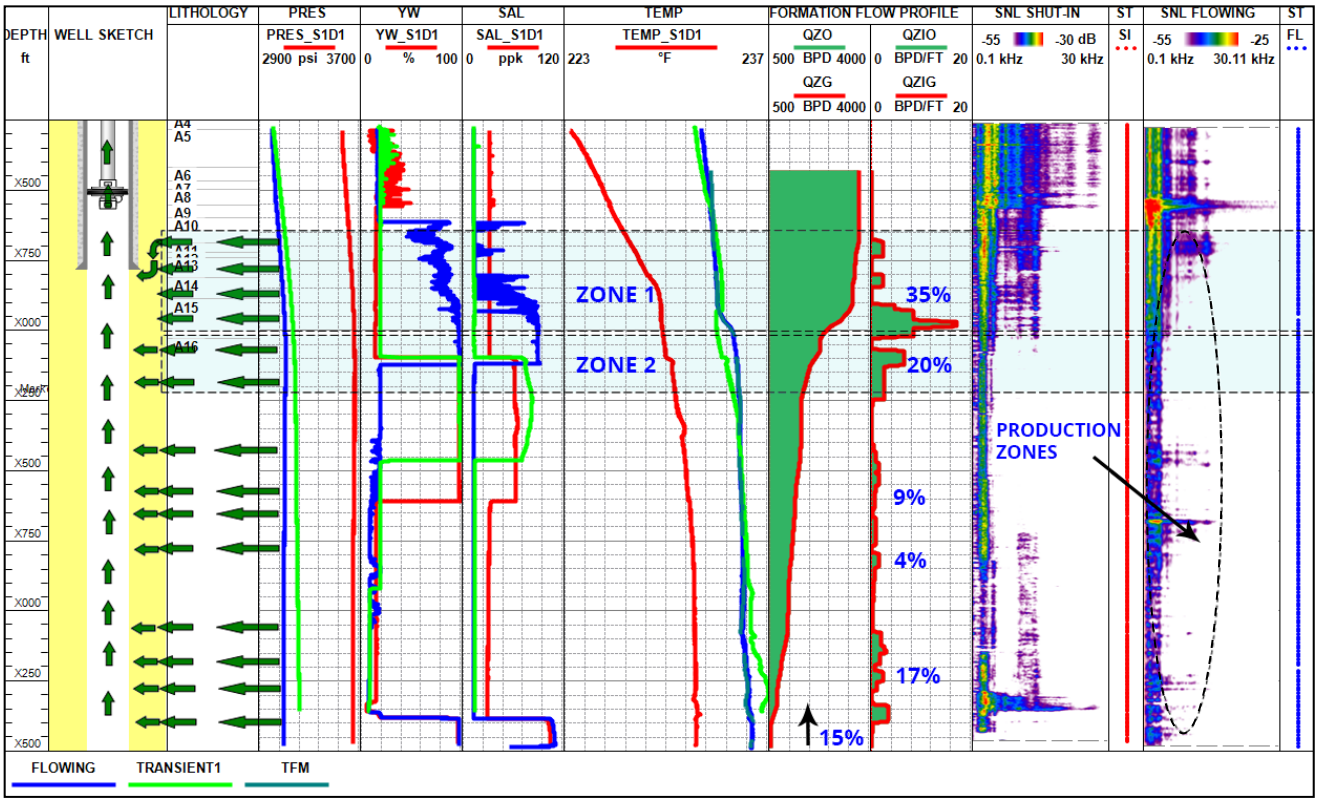

Fig. 1. Reservoir Flow Analysis. Horizontal well

pressure variance graph shows pressure spikes at wellhead, which means that static conditions were unstable. This instability can be seen on SNL logs.

Fluid inflow zones are distributed uniformly along the survey interval. However, the major inflows within the survey interval were found from zone 1 and zone 2. The inflow from Unit A16 was coming through fractures identified by low-frequency SNL signals. The signals in the frequency range 4.3-16.3 *kHz* observed across Unit A16 indicate production through both the matrix and fractured zones. The temperature profile recorded under flowing condition didn't merge with shut-in temperature profile at the end of the survey interval, showing inflow below the survey interval.

The gas production is observed in the upper part of the open-hole section from A15 and overlying A13 and A11.

Example 4 (Job ID-11049)

This case illustrates the application of high-precision temperature (HPT) logging and spectral noise logging (SNL) in locating water absorption zones in the open-hole section of a horizontal well. According to client data, the bottom-hole depth was X9,170 ft but the tool failed to pass below X8,483 ft depth, the unsurveyed distance being 687 ft. Thus, 2016 ft out of 2703 ft were surveyed in the open hole.

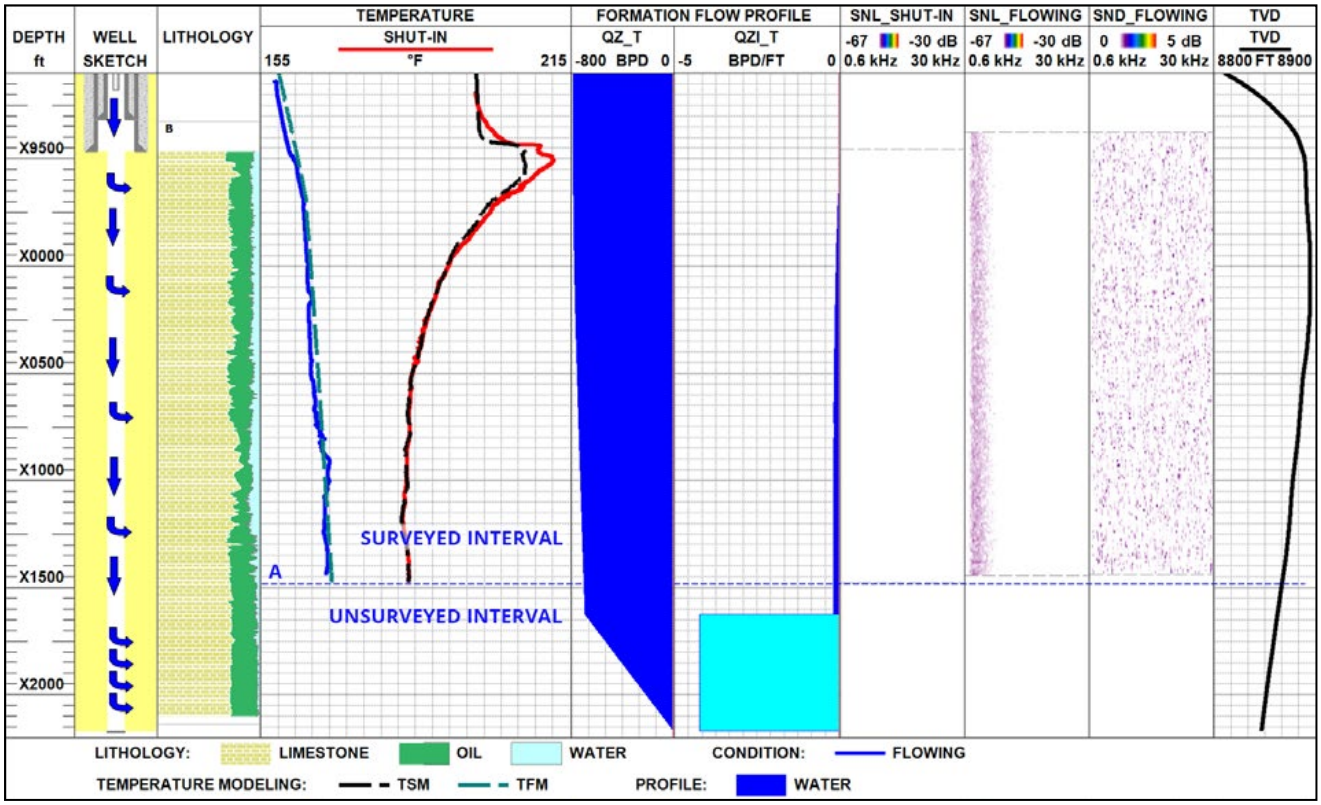

Fig. 1. Identification of major injected fluid loss below the survey interval by integrated SNL and temperature simulation

Static temperature logging detected cooling caused by water injection in the lower half of the open-hole survey interval. It is also seen that the temperature showed no recovery towards the geothermal profile near the bottom hole. Intense cooling is clearly seen at the top of the B formation above a casing shoe. Although no interpreted log data are available for this interval, data from nearby wells indicate that the upper portion of the B formation is highly permeable. Flowing temperature data showed that the temperature gradient slightly changed in the open-hole section. It was also observed that the temperature during injection became lower than the static temperature.

According to numerical temperature simulations, 90% of the injected water was absorbed below the tool running depth (Line A) and only 10% within the open-hole survey interval. This was probably due to the hook-shaped trajectory of the well, with the top of the highly permeable B formation being close to the bottom of the open-hole section of the wellbore (Fig. 1).

It can therefore be assumed that only a part of the water was absorbed in the surveyed open-hole interval; most of it was absorbed at the top of the B formation in the lower, unsurveyed portion of the wellbore, flowed laterally and caused the cooling observed above the casing shoe (Fig. 2), although no SNL data are available to support this assumption.

Static and flowing SNL did not detect any noise

in the survey interval. Water flow noise was not detected in the wellbore because of the absence of completion components in the survey interval that could generate low-

frequency noise. Moreover, the injection water velocity was too low to create turbulence and generate noise. SNL also did not detect any water absorption by reservoirs because each foot of the open-hole survey interval absorbed only 0.1 bbl/d of water, according to the simulation, and this water flow rate was too low for faults, fractures or the rock matrix to generate any detectable signal.

An analysis of all available data led to the conclusion that most of the injected water was absorbed outside the survey interval, most probably at the top of the B formation.

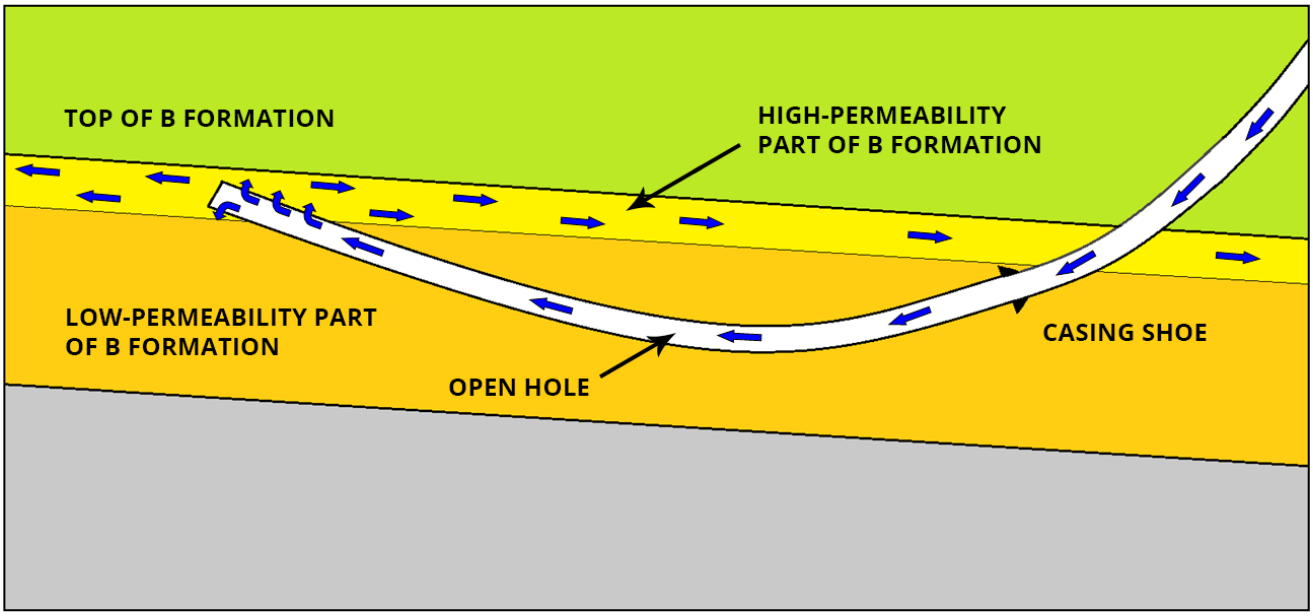

Fig. 2. Water flow pattern

Example 5 (Job ID-11018)

This case illustrates the application of high-precision temperature (HPT) logging and spectral noise logging (SNL) in locating gas absorption zones in the open-hole section of a horizontal well. A temperature simulation showed that despite the homogeneous permeability of the open-hole section (except the tight reservoir units A5–A7), most of the injected gas was absorbed at the top of the A formation, with the upper half of Unit A2 receiving 70% of the total injected gas. The remaining 30% of the injected gas was absorbed below, in the zone extending down to the top of the tight Unit A7. Unit A8 located in the lower portion of the wellbore was not observed to absorb gas, despite its high permeability (Fig. 1).

Flowing SNL indicated a number of narrow streaks with low-frequency, low-intensity noise

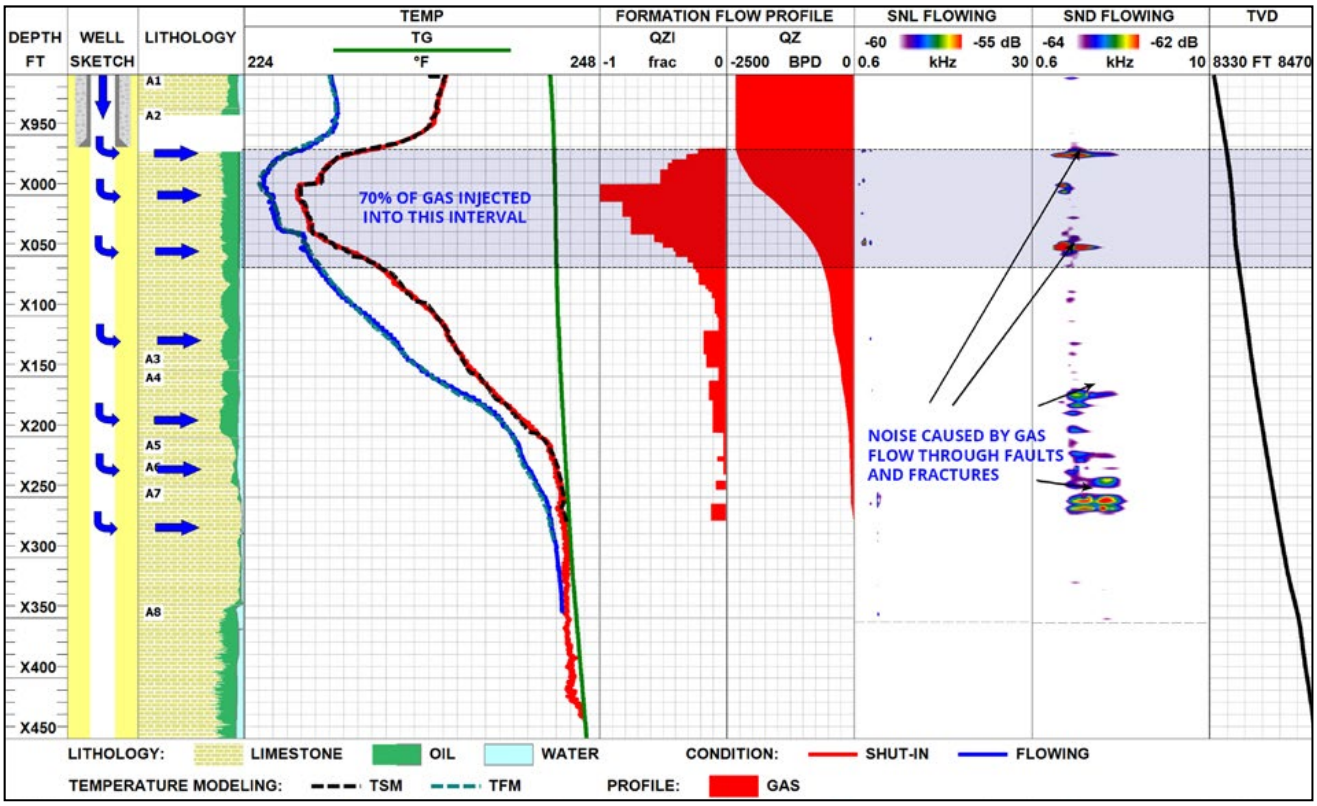

Fig. 1. Construction of an injection profile for a gas injector by integrated use of temperature simulation and wavelet-filtered SNL data

caused by gas absorption within Unit A2 and at the top of Unit A7, in accordance with simulation data. After wavelet filtration, flow zones became clearly visible as 1.6–5.6 *kHz* noise intervals. This noise frequency identified fluid flow through faults or fractures. It can therefore be concluded that most of the gas in this well was injected into fractures, which should be taken into account in further hydrodynamic modelling.

2.2.1.8 MULTI-WELL ANALYSIS

Example 1 (Job ID-9001, Job ID-10036, Job ID-10030, Job ID-11023)

Two pay formations – A3 and A5 – are under development in this oil field by commingled production without multi-string production equipment. Under such conditions, the pressure in the A3 and A5 reservoirs should be monitored closely and constantly for efficient field development and for the detection of cross-flows that may occur between them. The terrigenous sequence of the oil field is heavily complicated by both lateral and vertical heterogeneity.

An integrated HPT-PLT-SNL survey was conducted in three wells – WP1, WP2 and WP7. Well WP1 was surveyed twice at a one-year interval.

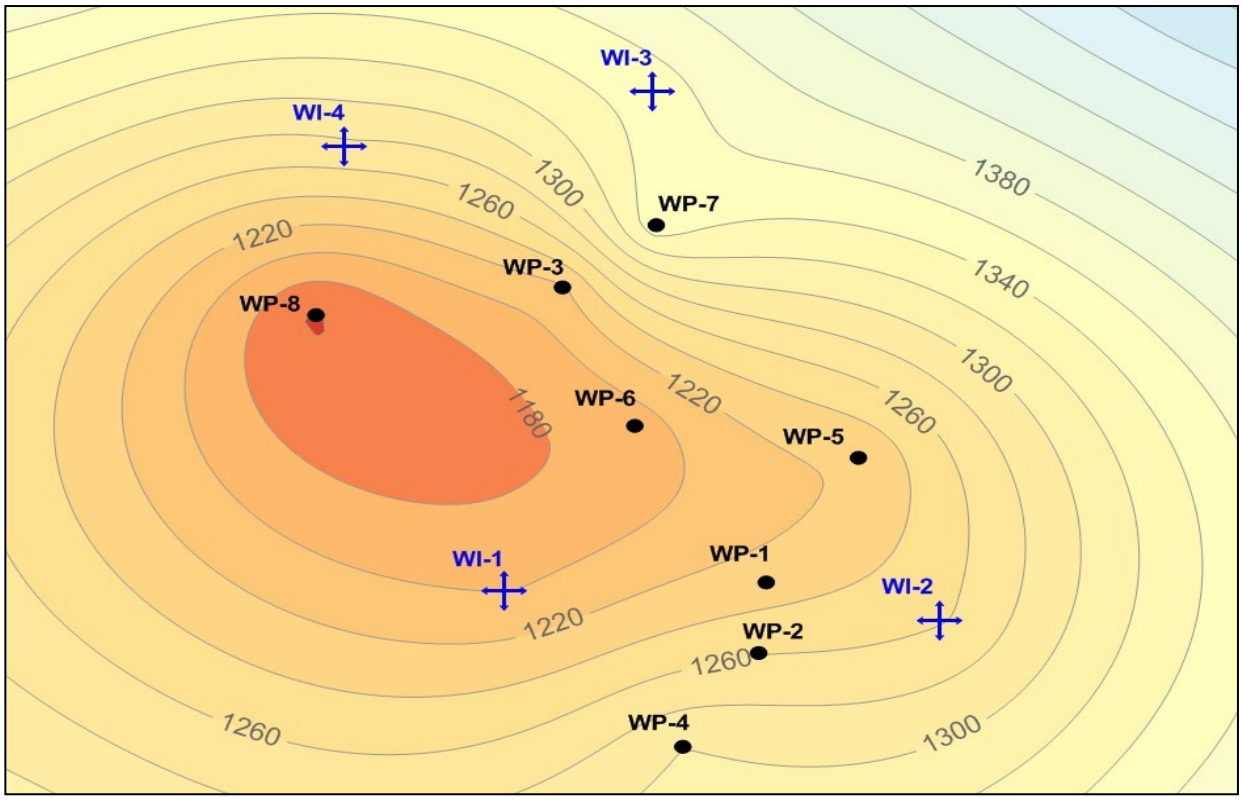

Fig. 1. Field map

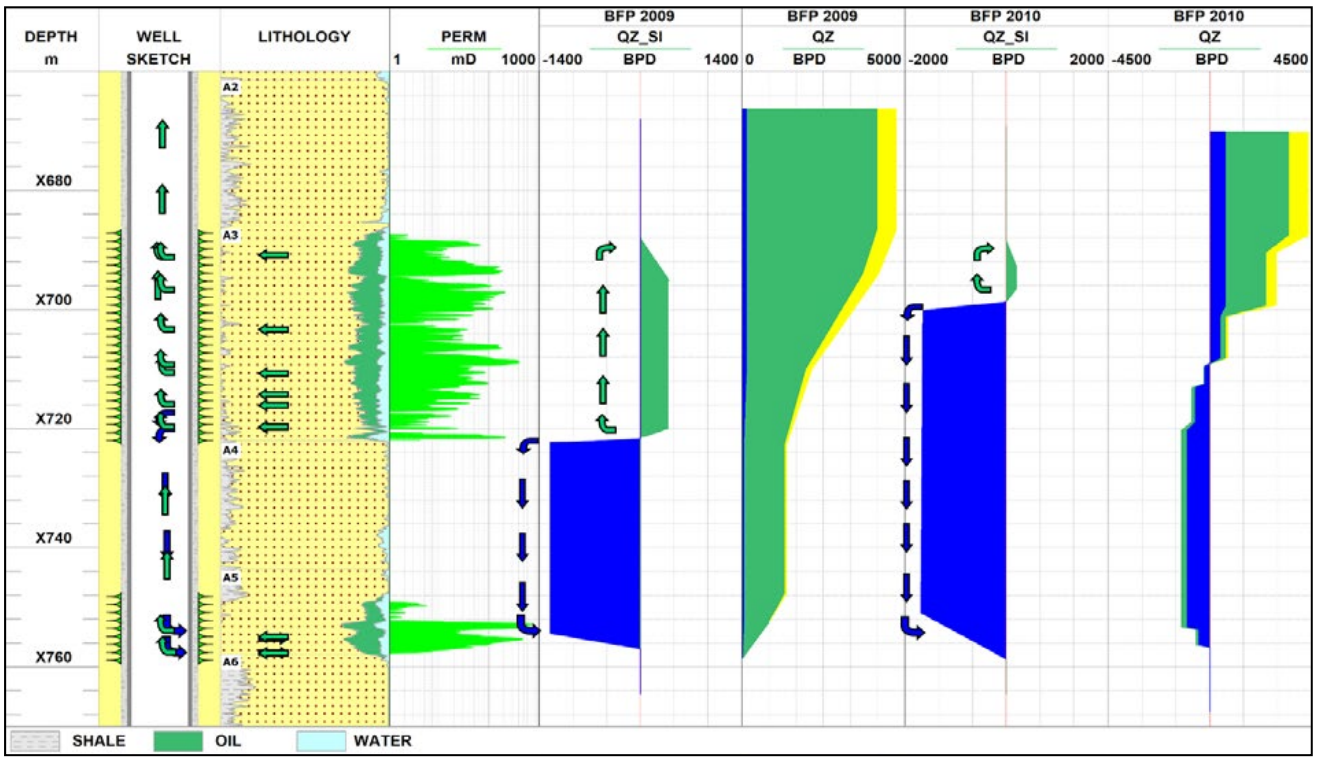

Fig. 2. Multiwell Analysis. Well WP-1 data for 2009 and 2010

WP2 was found to produce mainly from the A3 reservoir (Fig. 3). According to the PLT profile, inflow was mainly confined to the bottom of the reservoir. However, SNL indicated fluid inflow not only at the bottom but also at the top of the A3 reservoir. Inflow from A5 was extremely low. Under static conditions, borehole cross-flow occurred between the top and the bottom of the A3 reservoir. This leads to the conclusion that A3 had a non-uniform reservoir pressure pattern.

Survey results on Well wp1 are shown in Fig. 2. As mentioned above, the well was surveyed twice – in 2009 and 2010. According to the 2009 PLT survey data, reservoir inflows during production were distributed uniformly within reservoir intervals. However, cross-flows occurred under shut-in conditions from the bottom part of the A3 reservoir. As indicated by interpreted open-hole data, this zone had the highest permeability among all the rocks penetrated by this well. Most of the fluid from this reservoir unit flowed into the A5 reservoir and a minor portion into the top part of A3.

A repeated survey conducted a year later revealed increased water cut. Water inflow was found mainly in the bottom portion of the A3 reservoir. Moreover, cross-flow was observed during production. Some of the produced fluid flowed from the A3 reservoir into A5. This indicates that the pressure difference between the A3 and A5 reservoirs kept increasing over the last year.

As seen in the map (Fig. 1), WP1 and WP2 are neighbouring wells with similar conditions: in both of them, the A3 reservoir pressure was higher than the A5 pressure. The production

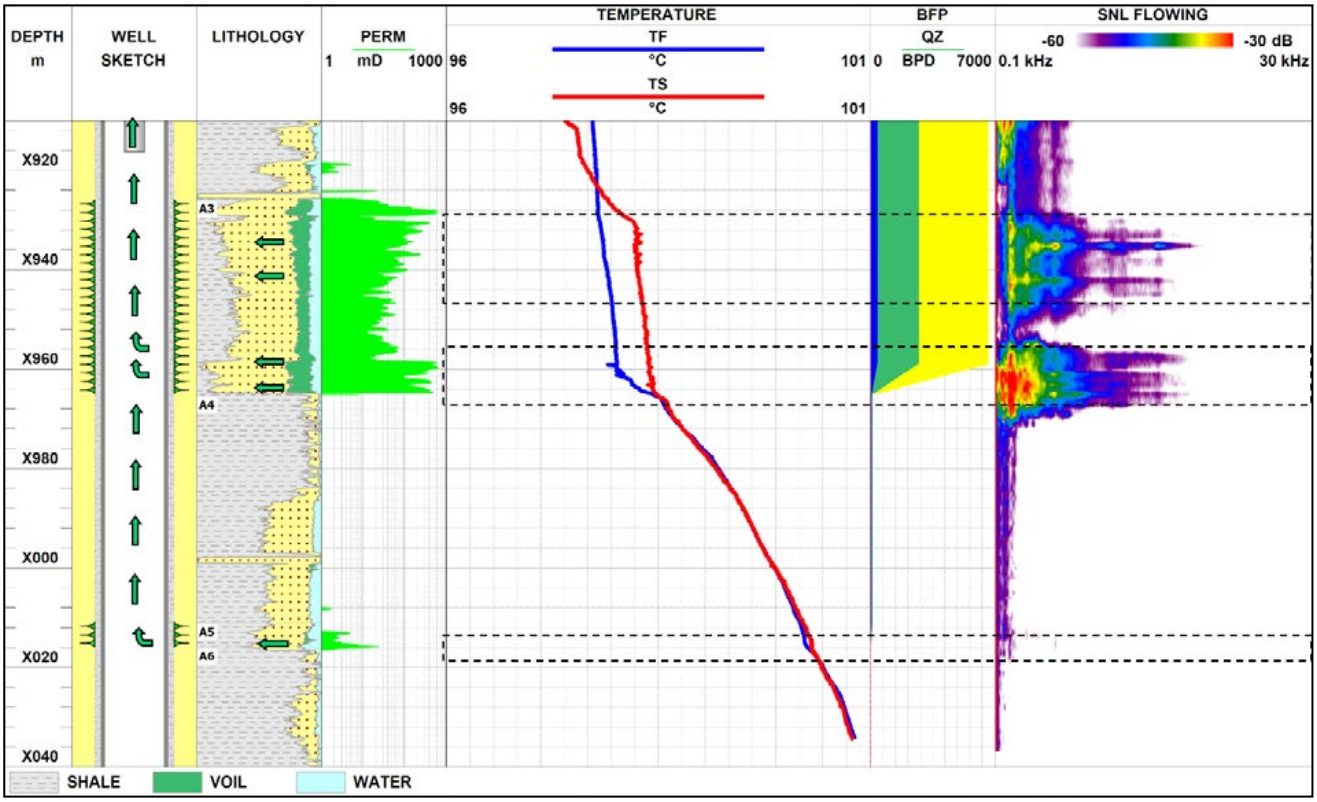

Fig. 3. Multiwell Analysis. WP-2

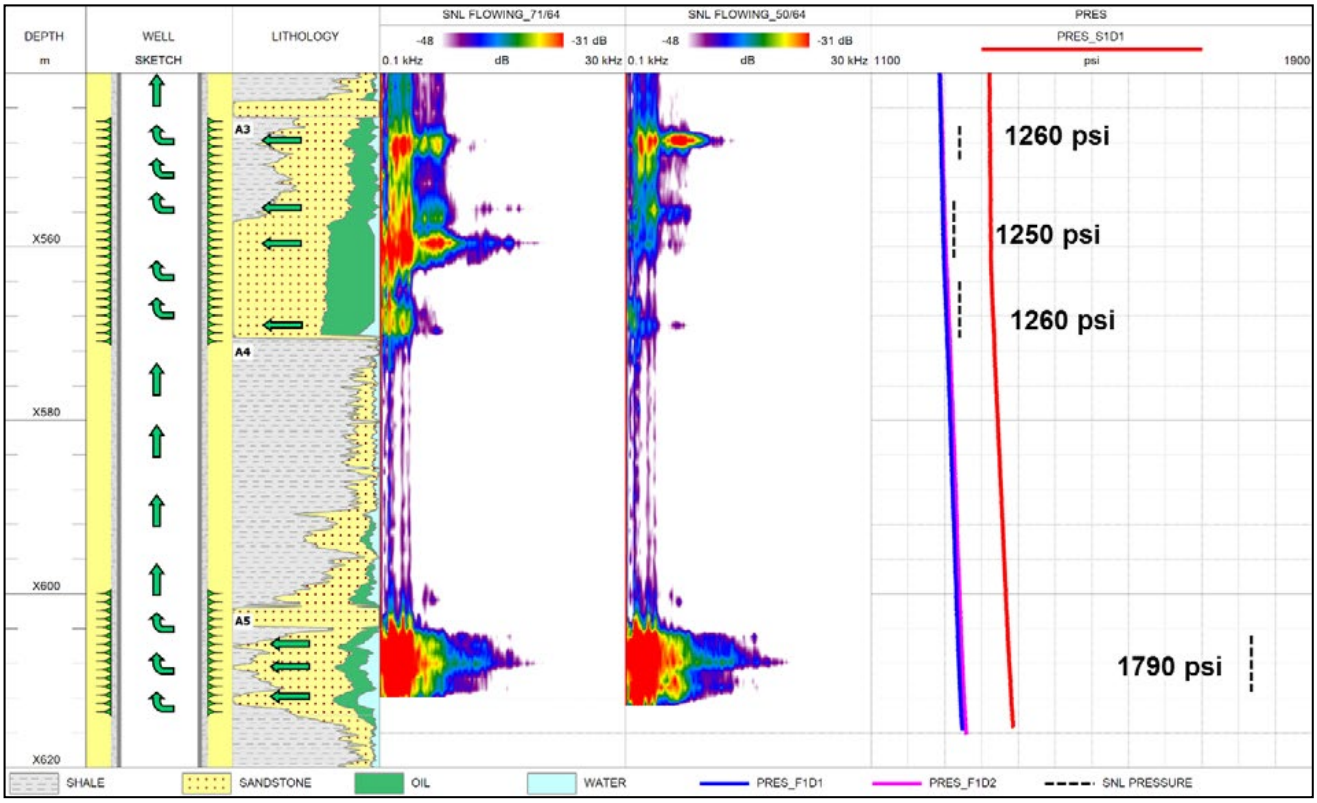

Fig. 4. Multiwell Analysis. WP-7

well WP7 is located at some distance from these wells, and it was also surveyed by HPT-PLT-SNL(Fig. 4). The survey was conducted in two steady modes to determine the near-wellbore zone pressure. According to the obtained results, the A5 reservoir pressure was higher in this well than the A3 pressure. This is indicated by both pressure calculations and cross-flow from A5 into A3 detected under static conditions and apparently indicates non-uniform pressure distribution in the A3 and A5 reservoirs. In the southern part of the field, the A3 reservoir pressure was higher than the A5 pressure, in contrast to its northern part. All these conclusions indicate the need to optimise the reservoir pressure maintenance system.

2.2.1.9 QUANTITATIVE ANALYSIS USING THE TERMOSIM SIMULATOR

Example 1 (Job ID-14231)

This case describes a survey conducted in the deviated well to determine production distribution between perforated intervals and to check for communication and fractures if any. This challenging objective was achieved by the integration of high-precision temperature, multiphase capacitance and salinity, and spectral noise logging techniques. The survey was performed in three modes: flowing, static and transient.

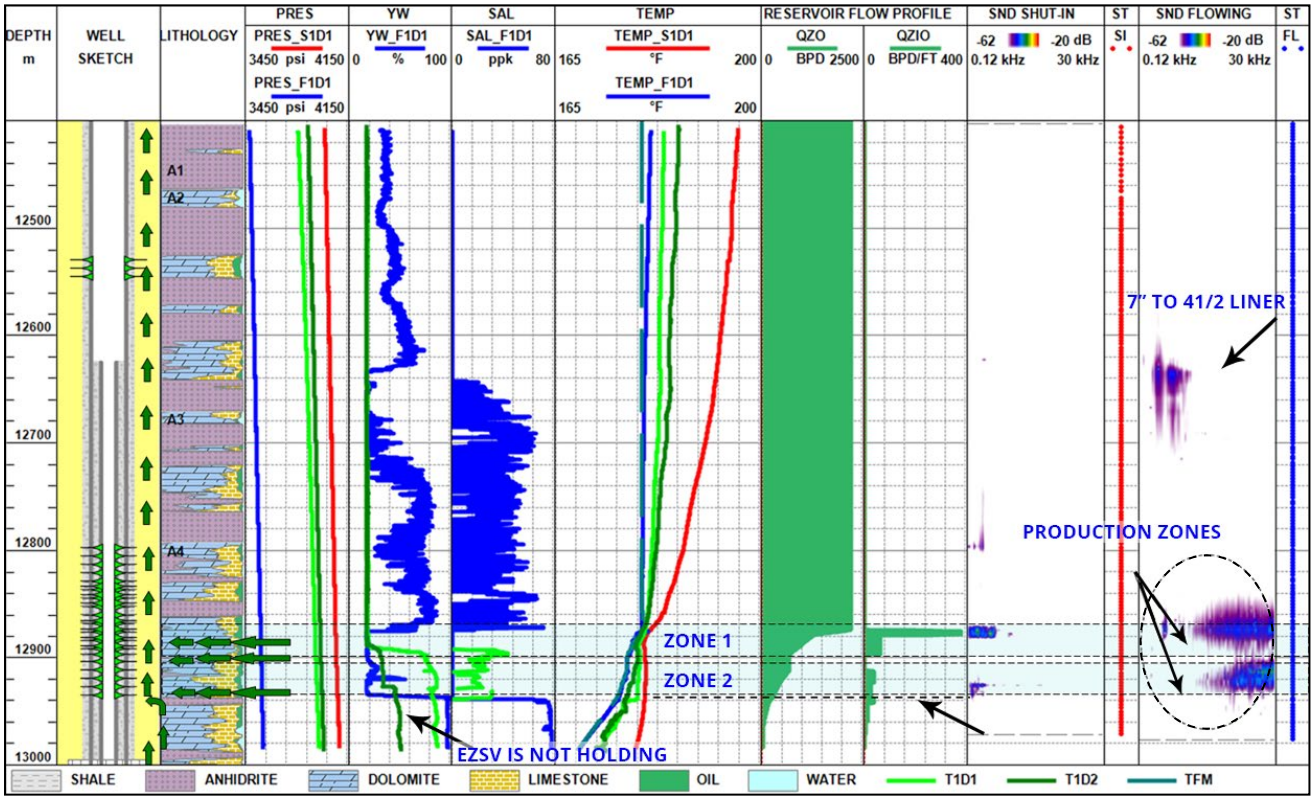

Fig. 1. No flow zone identification

To achieve these objectives, High Precision Temperature (HPT) and Spectral Noise Logging (SNL) surveys were carried out in this well under shut-in and flowing conditions. Shut-in bottom hole pressure recorded during HPT survey at the top of A2 was 4,007.3 psi, flowing bottom hole pressure was 3,482.8 psi at the same depth, producing a differential pressure of 524.5 psi. The shut-in pressure value is lower than the initial A4 reservoir pressure (4,400 psi) but higher than the bubble point pressure for A4 (3,062 psi). The flowing pressure value is higher than the bubble point pressure as well.

Shut-in temperature showed almost vertical gradient and shut-in SNL captured noise signals induced most probably by upward cross-flow from the zone below the survey interval into perforated interval in A4.

High frequency (10-30 *kHz*) signal corresponding to the matrix flow was detected within the perforated interval across the major oil inflows in intervals Zone 1 and Zone 2. The flowing and static temperature profiles did not merge below the perforated interval, indicating inflow below the perforation (LINE A). The different water holdup values in the sump area under flowing and transient conditions indicate that EZSV is not holding. Flowing temperature and flowing SNL did not show any indication of inflow zone through perforation interval across A2 formation.

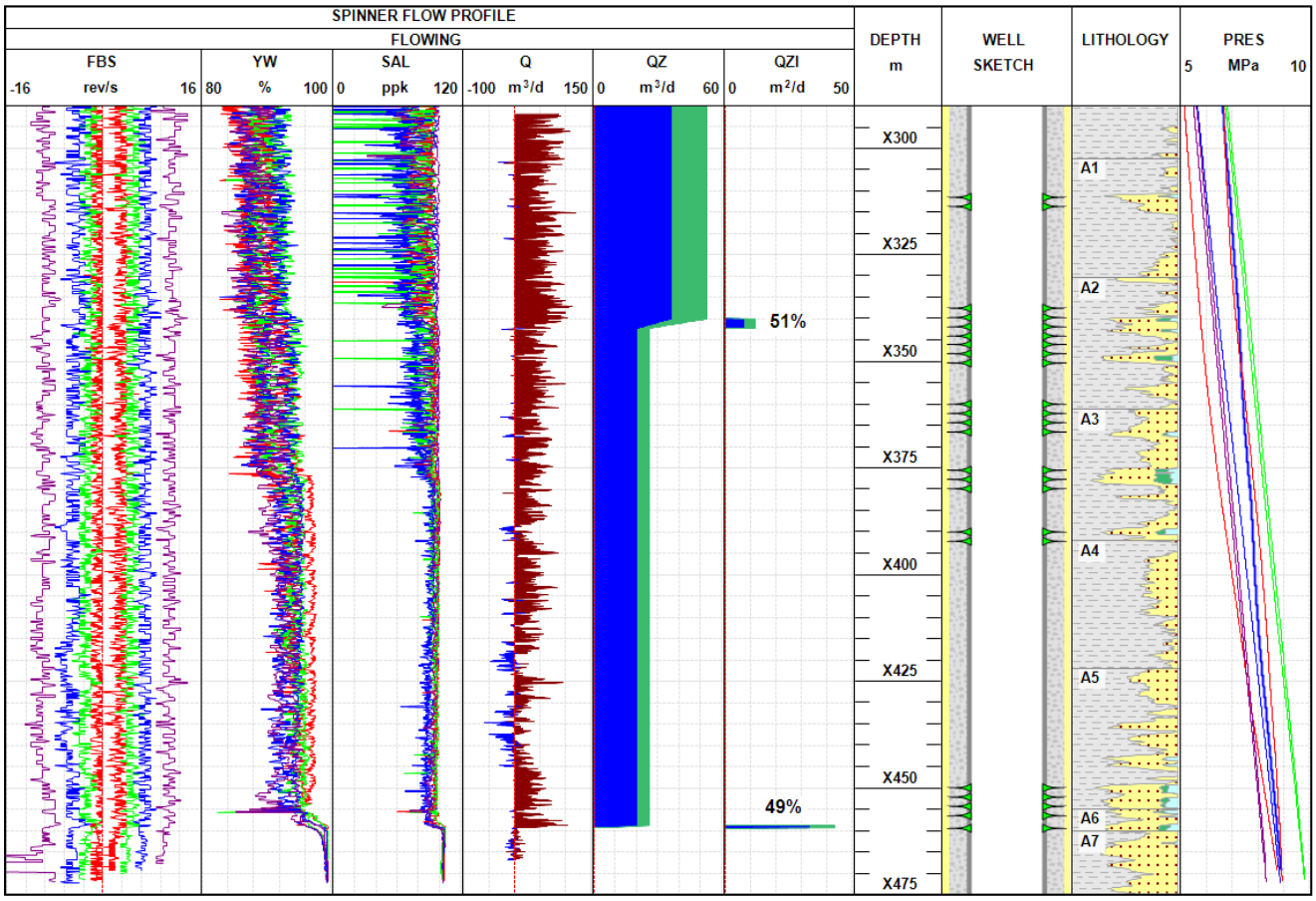

Fig. 1 Flowing PLT survey. Fullbore spinner data are given in the FBS panel and wellbore pressure in the PRESS panel. YW is water hold-up from capacitance sensor and SAL is wellbore fluid salinity from the induction resistivity sensor. Q is the spinner-based flow-rate profile, QZ is the interpreted wellbore flow profile and QZI is the differential flow profile.

Example 2 (Job ID-13443)

The well is shown in the example is a slightly deviated gas-lift oil producer with currently high water cut after eight years of production, with three perforated intervals across the A1, A2, A3, A5 and A6 formation units [27]. The well was surveyed under both flowing and shut-in conditions. The spinner detected production at 53 m^3/d with a mean water cut of about 70% from two inflow zones: X340.0–X342.2 m (A2 unit) and X458.9–X459.4 m (A6 unit). Fullbore spinner data suggest that production was equally split between the narrow A2 and A4 perforated intervals (Fig. 1).

The temperature logging programme consisted of one stabilised flowing survey, one transient survey after 13 hours and another transient survey after 17 hours of well shut-in. The flowing temperature profile of Fig. 2 provides additional details on the inflow profile and shows that the upper flow had multiple contributing zones, some of them with lower flow rates than the spinner could detect. One can pick these zones as temperature gradient

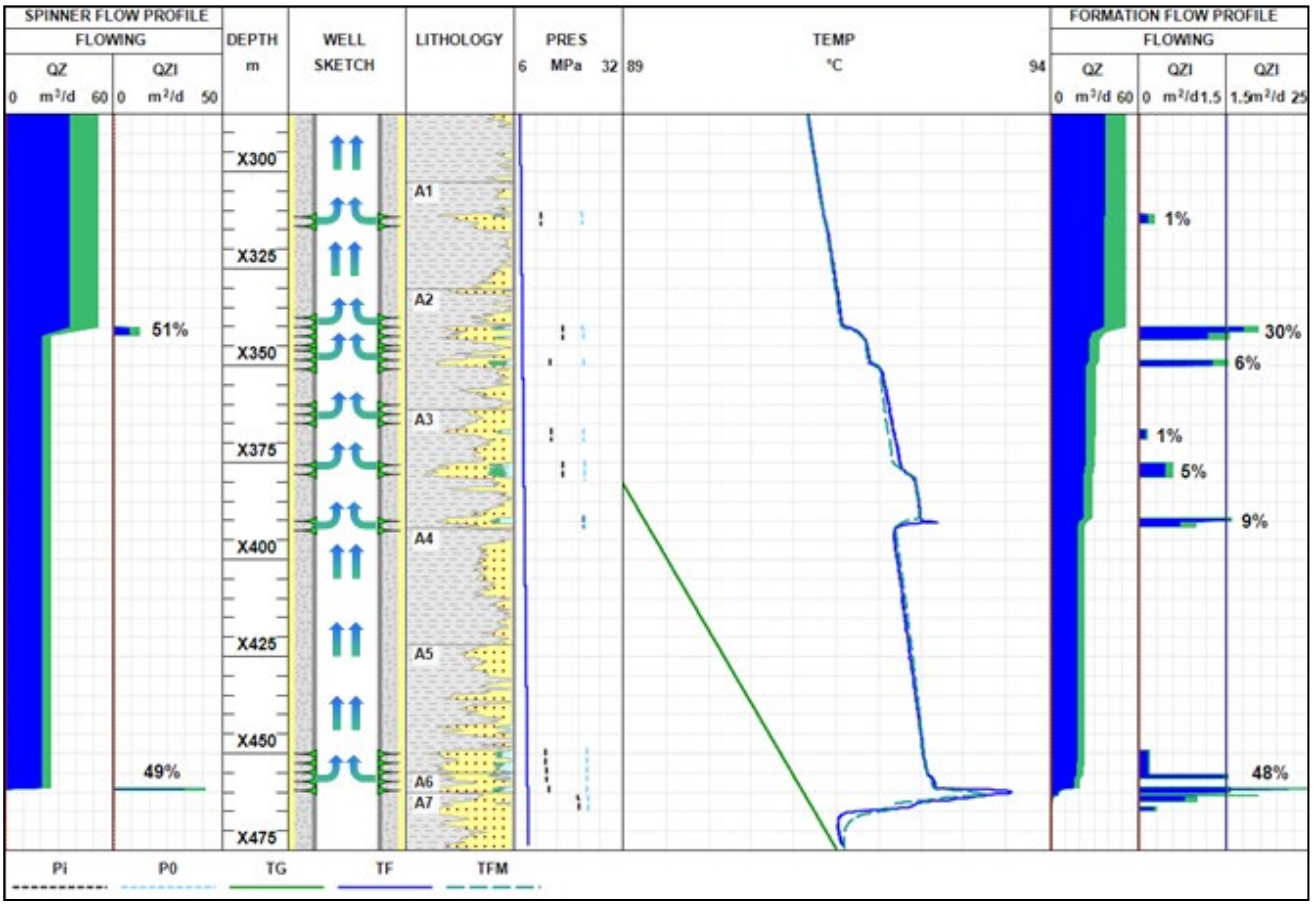

Fig. 2 Flowing HPT survey. Flowing temperature TF (solid blue line), simulated flowing temperature TFM (dashed cyan line) and geothermal profile TG (solid green line). The Formation Flow Profile panel (on the right) features the same QZ and QZI profiles as the FBS survey (on the left). The additional QZI panel is for a zoomed-in view at low inflow rates. The pressure in flowing formation units is shown by black dashes and the initial hydrostatic pressure by blue dashes.

anomalies. Whether a given temperature anomaly is positive or negative depends on a combination of factors, such as the far-field formation temperature, inflow rate and the total rate and temperature of the upward wellbore flow passing through this zone. This is what TSMp simulator handles based on the user inputs.

For instance, a cooling of 0.9°C at a depth of X460 m would originate from relatively cold but strong inflow from the upper part of the A6 unit merging with weaker but warmer upward flow from the lower part of the A6 unit. The overall production profile for this well was estimated with TSMp simulations at 55 m^3/d, i.e. very close to spinner readings.

The overall inflow profiles from spinner and temperature data modelling (QZ and QZI in Fig. 2) are the same but the latter resolves more details and picks small inflow zones missed by the spinner.

One can see that formation pressure varied between different flow units with particularly

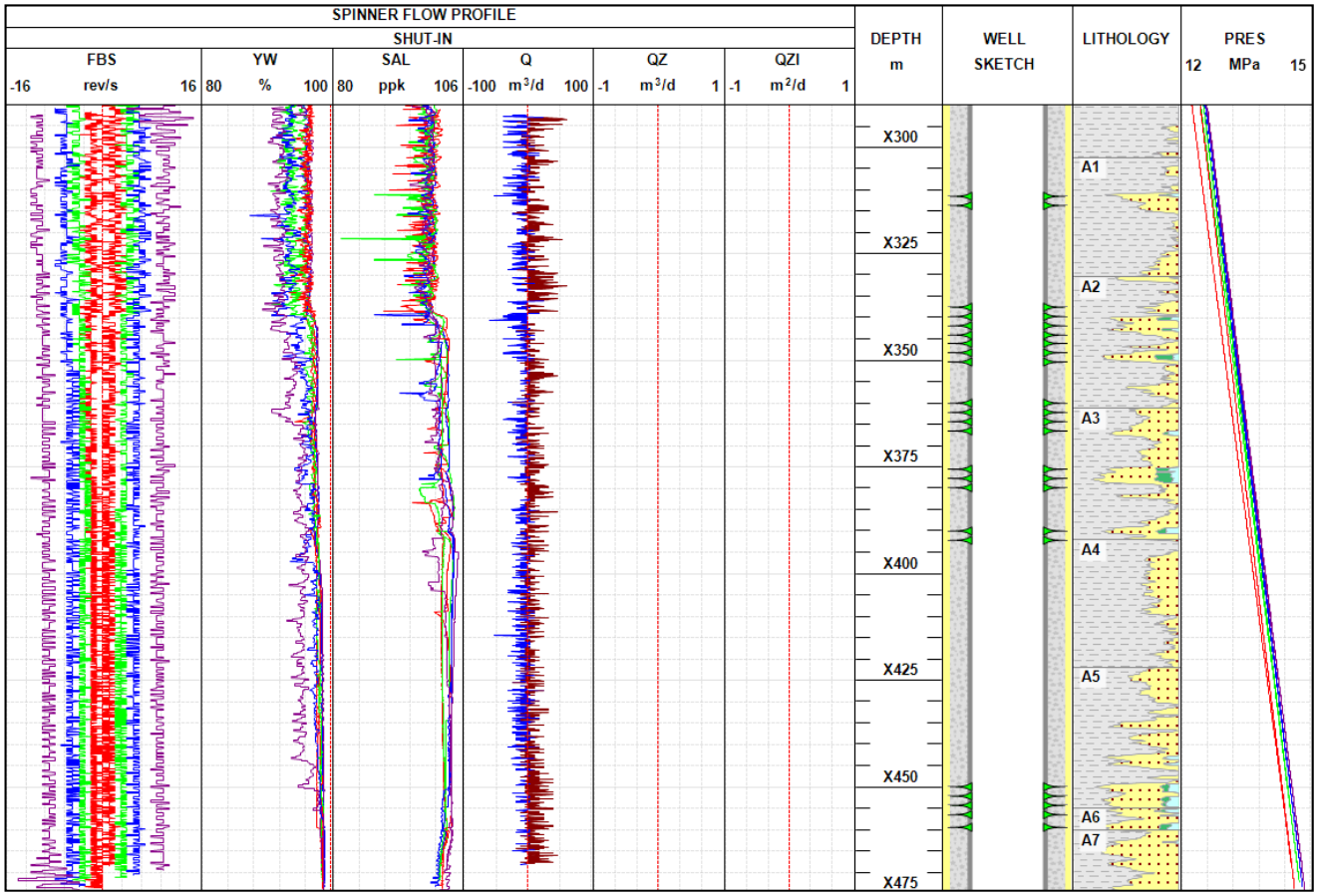

Fig. 3 Shut-in PLT survey. Fullbore spinner data are given in the FBS panel and wellbore pressure in the PRESS panel. YW is water hold-up from capacitance sensor and SAL is wellbore fluid salinity from the induction resistivity sensor. Q is the spinner-based flow-rate profile, QZ is the interpreted wellbore flow profile and QZI is the differential flow profile.

high formation pressures in the X389–X391 m interval.

Importantly, formation pressure was determined by simultaneous fitting of flowing and shut-in temperatures, and any attempt to change formation pressure and then compensate for this change by varying skin factors would most likely run the matching between either flowing or shut-in temperature logs and the corresponding modelled profiles.

The shut-in FBS survey did not reveal any flow, although multiphase sensors detected disturbance across perforations (Fig. 3).

The shut-in temperature transition logs show a clear response to these zones with a strong indication of upward and downward cross-flows (Fig. 4). TSMp simulations did not match the recorded logs very accurately because the cross-flow rate was changing uncontrollably during the survey, although the inflow points, drain points and cross-flow rates were accurately verified

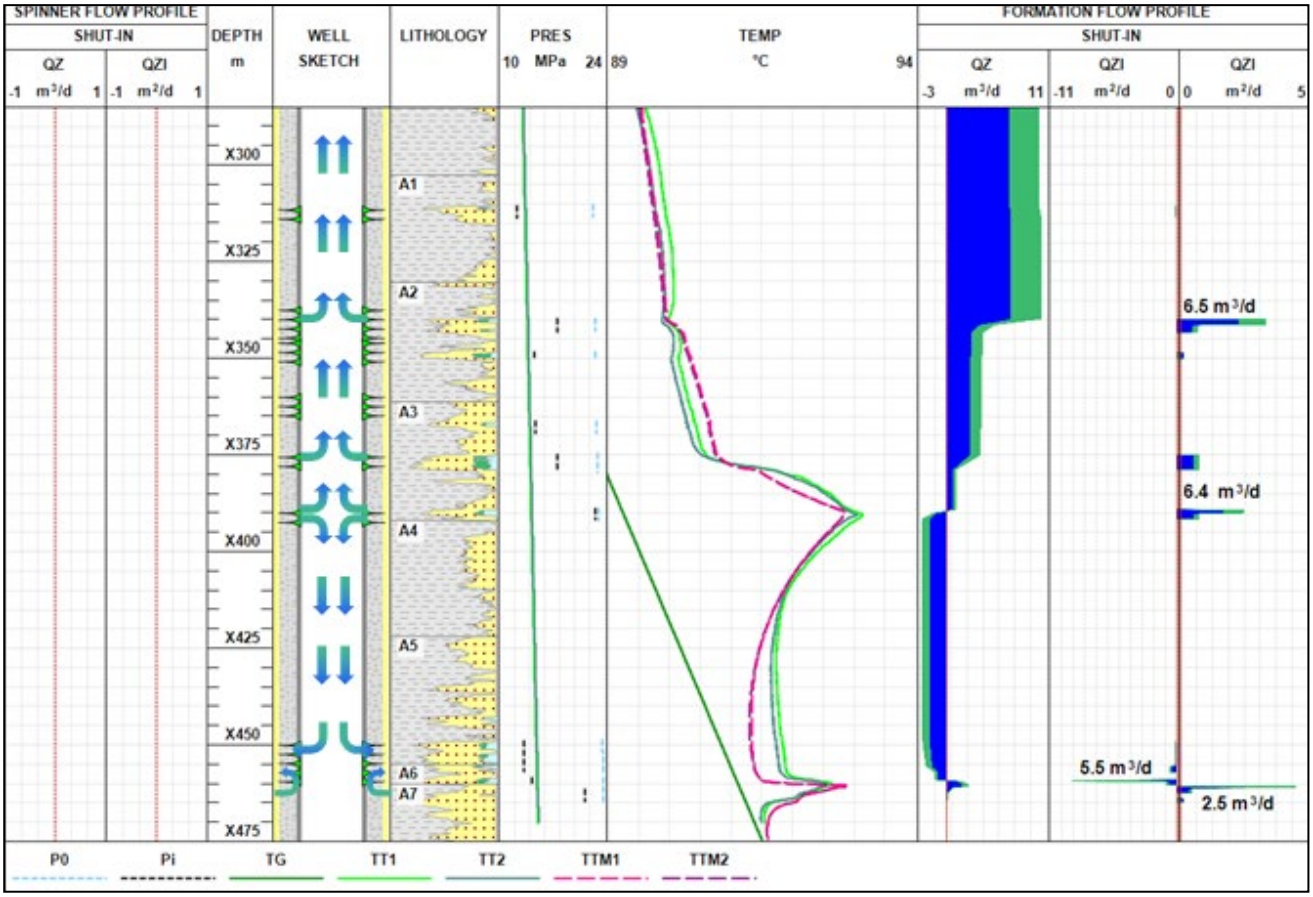

Fig. 4 Shut-in HPT survey. Transient temperatures TT1 13 hours after shut-in (solid light green line) and TT2 17 hours after shut-in (solid dark green line), simulated shut-in temperatures TTM1 (dashed pink line) and TTM2 (dashed purple line) and geothermal profile TG (solid green line). Temperature simulations revealed multiple wellbore cross-flows between formation units. The pressure in flowing formation units is shown by black dashes and the initial hydrostatic pressure by blue dashes.

by modelling. It is important to note here that the TSMp solver always assumes that formation pressure does not change between flowing and shut-in conditions, which is key in determining the only correct flow profile and formation pressure simultaneously from flowing and shut-in temperature logs. Anyway, this case provides a learning point to start monitoring pressure and temperature changes during a transition period after stopping production and to account for this change in the model. These data can be recorded at stations, normally above all perforated intervals, when the tool is on standby until the next transient pass.

In full agreement with the flowing temperature logs, shut-in cross-flow had its source at the bottom of the A3 unit, X389–X391 m, with the highest pressure among all flowing units. This flow rate is far below the spinner's threshold, and this explains why it was not captured by a conventional PLT survey (Fig. 5).

The source inflow then split into upward and

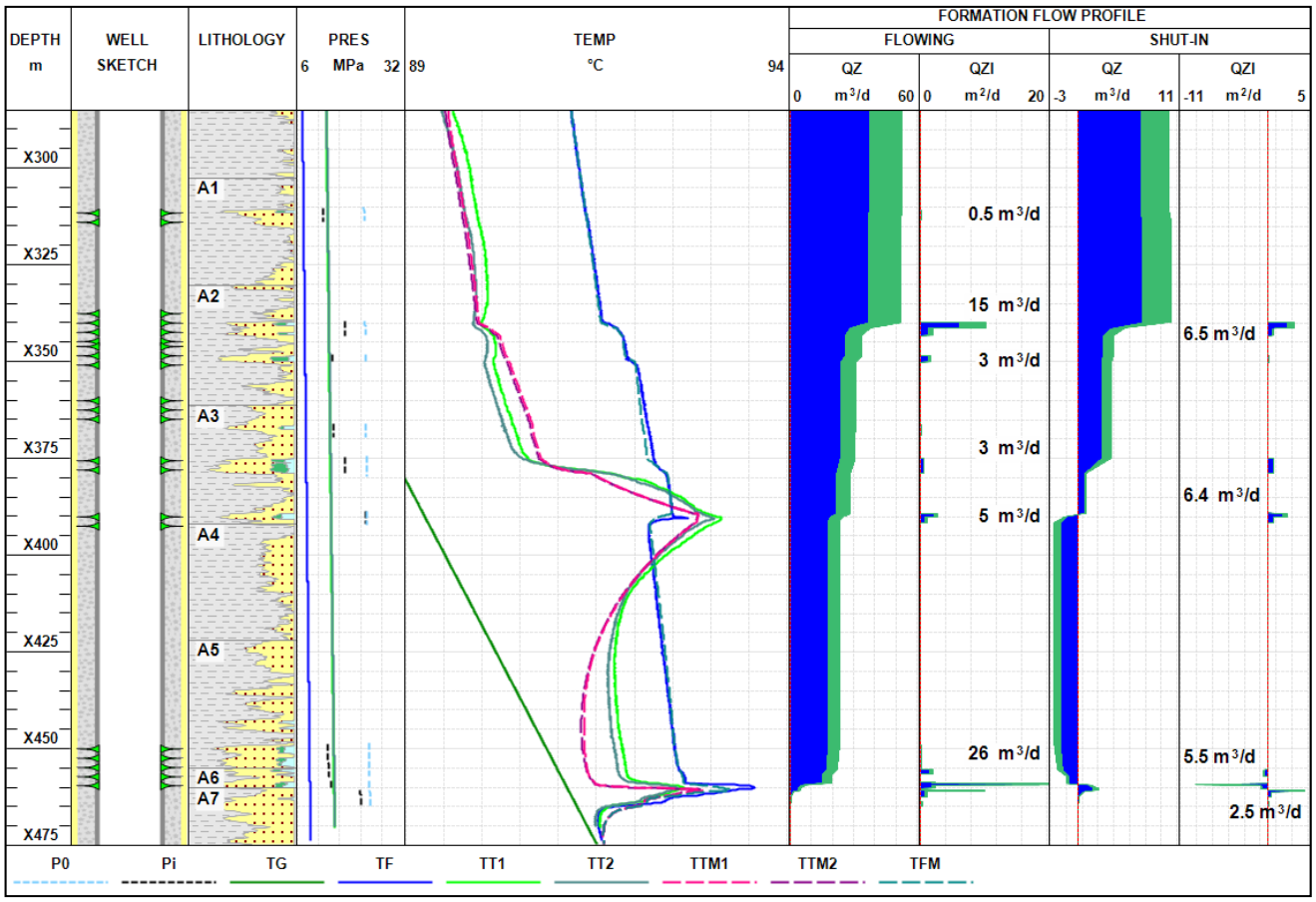

Fig. 5 Shut-in and flowing inflow profiles produced by temperature modelling.

downward flows. Upward 1-m^3/d flow met colder 2.5-m^3/d inflow from X375–X379 m, which resulted in cooling observed in the transient logs, then merged with 6.5-m^3/d flow from X345 m depth and went up beyond the survey interval.

The downward 3-m^3/d flow was absorbed at the top of the perforations within X458.5–X459 m. To model transient temperature profiles, one has to assume a minor upward flow of about 2.5 *m^3/d* from A7 to A6 that could not be detected by multiphase sensors because it occurred behind the casing. This flow pattern is in agreement with the fact that the A6 unit had the lowest formation pressure among all units below X389 m depth.

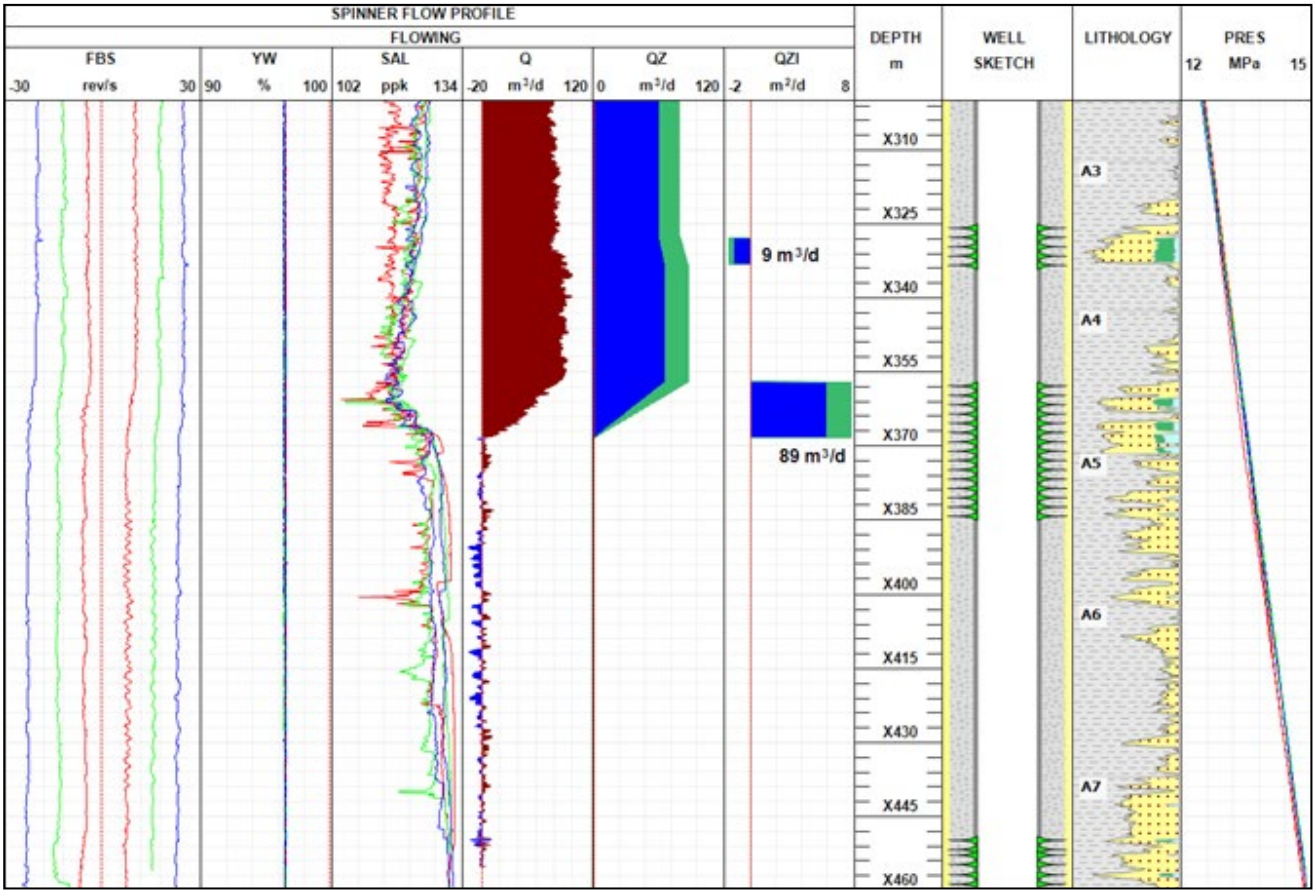

Fig. 1 Flowing PLT survey. Fullbore spinner data are given in the FBS panel and wellbore pressure in the PRESS panel. YW is water hold-up from capacitance sensor and SAL is wellbore fluid salinity from the induction resistivity sensor. Q is the spinner-based flow-rate profile, QZ is the interpreted wellbore flow profile and QZI is the differential flow profile.

Example 3 (Job ID-13413)

This well is gas-lift oil producer with currently high water cut after eight years of production, with three perforated intervals across the A3, A4, A5 and A7 formation units [27]. The well was surveyed under both flowing and shut-in conditions. The spinner detected production at 89 m^3/d with a mean water cut of about 70% from perforations across the A4 formation, as well as small 9-m^3/d loss of upward flow through perforations in A3 (Fig. 1). The total flow rate above all perforations was 80 m^3/d, in good match with surface tests.

The flowing temperature survey indicated that not only A4 but also A5 and A7 contributed to production at 105 m^3/d and 0.5 m^3/d, respectively, while the fluid loss across A3 was 28 m^3/d, confirming that A3 had the lowest formation pressure among all flowing units and even lower than the wellbore flowing pressure. The temperature survey also suggest that the main A7 flow came from a very thin layer above the perforations and then went down towards their top where it was detected by a salinity sensor.After the well was shut in for 20 hours, a transient survey was performed and the spinner

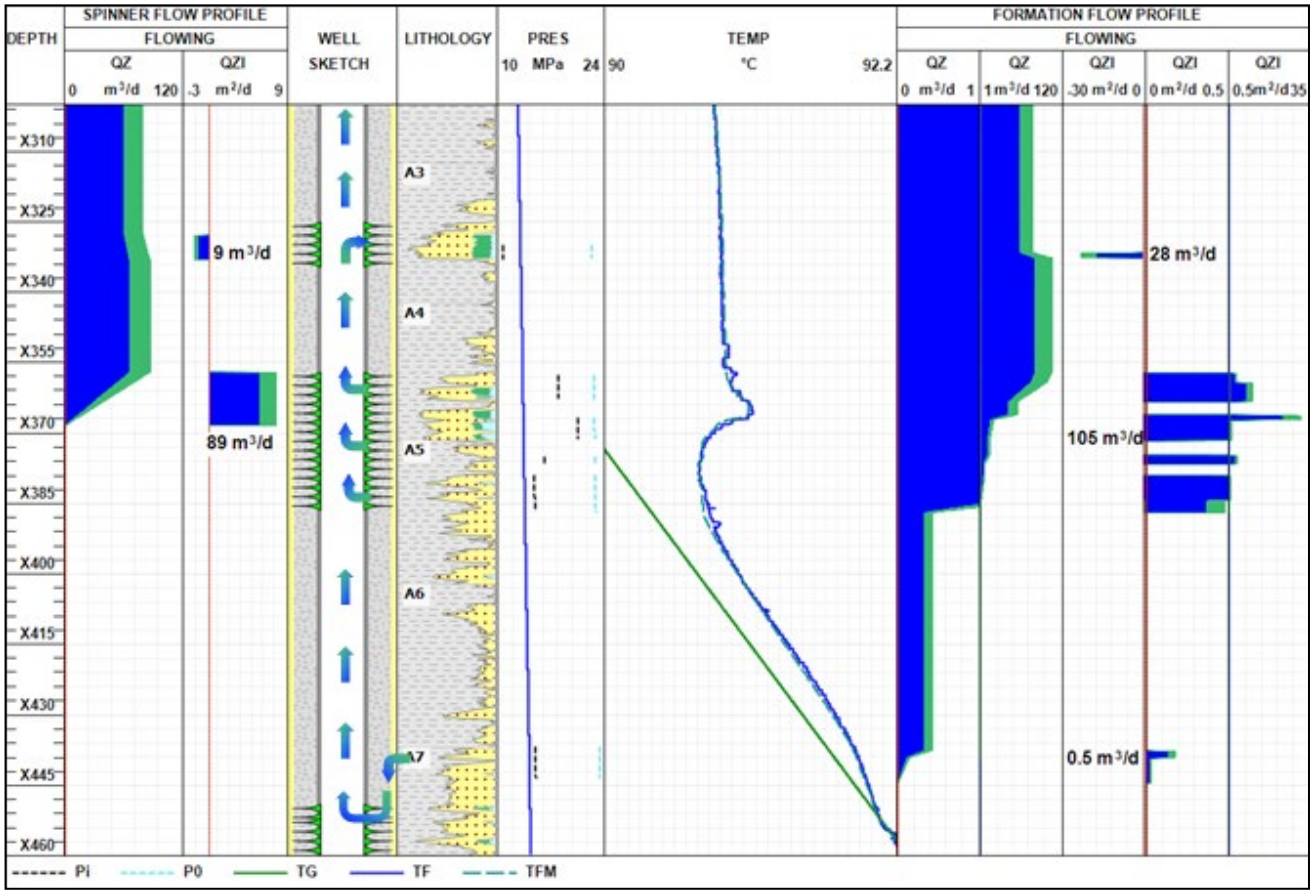

Fig. 2 Flowing HPT survey. Flowing temperature TF (solid blue line), simulated flowing temperature TFM (dashed cyan line) and geothermal profile TG (solid green line). The Formation Flow Profile panel (on the right) features the same QZ and QZI profiles as the FBS survey (on the left). The additional QZI panel is for a zoomed-in view at low inflow rates. The pressure in flowing formation units is shown by black dashes and the initial hydrostatic pressure by blue dashes.

captured upward 34-m^3/d cross-flow from the A4 to A3 perforations (Fig. 3). The temperature logs (Fig. 4) estimated upward cross-flow at 63 *m^3/d* and indicated that part of the inflow went down at 0.3 *m^3/d* to the A7 perforations and then channelled up behind the casing to the top of the thin A7 layer that was producing under flowing conditions.

The difference between upward flow rates from spinner and temperature surveys was caused by varying flow conditions after stopping the production. The pressure gradually recovered and the drawdown pressure in the A4 unit during the temperature survey was twice higher than during the spinner survey (Fig. 4).

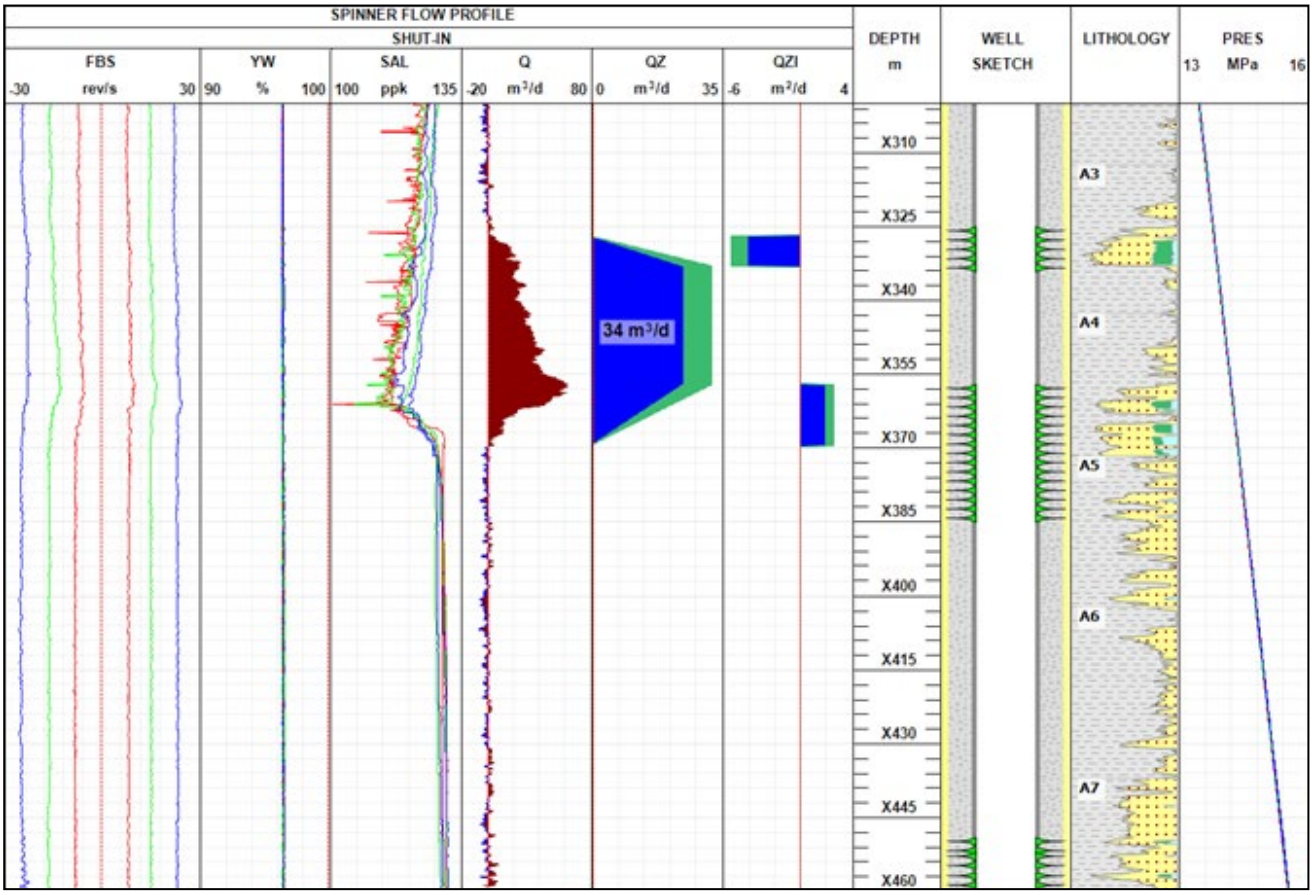

Fig. 3 Shut-in PLT survey. Fullbore spinner data are given in the FBS panel and wellbore pressure in the PRESS panel. YW is water hold-up from capacitance sensor and SAL is wellbore fluid salinity from the induction resistivity sensor. Q is the spinner-based flow-rate profile, QZ is the interpreted wellbore flow profile and QZI is the differential flow profile.

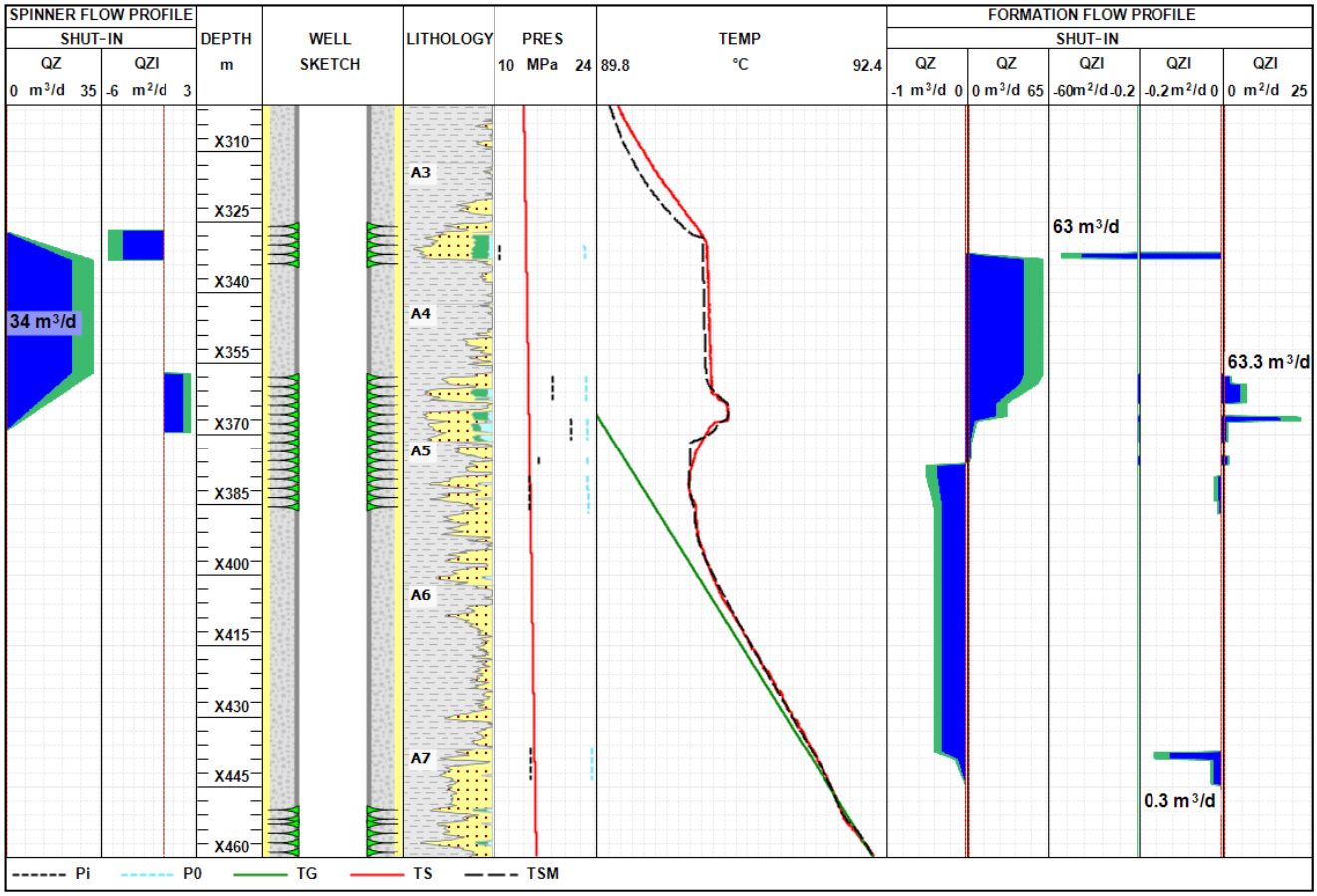

Fig. 4 Shut-in HPT survey. Shut-in temperature TS (solid red line), simulated shut-in temperatures TSM (dashed black line) and geothermal profile TG (solid green line). Temperature simulations revealed multiple wellbore cross-flows between formation units. The pressure in flowing formation units is shown by black dashes and the initial hydrostatic pressure by blue dashes.

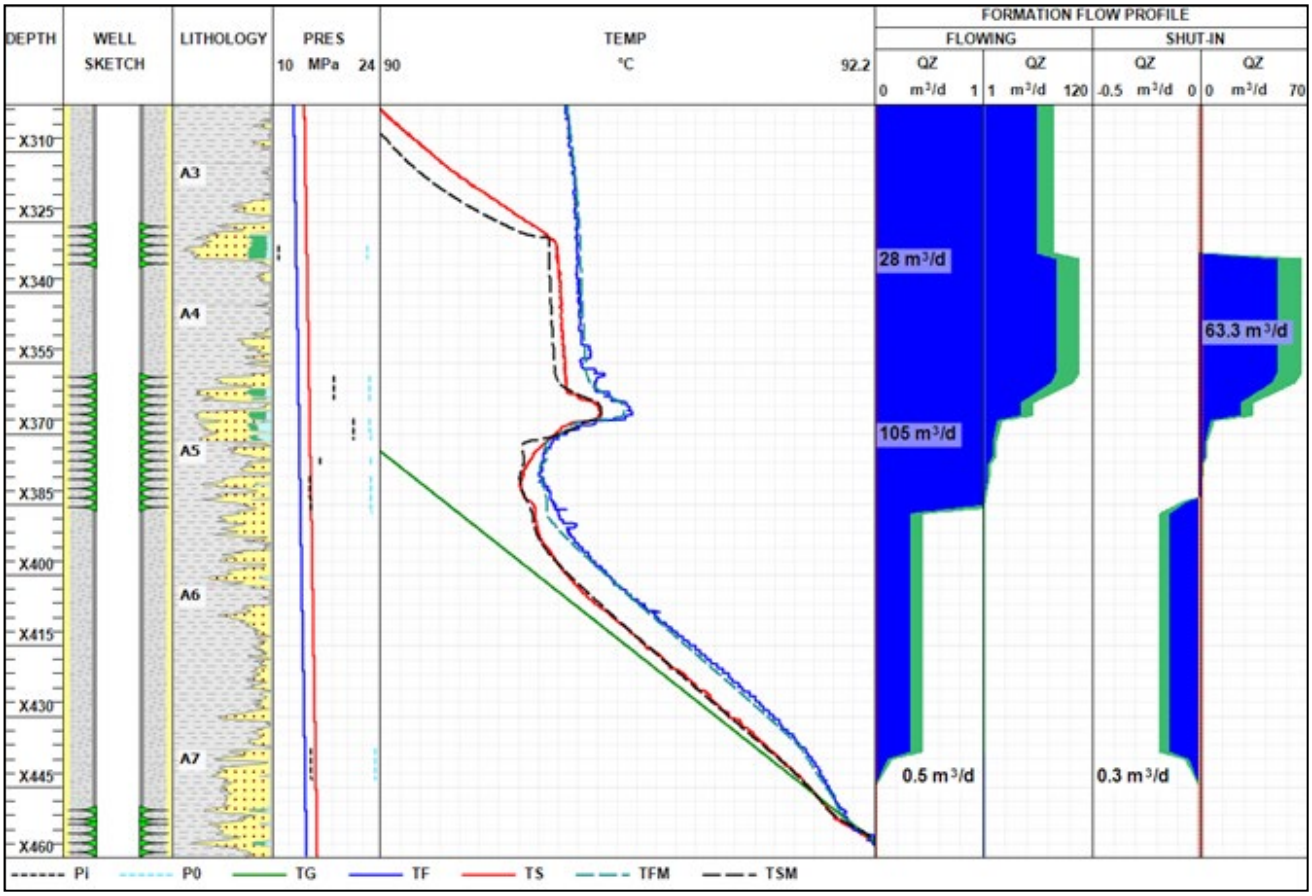

Fig. 5 Shut-in and flowing inflow profiles produced by temperature modelling

2.2.1.10 STEP TEMPERATURE RESPONSE TECHNIQUE

Example 1 (Job ID-14160)

This well is one of the eleven wells selected for acquisition of HPT-SNL data for flow calibration as part of hydrodynamic Micro-Grid Flow Modelling (MGFM) project for B. It has also been selected as a candidate for pressure pulse testing (PPT) in Cell 1. The objective of PPT will be to determine the dynamic permeability of B formation and check communication between B and C.

The short string was shut-in in October 2010. April 27, 2014 injection to the long string was stopped and the short string was brought on-line to injection. The average injection prior the intervention was 5690 BPD.

The objectives of the integrated production logging consisting of High Precision Temperature (HPT) logging and Spectral Noise Logging (SNL) in well were as follows: Estimate effectiveness of injection in B, Identify possible thief zones above and below B, Check well integrity (Communication between LS & SS)

HPT (High Precision Temperature) – SNL (Spectral Noise Logging) technologies were utilised during the survey. All the logging operations were conducted in the short string when the long string was shut-in. HPT and SNL surveys were conducted under flowing, transient and static conditions.

The first HPT-SNL survey was done under shut-in condition. Afterwards, the short string started

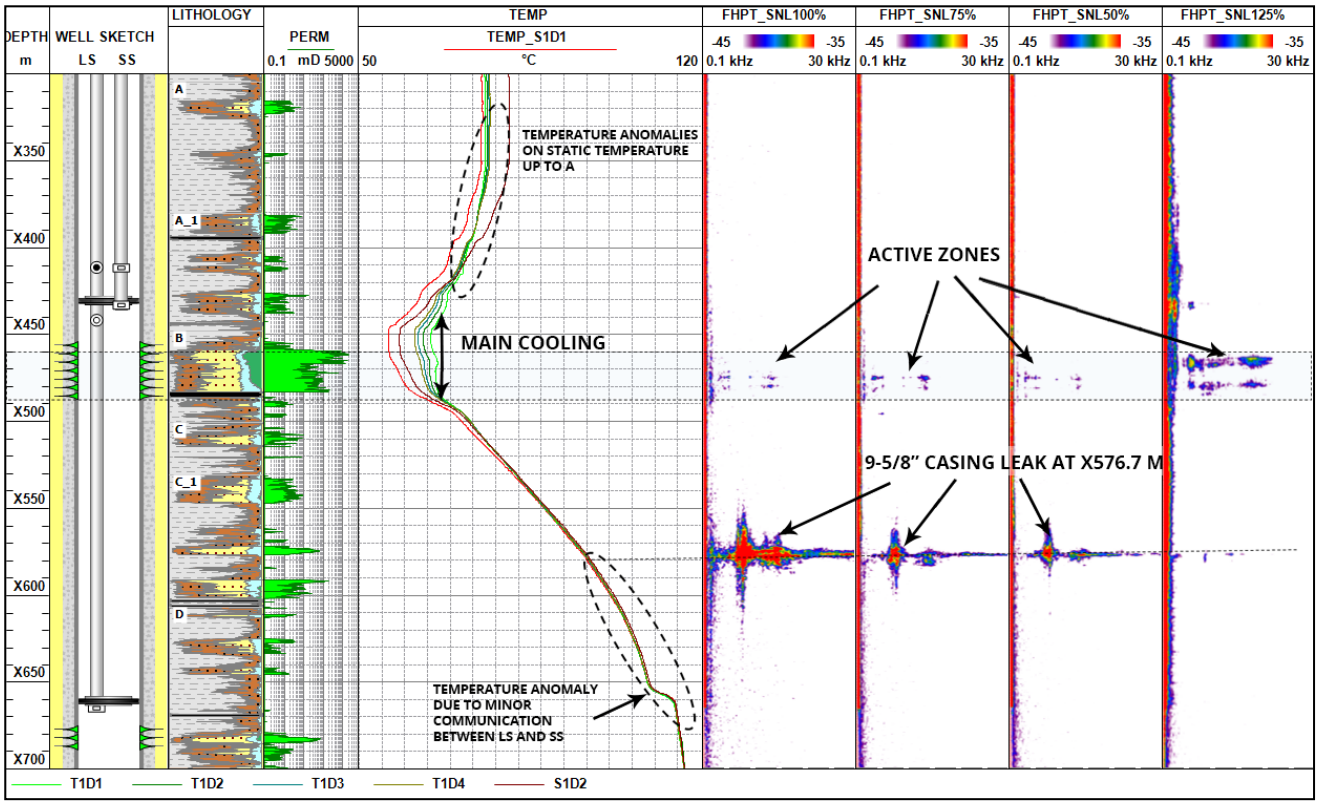

Fig. 1. Temperature and SNL measurements in the reservoir zone.

injecting for 1 hour 08 minutes at a rate of 450 m^3/d. Upon shutting-in the well, four transient temperatures were measured (STR technique).

The flowing HPT – SNL was conducted in 4 injection regimes: 100%, 75%, 50% and 125%.

Static temperature log shows some anomalies associated with upward cross-flow of a minor volume of injection water behind casing to A. The STR (Step temperature response) was performed in this well to assess injection allocation across B. It confirmed the response on temperature flux from B only. It means the temperature anomalies on A were not caused by active injection into these reservoir units. (see Fig. 1)

Infectivity test performed at 4 different injection rates shows that on regimes with rate 50%, 75% and 100% the upper part of B was not contributing to injection. The upper part of B turns to injection at a rate of 125%. This regime corresponds to the regular regime, which was set before the intervention in this well as per injection history.

The 9-5/8" casing leak at x576.7 m was detected at all performed regimes, but it was less pronounced at maximum rate of 125%. It might refer to C injection performance drop down after injection pressure was increasing. Also, it was detected the better injection performance of B at rate of 125%. It affects to volume of behind 9-5/8" casing flow to be less than during other injection regimes. (see Fig. 1)

According to HPT-SNL survey results, most of the fluid (90%) was injected into B reservoir. (for more details see Fig. 2)

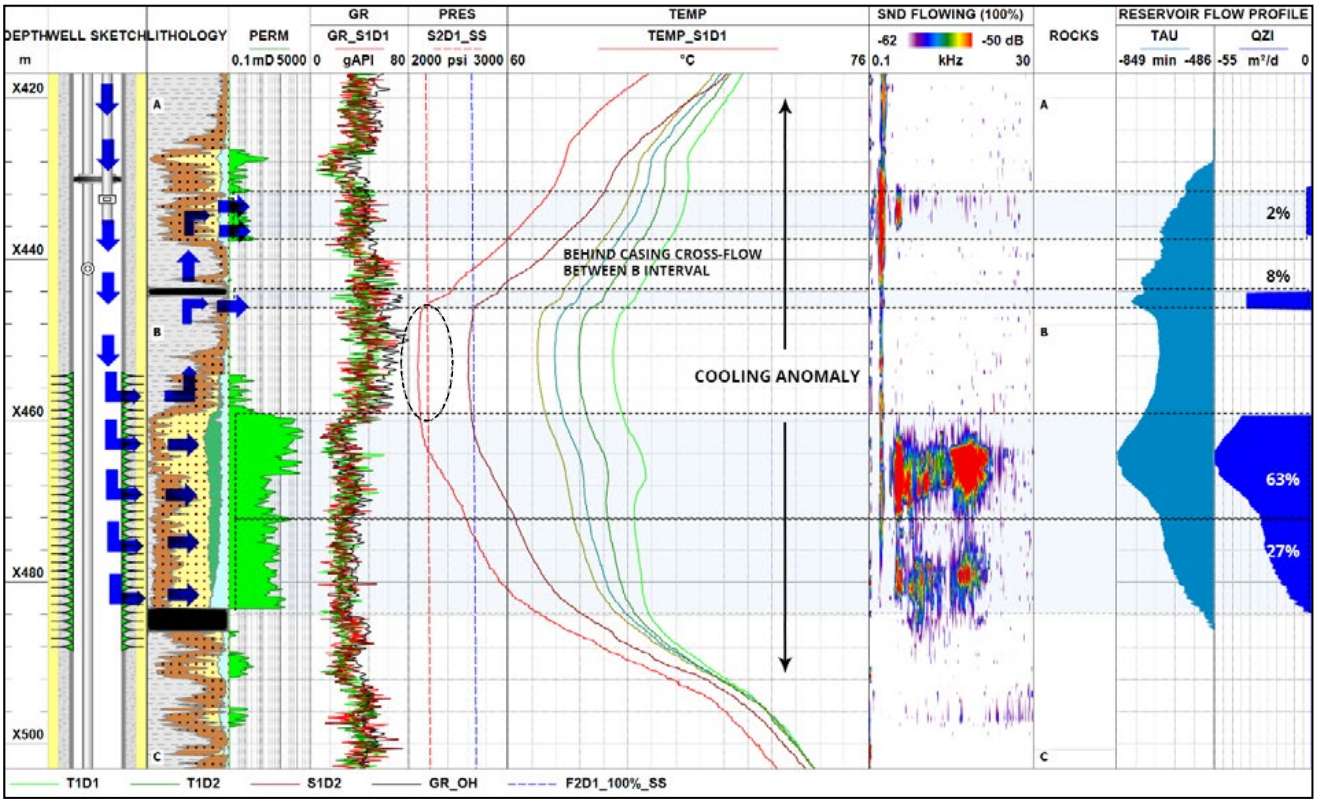

Fig. 2 Step Temperature Response Technique

2.2.1.11 EFFECT OF DAILY AND SEASONAL VARIATIONS OF INJECTION WATER TEMPERATURE

Example 1 (Job ID-11050)

This case presents the analysis of two time-lapse static temperature measurements made on 1 May 2009 and 27 July 2011. The survey well was shut-in for five days before static measurements in 2009 and for three days in 2011. The 2009 PLT and temperature profiles revealed that the C1 and C2 reservoir units had the maximum injectivities and C3 had a low injectivity. The PLT-based flow rate was 200 m^3/d, as shown in the figures below.

By 2011, the maxima and minima of the cooling zones had swapped places relative to the 2009 log. However, the PLT profile has not changed: most of the fluid continued to enter the C1 and C2 reservoir units at a rate of 200 m^3/d. Temperature simulations suggest two possible scenarios for the distribution of injected fluid in reservoirs units.

Scenario 1:

The temperature could change because of the effect of seasonal temperature variations on the injection fluid temperature. In 2009, injection was stopped on 26 April at 16:45, and the temperature at the surface on 1 May was 35°C. In 2011, injection was stopped on 25 July at 07:30, and the temperature at the surface on 27 July was 40°C. The simulation parameters are given in the table below.

By 2011, the temperature within the receiving reservoirs increased by ~4°C relative to 2009. The surface temperature was found to affect the wellbore temperature within the receiving reservoirs that had high injection rates. The hot fluid heats the receiving intervals, in contrast to the non-receiving ones that are cooled conductively by the previously injected cold fluid. Accordingly, static temperature logging revealed that the C2 reservoir unit with the highest injectivity was heated and cooled by fluids that were hotter and colder than the reservoir itself (Fig. 1).

	Regional data	**2009**	**2011–S1**
Average annual temperature	40°C	39°C	40°C
Seasonal maximum date	1 July	1 August	15 July
Annual variation	±10°C	±5°C	±5°C
Daily maximum time	16:00	16:00	16:00
Daily variation	±10°C	±10°C	±20°C
Maximum temperature	60°C	49°C	50°C
Minimum temperature	20°C	19°C	20°C

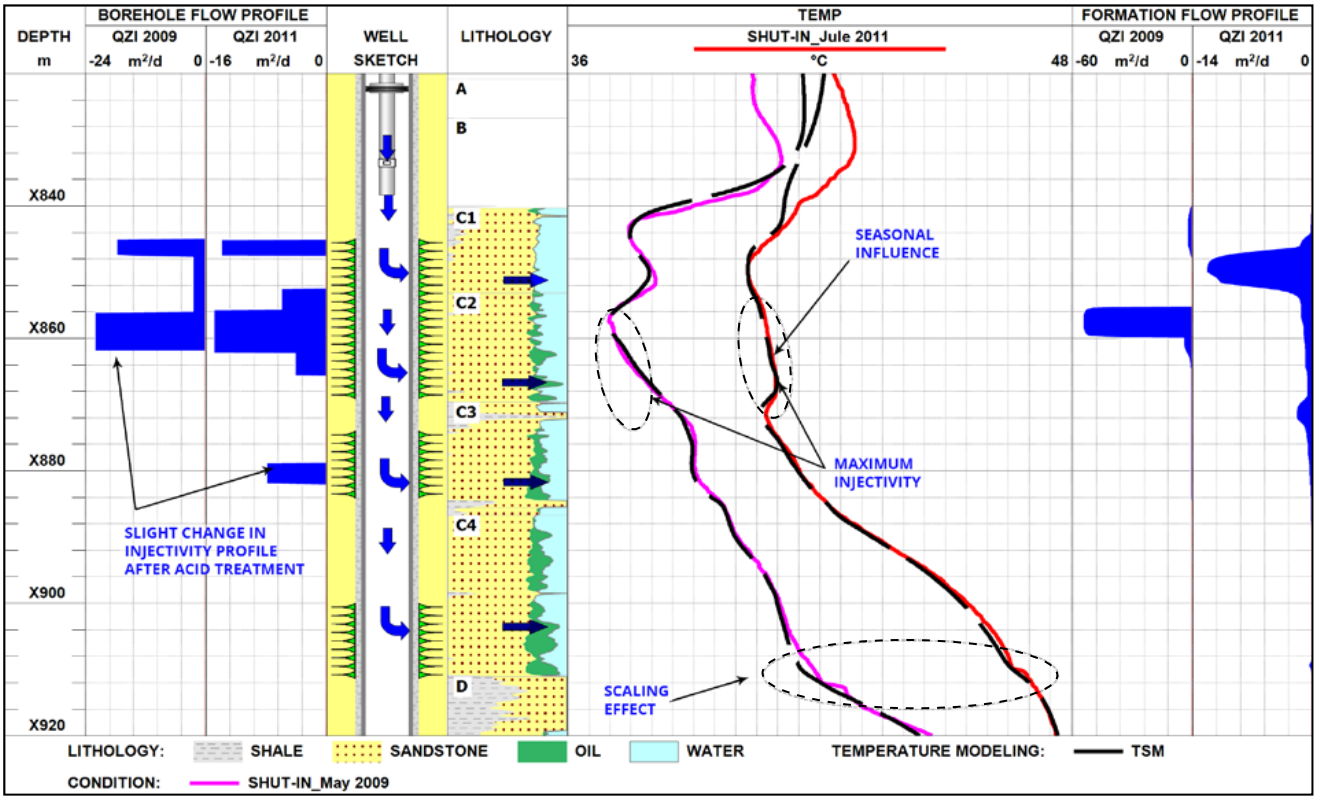

Fig. 1. Seasonal influence on the injected fluid temperature distribution in the reservoir

Scenario 2:

The change in the injectivity profile that occurred between 2009 and 2011 was caused by well operations. According to the well history, the volume of injected fluid increased three-fold after an acid treatment on 12 January 2011 (from 100 m^3/d to 300 m^3/d, then remaining at 250–300 m^3/d for 1.5 months) which could have caused fracturing and thus changed the injection profile. The C1 and C3 reservoir units received most of the injected fluid.

The simulation parameters are given in the table below.

	Regional data	**2009**	**2011–S2**
Average annual temperature	40°C	39°C	39.5°C
Seasonal maximum date	1 July	1 August	1 June
Annual variation	±10°C	±5°C	±5°C
Daily maximum time	16:00	16:00	16:00
Daily variation	±10°C	±10°C	±10°C
Maximum temperature	60°C	49°C	49.5°C
Minimum temperature	20°C	19°C	19.5°C

It should be noted that the injectivity of the C4 reservoir unit was low in both 2009 and 2011. The injection rate in this unit was too low to be detected by the full-bore spinner and was estimated by temperature simulation at 3.1% of the 2009 total injectivity (Fig. 2). The injectivity of the C4 reservoir unit in 2011 was 0.9% of the total injectivity in Scenario 1 and 1.5% in Scenario 2

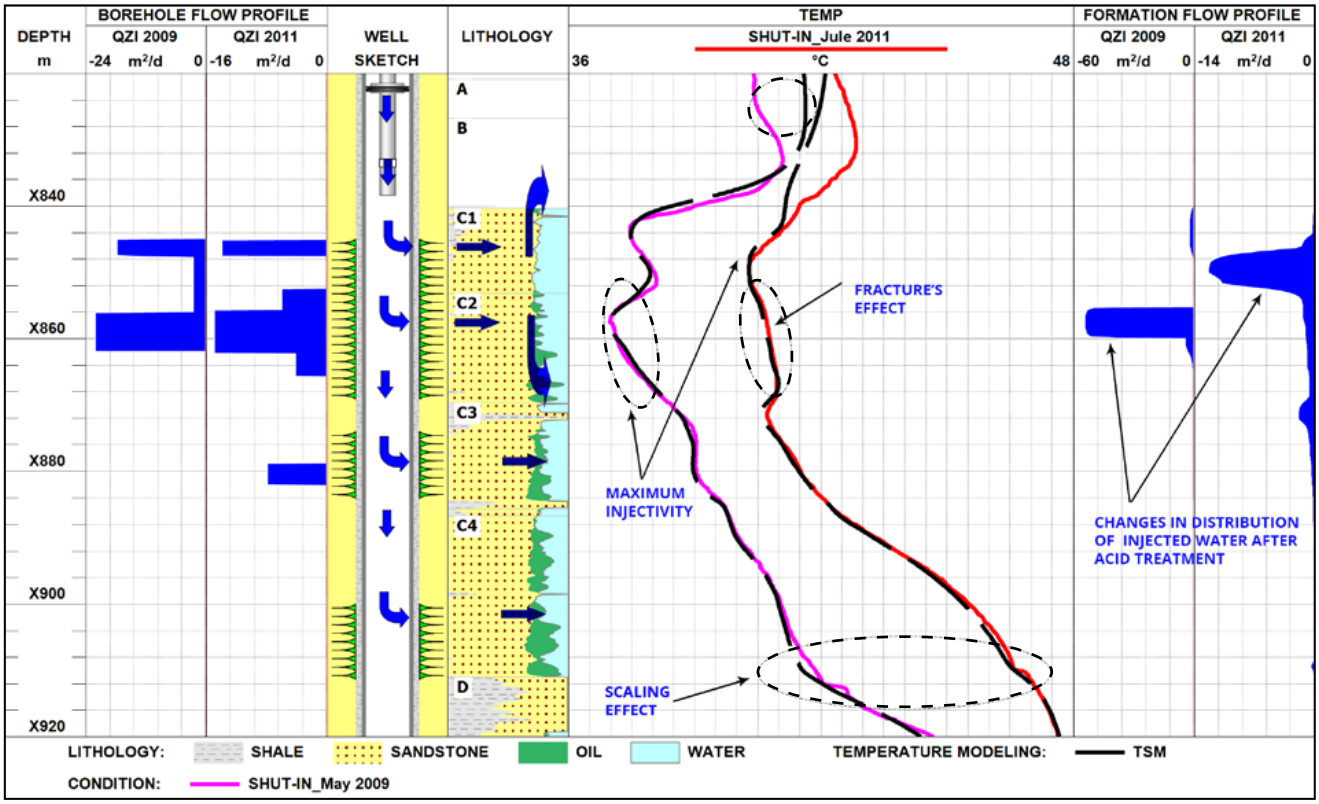

Fig. 2. Effect of fracture on the injected fluid temperature distribution in the reservoir

Example 2 (Job ID-10050)

This example demonstrates the effect of injection fluid temperature variations on wellbore temperature in an onshore injection well under static and flowing conditions. This effect was analysed using the RFI (Radial Flow in Injectors) temperature simulator.

Injection fluid temperature is known to be affected by daily and seasonal temperature variations. Average annual injection water temperature and daily and seasonal temperature amplitudes and phases impact static and flowing temperatures and are key input parameters for temperature simulations performed for injection wells.

Temperature measurements at the surface were in this case made with a high-resolution temperature sensor installed on a pipeline near the well and insulated with a special material. The sensor measured injection fluid temperature for several days and fed these data into the simulator.

Fig. 1 shows the measured temperature of injected water as a red line, and the modelled

temperature (with the selected amplitude and phase of injection water temperature fed into a simulator) as a dashed blue line. This took into account daily temperature variations. The modelled curves are shown in Figs. 3 and 4 as dashed black lines. As seen in the figures, the modelled flowing and static temperature curves based on the correct temperature history correlate with the measured temperature curves.

The effect of daily variations of injected water temperature on the wellbore temperature profile was analysed by generating and feeding into the simulator a knowingly incorrect injection temperature history with a changed average temperature and amplitude and phase of daily temperature variations (Fig. 2). The resulting curves are shown in the figures as dashed pink lines. The modelled flowing temperature is seen to deviate from the measured temperature, which affects the static temperature simulation.

This illustrates the importance of using correct daily temperature variation data in the simulation of flowing and static wellbore temperatures. Temperature measurements must always be made at the surface for at least a day before and during wellbore measurements, in order to design a proper temperature survey. The lack of data on daily temperature variation phases, survey schedules and injection volumes otherwise renders the injection profile based on temperature simulations uncertain.

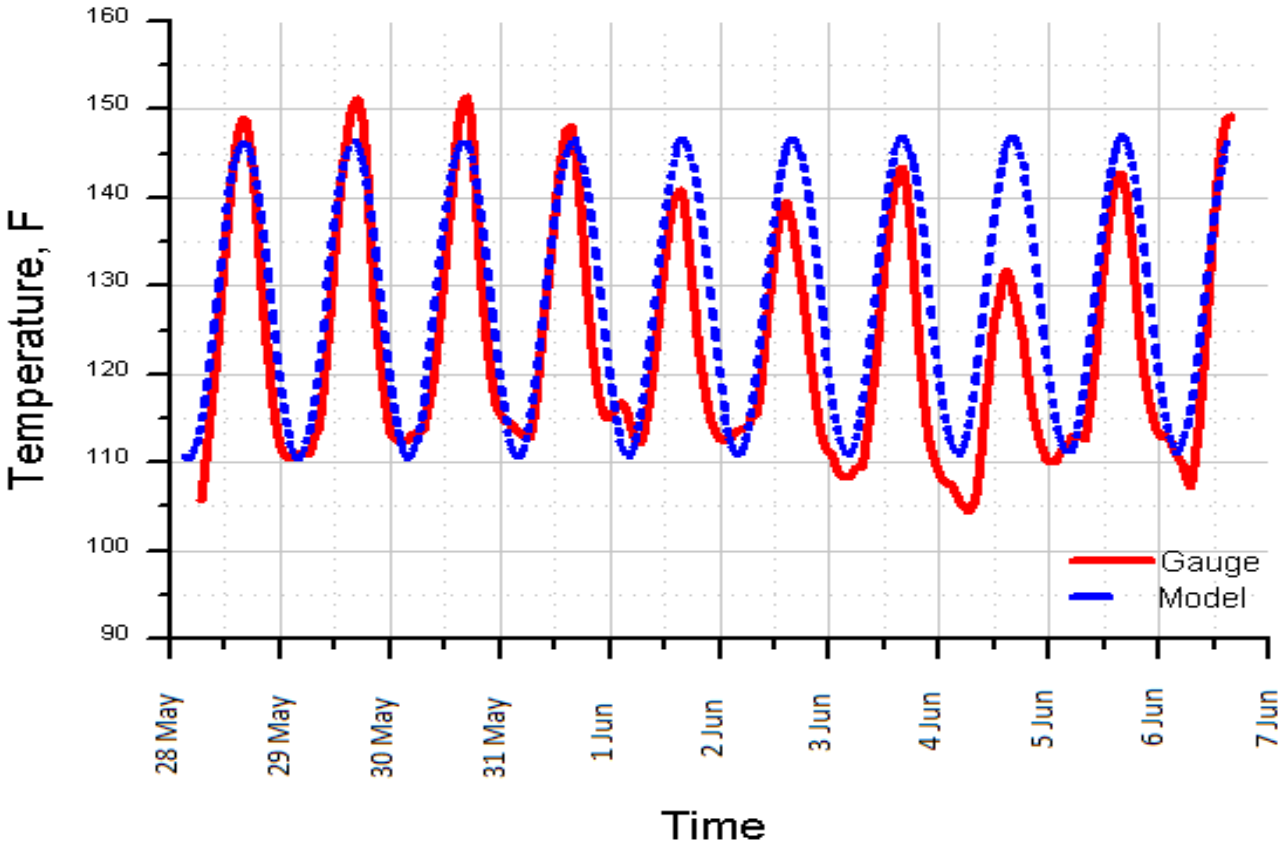

Fig. 1. Surface temperature variations

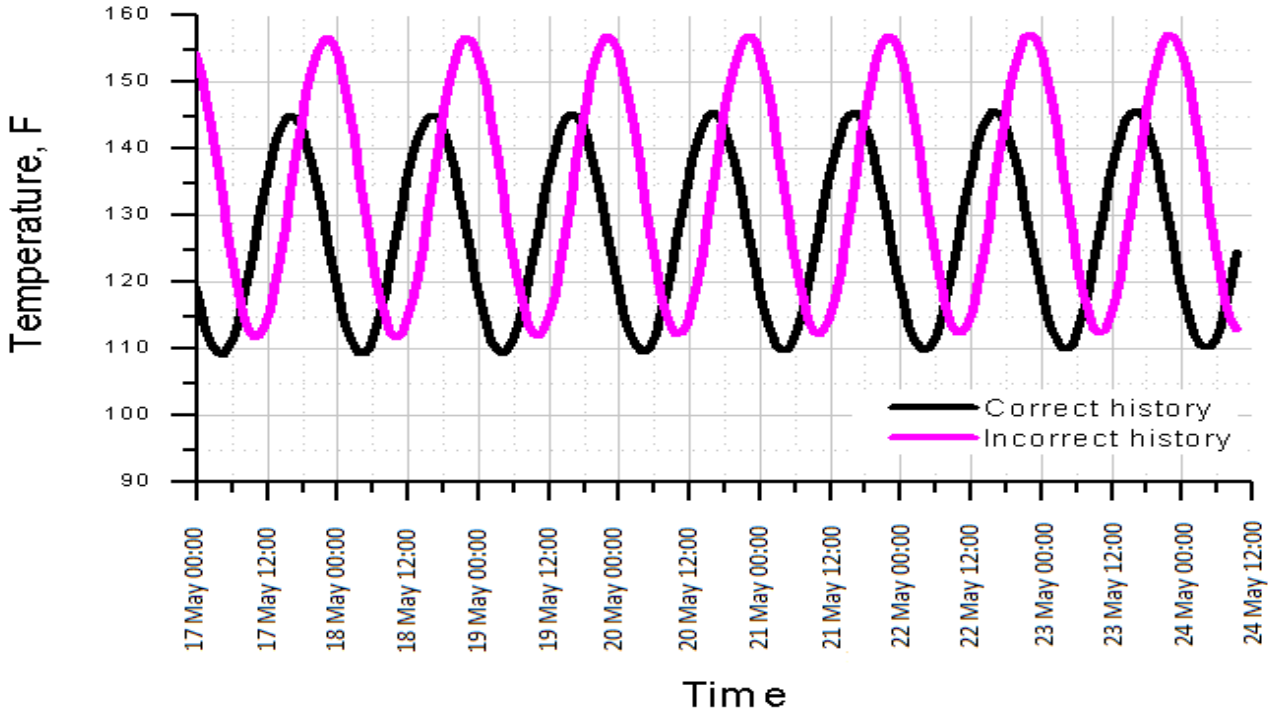

Fig. 2. Correct and incorrect temperature histories

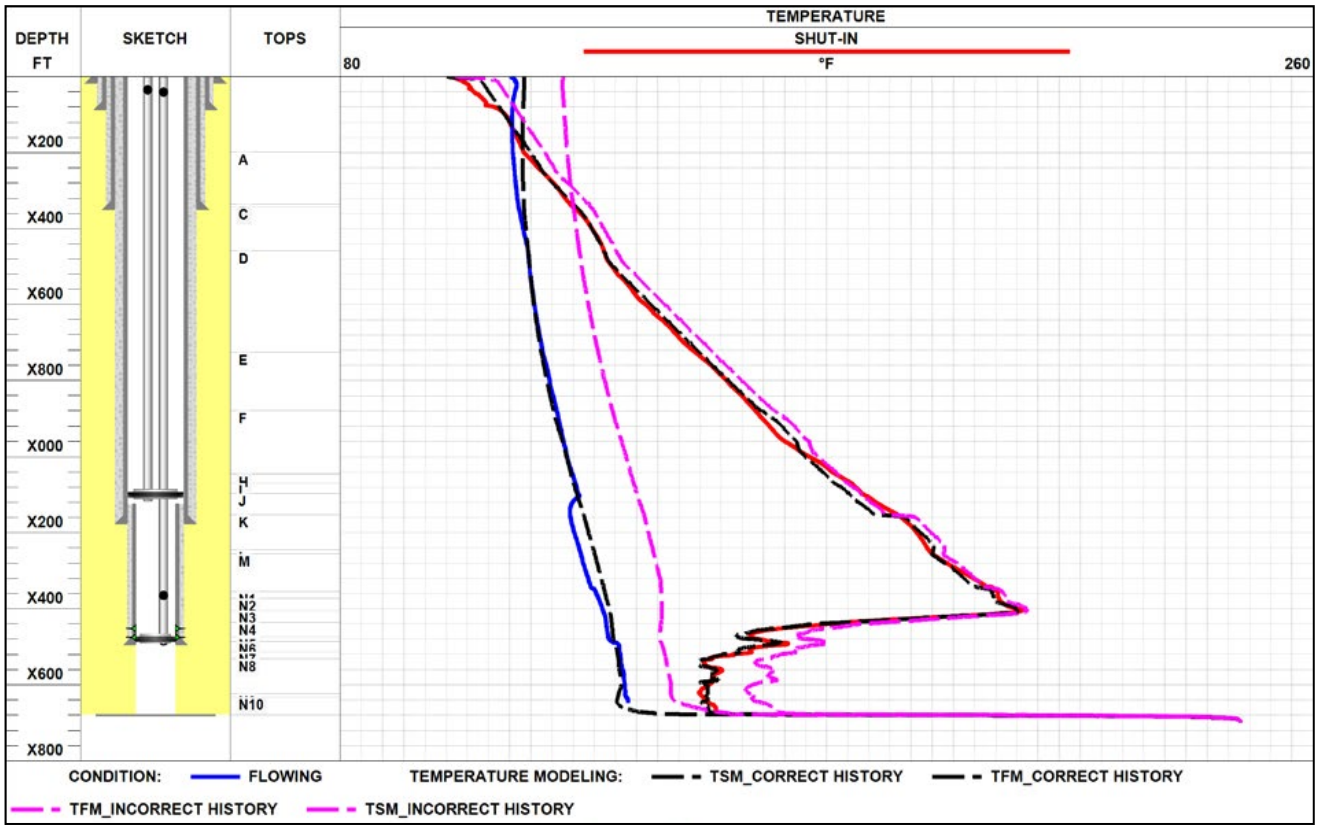

Fig. 3. Effect of history matching on the modelled and measured curves

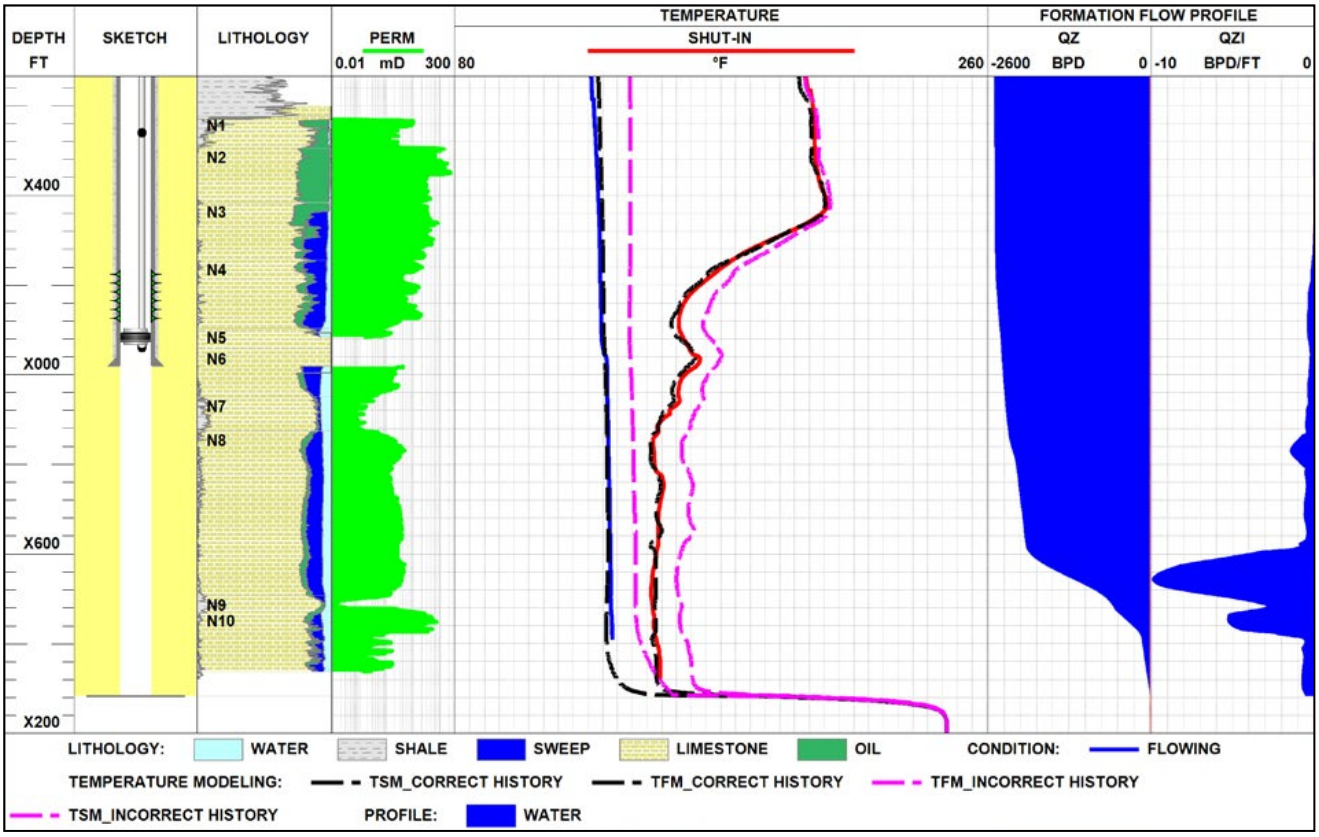

Fig. 4. Modelled and measured curves for an injection zone

2.2.1.12 HISTORICAL INJECTION ALLOCATION

Example 1 (Job ID-11052)

This example illustrates a temperature simulation performed to determine the historical and current cold-water injection profiles in this well.

The recorded static temperature log indicated cooling within the upper and lower perforated intervals. An SHPT log data simulation showed that more than 90% of injected water with an average annual temperature of 36C was absorbed by the upper perforated interval.

The flowing and static curves merged below X261 m suggesting no fluid loss below this depth. A flowing temperature simulation indicated injected water absorption within the upper perforated interval and no absorption below a depth of X261 m. A fluid flow rate of 170 m^3/d was used for the simulation of a temperature profile, and the result was in agreement with that for a flow rate of 156 m^3/d. The simulated QZI_T profile agrees with the QZI profile determined by HEX data interpretation. The fluid flow rate based on HEX data was calculated at 155 m^3/d (Fig. 1).

A low-temperature anomaly below a depth of X275 m could be due to breakthrough of injected water in this well in the past or from a nearby injection well.

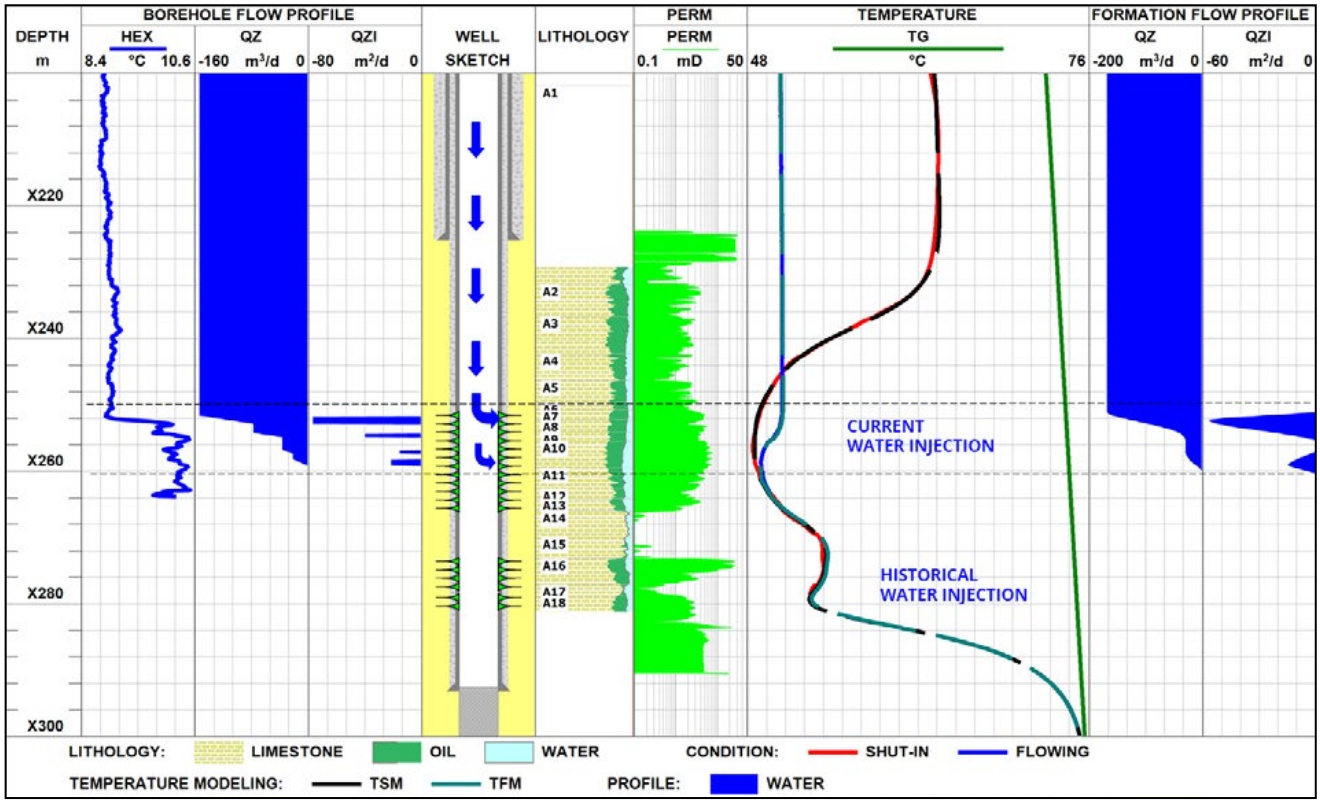

Fig. 1. Construction of current and historical injection profiles by HEX logging and temperature simulation

2.2.1.13 TEMPERATURE GRADIENT VERIFICATION

Example 1 (Job ID-7001)

This case illustrates the influence of geothermal rock temperature on static temperature in an injection well measured four to five days after shut-in. This effect was analysed using the RFI (Radial Flow in Injectors) temperature simulator.

One of the wells in this field was studied to reconstruct the geothermal profile. The selected well was never put on production and was far from other production and injection wells. The recorded geothermal profile was used to determine thermal conductivities for all of the reservoirs, and temperature simulations performed for one of the injection wells verified these data.

Figs. 1 and 2 show the reconstructed local thermal conductivities of rocks: LROCK CORRECT (a solid black line) and the corresponding geothermal curve TGM CORRECT (a dashed black line). As seen in the figures, the simulated static temperature (TSM CORRECT) correlates with the recorded temperature log, which indicates the correct selection of all parameters, including the geothermal profile. To demonstrate how geothermal temperature, and therefore thermal conductivity, affect static temperature, the knowingly incorrect thermal

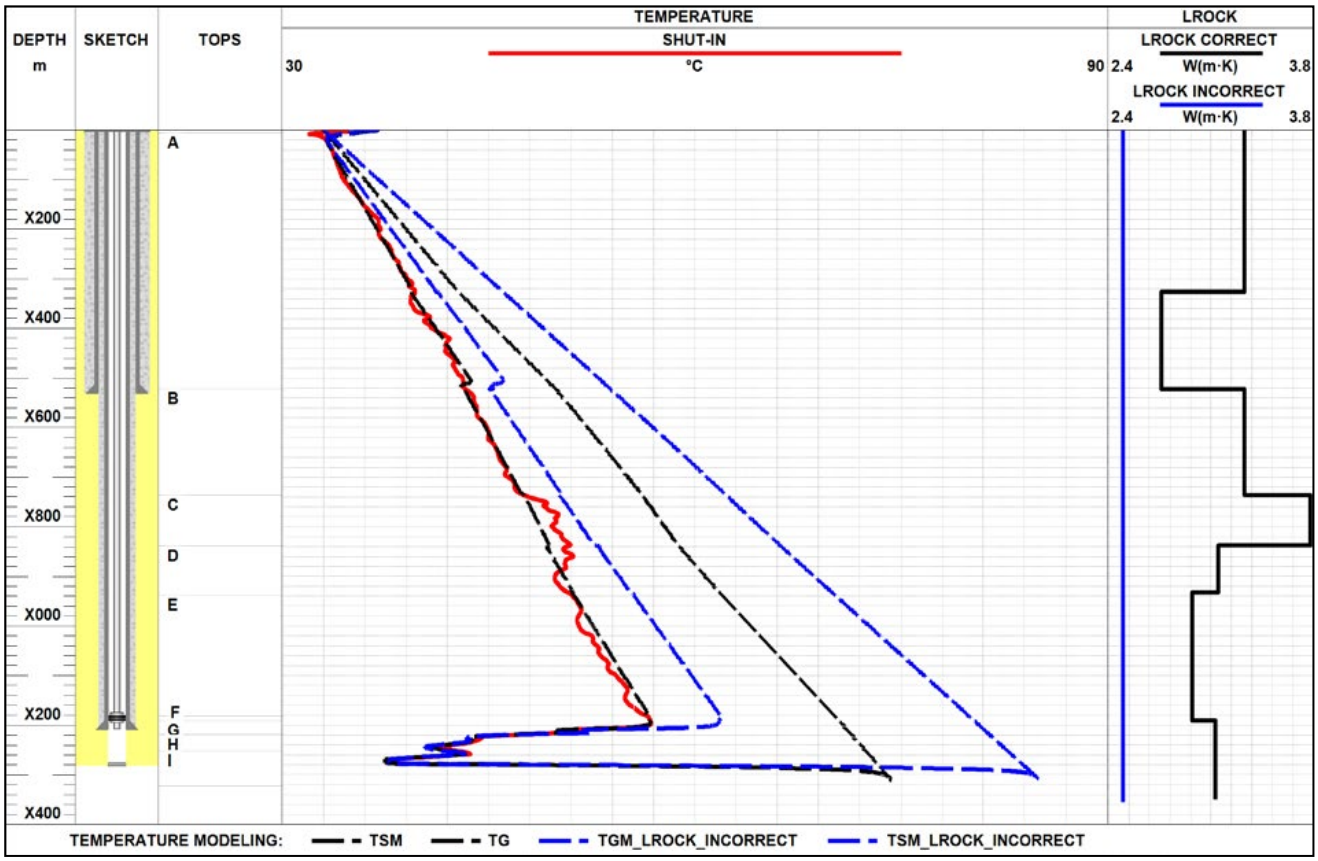

Fig. 1. Effect of LROCK parameter selection on the modelled and measured curves

conductivity profile LROCK INCORRECT (shown in blue in the LROCK panel) was fed into the simulator. The resultant thermal conductivities of the rocks correspond to the simulated curves TGM INCORRECT and TSM INCORRECT. The new simulated temperature curve, shown in blue, obviously does not match with the measured static temperature.

In this way we can see how geothermal temperature affects static temperature and that static temperature simulations can therefore be used to verify the geothermal profile of the field, as a basis for further temperature modelling.

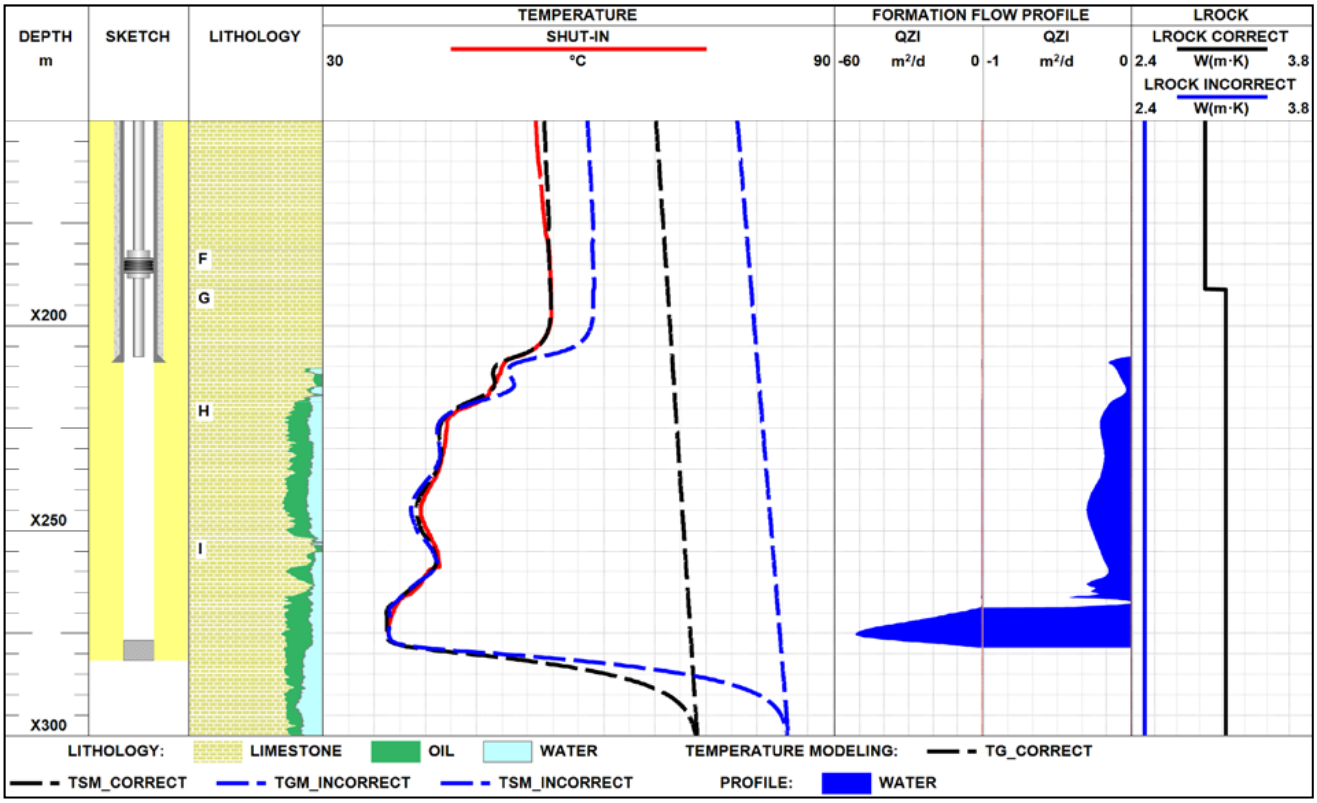

Fig. 2. Modelled and measured curves for an injection zone

2.2.2 WATER/GAS BREAKTHROUGH

2.2.2.1 SMART COMPLETION WELLS

Example 1 (Job ID-11027)

This case illustrates the application of the downhole memory pressure and temperature gauge (DMPT) and spectral noise logging (SNL) to locating sources of water encroachment in smart wells equipped with packers swelling upon contact with water to prevent water entry from water-breakthrough intervals.

The survey was performed in two modes: flowing and transient (with short-term shut-in). The flowing survey detected temperature perturbations within perforated zones caused by the choke effect (Fig. 1). These data showed that all three perforated zones within the survey interval produced fluid. The first perforated zone (Reservoir A3) was the main producing interval, as indicated by flowing temperature and noise logging data.

High-frequency 9–25 *kHz* noise, characteristic of reservoir flow, was detected in Zones A, B and C of Reservoir A3. Wavelet filtration of the recorded signal detected even low amplitude noises (Fig. 1). An insignificant temperature variation and low noise identified by filtration of the SNL signals from the second, third and fourth perforated intervals (below Level 3) indicated their low productivity.

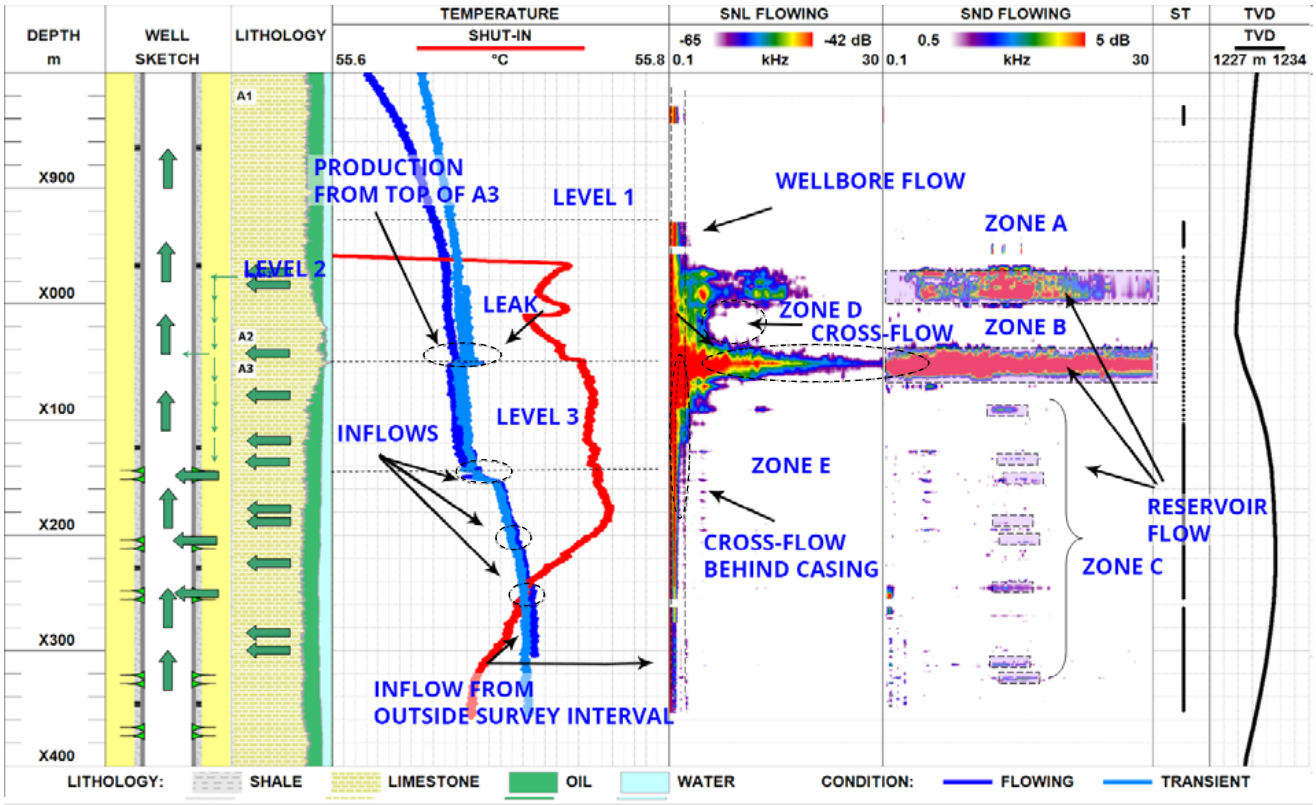

Fig. 1. Production from outside the survey interval and through a casing leak

A heating anomaly was observed under flowing conditions above the perforated intervals (Level 2). This temperature anomaly, caused by the choke effect, and high-amplitude noise detected within the whole frequency range (Fig. 1) indicated a casing leak at this depth, which could be verified by magnetic imaging defectoscopy.

The static temperature profile shows heating within flow zones. No heating was detected above Level 1. Therefore, there was no inflow from above Level 1. A packer installed at Level 1 opened up and prevented water production from an overlying productive interval. Spectral noise logging performed under flowing conditions confirmed that no production occurred from above Level 1 (Fig. 1). Flow behind casing between the open packers that generated low-frequency 1.6–2.6 *kHz* noise was found in Zones D and E.

In this way, high precision temperature and spectral noise logging can effectively locate flow intervals as well as water breakthrough zones shut-off by swelling packers.

The correlation of flowing and transient temperatures indicated strong upflow from below the survey interval.

The trajectory of this well suggests that noise detected in Zones A and B was generated by a permeable unit of Reservoir A3 (see a 3D view in Fig. 2).

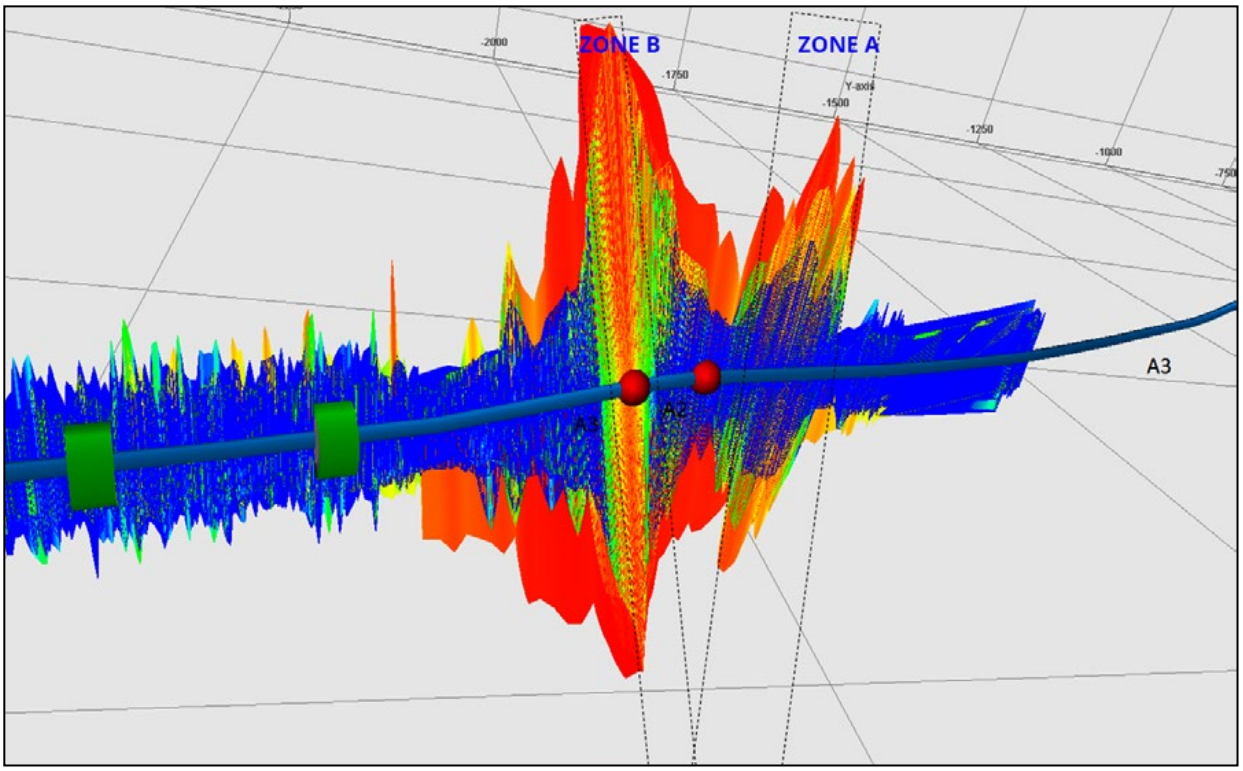

2.2.2.2 SINGLE-STAGE AND MULTI-STAGE FRACKING

Example 1 (Job ID-13022)

This is the vertical producer with hydro-frac completion. The frac water was flushed back in a few days but the water cut sustained at 80 % [26]. The HPT-SNL-PLT survey was performed two months after completion of the frac job. The well was flowing at a constant rate the entire time and the survey was started with flowing passes. The well was then shut in and the shut-in pass was recorded after three days (see Fig 1.).

The PLT interpretation (mechanical spinner and multiphase sensors) suggests that the main oil inflow to the wellbore occurs from the bottom part of the perforated zone while water is coming from the middle part (see BOREHOLE FLOW PROFLE at Fig. 2). The total water cut is estimated as 15%.

SND flowing shows reservoir noise across permeable zones (see Zone 3 at Fig. 2). Some low-frequency noises typical for fluid flows through hydraulic fractures and/or a cement sheath channel were captured both above and below perforations (see Zone 3 on LFD FLOWING Panel at Fig. 2) in the interval from Line A down to Zone 3.

Termosim numeric flow modelling was performed based on SNL flowing units and allowed more insight into the flow geometry behind casing at reservoir level.

The geothermal profile TG (green log at Fig. 2)

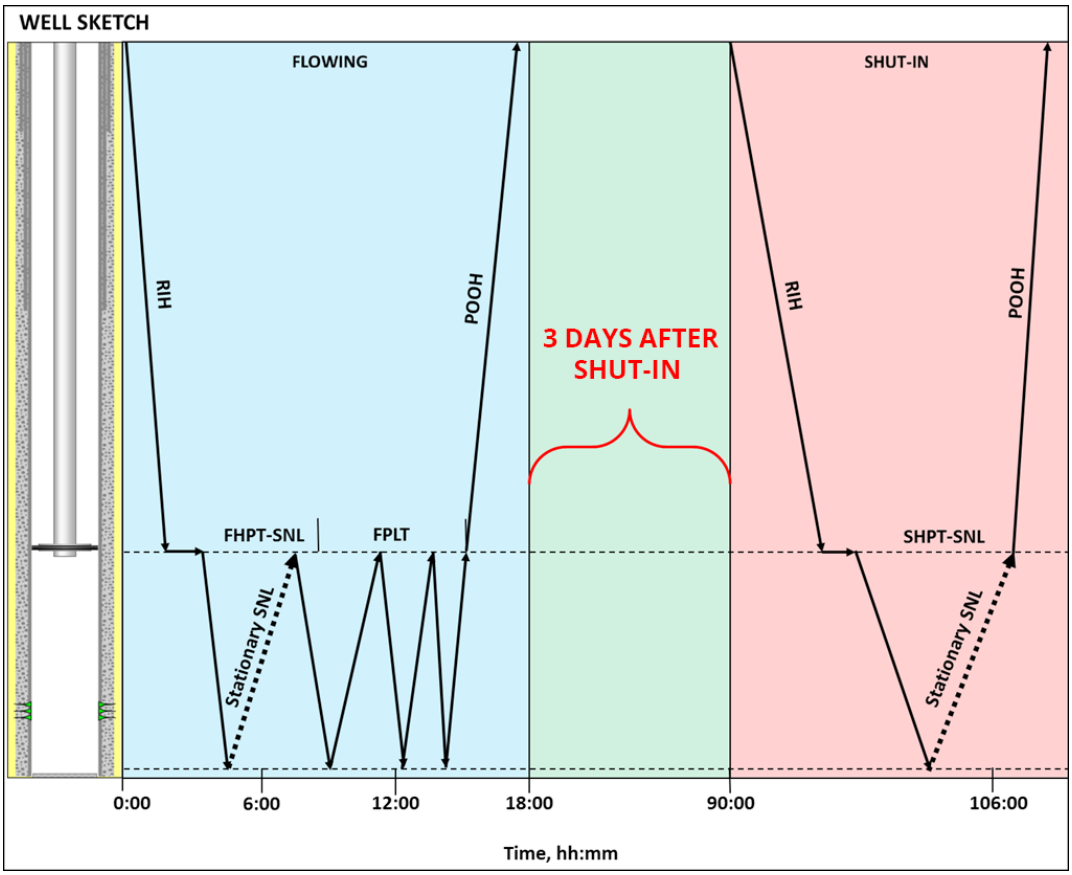

Fig. 1 HPT-SNL-PLT logging procedure.

was reconstructed using reverse modelling from the three well shut-in surveys (see Appendix A). Reservoir pressure in each reservoir zone was assumed to be equal to wellbore pressure after three days of shut-in. The temperature logs at P1 were recorded both in quasi-stationary flow regime (blue log at Fig. 2) and shut-in temperature logging regime (red log at Fig. 2).

The simulation results are shown on the FORMATION FLOW PROFILE panel at Figure 2. They suggest that perforations are connected to both overlying and underlying reservoirs. The underlying reservoir BP161-2 contributes to production from perforations with oil. The overlying formation BP15 contributes to production from perforations with water.

Combined noise and temperature analysis suggest that communication with BP15 is created by fracture, most probably induced during the frac jobs.

The cooling anomaly of shut-in temperature SHUT-IN (as against TG) suggests that hydraulic facture initially extended all the way down to the E-line, but the flowing temperature and SNL suggest that the bottom part of the fracture is currently closed and the inflow starts from D-line. The temperature simulations (dash line TFM) provide a good match to the scenario in which all the water cross perforations arrive from the overlying BP15 formation.

One can also note a packer noise across the A-line, which is created by flow turbulence.

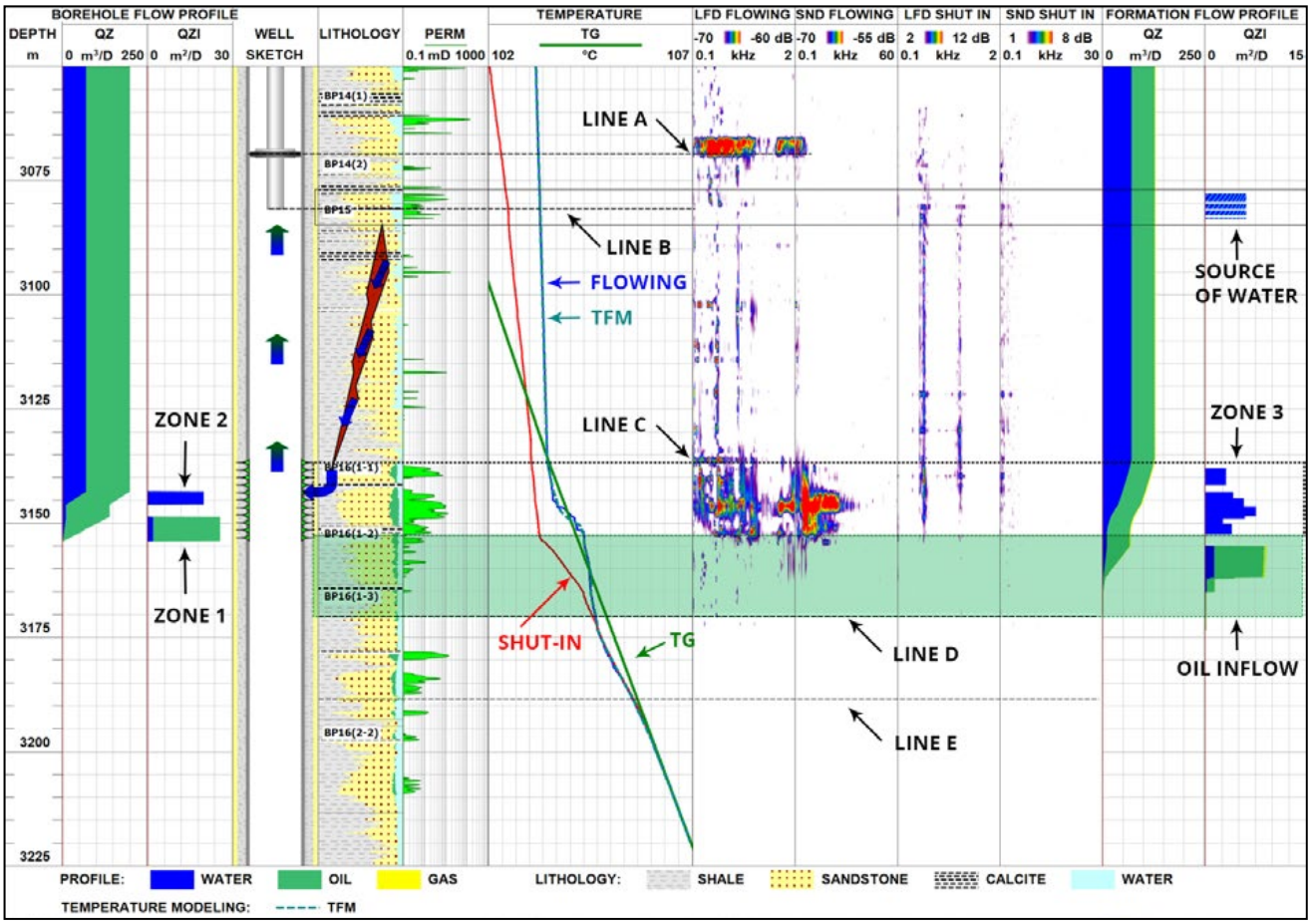

Fig. 2 PLT (to the left) and HPT-SNL (to the right) interpretation of borehole and formation inflow.

Example 2 (Job ID-13506)

The HPT-SNL-PLT survey at horizontal this well was conducted two years after drilling. Multi-stage hydraulic fracturing with several zones being separated by packers was performed in this well, after which the well was put on production though a ported liner [26]. During five months of operation, the water cut increased from 60 % to 95 % and the well was suspended. Two weeks prior to the survey, frac sleeves were milled out, and the well was recompleted by injecting nitrogen through coil tubing. The water cut remained at the same high.

The objective of the HPT-SNL-PLT survey was to locate the source of water.

The pressure in BP16 formation turned to be below bubble point, which resulted in substantial free gas production.

Since the well was shut-in long time, the HPT-SNL-PLT survey has started with shut-in passes and then proceeded with flowing pass (see Fig. 1).

The PLT interpretation (mechanical spinner and multiphase sensors) suggests that the main water inflow to the wellbore occurs from below the survey interval at 4348 m and there is also some

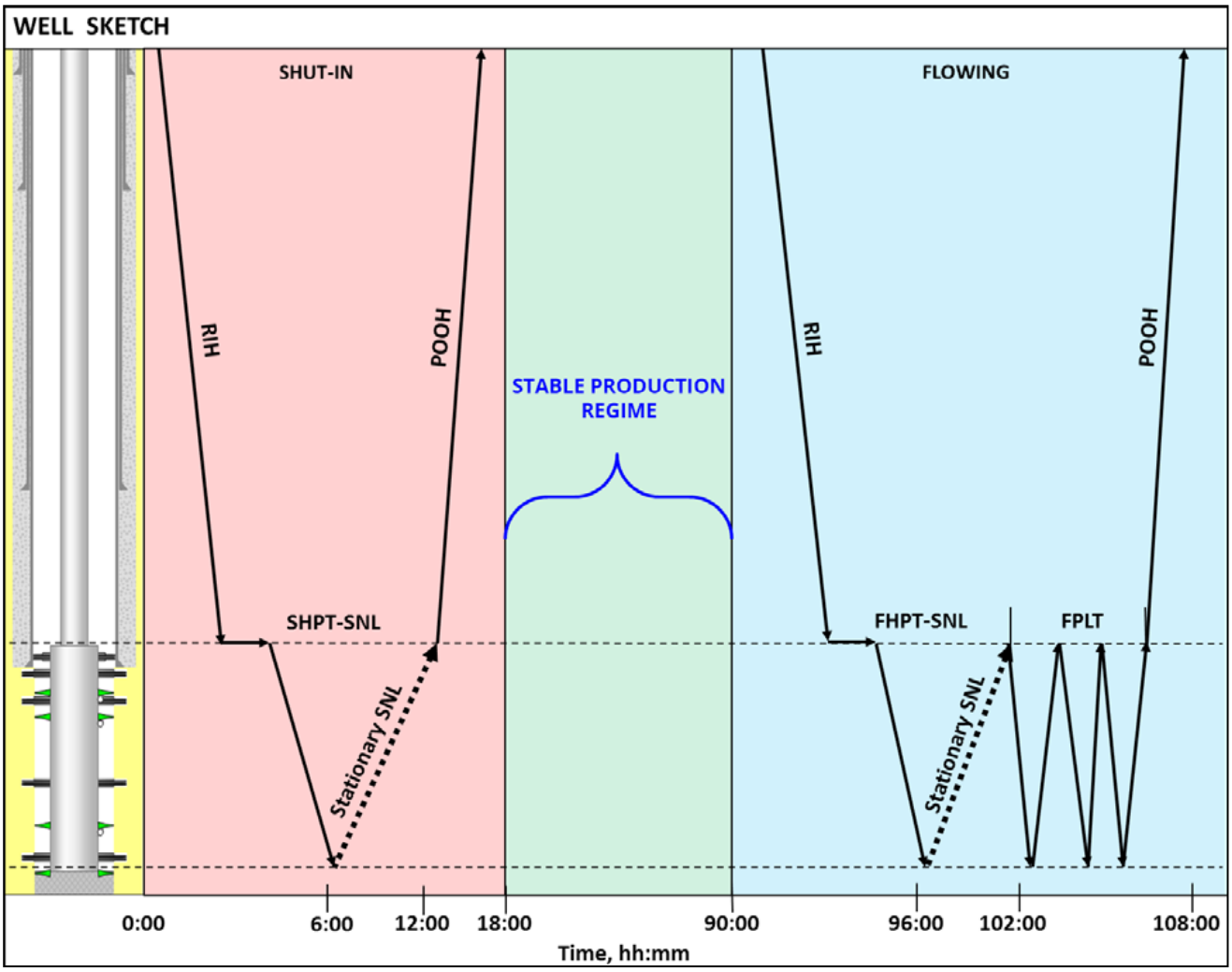

Fig. 1 HPT-SNL-PLT logging procedure

minor water contribution from all frac sleeves (see BOREHOLE FLOW PROFILE at Fig. 2).

SND flowing shows reservoir noise across permeable zones (see Zone 1 to 6 at Fig. 2). High frequency SND panel has picked up the flow through the frac sleeves and the flow behind the liner. The connection between reservoir noise across Zone 1 and frac sleeve #3 is a clear indication that the packer at 3740 m is not holding. The SND/LFD panel also suggests that frac sleeve#1 is connected to two reservoir fractures.

Termosim numerical flow modelling used the SND flow zones and ended up with the FORMATION FLOW PROFILE panel at Fig. 2. It suggests two water sources: most of the water (140 m^3/d) is coming from below the survey interval at 4348 m and some minor water inflow 10 m^3/d is expected from the bottom fracture of Zone 6.

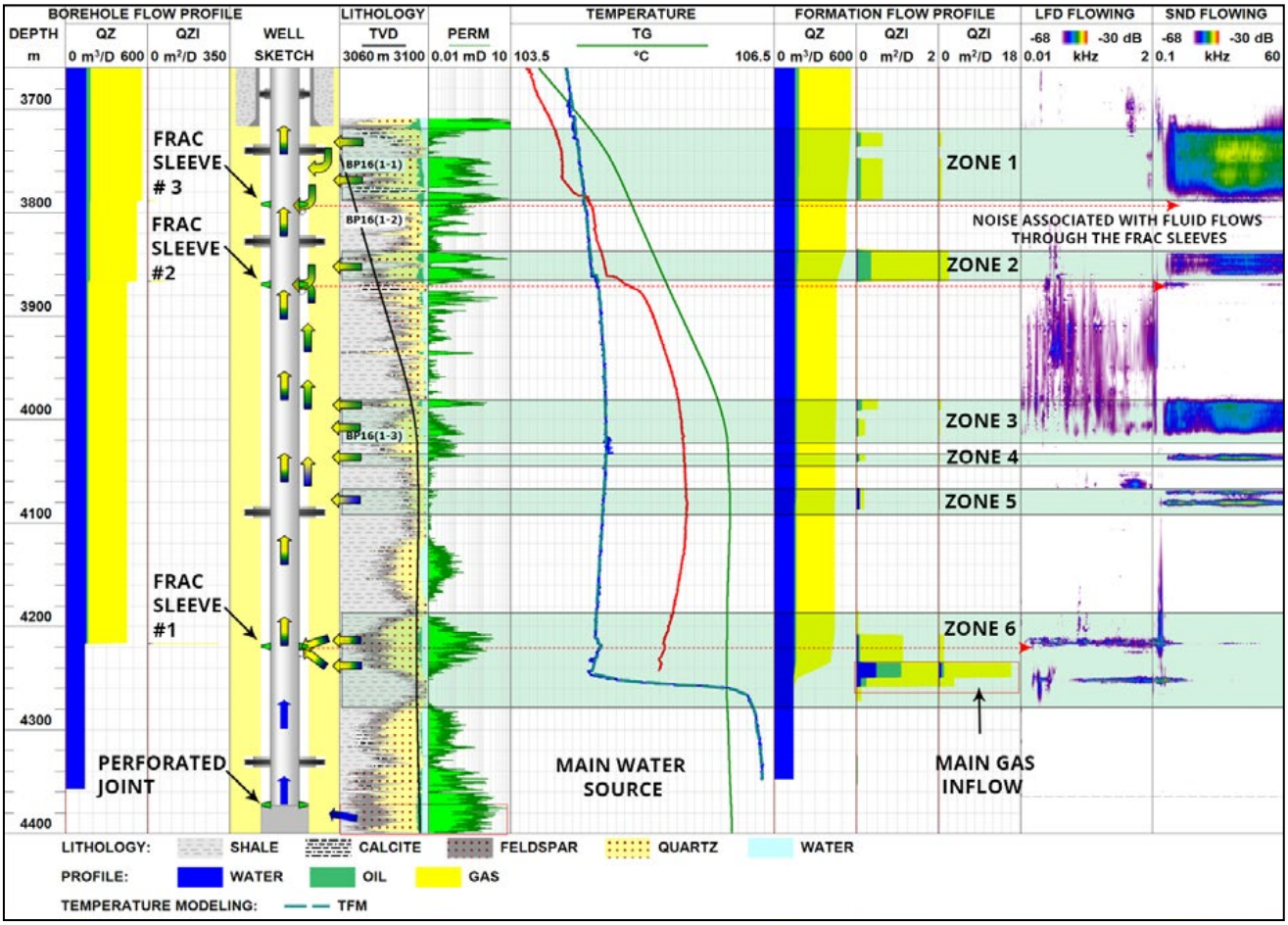

Fig. 2 HPT-SNL-PLT survey results with subsequent temperature simulation showing inflow profile in the wellbore and behind casing.

Example 3 (Job ID-13511)

The HPT-SNL survey at this horizontal well was conducted one year after drilling. Multi-stage hydraulic fracturing with several zones being separated by packers was performed in this well, after which the well was put on production though a ported liner. An ESP was run into the well after it had been flowing for three weeks. After only two months of producing the well by artificial lift, it was shut in due to a high water cut that amounted to 50 %. Fluid production rate at surface conditions was 150 m^3/day and gas rate varied from 10,000 to 23,000 m^3/day.

The objective of HPT-SNL survey was to locate the source of water [26].

The survey started with flowing passes: the ESP was pulled out after and the flow was stabilised with nitrogen lift. The well was then shut in. The shut-in pass was recorded after two days (see Fig. 1).

SNL suggests numerous inflow zones from formation fracs. It also tracked inflow through three frac sleeves. Frac sleeve #3 produces mostly water.

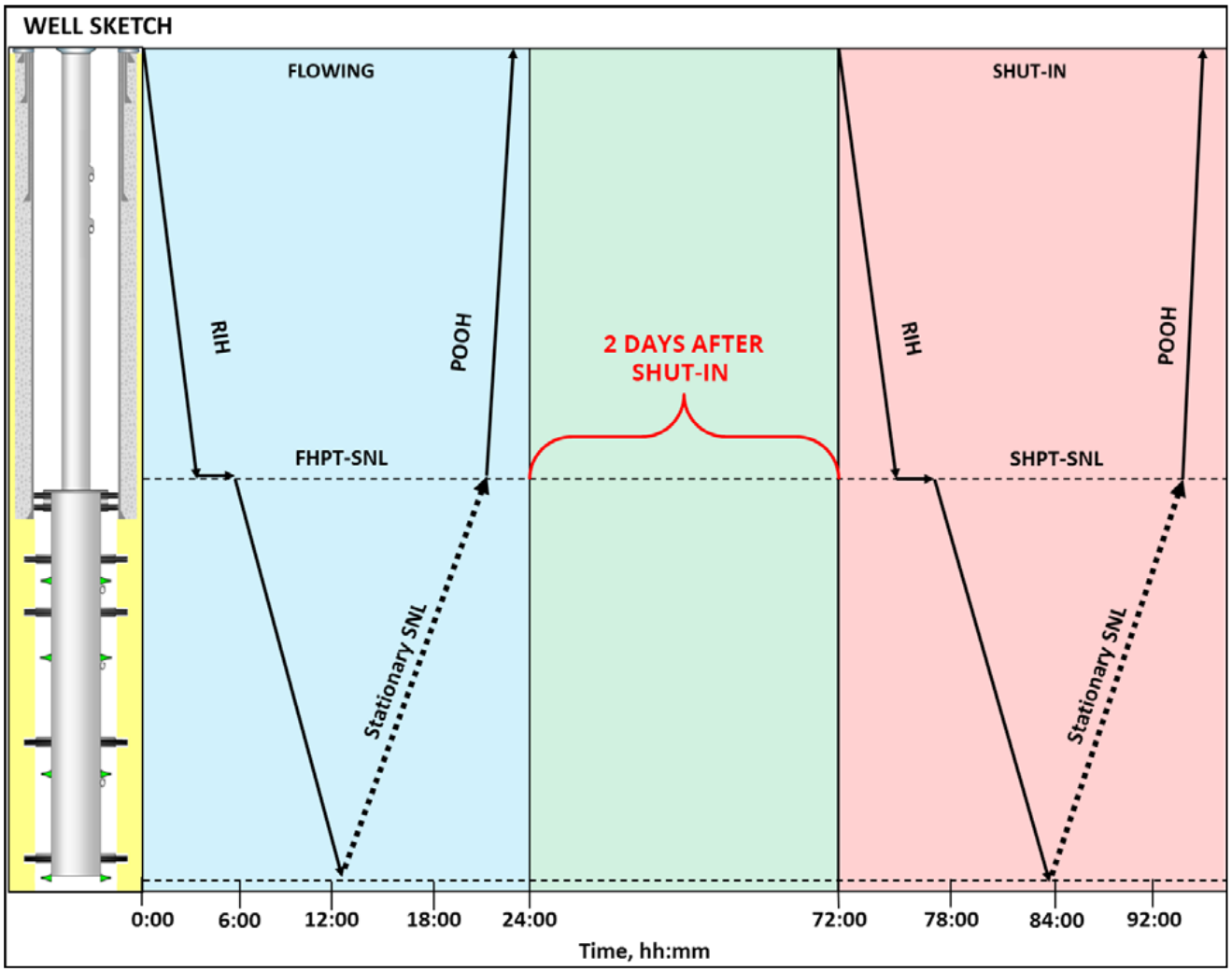

Fig. 1 HPT-SNL logging procedure.

There is a cooling anomaly confined to formation fracs picked up by SNL at 3840 m, which is a clear indication of induced frac communication with overlying BP15 formation.

Based on the survey results, the remedial workover was carried out and cement was squeezed through the frac sleeve #3 into the zone between the two packers, which resulted in complete water shut-off.

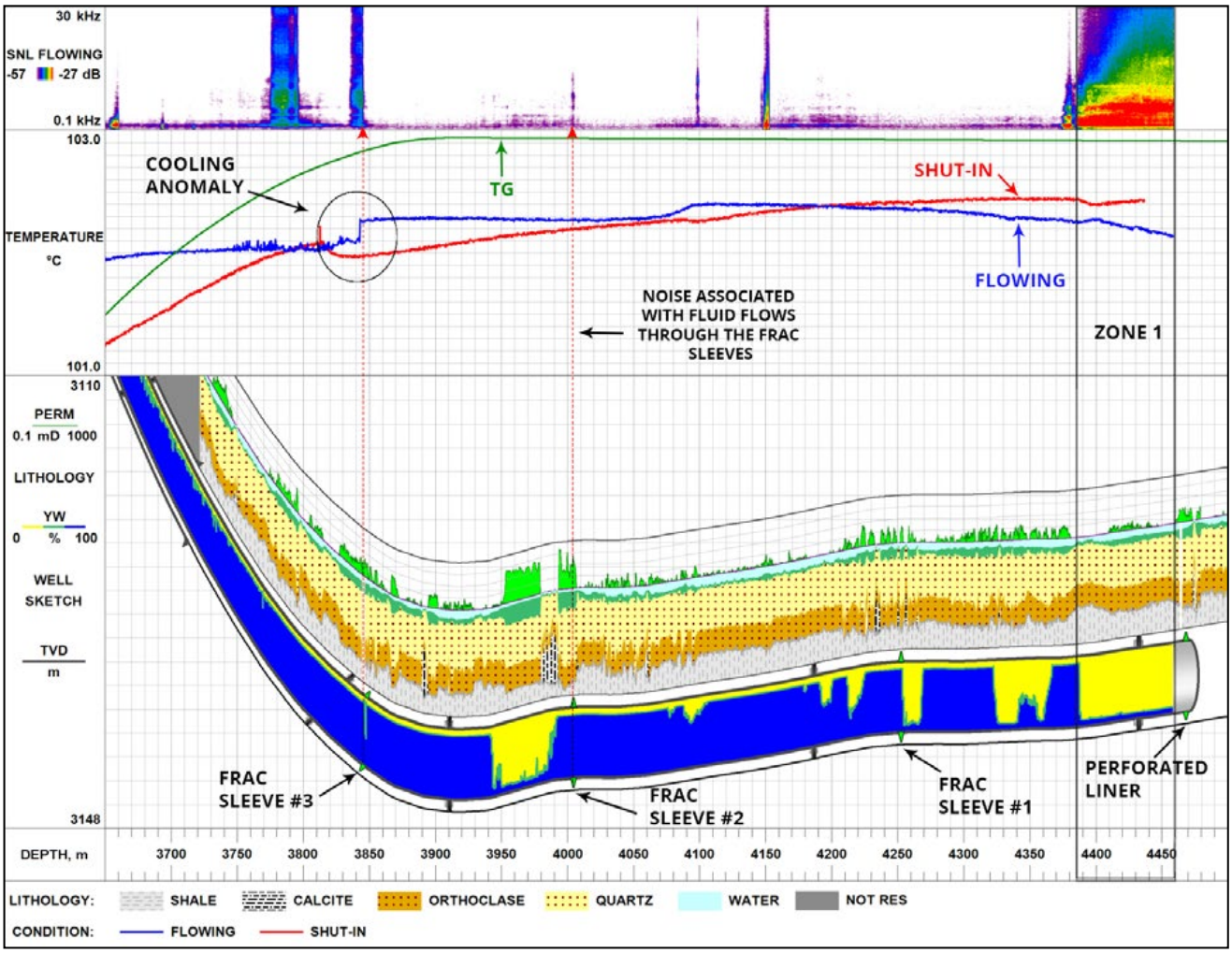

Fig. 2 Water Breakthrough Identification after Multi-Hydrofrac Jobs

2.2.2.3 DUAL-STRING COMPLETION WELLS

Example 1 (Job ID-11058)

This case presents a slanted dual-string well selectively producing from the A and B reservoirs through long and short tubing respectively, and focuses on the lower reservoir B with the objective of locating its flowing intervals. This objective was achieved by integrated high-precision temperature and spectral noise logging (HPT-SNL) [25].

An inflow profile for the B reservoir was constructed by the simulation of flowing temperature for the long string. The advantage of temperature simulations for inflow profiling

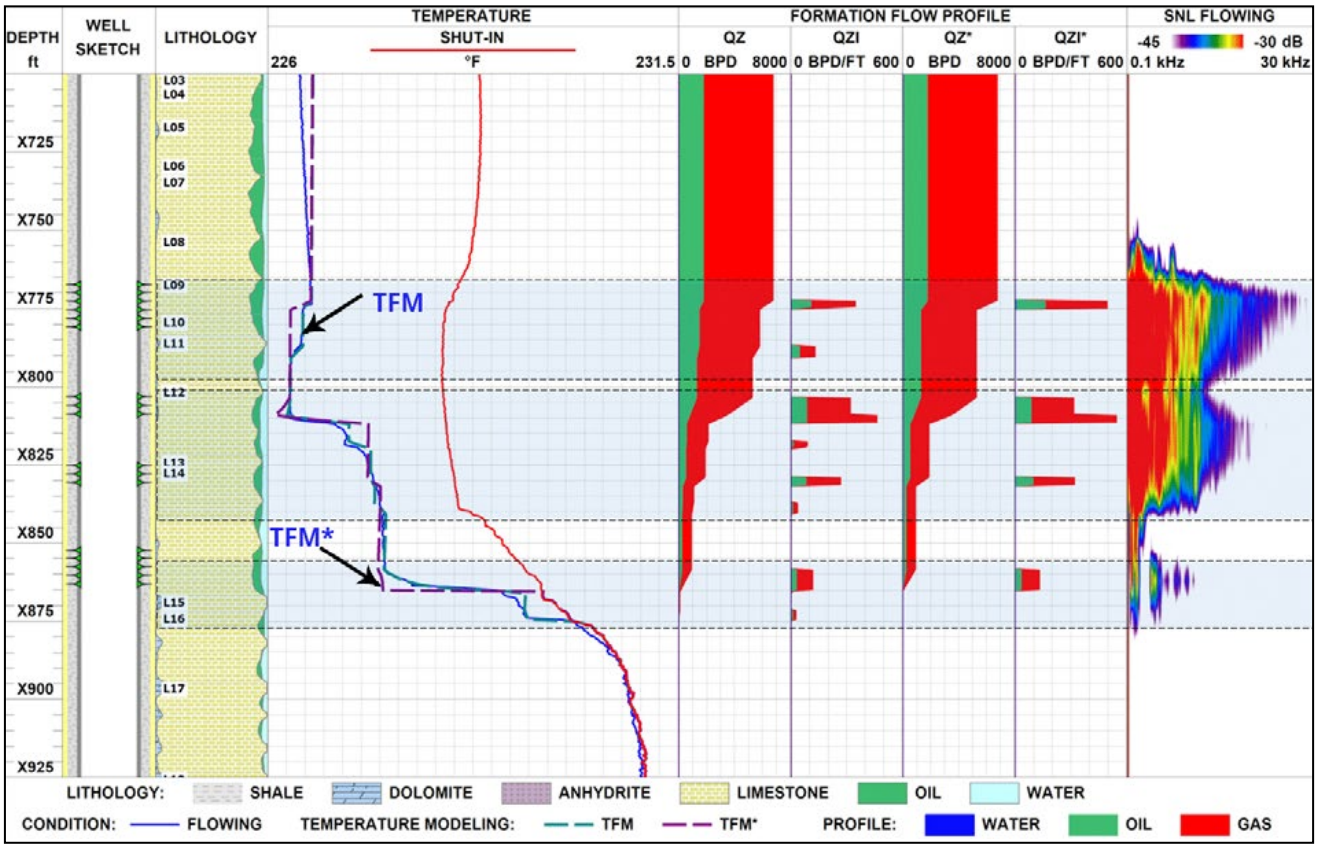

Fig. 1. Identification of inflow intervals by temperature simulations for both perforated and unperforated intervals. SNL data detected gas inflow caused by pressure decrease to below the bubble point

is the possibility to identify flowing zones in the reservoir, including those outside the perforated intervals. This was confirmed by the construction of the QZI* profile that had no unperforated but flowing reservoir intervals. The simulated temperature TFM* corresponding to the QZI* profile is seen to substantially deviate from the measured curve due to flow outside the perforations (Fig. 1).

SNL located flowing reservoir intervals in agreement with the temperature-based production profile. Noise amplitudes in Zone 1 and Zone 2 indicated large amounts of gas in the reservoir due to low pressure in the operating well, which was below the bubble point pressure. According to the SNL noise frequency distribution, fluid flowed in the reservoir through fractures, while the maximum noise amplitudes were within a frequency range of 3–6 *kHz*. In Zone 3, SNL detected only low noise, possibly due to the small amount of gas or low flow rate.

Example 2 (Job ID-11019)
This well, producing from the D and E formations, was surveyed by the high-precision temperature (HPT) logging tool and conventional memory production logging tool (MPLT) to determine the reservoir-to-wellbore flow path. Production from the D reservoir was suspended by closing the Sliding Side Door (SSD).

The strong cooling detected in the interval X187.2–X242.5 m by SHPT logging was caused by breakthrough of injected water from a nearby injection well. This indicates that the injected water repeatedly washed this interval.

The spinner profile shows that fluid entered the wellbore mainly through the SSD at a depth of X214.5 m and that the D reservoir contributed significantly, with a properly working packer. A flowing high-precision temperature (FHPT) log indicates that the temperature gradient changed sharply at the SSD depth (Fig. 1).

The SHPT and FHPT logs diverged below a depth of X283.0 m because of minor cross-flow from below the perforations. This is suggested by the presence of stagnant water detected by salinity data below the perforations, which means that no inflow occurred from beneath the cement, i.e. that the bottom hole did not leak. Therefore, inflow most probably occurred from the E9 reservoir.

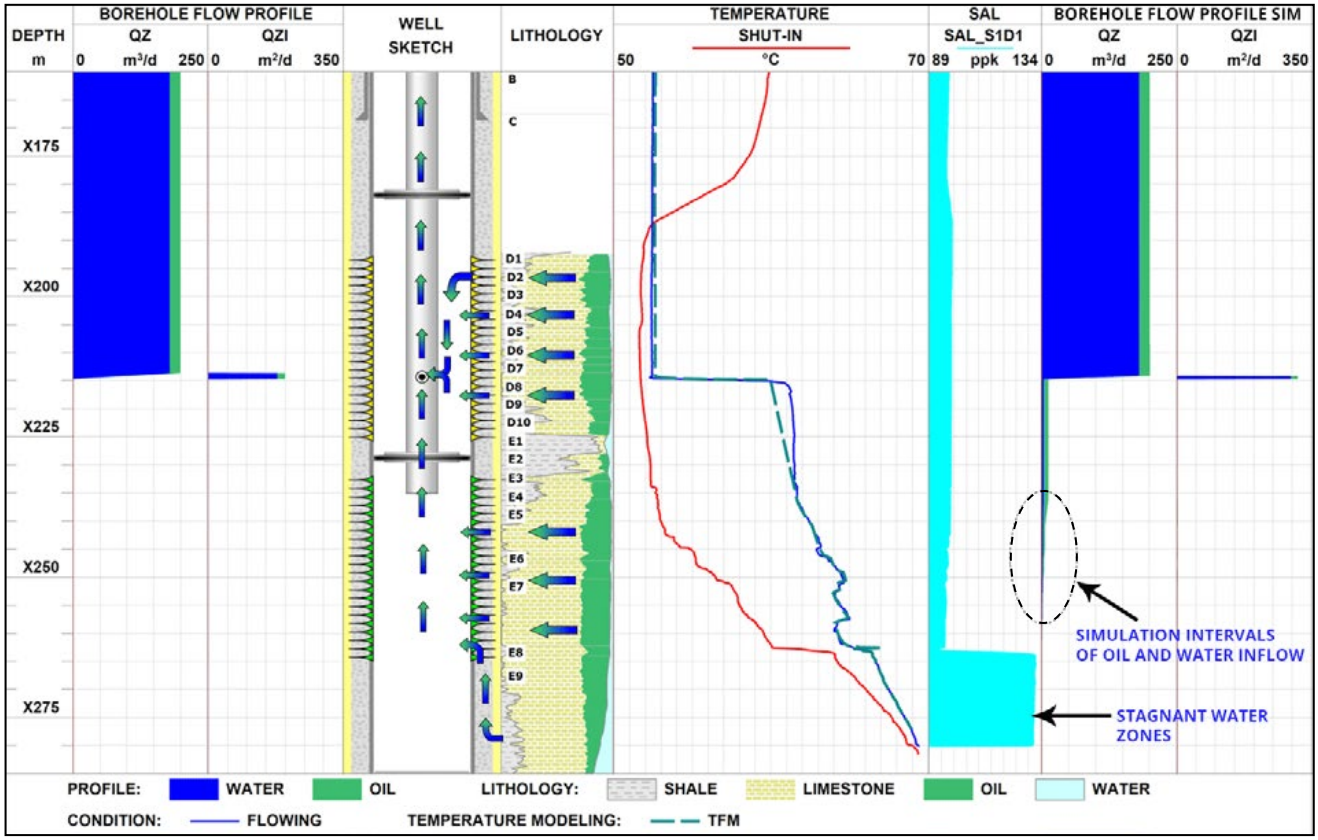

Fig. 1. Identification of a water breakthrough interval and the main fluid inflow interval by temperature simulation and spinner logging

The current inflow profile was constructed using the flow temperature simulator. The inflow profile was in good agreement with the PLT profile above the SSD but indicated that fluid entered the wellbore also from the E5-E7 reservoirs, which the PLT survey failed to indicate because of the spinner sensitivity threshold. The temperature simulation showed that only half of the total amount of oil was produced from the E reservoir and the other half from the D reservoir that was supposedly suspended from production.

Example 3 (Job ID-13054)

Well OP-1 was drilled and put into operation in September 2006. It was completed as a dual string naturally flowing production well with separation packers. The short string produced from the A3 and A4 reservoirs and the long string from A5.

The total fluid production rate from A3 and A4 was 1000–1200 BPD. After two years of operation, water cut for SS from A3 and A4 increased to 12%. During the same period, wellhead pressure dropped so much that natural flow of the well ceased. To help resume flowing through SS swabbing was carried out but without success. Since 2008, SS has been out of operation.

The total fluid production rate from the A5 reservoir through LS was 1500 BPD. In September 2012, reservoir A5 water cut was 60%. When the survey commenced, the well was naturally flowing through LS.

The survey was conducted to identify the source of increased water cut and cross-flows behind casing above and below perforated intervals, and to assess integrity of completion components and downhole equipment. The integrated HPT-SNL technique was employed to reach all these objectives. The survey was conducted during inflow through LS during a short stop and as a baseline measurement made two days after well was shut-in.

Specific to this survey, the pressure drawdown on the top of A5 reservoir in quasi-stationary inflow mode was as low as 33 psi relative to the baseline measurement made two days after well was shut-in. Another specific feature was the detection of low-amplitude acoustic noise used to confirm the results of integrated HPT-SNL and identify reservoir flow intervals.

For the given downhole conditions, the integrated survey revealed the following:

No leaks in completion components or downhole equipment and no communication between tubing strings were found over the survey interval.

Short tubing string

Upward cross-flow between the perforated interval of the A3 reservoir and the top part of the perforated interval of A4 was found in Zone 1. This cross-flow is indicated by near-zero temperature gradient in the Shut-in, Transient 1, Transient 2 and Transient 3 logs and by acoustic noise which was detected in this zone by SNL. It is highly probable that this cross-flow entered the A annulus between the packers. The potential flow path is impossible to trace accurately because of LS tubing wall. The source of increased water cut from A3 and A4 is impossible to identify reliably without putting the well under the inflow regime through the short string. However, it can be assumed that high water-cut fluid

came from the perforated interval of A3 and A4. In combination with low reservoir pressure, this was the reason why the well stopped flowing naturally through the short tubing string.

Long tubing string

Temperature and Spectral Noise Logging data indicated that fluid inflow mainly occurred from the perforated interval of the A5 reservoir, i.e. Zone 2. Wellbore inflow was also detected in the perforated interval by the salinity and capacitance sensors included in the integrated HPT logging.

The source of increased water cut from the A5 formation was the upward shift of the OWC. Different temperatures and temperature gradients recorded during shut-in and flowing passes below the perforated interval of A5 i.e. in Zone 3, indicated formation water coning, possibly including flow behind casing.

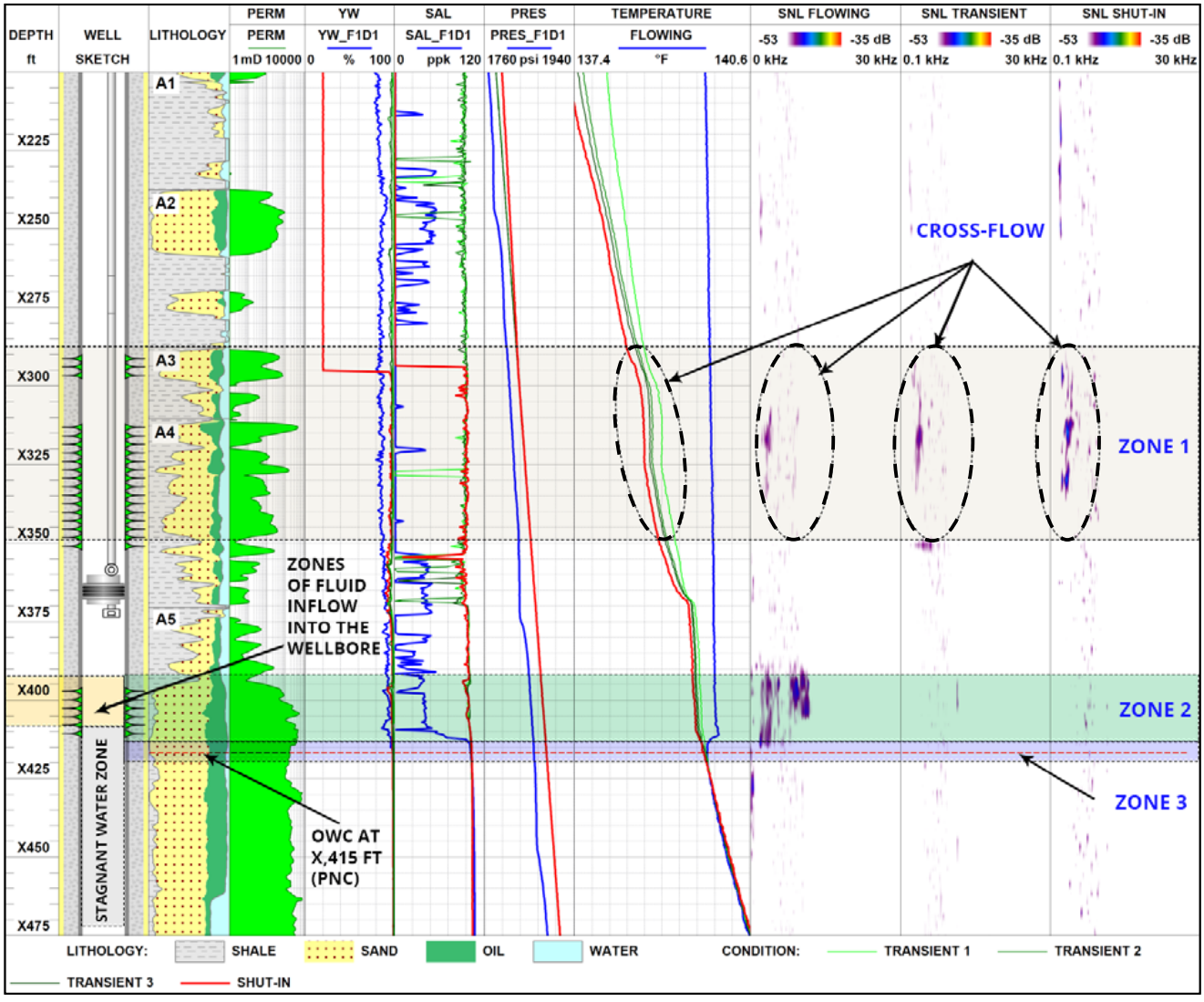

Fig. 1. Water Breakthrough Identification in Dual string completions well

2.2.3 FRACTURE FLOW ANALYSIS

Example 1 (Job ID-11020)
This example illustrates the correlation of data acquired by memory PLT (MPLT) survey, Formation MicroImager (FMI) and static high-precision temperature (SHPT) logging.

The spinner profile shows that the injection during the survey was into the interval X52.0–X55.9 mbdf of the C2 formation, which was found by an FMI survey to contain a fault. However, a temperature profile indicates the strongest cooling at a much lower depth, within the C3 and C4 formations, which is in agreement with a historical injection profile constructed by a temperature simulator (shown by a dashed line). This cooling could be caused by injections into this well and/or by lateral flow from nearby injectors. According to another possible flow pattern, water flowed from this injector into a fault crossing the well within the C2 reservoir unit, then entered fractures at a distance of more than 3 m from the well, flowed downwards through them, and finally entered the C3 and C4 reservoir units (Fig. 1).

The source of cooling can be located by combined analysis of flowing and static temperatures and noise logging data.

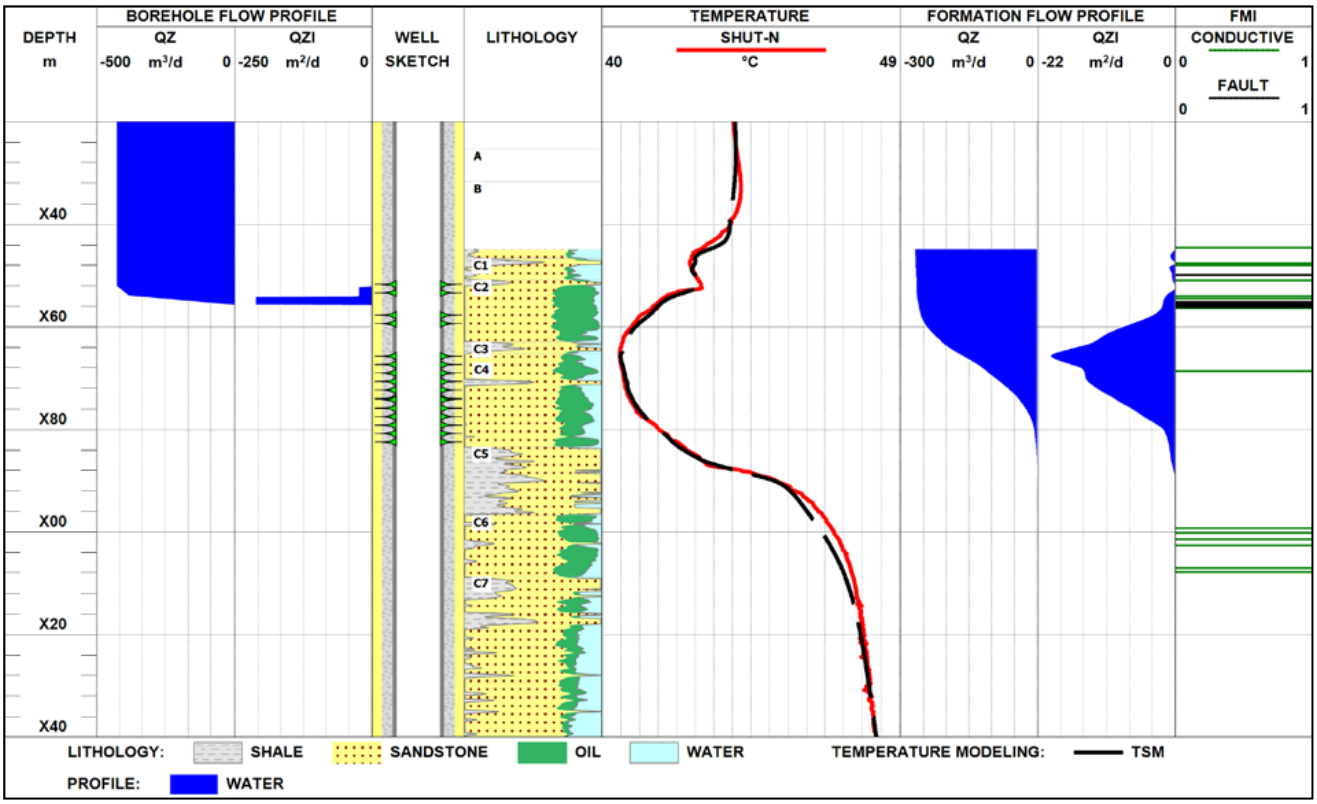

Fig. 1. Location of the main fluid loss interval by correlation of PLT and FMI data and analysis of injected fluid distribution by temperature simulation

Example 2 (Job ID-10047)

This case presents a classic example of injection into fractures (Figs. 1). This well injected water into two perforated intervals in Zones A–C. One of the objectives of the survey performed in the well was to construct the current injection profile for these zones. The integrated survey consisted of spinner logging, high-precision temperature (HPT) logging and Spectral Noise Logging.

Spinner data showed that all injected water left the wellbore through two narrow zones in the upper perforations, with a 30–40-ft no-flow section between them. No water was found to flow through the lower perforations. SNL detected only low-frequency noise throughout the survey interval and no medium- or high-frequency noise characteristic of injection into the rock matrix. This low-frequency noise was generated by turbulent flow in the wellbore. Zones of sharply reduced noise corresponded to flowing perforations detected by spinner data.

Thus, in this intricate case, when the SNL signal is strongly masked by wellbore flow, a signal component generated by injection into the reservoir through a fracture must be extracted from the overall signal. After wavelet filtration, SNL data clearly showed two injection zones correlating with the spinner-detected ones (Fig. 1).

Temperature logs recorded under static and flowing conditions clearly detected two fractures across the upper perforations and no current injection into the reservoir across the bottom perforations, as both the flowing and static logs merged below Line A. The shape of the static temperature profile indicated two intervals of uniformly distributed injection into fractures (Figs. 1 and 2). It should be noted that

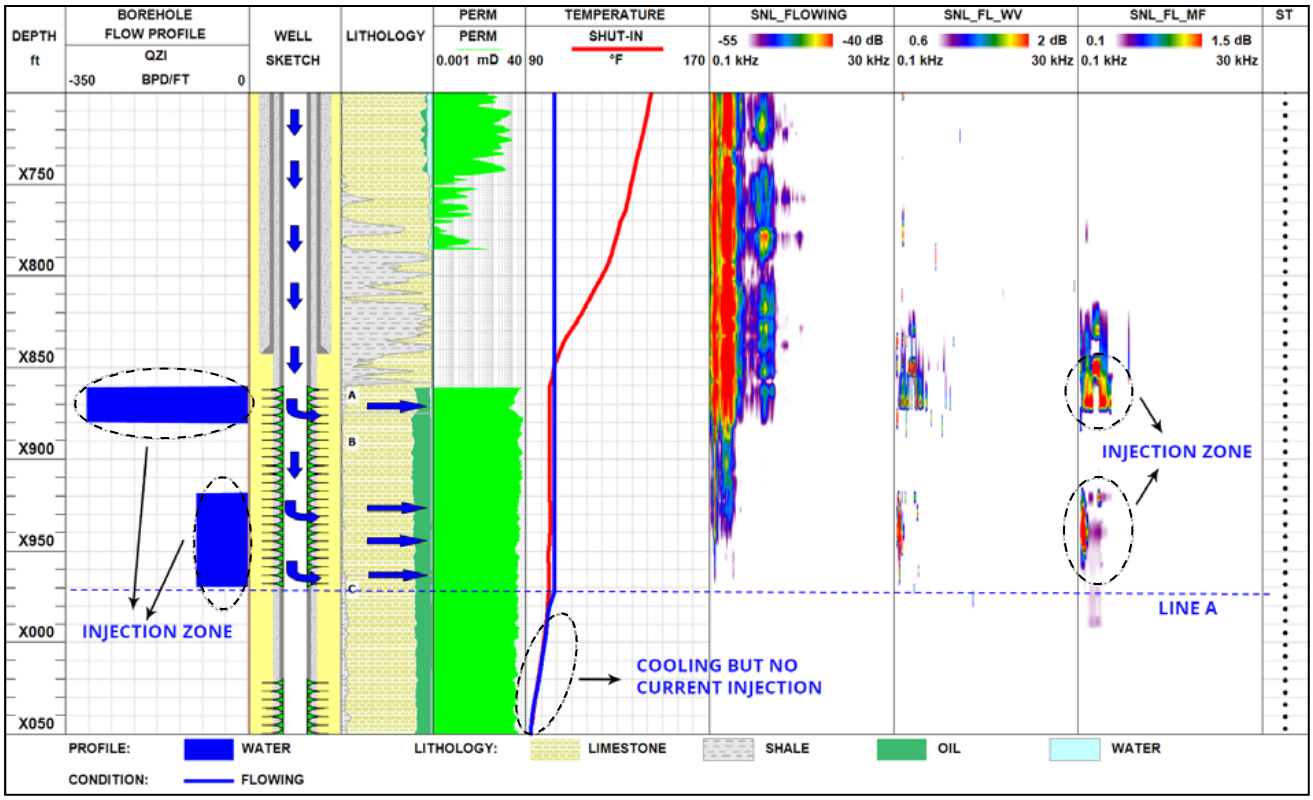

Fig. 1. Injection profile based on HPT, spinner and SNL data

the reservoir was cooled at the bottom but was not under injection during the survey, according to SNL data. Therefore, this cooling was possibly caused by injection in the well vicinity or by injected water from offset injectors.

The fact that injection around this injector occurred mainly into fractures should be taken into account in dynamic modelling. The results of the survey suggest the following actions: (1) The lower perforations can be reperforated and stimulated, 2) Sidetracking is recommended to increase injection into the rock matrix in this zone because of fracture flow and channelling across the upper perforation.

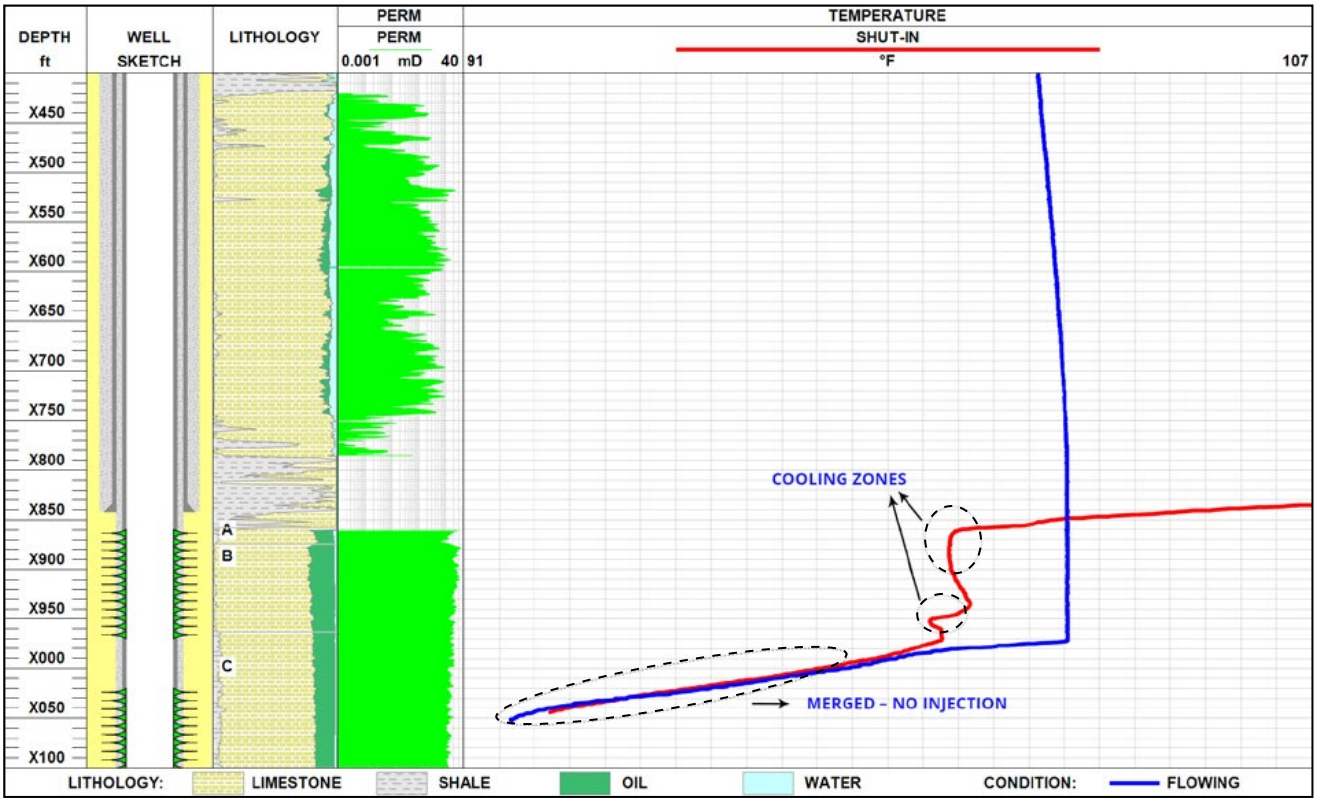

Fig. 2. Lower injection limit according to temperature logs

2.2.4 PRE-STIMULATION AND POST-STIMULATION FLOW ANALYSES

Example 1 (Job ID-11054)

This well, injecting into the A reservoir, was surveyed by the integrated high-precision temperature, spinner and spectral noise logging technique to control the effectiveness of reservoir stimulation jobs.

According to the previous spinner survey, Zone 1 and Zone 2 received small amounts of injected fluid while Zone 4 received most of it. The perforated intervals that were not picked by the spinner did not receive any fluid (see the 2010 spinner column in Fig. 1). The survey was repeated after

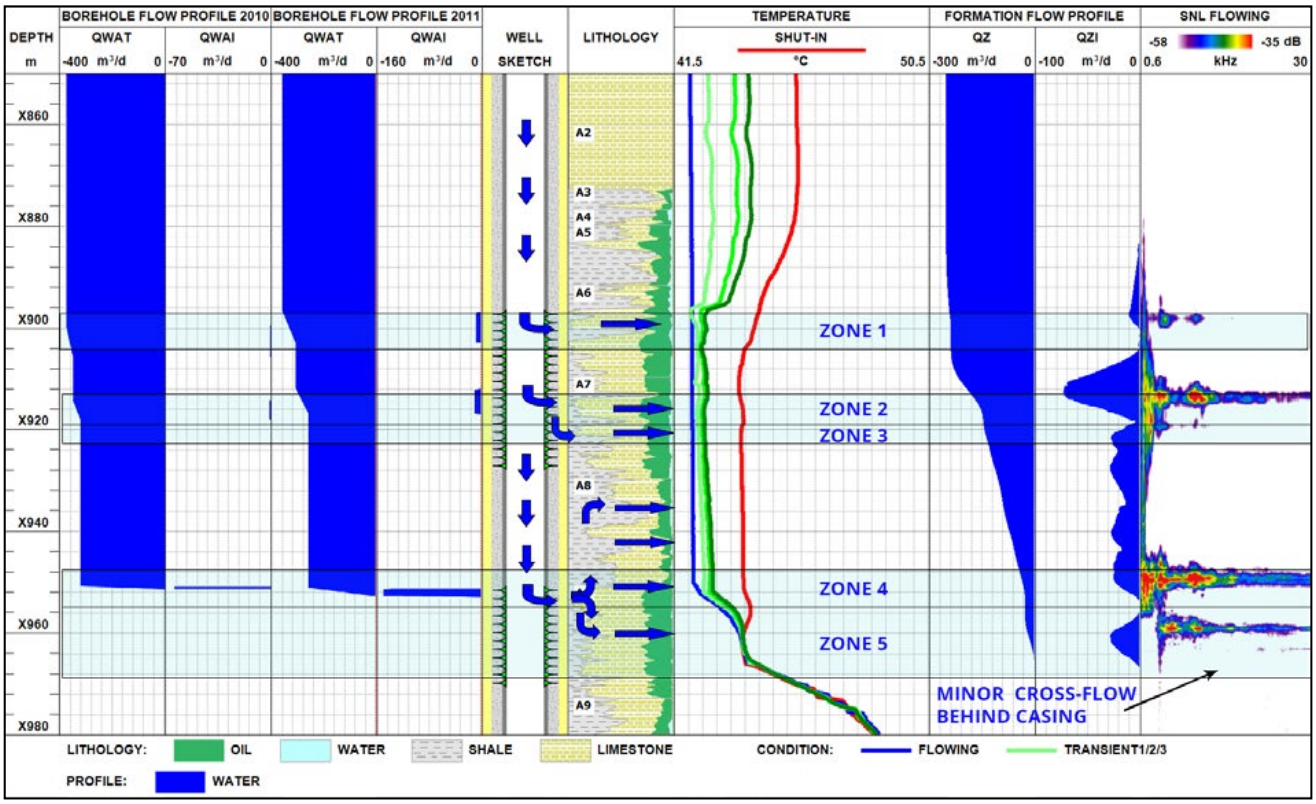

Fig. 1. Post workover monitoring

the acid treatment of the perforated intervals. The repeated flow-rate measurement showed that the injection profile did not change essentially: the receiving zones remained the same (Zones 1, 2 and 4 in Fig. 1), with most of the injected fluid still entering the upper portion of the lower perforations (Zone 4). However, temperature logging detected cooling in A7 and A8 (Zones 3 through 4), indicating that the fluid injected within A9 (Zone 4) flowed behind casing and entered A7 and A8. Noise data generally correlate with the spinner and temperature logs but additionally feature minor downward cross-flow behind casing from the upper portion of A9 (Zone 4) into the middle portion of A9 (Zone 5).

Integrated analysis of all acquired data allowed the conclusion that, despite the slightly increased fluid injection into A6 and A7, the overall effect of the performed operations was low. Some large zones were left unswept. This lack of effect was probably due to poor perforations across A6 and A7. The fluid could easily enter high-quality perforations within Zone 1, Zone 2 and Zone 4, and then flow behind casing into overlying formations. This assumption can be verified by analysing perforation quality using magnetic imaging defectoscopy (MID).

2.3 WELL INTEGRITY PLATFORM

2.3.1 LEAK DETECTION

Objectives
Location of leaks in completion components and channelling from/to the reservoir

Technology
1. Hardware and software tools
- SNL – Spectral Noise Logging tool
- Micro T – High precision temperature sensor
- EmPulse – Magnetic Imaging Defectoscope
2. Methodology
- Location of leaks in the A, B and C annuli
- Location of annular flow/channelling behind tubing/casing
- Location of flow sources and drain paths in rocks

Criteria for Candidate Selection
1. Pressure test failure
2. Sustained annulus pressure (SAP)

Inputs for Candidate Selection
1. Wellbore accessibility
2. Availability of conveyance equipment for stationary measurements
3. Integrity tests
4. Well sketch and zones of interest

Inputs for Job Proposals
1. Integrity tests
2. Well sketch and zones of interest

Inputs for Interpretation and Analysis
Raw logs recorded by TGT

2.3.1.1 CASING INTEGRITY

Example 1 (Job ID-11074)
This case illustrates the application of high-precision temperature (HPT) logging, spectral noise logging (SNL) and magnetic imaging defectoscopy (MID) for identification of well integrity problems.

The survey was conducted under gas injection into the tubing annulus. The well could not be put onto stable production using a compressor. Only the upper gas-lift valve was activated at a depth of X1, with no further increase in compressor pressure. The resulting drawdown pressure was below 10 bar, i.e. much lower than during ESP operation. As a result the producer performed abnormally, however it was possible to acquire some useful information. The discharge pipe gave a small amount of liquid-free gas, which was disproportionate to the compressor rate and implied substantial gas leakage. This assumption was confirmed by a combined data analysis of temperature logging, spectral noise logging and magnetic imaging defectoscopy that detected a production casing leak.

The static temperature curve features a number of anomalies in Zone 1. The anomalous

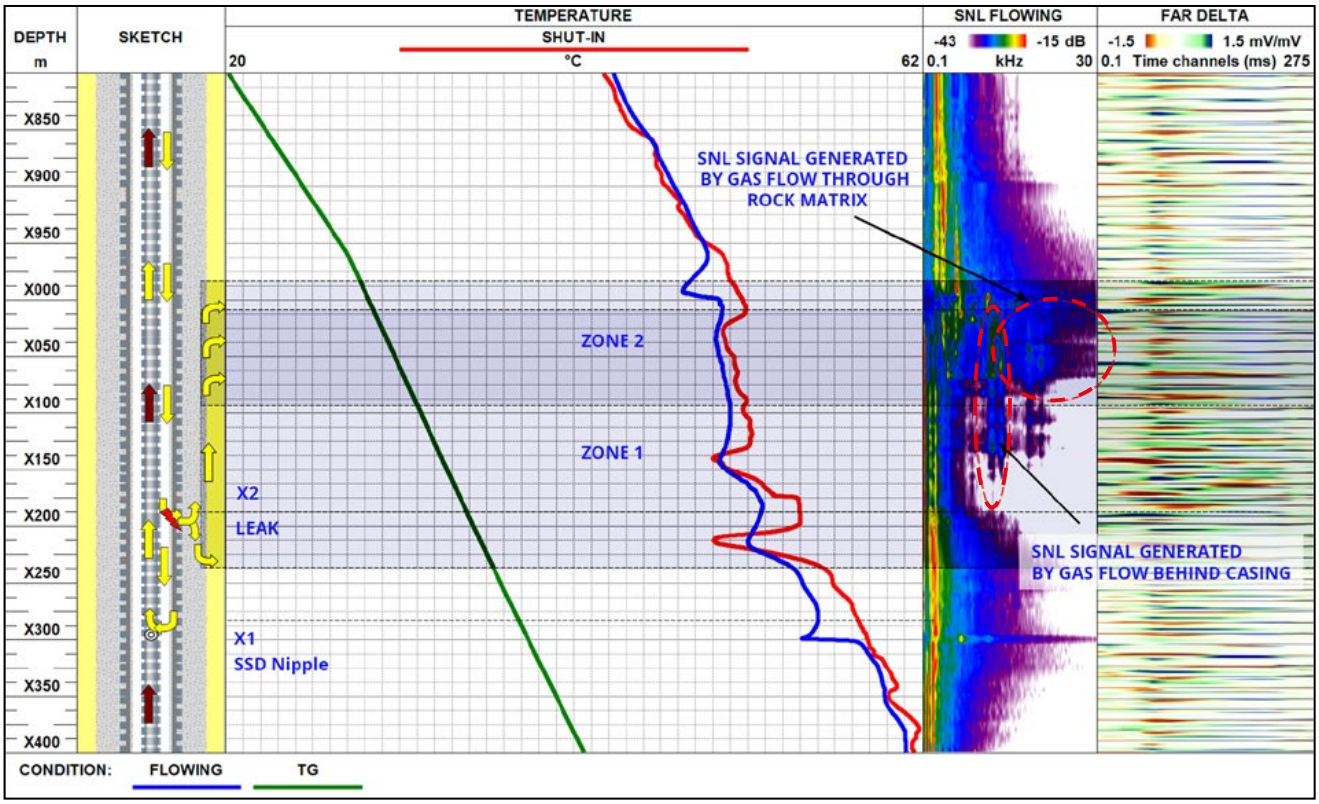

Fig. 1. Correlation of static and flowing temperature anomalies with SNL data

temperature tended to the geothermal, which meant lateral fluid flow through permeable reservoir units. These anomalies were most likely generated by local processes in this particular well, since no similar anomalies were observed in nearby wells at the same depth.

During compressor operation, some temperature anomalies were also observed in Zone 1. A cooling anomaly at a depth of X1 was caused by injected gas that broke through a gas-lift valve. At the same depth, SNL detected 2.5–30 *kHz* noise generated by turbulent gas flow through the gas-lift valve. MID indicated substantial loss of metal from casing at a depth of X2. Gas entered the casing annulus through this leak and flowed through cement fractures into porous rocks. This flow pattern is evidenced by the shape of the flowing temperature curve and by noise typical of fluid flow through the casing annulus (Zone 1). High-frequency noise that appeared in Zone 2 indicated fluid filtration through the rock matrix.

The detected casing leak was isolated, and the resulting watercut decreased.

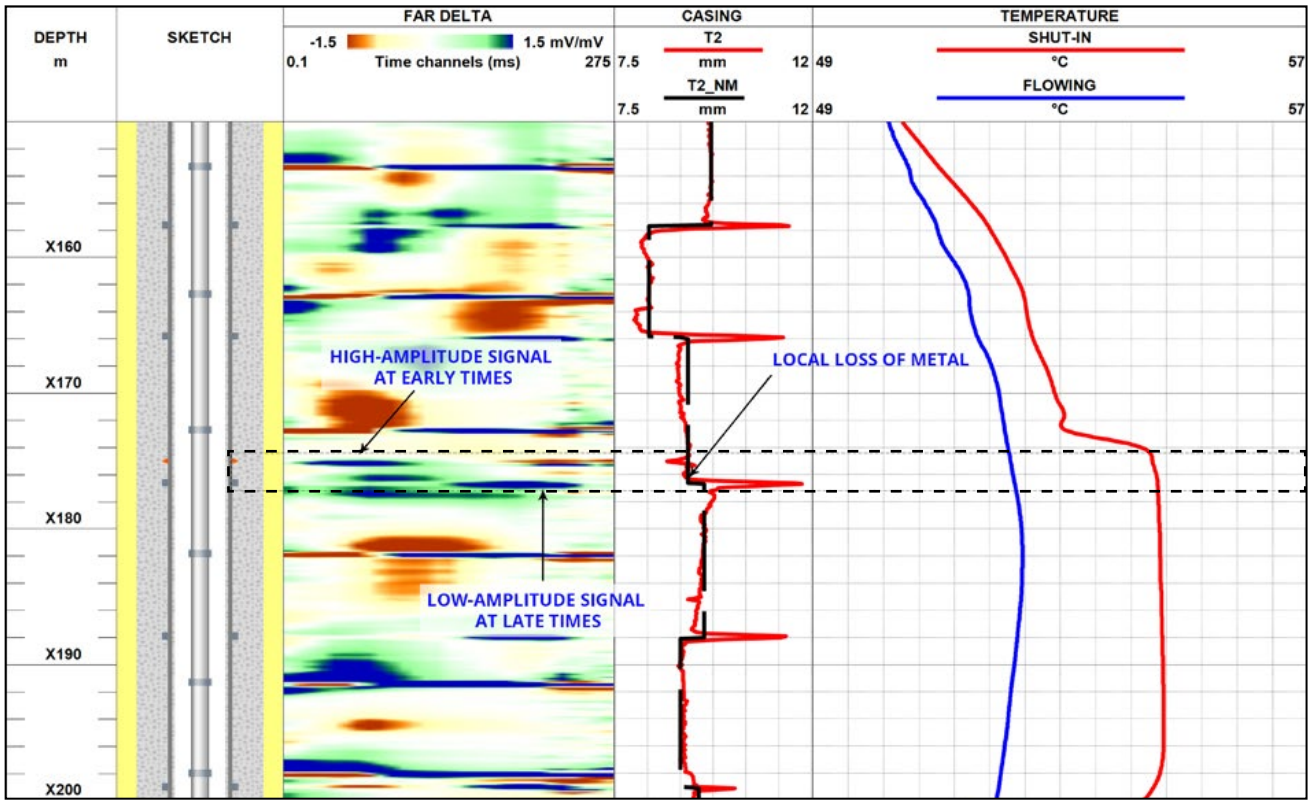

Fig. 2. Casing corrosion identified by MID

Example 2 (Job ID-13055)

The main objectives of the survey on the given producer well, were to evaluate the quality of the perforation job and determination of corrosion intervals on 7” production casing and 3 ½” tubing.

HPT (High Precision Temperature) – SNL (Spectral Noise Logging) – MID (Magnetic Imaging Defectoscope) technologies were utilised during the survey. HPT and SNL surveys were conducted under flowing and static conditions. The first HPT-SNL survey was done under flowing condition. After that the well was closed and MID survey was performed. Finally, HPT-SNL measurements were taken under static condition.

The warming anomaly on temperature curve in flowing mode and high amplitude noise in wide frequency spectrum across the perforated interval in A8 formation indicate fluid inflow into wellbore through perforated interval. The MID data characterises the perforated interval as an equivalent metal loss area, which confirms satisfactory quality of perforations.

Above the perforated interval across the A2 formation HPT data shows cooling anomaly in both regimes (static and flowing) and noise on SNL panel. This anomaly is caused by gas inflow into the borehole through 7” casing leak. Thickness log calculated from MID data confirms casing leak at the same depth.

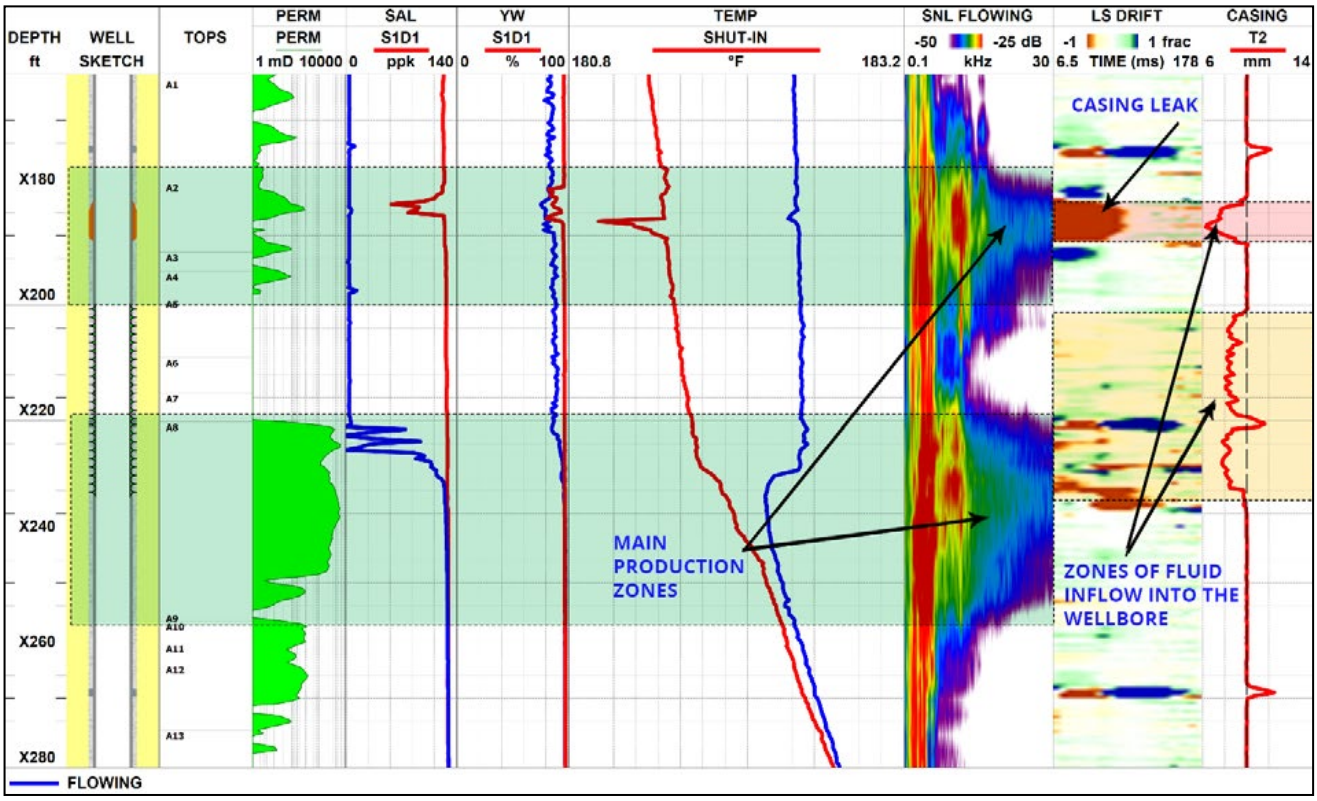

Fig. 1. Temperature, noise and MID measurements in the reservoir zone.

2.3.1.2 WELLS WITH SUSTAINED ANNULUS PRESSURE

Example 1 (Job ID-11048)

This case illustrates the application of static high-precision temperature (SHPT) logging and Spectral Noise Logging (SNL) in a water injection well to locate the source of water entering the casing annulus and then rising to the surface because of a well integrity problem. Logging runs were made only under static conditions to avoid accidents.

A cooling anomaly detected below X120 m was caused by cold water injection into a producing unit. As no noise was captured, it was concluded that no leaks occurred at this depth.

A comparison of static temperature logs recorded in this and nearby wells showed that a temperature anomaly detected within the C and D formations was a result of lateral flow and was not caused by well integrity issues (Fig. 2).

A total of two narrow intervals with noise generated by fluid flow were found in the B formation, and a wide one in the A formation:

1. Noise with a wide frequency range detected by SNL in the interval X071–X072 m at the bottom of B formation indicated fluid flow through the rock matrix. A time-lapse comparison of 2006

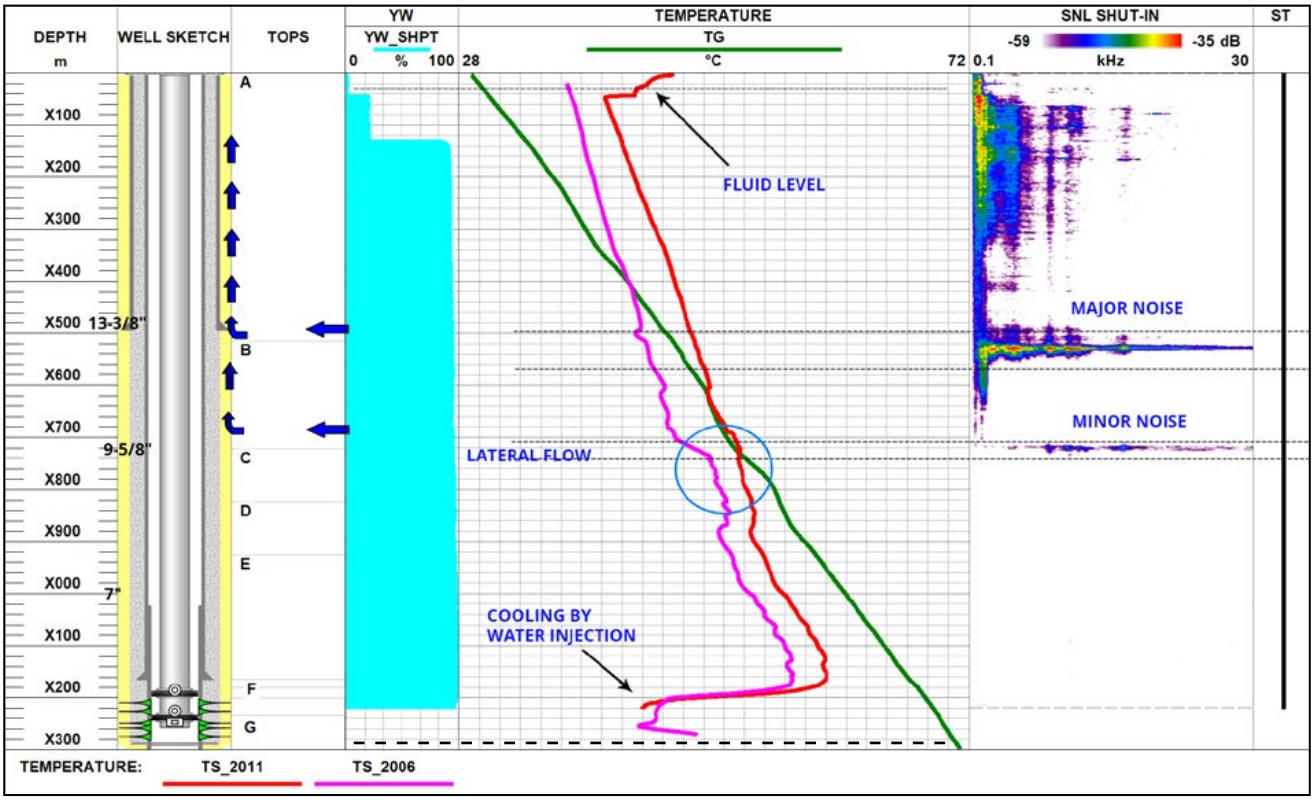

Fig. 1. Comparison of 2006 and 2011 shut-in temperature logs

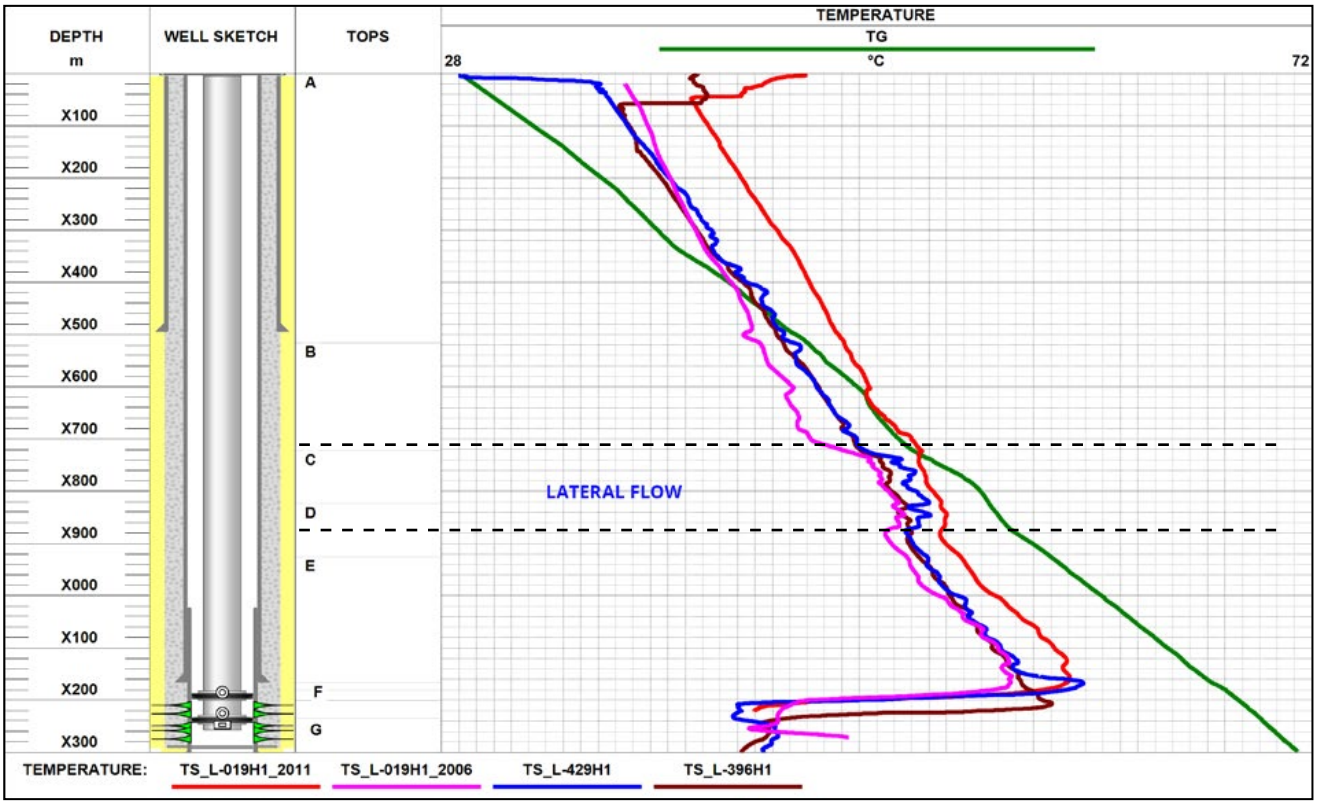

Fig. 2. Lateral flow within the C and D formations

and 2011 shut-in temperature logs enabled the analysis of anomalies possibly caused by a well integrity problem. The 2011 temperature curve features a heating anomaly that appeared after the 2006 temperature survey, probably due to water entry into the casing annulus (Fig. 1).
2. Intense noise detected in the interval X049–X055 m was caused by fluid flow through the rock matrix. A temperature anomaly indicating fluid entry into the casing annulus in this interval is not distinguishable due to a masking effect caused by upward fluid flow. However, the temperature gradient above the interval decreased, and the temperature curve became vertical instead of tending towards the geothermal profile. This points to the fact that the leaking fluid partly entered this interval and partly flowed up towards the wellhead.
3. Noise detected in the frequency range 2–21 *kHz* above a depth of X042 m was generated by the partial entry of the leaking fluid into the A formation. This reservoir has for a long time been used as a source of drinking water and now apparently has low reservoir pressure.

The rest of the water from the B formation, that did not enter A formation, flowed behind the casing to the surface and was the pressure source for the C annulus. Low-frequency 0.6–2 *kHz* noise detected by SNL between a depth of X071 m and the surface was caused by water flow through the casing annulus.

Well integrity could be restored in this well by recementing.

Example 2 (Job ID-14472)
The well was drilled in 1970 and completed as a gas producer. The well was abandoned in 2007 and Surface Casing Vent Flow was detected in September 2008 at rate of 18 drops per minute of water.

Spectral Noise Log (SNL) and High Precision Temperature (HPT) was run in the subject well to identify the source of Surface Casing Vent Flow-SCVF. Vent Flow rate is 18 drops of water per minute. The measured surface annulus pressure after 9 days of shut-in time was about 80 kPa.

Based on the diagnostic and analysis of logs, in shut-in condition, water from high pressure aquifer inflows the channel at depth of 183.2m behind surface casing up to the shallow depth (10.7m to 24.6 m). This can be inferred from the Noise anomalies recorded during the shut-in condition in the interval of 7.1m-183.2 m (low frequency range 0.1 *kHz* to 0.3 *kHz*). Flow in cement channels, appears as a separate satellite line on SNL track. This upwards cross flow in shut-in condition also is supported by positive anomaly on temperature profile starting from below survey interval to 183.2m. Such temperature anomaly is a typical signature of upwards water encroachment in reservoir (Aquifer).

Like the shut-in survey, the same noise anomalies and patterns were recorded in the bleed-off survey, the cross flow from 183.2m to shallow depth of 10.7m to 24.6 m appears to be more active inferred by increase in noise intensity and amplitude. The temperature difference in bleed of condition across the aquifer (below 183.2m) is higher than other intervals. Some noise appear

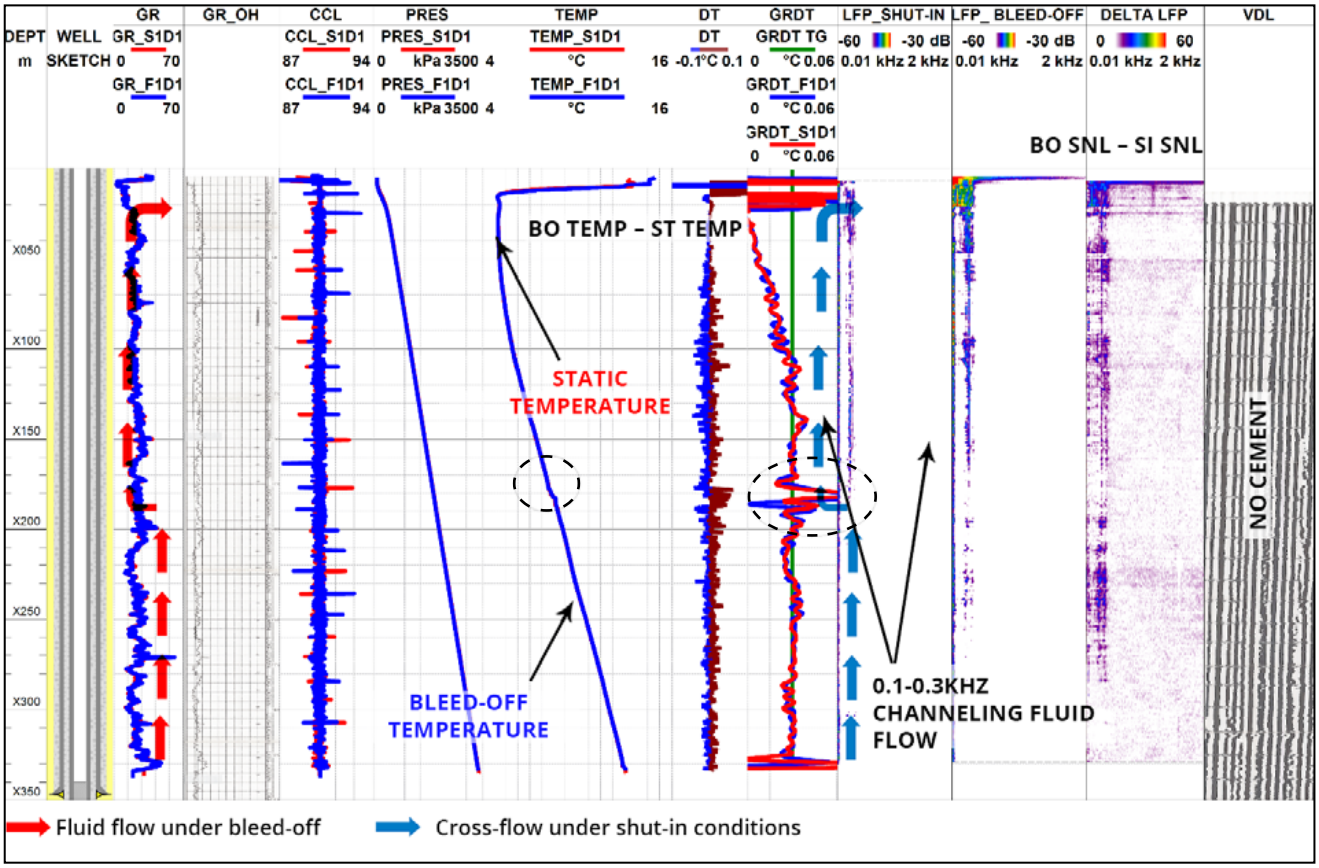

Fig. 1. Channeling Identification

below 183.2 m only in bleed-off condition, this indicates contribution of aquifer under bleed-off conditions.

Further analysis on noise amplitude, noise frequency and temperature profile suggests a corroded spot in 339.7mm surface casing at shallow depth of 15.7m and this spot is supposed to be an entry point of water to surface casing annulus.

Example 3 (Job ID-13000)

Well was drilled in April 1997 and brought in as a gas producer targeting the Barik reservoir. The well was perforated in the interval from 4271.4 m to 4369.5 m. Hydraulic fracturing was conducted in September 1997. The A-annulus pressure reached 100 bar, which was first determined in May 2002. Integrity Test showed that the pressure came back within a day after bleeding off. In line with the well-failure model, the well was suspended with a 50-m cement plug set on top of perforations in December 2002. Then, in February 2005, some activities to bring the well back to production were taken as follows: USIT in Corrosion mode was run in the 3 1/2” tubing through interval from 4124 m to 2691 m to assess the integrity of the 7” liner and

the tubing followed by the second run from the surface to 2685 m to assess the condition of the 9 5/8" casing and the tubing, which did not reveal any serious integrity issues of 9 5/8" casing, 7" liner and 3 1/2" tubing. The well resumed to produce in June 2005. The A-annulus pressure measurement showed that the pressure reached 21 bar.

The 2011 Integrity Tests confirmed the A-annulus pressure at 29 bar, which was then bled down to 25 bar for 5 minutes. There was no communication detected between A and B annuli.

In November 2012, the HPT logging was conducted in the shut-in well and HPT-SNL survey was run while bleeding off the A-annulus, which pressure was 14 bar at the time of bleed-off operation. As the logging operations were restricted in time, the SNL bleed-off zone was specified by the analysis of temperature anomalies and anomalies in the intervals of possible leaks, including the 9 5/8" casing shoe installation depths. According to the static temperature, the anomaly observed at the interval of 9 5/8" casing shoe meant a possible leak and source of gas in A-annulus. This interval was included into the scope of SNL bleed-off measurements. The bleed-off temperature profile was measured from surface to the reservoir section and spectral noise logging was conducted in the zone of 9 5/8" casing shoe installation. Both the water and the gas were recorded at the wellhead from A-annulus during the bleed-off operation. The HPT data show difference between static and bleed-off temperatures from the A6 depth to the surface, which means flow in the A-annulus starting from the leak point in the zone of 9

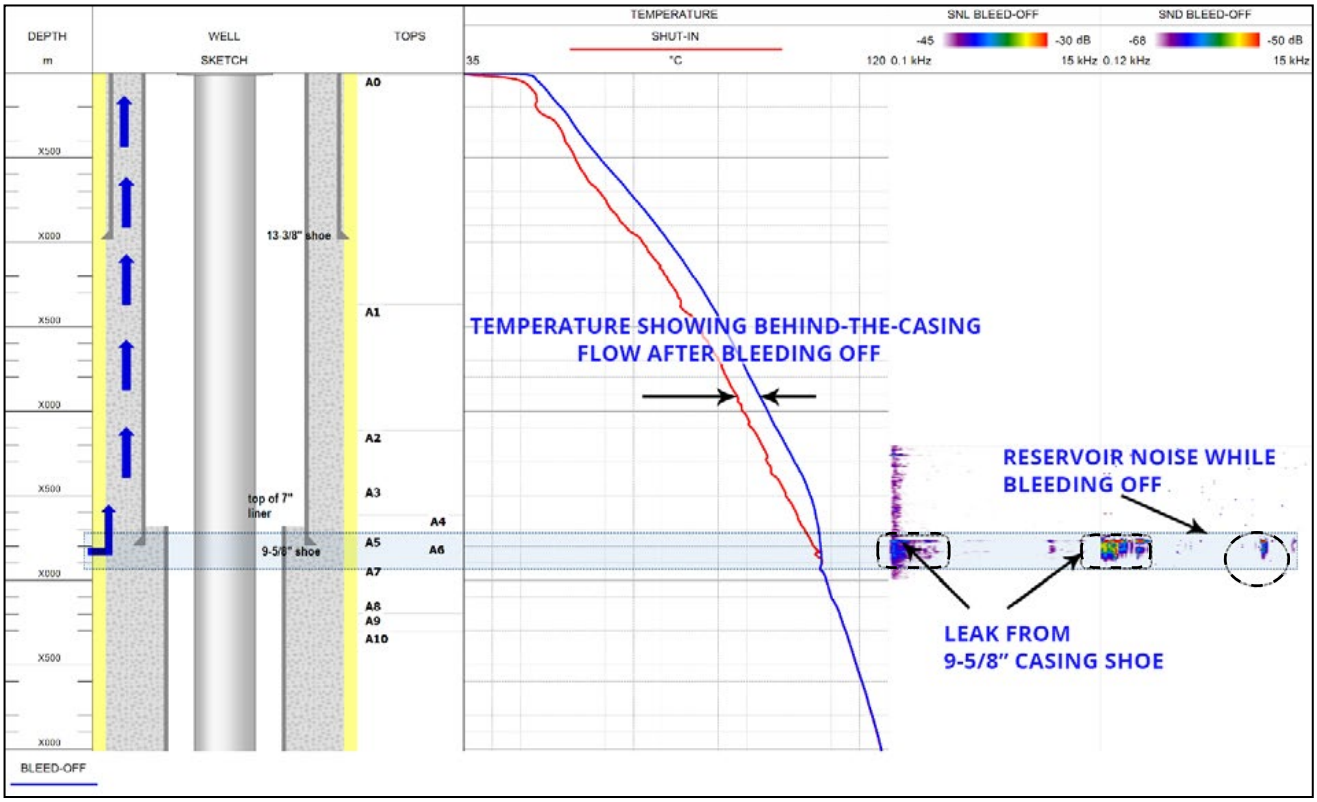

Fig. 1. HPT-SNL Logging data to determine a source of A-annulus pressure

5/8" casing shoe. Both the SNL BLEED-OFF and SND BLEED-OFF captured noises ranged in frequencies from 11 to 14 *kHz* at A5 and A6, suggesting flow from these A5 and A6 units, and low-frequency signals corresponding to the noises produced by flows through the leak from the seal between 9 5/8" casing shoe and the top of 7" liner is attached.

The survey resulted in the recommendation to conduct an additional MID logging to assess the tubing and casing corrosion.

Example 4 (Job ID-13110)

This well was drilled as a subsea gas condensate producer, Slight gas bubbling in Annulus D was observed after 3 years of production with leak rate of 100 L/h at 113 m below sea level.

As per technology, TGT recorded high-precision temperature and pressure logging data while running in hole and SNL at stations while pulling out of hole. Surveys were carried under D-annulus bleed-off and A-annulus injection conditions.

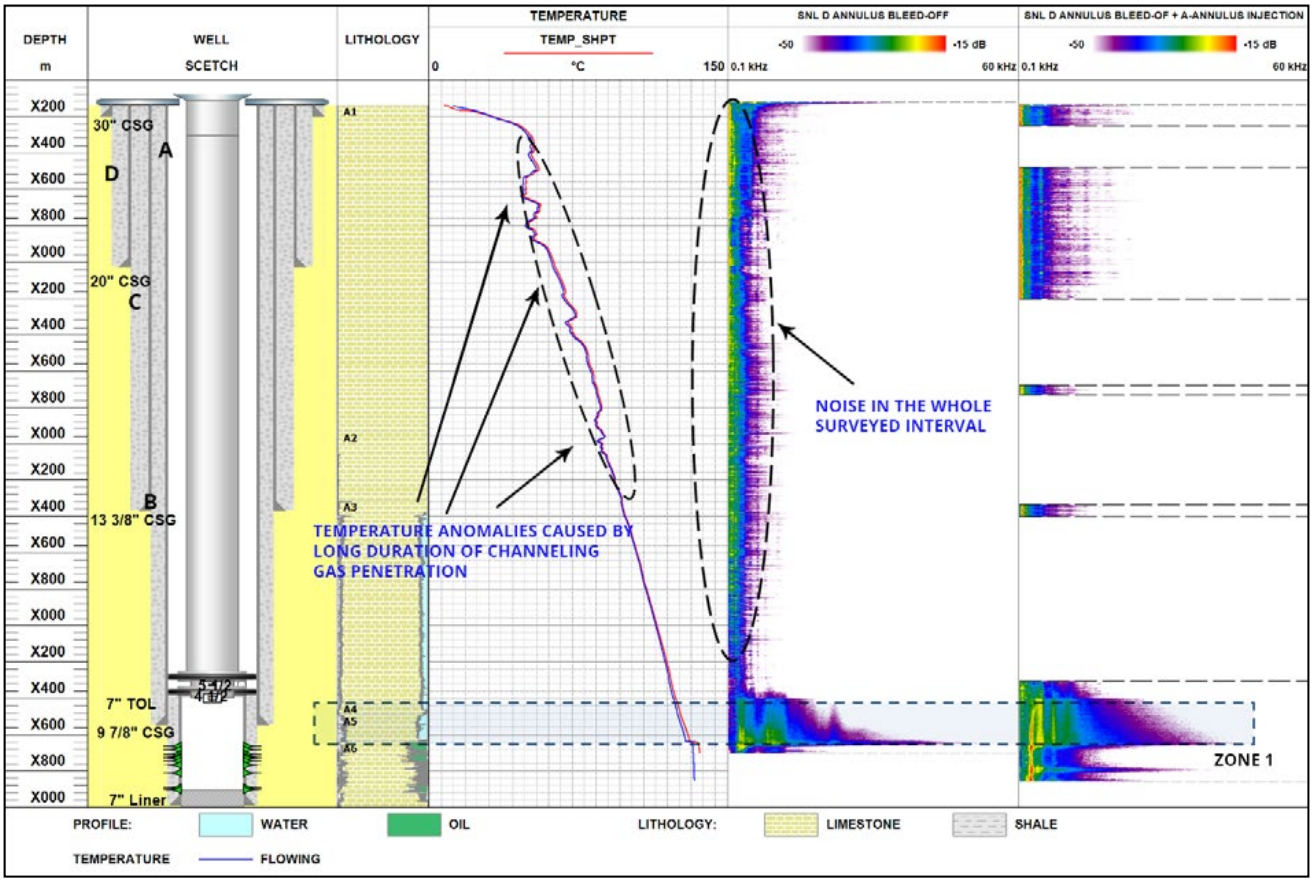

Fig. 1 Leak detection survey (Temperature survey and Noise logging under 1) gas leakage to the surface through Annulus D and 2) during MEG 65% fluid injection into Annulus A).

During injection mode the pressure in Annulus A increased to 1945 psi while the tubing head pressure remained at 2405 psi during the survey suggesting no communication between the tubing and the Annulus A. This is confirmed also by the fact that pressure, temperature and the noise spectrum remained unchanged in both survey modes.

High-frequency reservoir noises detected across the main formation in the narrow intervals in Zone1 were caused by reservoir gas flow (Fig. 1). Apparently, this gas escaped to the surface. The perforated interval was logged incompletely, and fluid inflow was assumed to have also come from below the survey interval.

The facts that low-frequency noise was detected all the way from the Main formation to the surface under both conditions and the temperature between the 13-3/8” casing and the surface had numerous anomalies (see Fig. 2)

Behind-casing cross-flow is confirmed by an increase in low-frequency noise amplitude above the 20”casing shoe where the cement bond was supposedly better (Fig. 2).

In addition, conditions for cross-flow are indicated by poor cement quality behind at least three strings of 7”, 9-7/8’’ and 13” sizes detected by CBL, the results of which were not trusted by the clients.

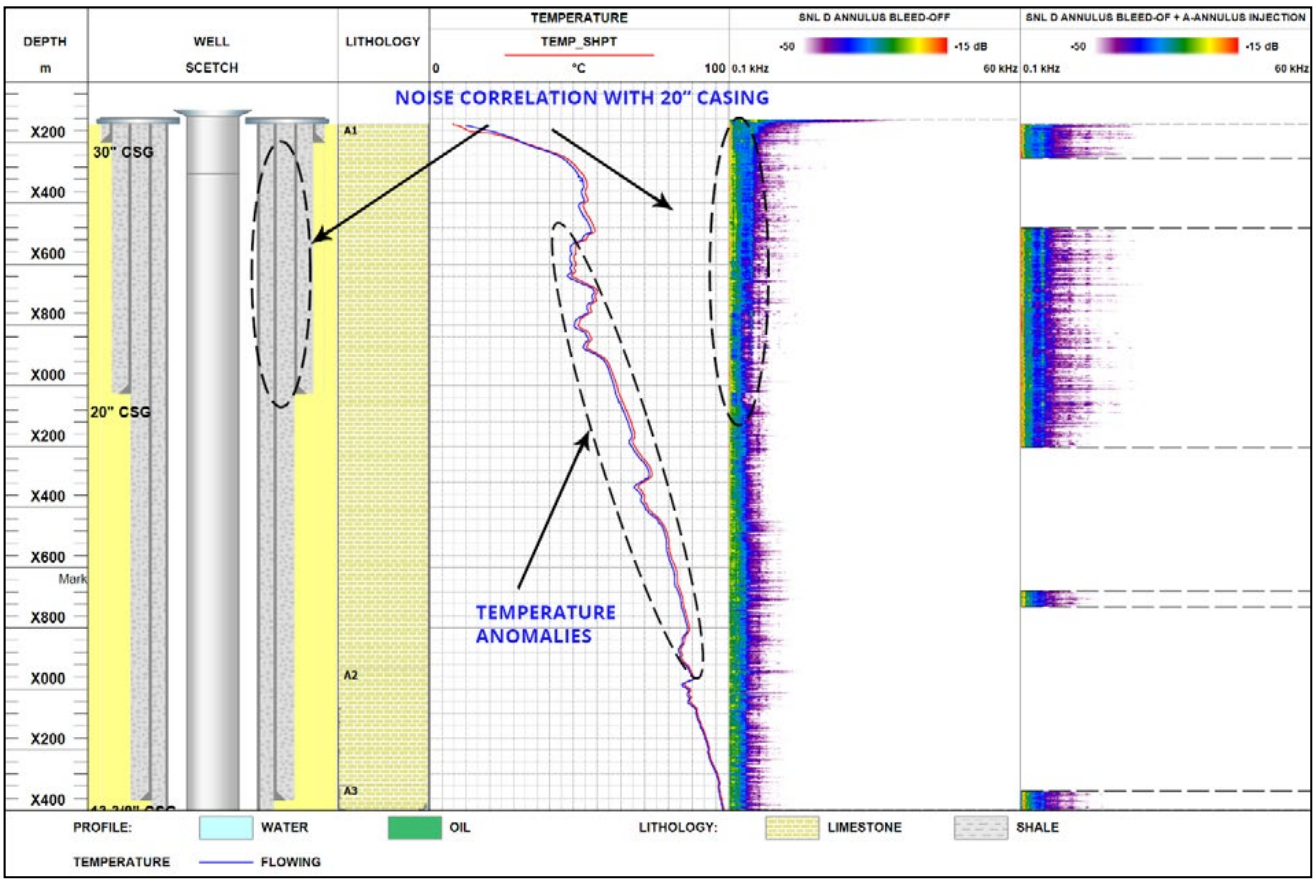

Fig. 2 Low frequency SNL data. Correlation of noise data and 20” casing shoe

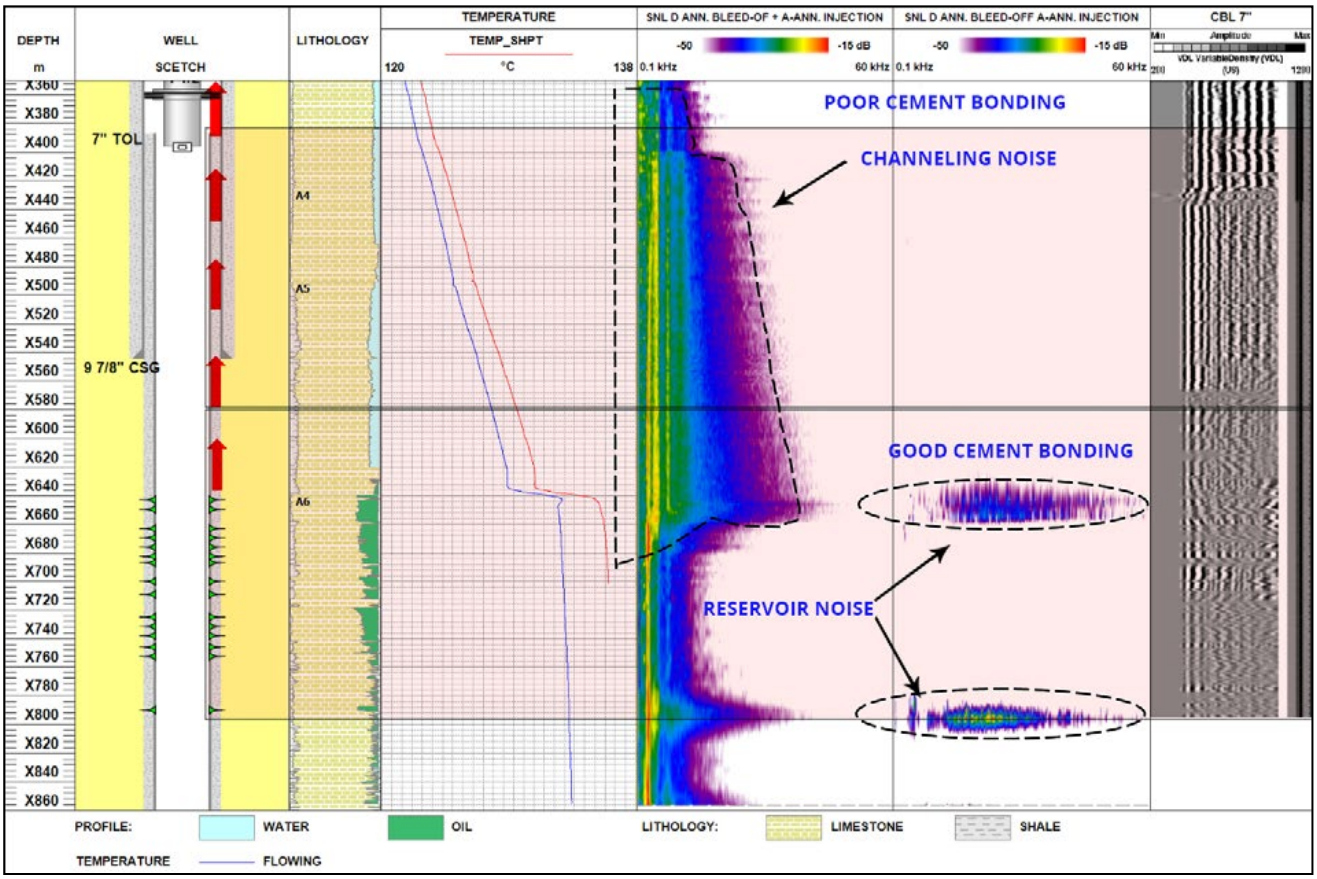

Fig. 3 CBL Data Across main reservoir zone

2.3.1.3 PACKER INTEGRITY

Example 1 (Job ID-11030)

The main objective of the survey was to identify the source of pressure for the C annulus (9-5/8" x 3-1/2") in a deviated well producing from a terrigenous reservoir by natural lift. Additionally, the client reported excess pressure in the B annulus (13-3/8" x 9-5/8"). The well was surveyed by integrated high-precision temperature and spectral noise logging (HPT-SNL).

HPT-SNL was performed in two modes: under shut-in conditions and during pressure bleed-off from the C annulus (9-5/8" x 3-1/2") (Fig. 2). The well was shut-in for two days before the survey. During this period, the pressure in the C annulus (9-5/8" x 3-1/2") increased to 170 psi and in the B annulus (13-3/8" x 9-5/8") to 50 psi.

A comparison of static and bleed-off measurements showed that the wellbore temperature decreased after pressure bleed-off from the C annulus. The highest temperature variation was detected between the packer and the wellhead. The bleed-off temperature gradient changed substantially at the packer, as compared to the static temperature gradient.

SNL reliably detected noise at the packer during pressure bleeding from the C annulus (Fig. 1). It should be noted that this noise occurred only during pressure bleed-off. During static measurements, no noise was detected at the packer. The absence of leak-related anomalies or noise sources below the packer suggests that the pressure source for the C annulus was located below the survey interval and was most likely the perforated reservoir itself, which explains the difference between the static and bleed-off temperatures.

All of the above indicates a leaking packer, which was probably the cause of the pressure increase in the C annulus.

Noise detected by SNL near the surface peaked within the B formation (Fig. 2). A leak in this interval could cause a pressure increase in both the C and B annulus.

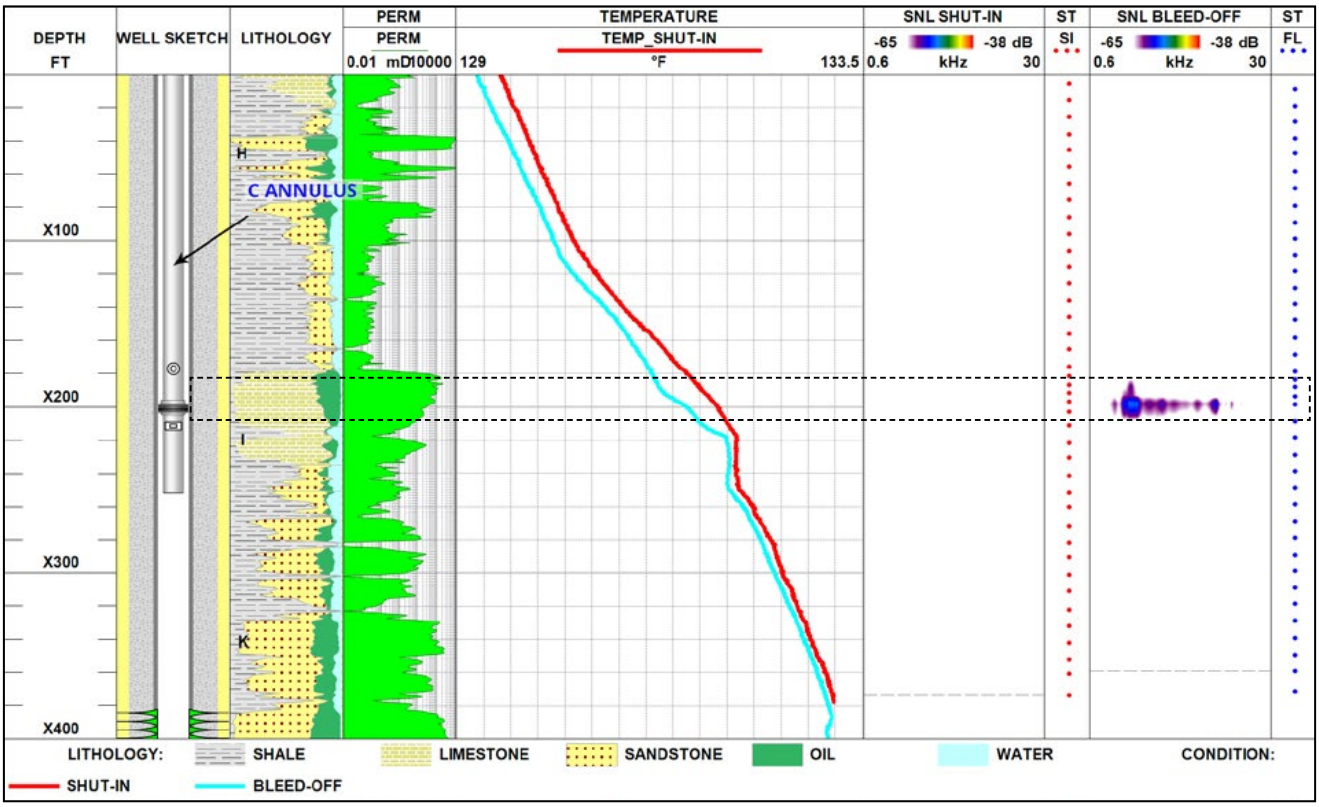

Fig. 1. Temperature and noise measurements showing a packer leak

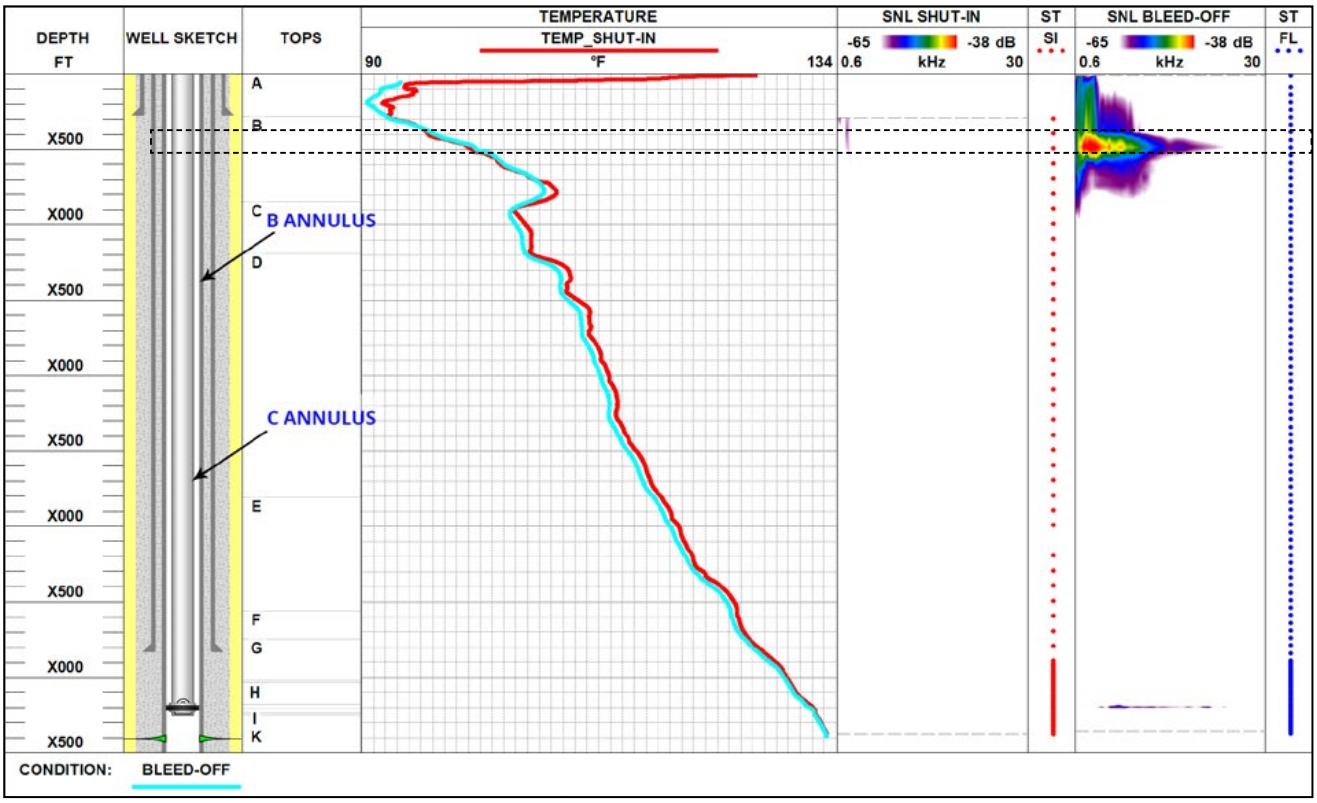

Fig. 2. Wellbore temperature and noise measurements

Example 2 (Job ID-12064)
The survey objective was to identify the source of annulus pressure in a gas injection well, which was achieved using the integrated HPT-SNL technique.

The survey was performed in two modes: under static conditions and during pressure bleed-off from Annulus A. A static logging run was made after a long shut-in period. A significant cooling anomaly indicating gas leakage was found at the packer during pressure bleed-off from Annulus A. The noise data panel shows intense noise in the entire frequency range indicating a leak at the packer, while temperature data also contain an anomaly at its depth.

Noise, temperature and pressure behaviours while changing pressure bleed-off parameters in Annulus A

During an upward logging run, the packer was stripped. The annulus was closed for HSE reasons half an hour later and opened again 10 minutes after that on a smaller choke. These changes in pressure bleed-off conditions affected HPT-SNL readings immediately and simultaneously.

For instance, packer stripping was visualised as temperature and pressure anomalies at Line A: Annulus A produced substantial gas flow, and well pressure started to decrease. As the packer was open, Annulus A communicated with tubing and its pressure started to recover.

When the tool was pulled up to Line B, Annulus

A was closed to stop the gas leak to the surface, and annular pressure also started to recover.

When the tool reached Line C, Annulus A was reopened on a small choke.

SNL detected noise caused by gas flow through the annulus under different conditions, and the signal frequency depended substantially on bleed-off modes.

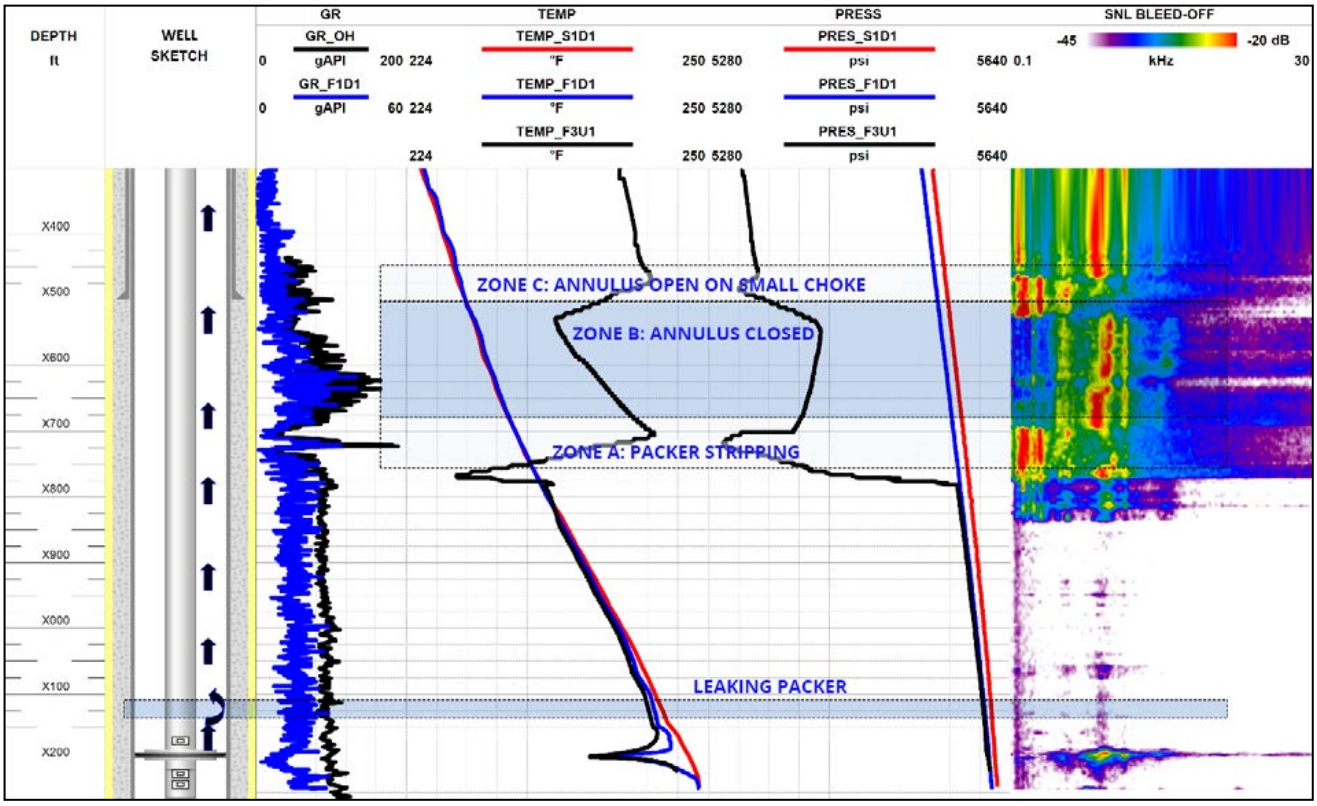

Fig. 1. HPT-SNL data: temperature and pressure recorded under static conditions and temperature, pressure and noise recorded during pressure bleed-off from Annulus A.

2.3.1.4 DETECTION OF CHANNELLING IN A GAS STORAGE WELL

Example 1 (Job ID-16036)

Checking for potential behind-casing cross-flows prior to perforation is a fairly common task in oilfield operations.

Such a survey, conducted to identify behind-casing cross-flows, was particularly critical for an oil company operating an underground gas storage reservoir for which it was necessary to make sure that no gas was lost into other formations from a well that was drilled a few years after gas injection started in this field.

In this case, behind-casing cross-flow was

suspected after acquisition of CBL data showing a poor cement bond above and below the gas storage.

To make sure there were no wellbore integrity problems, a spinner survey was conducted and then the wellbore was scanned with the Electromagnetic Pulse (EmPulse) to check on casing and tubing integrity. Logging data showed no cross-flows inside casing (Fig. 1).

To identify any potential behind-casing cross-flows, reservoir-oriented surveys were conducted, including Pulsed Neutron Logging (PNL), Spectral Noise Log High Definition (SNL-HD) and High-Precision Temperature High Definition (HPT-HD) logging.

SNL captured high-intensity, high-frequency noise signals across a gas injection zone (A5). Such signals are normally associated with reservoir gas flows (Fig. 1). Similar noises were also detected in the overlying (A2, A3 and A4) and underlying (A6) formations.

The cooling anomalies in the static temperature curve were caused by both lithological features above A2 and adiabatic gas expansion during pressure jumps in A5 and A4.
The recorded low-frequency noise signals and an analysis of temperature logs revealed communication between the gas storage Unit A5 and the overlying and underlying formation Units A2, A3, A4 and A6 and determined the cross-flow direction (Figs. 1 and 2).

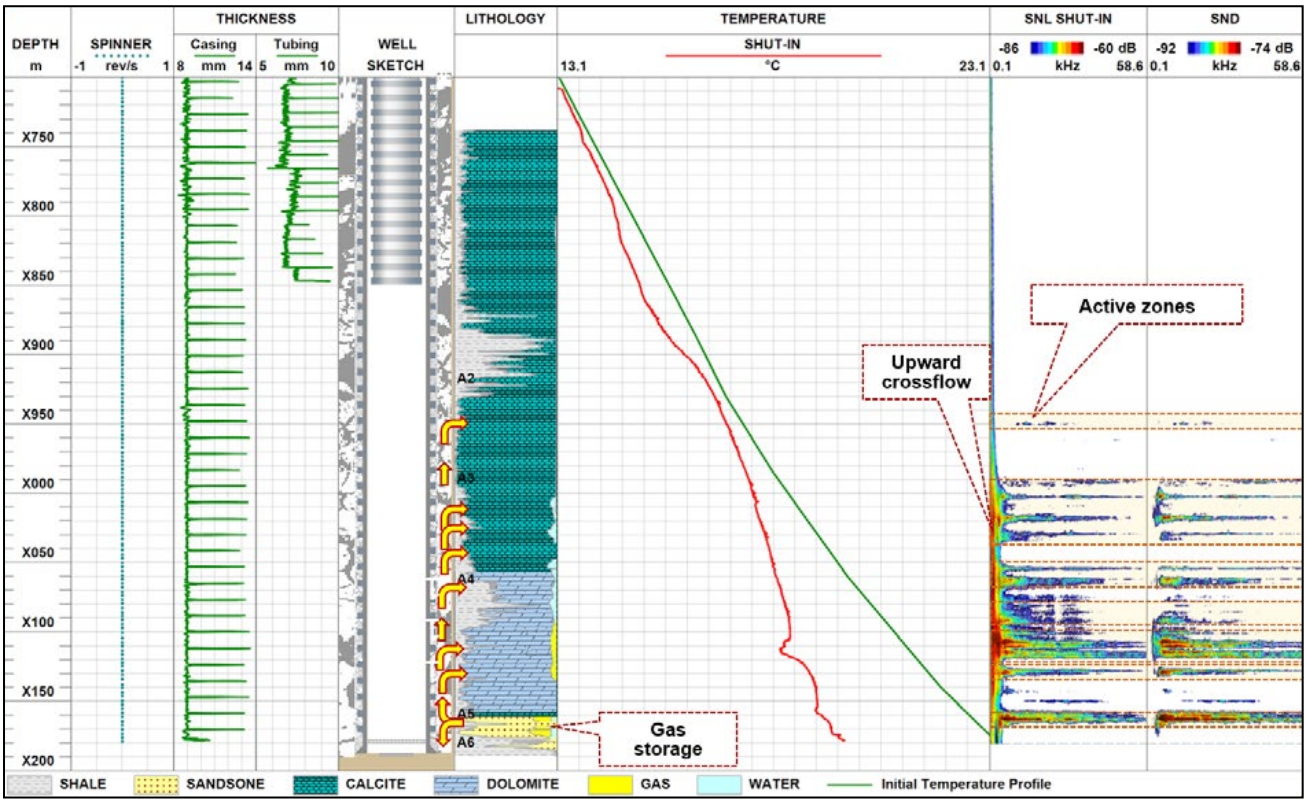

Fig. 1. SNL indicated gas movement within the gas storage itself (A5) as well as above and below it, whereas PNL detected gas in permeable strata and in the casing annulus. A temperature gradient change below A2 was due to upward cross-flow behind casing from the gas storage. The temperature and noise logging data also showed that some gas flowed below the survey interval into the A6 reservoir.

A PNL data analysis confirmed the presence of gas in those formations where SNL data indicated fluid flows. Some gas was also found in shales, which could be due to gas channelling behind casing (Figs. 1 and 2).

In summary, a comprehensive analysis of reservoir-oriented SNL-HD, PNL, HPT-HD, EmPulse and spinner surveys identified cross-flow from the gas storage into the upper and lower zones.

The results of the integrated SNL-HD, PNL, HPT-HD, EmPulse and spinner surveys have been used to successfully eliminate cross-flow behind casing.
This complex approach should be applied in any well prior to perforation to make sure that it does not lose hydrocarbons during operation.

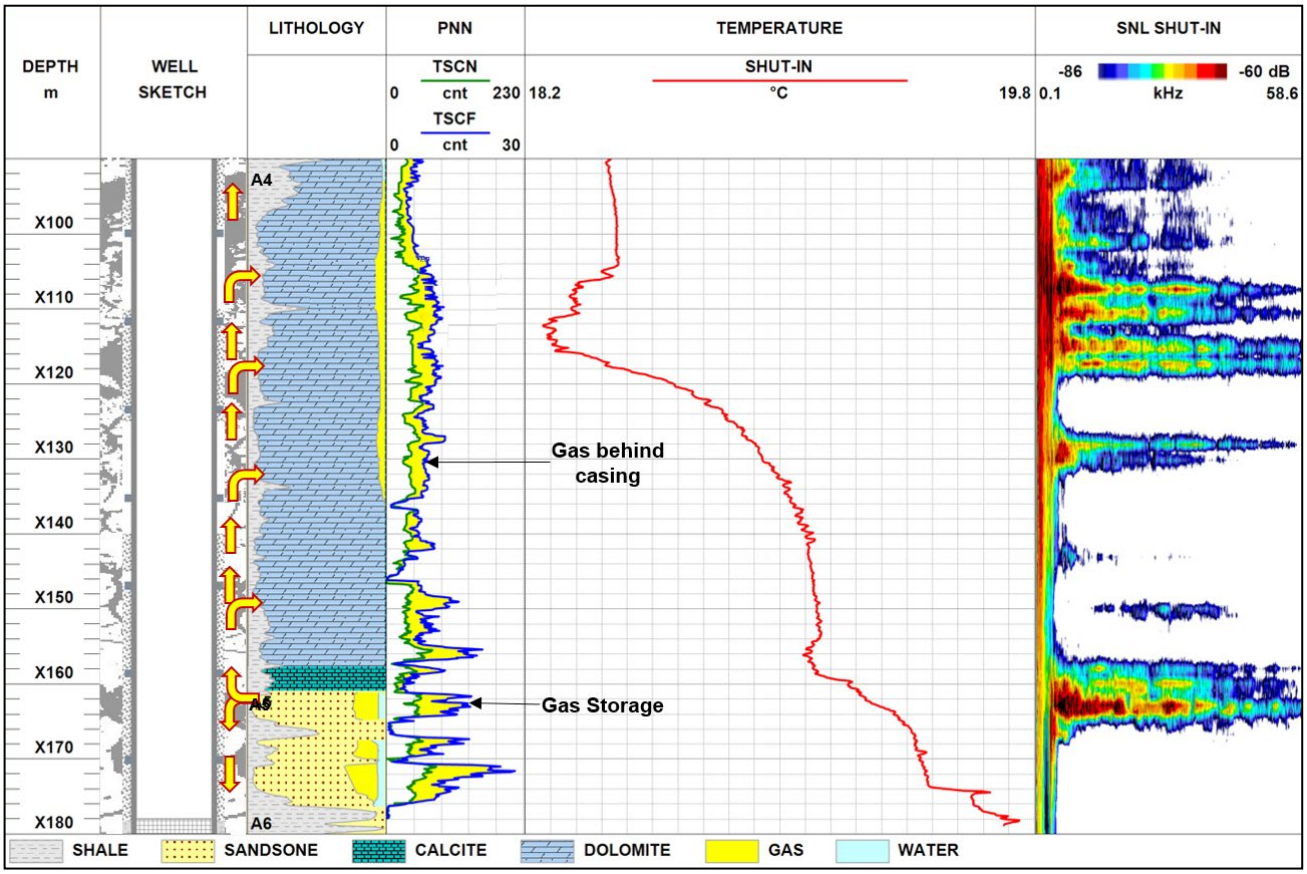

Fig. 2. Gas invasion by PNL data (shown in the "Lithology" column in yellow). Gas was found to accumulate in Units A5 and in the casing annulus.

2.3.2 CORROSION ASSESSMENT

Objectives

Evaluation of the individual thicknesses of the first and second metal barriers (tubing and casing) and location of corrosion zones in them

Technology

1. Hardware and software tools
- EmPulse-2 – Magnetic Imaging Defectoscope
2. Methodology
- Location of corrosion zones in the first and second metal barriers independently
- Location and identification of completion components
- Evaluation of the perforation quality of the first barrier

Criteria for Candidate Selection

1. Wellbore accessibility
2. Pressure test failure
3. Sustained annulus pressure (SAP)
4. Abnormally increased water/gas production
5. Completion features susceptible to corrosion

Inputs for Candidate Selection

Well sketch and zones of interest

Inputs for Job Proposals

Well sketch and zones of interest

Inputs for Interpretation and Analysis

Raw logs recorded by TGT

2.3.2.1 CORROSION HOLE IN A LONG TUBING STRING

Example 1 (Job ID-13207)

This case shows how the EmPulse tool captures a tubing defect in a dual-barrier completion (Figs. 1a and 1b). Well OP-1 is a dual 3-1/2”-string oil producer completed with 9-5/8” casing in two pay zones. Its upper section contains two 3-1/2” tubing strings, 9-5/8” production casing, 13-3/8” surface casing and 18-5/8” conductor casing. Both long and short strings have the same wall thickness of 0.254 inch, and the wall thickness of 9-5/8” production casing is 0.435 inch.

The tubing-head pressure survey revealed the same pressure in the long and short strings, suggesting downhole communication between them. A Multi Barrier Imaging survey was conducted in long string to check tubing for corrosion and defects.

Long string tubing thickness data revealed 30% metal loss at X,907 ft between the packers (see the Thickness 1 profile in Fig. 1a). Brown spots indicating corrosion are present in both the NEAR and FAR DELTA panels at the same depth, which means that the actual response is lower than the simulated. The centre of the brown spot is closer to the dashed line CL1, which qualifies it as corrosion in the first barrier [28].

The second barrier has the nominal thickness, as seen in the Thickness 2 profile, and no brown spots are intersected by the CL2 line, which suggests no corrosion in 9-5/8” production casing.

A temperature log was recorded simultaneously with the EmPulse log (Fig. 1a) and shows a gradient change across a defect located by EmPulse, which indicates a leak through a corrosion hole (6).

After completion of logging operations, the tubing strings were retrieved and a 1.6”-by-1.2” corrosion hole was found across the leak area

detected by EmPulse and temperature logs. It should be noted that this particular defect is larger than the minimum defect the EmPulse tool can capture. Also note that, despite the close proximity and electromagnetic interference between the tubing and casing collars at X880 ft, both were automatically identified by the EmPulse tool and software using a time response pattern.

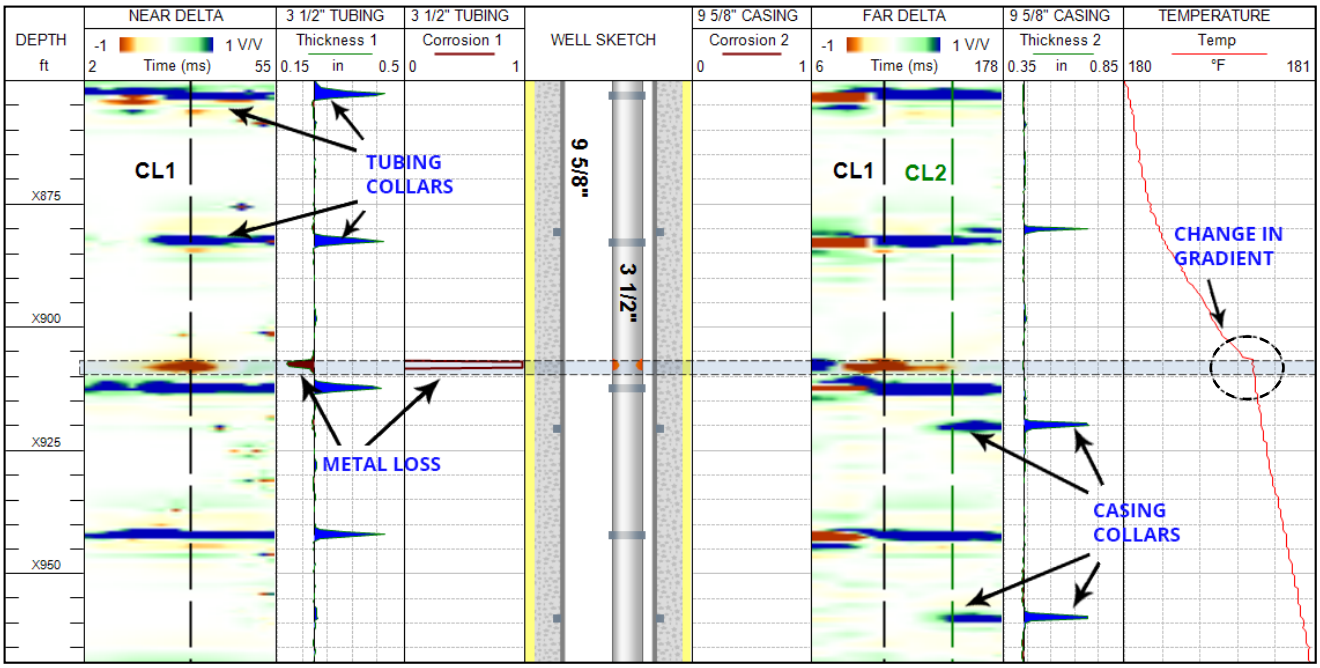

Fig. 1a. Corrosion hole in a long tubing string at X,907 ft. The short string was located at a shallower depth and was not captured in this depth interval

Fig. 1b. Corrosion hole found in the long string at X,907 ft after retrieval

2.3.2.2 CORRODED TUBING SECTION

Example 1 (Job ID-13545)

This case shows how the EmPulse tool captures a tubing defect in a dual-string three-barrier completion, which is a challenging environment for electromagnetic scanning because of the asymmetric position of tubing strings in the wellbore. The current model describes axisymmetric systems (see Section 1.5), and the calculation of the second barrier's thickness is impossible because of the influence of the short string. The 9-5/8" casing was analysed only qualitatively in the two-string zone. For the zone containing only the long string, the thickness of the second barrier can be quantified. Well OP-2 is a dual 3-1/2"-string oil producer completed with 9-5/8" casing in two pay zones. The objective of the Multi Barrier Imaging survey in this well was to check the integrity of the long string and locate zones of metal loss. The tool was run only once in a long string.

Most of the well contains 13-3/8" casing, i.e. the third barrier, that complicated the electromagnetic scanning of the second barrier.

The survey revealed three corroded zones in tubing at X417 ft, X427 ft and X442 ft (Fig. 1). This section contains two 3-1/2" tubing strings, 9-5/8" casing and 13-3/8" casing.

The centres of the brown spots are closer to the CL1 corrosion line on the NEAR DELTA and FAR DELTA panels, which indicates corrosion in the first barrier (the long 3-1/2" tubing string). Tubing thickness data in the Thickness 1 profile of Fig. 1 shows a metal loss of at least 25% in all three zones.

Corrosion of more than 10% in the first barrier can significantly distort the measured response,

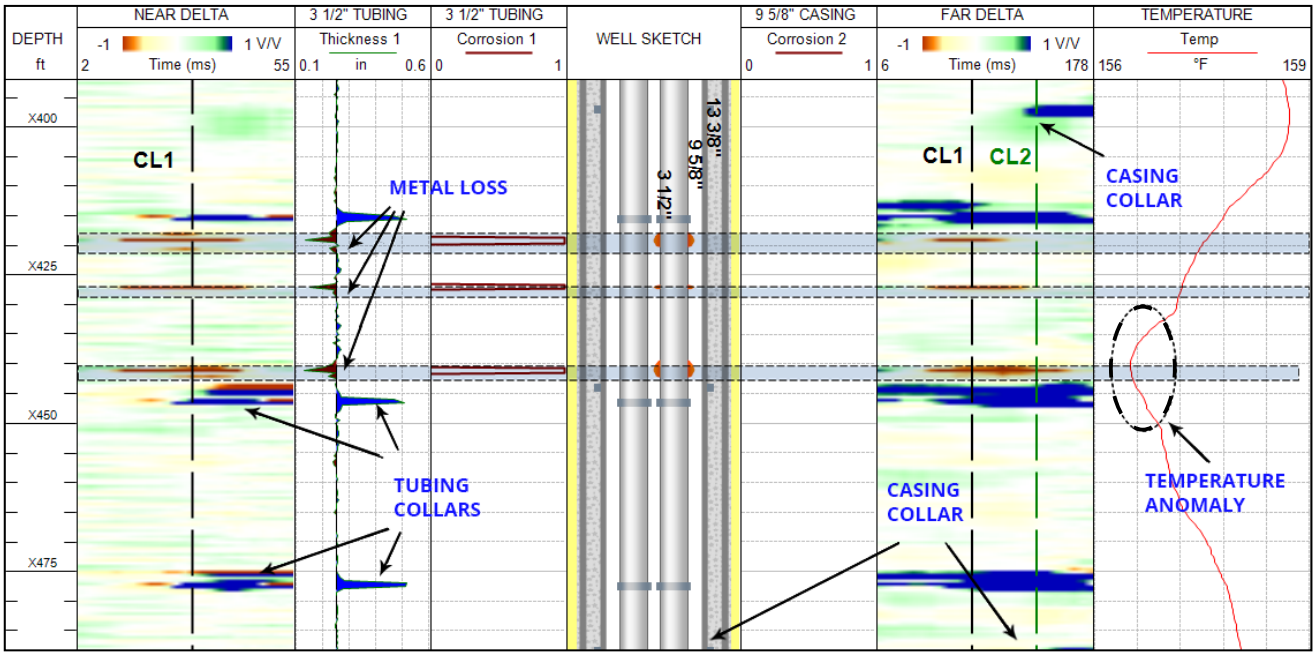

Fig. 1. A corroded tubing joint with three distinct zones of metal losses at X417 ft, X426 ft and X442 ft. The temperature log shows a cooling anomaly at X442 ft caused by leaking

and it can deviate from the modelled response in a wide time range. Red spots overlapping with CL1 and CL2 may appear in the Far Delta panel, with the maximum deviation (in their centres) still remaining on CL1.

The temperature sensor detected a cooling anomaly at X442 ft right across the lower defect detected by EmPulse, suggesting that this zone corroded into a through hole and started to leak [29].

The FAR DELTA panel data suggest no corrosion in 9-5/8" production casing.

2.3.2.3 TUBING COLLAR CORROSION

Example 1 (Job ID-13551)

This case shows how the EmPulse tool captures corrosion in a tubing collar. Well OP-3 is a dual 2-3/8"-string oil producer completed with 5" casing in two pay zones. Downhole communication between the tubing strings was suspected because of similar wellhead pressures in them. The objective of the Multi Barrier Imaging survey in this well was to check the integrity of the long string and locate zones of metal loss.

The survey revealed that a collar located at X850 ft had reduced thickness, as seen in the Thickness 1 profile (Fig. 1). Both the NEAR DELTA and FAR DELTA panels show a brown spot extending from early times through an intersection with the CL1 corrosion line, thus indicating metal loss in this collar. The temperature log shows a gradient change indicating that the collar was leaking. There is a strong indication of 15% metal loss in tubing one foot above the corroded collar. There are also some indications of smaller metal

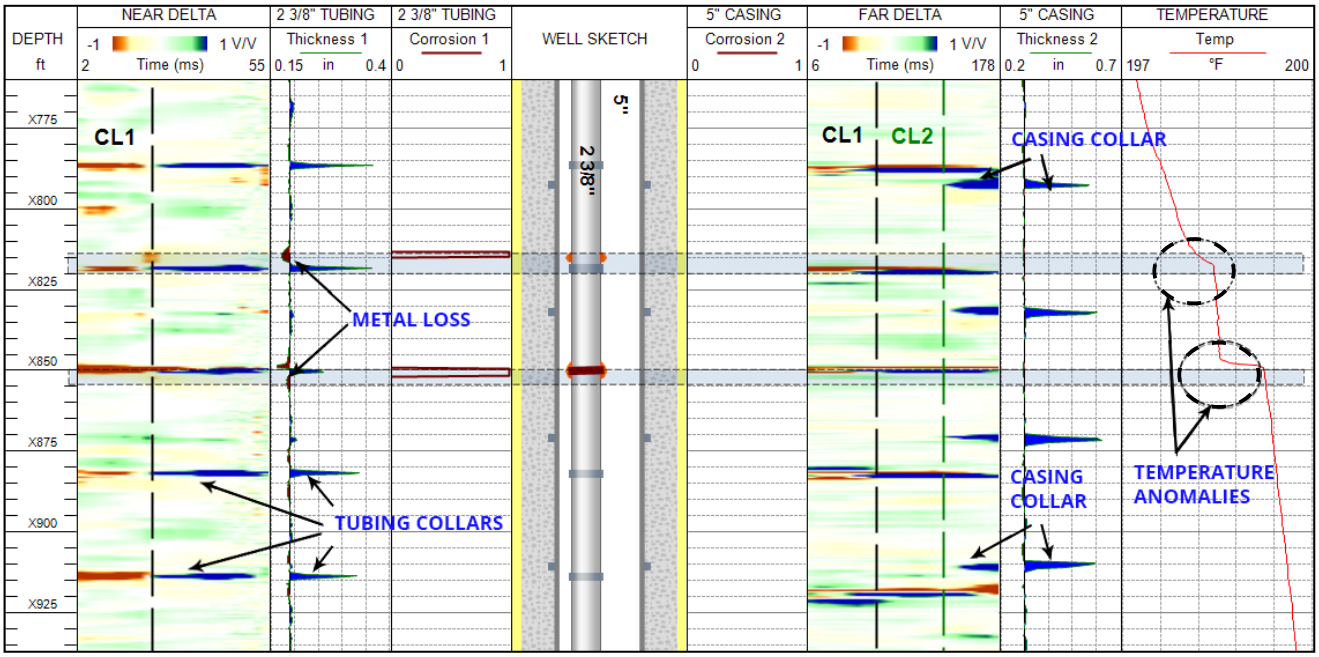

Fig. 1. Tubing collar corrosion at X850 ft and tubing joint corrosion at X815 ft. Both defects are through-hole leaks captured in temperature logs

losses below this collar as suggested by reduced thickness and a faint yellow spot intersected by the CL1 line at X850ft.

Another corrosion event was detected at X813 ft. The NEAR DELTA panel displays a decrease in tubing thickness and a brown spot intersected by the CL1 line. The temperature log shows a gradient change indicating a leak [29].
The thickness profile, calculated for the long-string interval containing no short string, indicated no metal loss in the 5” production casing.

2.3.2.4 CASING CORROSION

Example 1 (Job ID-13420)
This case shows how the EmPulse tool captures corrosion in the second barrier (10-3/4” casing).

Well OP-4 is a dual 3-1/2”-string oil producer completed with 10-3/4” production casing in two pay zones. Most of the well contains 13-3/8” casing, i.e. the third barrier, which complicated the electromagnetic scanning of the second barrier.

The objective of the survey was to check the tubing strings and 10-3/4” casing for corrosion.

The survey revealed no tubing corrosion, as seen in the Thickness 1 profile and the DELTA panels of Fig. 1.

However, the centre of a brown spot at X944 ft in the FAR DELTA panel is closer to the CL2 corrosion line, which indicates corrosion in 10-3/4” production casing.

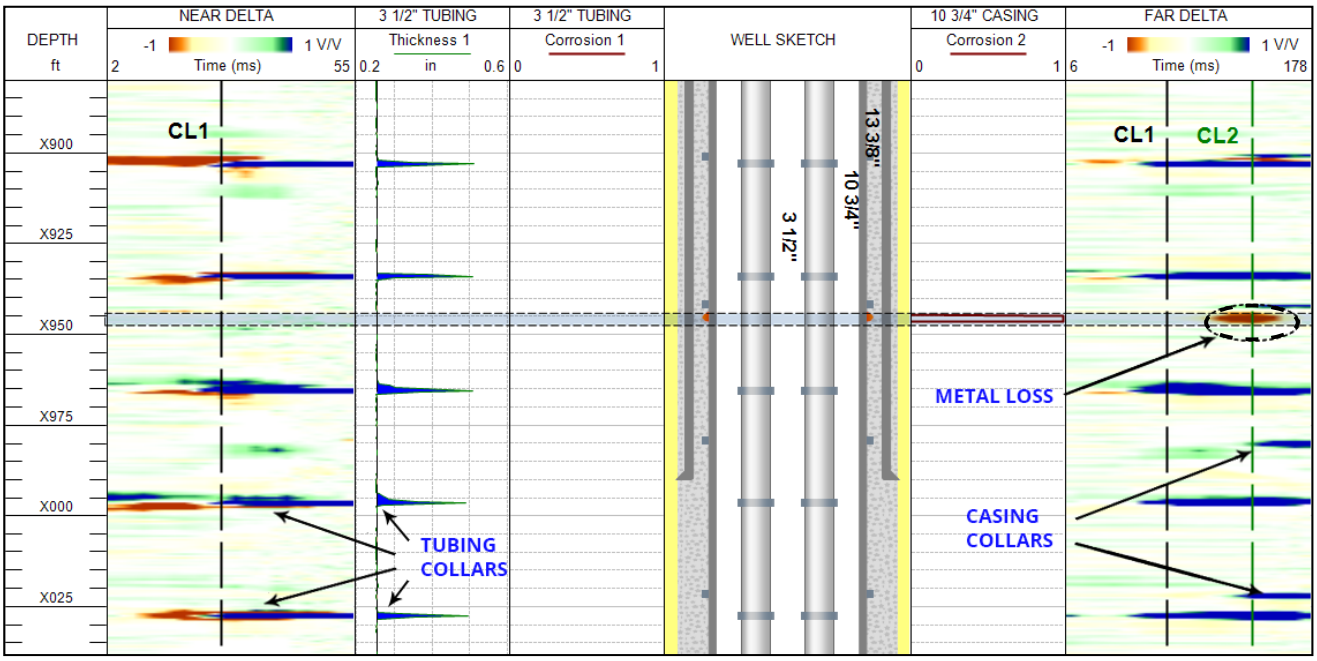

Fig. 1. Corrosion in the second barrier. Metal loss was found at X944 ft in 10-3/4” production casing

2.3.2.5 LEAKING CORROSION HOLES IN TUBING AND CASING

Example 1 (Job ID-14057)

This case shows how the EmPulse tool captured a leaking hole in tubing and multiple leaking holes in casing. Well WD-1 is a water disposal injector completed with 5-1/2” tubing, 9-5/8” casing and 13-3/8” conductor strings. A Multi Barrier Imaging survey in this well was combined with temperature and spectral noise surveys to check if water was injected into the target formation.

The survey revealed a massive metal loss of 80% in tubing at X051 ft that turned into a through-hole leak captured by the spectral noise logging tool (Fig. 1). The temperature log did not reflect this low-rate leak.

Below that depth, the survey revealed numerous zones of corrosion in the X070–X100 ft interval (Fig. 2).

The thickness log indicated 60% metal loss at X072 ft and 30% metal loss at X086 ft and X089 ft.

The spectral noise log suggested that all three defects were leaking [29].

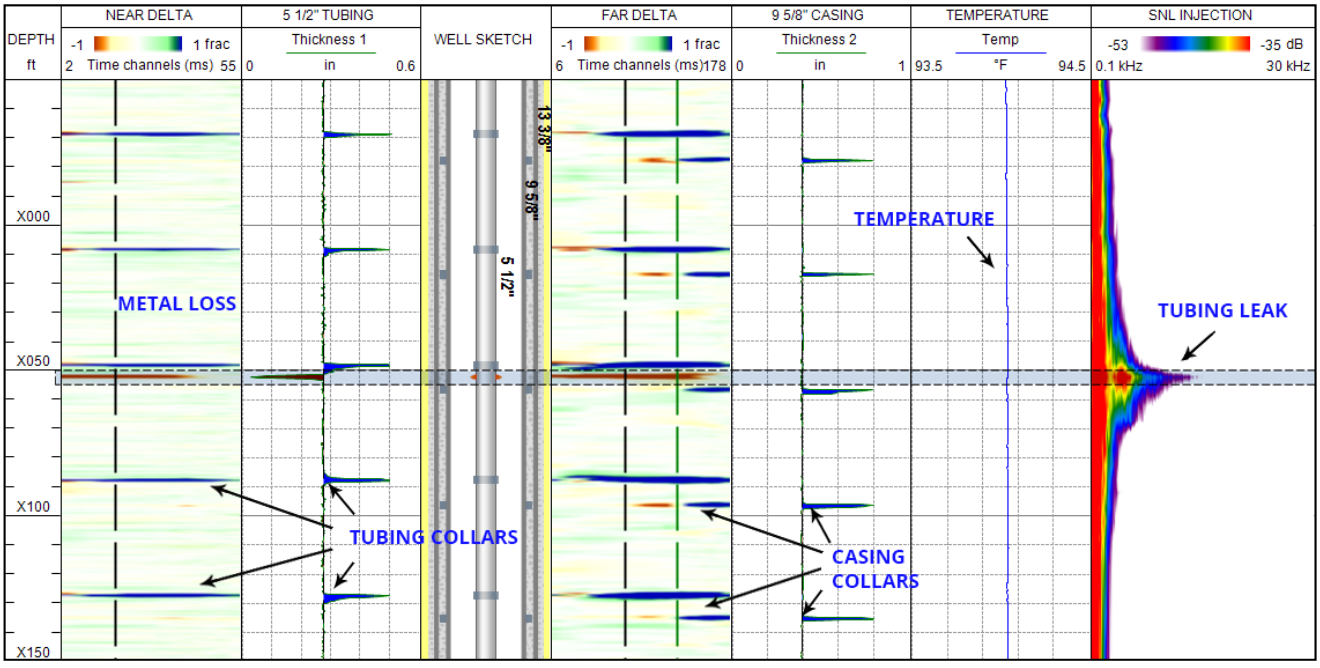

Fig. 1. Tubing corrosion. Almost 80% metal loss was found at X051 ft in 5-1/2” tubing. The spectral noise log (SNL) suggested that this was a through-hole leak, as noise energy extended to higher frequencies. The leak rate was low and was not picked up by temperature logging

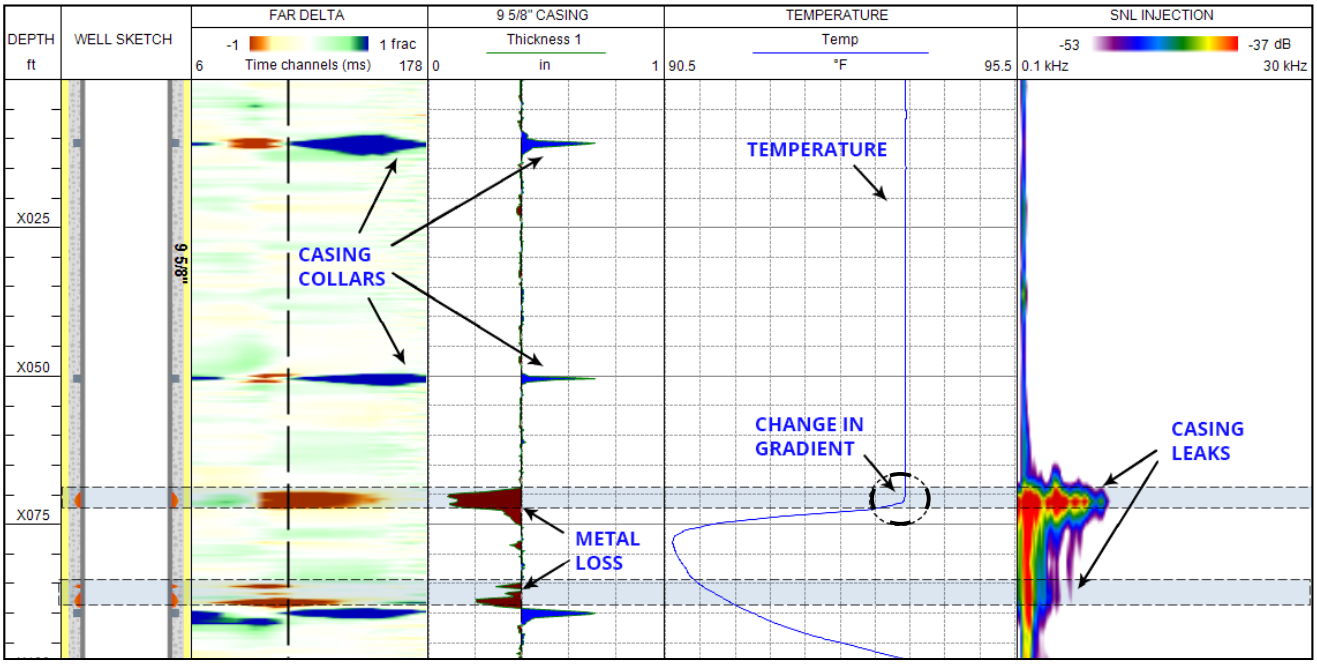

Fig. 2. Numerous corrosion holes in 9-5/8” casing. Three holes were picked up by the EmPulse tool, all with noise extending to higher frequencies above 1 *kHz*, which clearly indicated an active leaks

3. REFERENCES

1. M.A. Miheev, I.M. Miheeva. Foundations of heat transfer. In Russian, 1973, Moscow, Energiya Press.
2. H. Schlichting. Boundary-Layer Theory. In Russian, 1974, Moscow, Nauka Press.
3. V.E. Nakoryakov, A.V. Gorin. Heat and mass transfer in two-phase systems. In Russian, 1994, Novosibirsk, Institute of thermophysics of Siberian Branch of the Russian Academy of Sciences Press. 431 pp.
4. O. Bratland, Pipe flow 1. Single-phase Flow Assurance
5. O. Bratland, Pipe flow 2. Multiphase Flow Assurance
6. A.M. Ansari, N.D. Sylvester, O. Shoham, J.P. Brill. A Comprehensive Mechanistic Model for Upward Two-Phase Flow in Wellbores. SPE Annual Technical Conference and Exhibition, 23-26 September, New Orleans, Louisiana, 1990
7. D.H. Beggs, J.P. Brill. A Study of Two-Phase Flow in Inclined Pipes. Journal of Petroleum Technology, vol. 25, 1973
8. H. Shi, J.A. Holmes, L.R. Diaz, L.J. Durlofsky, K. Aziz. Drift-Flux Parameters for Three-Phase Steady-State Flow in Wellbores. SPE Annual Technical Conference and Exhibition, 26-29 September, Houston, Texas, 2004
9. H. Shi, J.A. Holmes, L.J. Durlofsky, K. Aziz, L.R. Diaz, B. Alkaya, G. Oddie. Drift-Flux Modeling of Multiphase Flow in Wellbores. SPE Annual Technical Conference and Exhibition, 5-8 October, Denver, Colorado, 2003
10. Y. Nicolas, E.J. Witterholt. Measurements of Multiphase Fluid Flow. Fall Meeting of the Society of Petroleum Engineers of AIME, 8-11 October, San Antonio, Texas, 1972
11. Hinze, J.O. 1959. Turbulence, McGraw-Hill Book Co., Inc., New York
12. S.A. Nikolaev and others, "Sound Generation by Percolation Flows through Porous Media" published in Acoustic Journal, 1992, 38, No. 1, 114–118 3
13. Y.M. Zaslavsky, "On the Theory of Acoustical Emission Accompanying Gas Filtration by Partially Fluid-Saturated Medium" published in Technical Acoustics Electronic Journal, http://ejta.org, 2005, 5
14. M.J. Lighthill, "On Sound Generated Aerodynamically: Turbulence as a Sound Source", 1954.
15. Wang Y, Jin J, Bai B and Wei M, "Study of Displacement Efficiency and Flow Behavior of Foamed Gel in Non-Homogeneous Porous Media", 2015, PLoS ONE 10(6): e0128414
16. SPE 177620-MS Quantification of Reservoir Pressure in Multi-Zone Well under Flowing Conditions Using Spectral Noise Logging Technique, Zubair Reservoir, Raudhatain Field, North Kuwait (2015)
17. SPE 162081 Spectral noise logging data processing technology (2012)
18. Arbuzov, A.A., Alekhin, A.P., Bochkarev, V.V., Minakhmetova, R.N., Chukhutin, D.V. and Zakirov, A.N. Memory Pulsed Neutron-Neutron Logging, SPE- 162074, SPE Russian Oil & Gas Exploration & Production Technical Conference and Exhibition, Moscow, Russia, October 16–18, 2012
19. Williams M.M.R. Effective diffusion coefficients in heterogeneous media. J. Nucl. Energy, v.26, pp. 189-209, 1972.
20. Crain, E.R., "Crain's Petrophysical Handbook., at http://www.spec2000.net, Rocky Mountain House, Alberta, Canada, 2013
21. TERMOSIM Software (https://tgtoil.com/technologies/hpt-high-precision-temperature-logging/itsm/)
22. Salamatin A., Karuzin A., Aslanyan I., Zaripov I. TERMOSIM Handbook – Kazan, Russia: TGT Oil And Gas Services, 2014. – 320 (https://www.prime-college.ru/courses/tgt/level/

advanced/wla-advanced/rfa-2/rfa-i/rfa-i-mc/)

23. Nikolaev S., Nikolaeva N., Salamatin A. Thermal physics of rocks. – Kazan: KSU , 1987. – 152 p.
24. Nelson Suarez, Ademola Otubaga and Nagendra Mehrotra et al. 2013. Complementing Production Logging with Spectral Noise Analysis to Improve Reservoir Characterisation and Surveillance. SPWLA 54 th Annual Symposium held in New Orleans, Louisiana, USA, 22-26 June.
25. Salim Ghalem, D. Elyes Draoui, Ayman Mahamed et al. 2012. Innovative Noise and High-Precision Temperature Logging Tool for Diagnosing Complex Well Problems. SPE-161712 presented at the Abu-Dhabi International Petroleum Exhibition and Conference held in Abu-Dhabi, UAE, 11–14 November.
26. A.A. Lutfullin, A.R. Abdrahimov, I.N. Shigapov, I.Yu. Aslanyan, A.M. Aslanyan, R.K. Kuzyutin et al. 2014. Identification of Behind-Casing Flowing Reservoir Intervals by the Integrated High-Precision Temperature and Spectral Noise Logging Techniques. SPE-171251-MS presented at the SPE Russian Oil and Gas Exploration and Production Technical Conference and Exhibition held in Moscow, Russia, 14-16 October.
27. Arthur Aslanyan, Irina Aslanyan, Andrey Salamatin, Andrey Karuzin, Yulia Fesina et al. 2014. Numerical Temperature Modelling for Quantitative Analysis of Low-Compressible Fluid Production. SPE 172090 presented at the Abu-Dhabi International Petroleum Exhibition and Conference held in Abu-Dhabi, UAE, 10–13 November.
28. A. Aslanyan, I. Aslanyan, A. Arbuzov, B. Zagidullin et al. 2014. Time-Domain Magnetic Defectoscopy for Tubing and Casing Corrosion Detection. SPE 169601 presented at the SPE International Oilfield Corrosion Conference and Exhibition held in Aberdeen, United Kingdom, 12—¬13 May 2014.
29. Ihab, N. M., El-Hamawi, M, Rasheed A.H. Arthur, A.A, Filenev, M, Aslanyan I.Yu, Bargouthi J., Salim,B,. Leak Detection By Temperature And Noise Logging. 2012. Abu Dhabi International Petroleum Exhibition & Conference, Abu Dhabi, UAE, 11-14 November.

TGT oilfield services DMCC

Dubai, UAE

PO BOX: 334585

TEL: +971 (4) 431-49-04

FAX: +971 (4) 431-49-08

E-MAIL: info-uae@tgtoil.com

WWW.TGTOIL.COM